Flash tube chambers for electron and photon detection

P. J. Doe

FLASH TUBE CHAMBERS

FOR

ELECTRON AND PHOTON DETECTION

by

P.J.Doe, B.Sc., M.Sc.

A thesis submitted to the University of Durham for the Degree of Doctor of Philosophy

Being an account of the work carried out at the University of Durham during the period October 1975 to October 1977

"He had been eight years upon a project for extracting sunbeams out of cucumbers, which were to be put into vials hermetically sealed, and let out to warm the air in raw inclement summers. He told me he did not doubt in eight years more, that he should be able to supply the Governor's gardens with sunshine at a reasonable rate ; but he complained that his stock was low, and entreated me to give him something as an encouragement to ingenuity, especially since this had been a very dear season for cucumbers"

Gullivers Travels, Voyage to Laputa.

Jonathan Swift. (1726)

C O N T E N T S

		Page Nos
ABSTRACT		i
CHAPTER ONE:	INTRODUCTION	1
	References	6
CHAPTER TWO:	THE ELECTROMAGNETIC SHOWER : ELECTRON-PHOTON DETECTION	7
	2.1 Introduction	7
	2.2 Interaction Processes	7
	2.3 Theoretical and Experimental Shower Studies	9
	2.4 Electron-Photon Detection	11
	2.4.1 Homogeneous Total Absorption Detectors	11
	2.4.2 Sampled Shower Total Absorption Detectors	12
	References	15
CHAPTER THREE:	AN ELECTRON-PHOTON DETECTOR EMPLOYING HIGH PRESSURE FLASH TUBES	17
	3.1 Introduction	17
	3.2 Characteristics of High Pressure Flash Tubes	17
	3.2.1 Factors Influencing Efficiency	19
	3.2.2 Factors Influencing the Digitisation Pulse	19
	3.2.3 Recovery and Sensitive Times	21
	3.3 Construction of Detector	22
	3.3.1 Shower Sampling Module	23
	3.4 The High Voltage Pulsing and Clearing Field System	25
	3.5 Data Acquisition	26
	3.5.1 The Positron Beamline	26
	3.5.2 Trigger Logic and Data Handling	28
	References	30

Page Nos

CHAPTER FOUR: INVESTIGATION OF THE PERFORMANCE OF THE HIGH PRESSURE FLASH TUBE CHAMBER AS AN ELECTROMAGNETIC SHOWER DETECTOR 31

4.1 Introduction 31
4.2 Electromagnetic Shower Parameters as Recorded by the Detector 32
4.3 Measurement of Primary Particle Energy 35
4.4 Energy Resolution 38
4.5 Determination of the Trajectory of the Primary Particle 39

4.5.1 Location of Shower Axis 40
4.5.2 Spatial Resolution of the Detector 44
4.5.3 Angular Resolution of the Detector 45

4.6 Performance of the Detector at High Event Rates 45
4.7 Reduction of Internal Fields 46

4.7.1 Use of Alternate Polarity H.T.Pulse 47
4.7.2 Use of Oscillating H.T. Pulse 48

4.8 Conclusions 49

References 51

CHAPTER FIVE: AN ELECTRON-PHOTON SHOWER DETECTOR EMPLOYING LOW PRESSURE FLASH TUBES 52

5.1 Introduction 52
5.2 Design and Construction of the Detector 52
5.3 Electronic Circuits, Trigger Logic and Data Acquisition System 55

5.3.1 H.T.Pulsing and Clearing Field System 55
5.3.2 Output Digitisation 56
5.3.3 Trigger Logic and Data Acquisition System 57

5.4 Operation of the Detector in the Positron Beam 58

5.4.1 H.T.Plateau and Module Efficiencies 58
5.4.2 Determination of Sensitive Time 59
5.4.3 Determination of Recovery Time 60

5.5 Electromagnetic Shower Parameters Recorded by the Detector 61
5.6 Energy Measurement 63

5.6.1 Energy Resolution 65

5.7 Spatial and Angular Resolution 66

5.7.1 Fitting the Shower Axis 67
5.7.2 Determination of the Position of the Primary Particle 69
5.7.3 Spatial Resolution 71
5.7.4 Angular Resolution 72

Page Nos

5.8 Operation of the Detector at High Event Rates 73

5.8.1 Effect of Rate on Efficiency 74
5.8.2 Effect of Rate on Sensitive Time 75
5.8.3 Effect of Rate on Recovery Time 76
5.8.4 Effect of Rate on Energy and Spatial Resolution 77

5.9 Discussion 78

References 81

CHAPTER SIX: A STUDY OF THE FLASH TUBE DISCHARGE MECHANISM AND FACTORS INFLUENCING THE INDUCED FIELD 82

6.1 Introduction 82
6.2 The Flash Tube Discharge Mechanism From a Study of the Digitisation Pulse 83

6.2.1 The Discharge Mechanism 83
6.2.2 Experimental Technique 86
6.2.3 The Digitisation Pulse Output 87
6.2.4 Percentage of Discharges Involving Streamer Formation as a Function of Applied Field 88
6.2.5 The Effect of Rate on the Probability of Streamer Production - The Induced Field 92
6.2.6 Townsend and Streamer Pulse Height as a Function of Applied Field and Event Rate 96

6.3 Effect of Induced Fields Upon the Performance of the Flash Tube 97

6.3.1 Influence of the Induced Field Upon the Sensitive Time 97
6.3.2 Experimental Arrangement 98
6.3.3 Effect of the Outer Surface Resistance Upon the Induced Field 99
6.3.4 Dependence of the Induced Field Upon the H.T. Pulse Length 101
6.3.5 Effect of an Oscillating H.T.Pulse on the Induced Field 103

6.4 Discussion 104

References 107

Page Nos

CHAPTER SEVEN: CONCLUSIONS AND FUTURE WORK 108

7.1 Conclusions 108
7.2 Suggestions for Future Work 110

References 114

APPENDIX I: RELATIONSHIP BETWEEN THE NUMBER OF PARTICLES INCIDENT UPON A LAYER OF FLASH TUBES AND THE NUMBER OF TUBES OBSERVED TO IGNITE 115

ACKNOWLEDGEMENTS 118

ABSTRACT

The construction and operation of a simple, inexpensive, electron-photon detector, of the sampled shower type, is described ; the sampling planes consisting of layers of high pressure, methane doped, neon flash tubes, with CAMAC compatible digitised outputs. The detector was tested in a positron beam at energies from 0.5 to 4.0 GeV. No adverse effects due to the high background radiation were experienced, and an energy resolution of 43% and spatial and angular resolutions of 5 mm and 4° (FWHM) were obtained. The maximum event rate at which the detector could operate was limited to ~ 1 sec^{-1}, by the presence of internal fields which resulted in spuriousness or inefficiency. The use of modified H.T. pulsing systems has also been investigated as a means of reducing the internal field.

A modified detector was constructed, utilising large diameter, low pressure flash tubes, in an attempt to improve the maximum event rate, yet maintain the same useful resolution. An energy resolution of 33% and spatial and angular resolutions of 11 mm and 2° (FWHM) were obtained, which compares favourably with more complex and expensive detectors. Unexpectedly, at event rates in excess of a few per second, the tubes behaved either spuriously or inefficiently, due to large internal fields.

Investigations into the mechanisms of formation and decay of the internal fields have been made by observation of the digitisation output pulse. This novel approach may, with refinement, be of use in future studies of gas discharges since it is particularly sensitive to the gas breakdown mechanism. The significance of the outer surface resistance of the flash tube has also been demonstrated to be of importance to the performance of the tube. A mechanism, which results in the flash tube igniting spuriously, is suggested and a threshold value of the internal field, at which spuriousness occurs, has been determined.

CHAPTER ONE

INTRODUCTION

The flashtube was introduced by Conversi and Gozzini [1] in 1955, and in its simplest form consists of a sealed glass tube, containing a noble gas such as neon, placed between plane parallel electrodes. This simple configuration is shown in Figure 1a. The passage of an ionizing particle through the tube is determined by means of auxiliary detectors, which provide a trigger for a large impulsive electric field to be applied across the gas volume. The primary ionization, left in the wake of the particle, avalanches under the influence of the electric field producing a discharge of copious secondary electrons and photons which fills the whole tube. The occurrence of a discharge is evidence therefore of an ionizing particle having traversed the tube, and may be recorded optically, or by means of a simple electrical probe.

A single flash tube is rather limited in its applications, however large sensitive volumes may be constructed by insertion of further tubes between the electrodes, and by stacking additional layers, as indicated in Figure 1b. In this manner complex detection geometries may be achieved quite simply. The fundamental geometry is not restricted to plane surfaces, cylindrical configurations have been constructed with comparable ease.

The emergence of the flash tube was closely followed by the parallel plate spark chamber [2], which may be considered as a development of the original flash tube concept. Despite its numerous advantages, the flash tube has not seen such universal acceptance as the spark chamber,

FIGURE 1a A SIMPLE FLASH TUBE ASSEMBLY

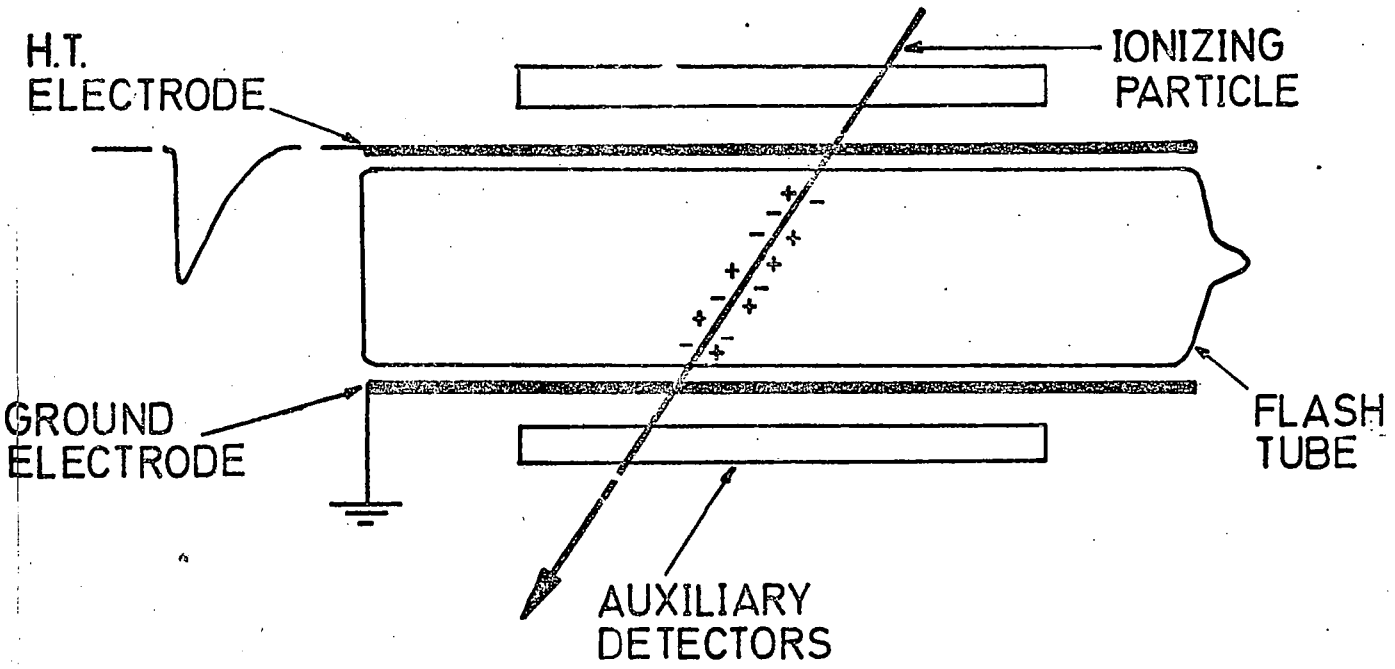

FIGURE 1b A FLASH TUBE ARRAY

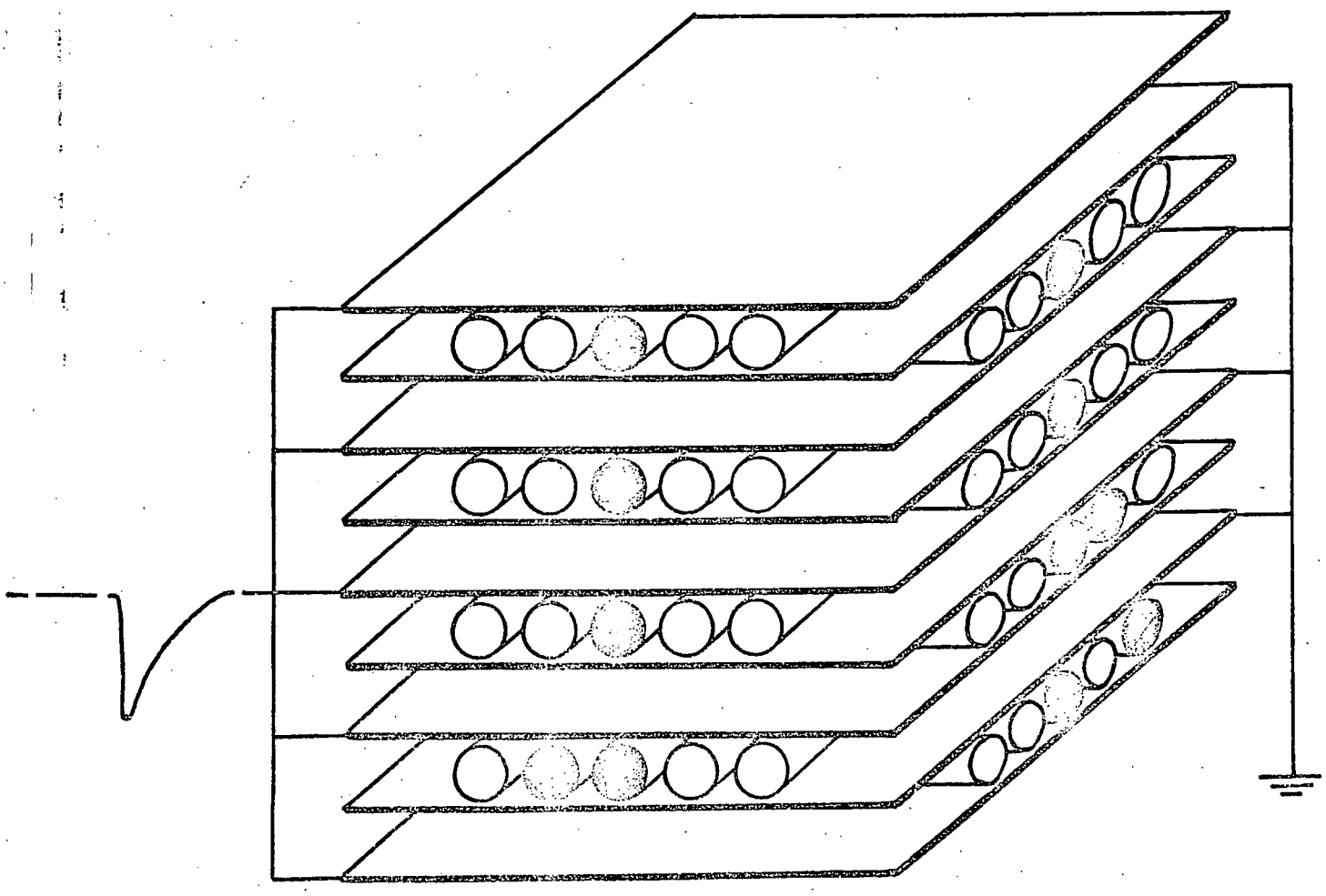

and is virtually unused outside the sphere of high energy cosmic ray physics. The reasons for this restricted use of flash tubes becomes obvious if one compares the properties of the two detectors, in the light of the general requirements of typical cosmic ray and accelerator based experiments.

The spark chamber has a number of advantages over the flash tube array ; it offers a superior spatial resolution, the sensitive time is simply adjusted, and the recovery time is short, allowing operation at high rates in a high background. The spark chamber contains very little insensitive material (such as glass tubes) and the resultant low scattering probability makes it ideally suited to magnetic spectrometers. Conversely, the flash tube at the time of its introduction exhibited long recovery and sensitive times which prevented its use at high trigger rates or in high background. Also, because of its relatively poor spatial resolution, dictated by the tube diameter, plus the large insensitive mass of glass, it did not lend itself to accurate track location. It is principally for these reasons that the accelerator based physicist has in the past chosen the spark chamber in preference to the flash tube array.

The requirements of a typical cosmic ray experiment differ from that of the accelerator experiment in many important respects. Cosmic ray experiments are usually concerned with particles of an energy unobtainable by accelerators, however the flux of these particles is very low and in order to obtain a realistic event rate detectors of large sensitive volume are required. As previously mentioned, flash tubes are ideal for this purpose, also they do not require continued replacement of gas, which for large volumes can be prohibitively expensive. The energy expended in discharging a tube is negligible compared with that involved in the formation of a spark, hence allowing the use of relatively

simple power supplies. Also, the rise time of the pulsed electric field can be made long compared with that required by spark chambers, without adverse effects and therefore is less likely to present a source of electrical interference to nearly equipment. The individual nature of the tubes allows statistical studies to be made of the number of particles in large showers, particle identification by way of its ionizing ability, and the efficient recording of many particle tracks at any incident angle. A number of ways of outputting the information from a tube is available, either by fibre optics [3] or electrical probes [4], neither of which require sophisticated electronics, or alternatively the intense light output is ideal for normal photographic techniques. The cosmic ray researcher was quick to utilize these possibilities, and the flash tube has rendered efficient and reliable service in such fields as extensive air showers[5], quark searches[6], neutrino studies[7], and high energy (TeV) cosmic ray spectroscopy[8].

The present trend of high energy accelerator physics is such that a need is frequently arising for an inexpensive, large area detector, capable of providing 4 π coverage without the need of particularly high spatial resolution, for example, the total enclosure of the intersection of colliding beams to record total particle production upon satisfaction of some trigger requirement, or neutrino type experiments which look for the particular signature of a rare event, but do not require a high degree of spatial resolution. It is these and similar demands, whose solution by conventional means would prove prohibitively expensive, that has motivated a reappraisal of the flash tube as a detector for accelerator based experiments, and stimulated investigation into the problems of long sensitive and recovery time, and high event rate effects, which have previously prevented the use of flash tubes.

The sensitive time and recovery time of flash tubes is typically

100 μs and 0.5s respectively ; this will limit the tube to event rates of approximately 1 event sec^{-1}, in backgrounds of less than 10^3 particles per tube, per second. This is clearly of little use to the majority of accelerator based experiments. However, the use of alternating clearing fields and the addition of a small percent of electro-negative gas to the NeHe, has reduced the sensitive and recovery times to 1 μs and 1 ms respectively[9], allowing event rates of up to 10^3 sec^{-1} in backgrounds of up to 10^6 particles per tube, per second. At these high event rates, it is expected that the field resulting from charges deposited on the inner wall of the flash tube will result in a reduction of the tube efficiency. However, the problems of these induced fields may be largely overcome by the use of commercially available low resistance glass, or by the replacement of glass by a plastic[10]. (This latter method unfortunately requires a constant gas flow to overcome outgassing, and is apparently still in a development stage).

In the light of the above mentioned improvement, the flash tube now represents an attractive possibility for the accelerator based experimenter requiring a large area detector. To demonstrate this, and also to investigate the use of flash tubes in one particular sphere, that of electron-photon detection, a detector of the sampled shower type was built. The decision to build an electron-photon detector was made, since there appeared to be an increasing requirement for large area electromagnetic shower detectors, offering some degree of both spatial and energy resolution. Previous detectors such as lead glass Cerenkov or lead-scintillator sandwich, only achieve both forms of resolution at the cost of great complexity and expense. It appeared that a total absorption detector, with sampling planes of flash tubes, could provide an inexpensive solution to the problem.

The results from this shower detector were particularly

encouraging[11], no effects of high background were detected, and data was taken at rates of 50 events sec^{-1} with no apparent deterioration in efficiency. It was decided, therefore, to construct a more refined detector to investigate further the potential of the flash tube in this particular application, and of its general use in an accelerator environment. It is the results obtained operating this detector, and a subsequent further shower detector, designed specifically to operate at high event rates whilst maintaining a useful degree of both spatial and energy resolution, with which this thesis is concerned.

REFERENCES : CHAPTER ONE

(1) Conversi M., Gozzini A, Nuovo Cin., 2, (1955) 189.

(2) Fukui S., Miyamoto S., Nuovo Cin., 1, (1959) 113.

(3) Conversi M., Federici L., Taccetti Q., Int.Conf. Instrumentation for High Energy Phys., Frascati, (1973), 184.

(4) Ayre C.A., Thompson M.G., Nucl. Inst.Meth., 69, (1969) 106.

(5) Bohm E., Nagano M., Van Staa R., Trumper J., Proc.Int.Conf. Cosmic Rays, 4, (1971) 1438.

(6) Ashton F., et al., J. Phys. A : Gen.Phys., 4, (1971) 895.

(7) Meyer, B., et al., Phys. Rev., D4, (1971) 80.

(8) Ayre, C.A., et al., Nucl. Inst. Meth., 102, (1972) 10 and 29.

(9) Chaney, J.E., Ph.D.thesis, Durham University, (1974).

(10) Conversi M., Federici L., Submitted to Nucl.Inst.Meth., August 1977.

(11) Chaney, J.E., Breare J.M., Tait I.D., Nucl. Inst. Meth., 125, (1975) 189.

CHAPTER TWO

THE ELECTRO-MAGNETIC SHOWER : ELECTRON-PHOTON DETECTION

2.1 INTRODUCTION

Electrons and photons are detected by recording the effects of their interaction with matter. There are a number of processes by which this interaction may take place, the dominant or most probable process depends principally upon the energy of the primary electron or photon. For high primary energies, the dissipation of this energy may involve many or all of these processes resulting in the production of the electromagnetic shower. The design and performance of a detector will depend upon the many parameters of this shower and the ultimate resolution of an "idealised" detector is set by the statistical fluctuations of these processes.

For the reasons given above, before embarking upon the subject of this thesis, a brief account of the principal electron-photon interactions with matter will be given, followed by a short description of the most common forms of electron-photon detectors in current use.

2.2 INTERACTION PROCESSES

A large number of physical processes are involved in the development and decay of an electromagnetic shower[1]. The probability of a particle undergoing a particular process depends very much upon its energy. This is illustrated for three major processes by Figure 2.1 and is summarised below :

(1) BREMSSTRAHLUNG, whereby a charged particle is accelerated by the nuclear electromagnetic or electron field and produces copious low

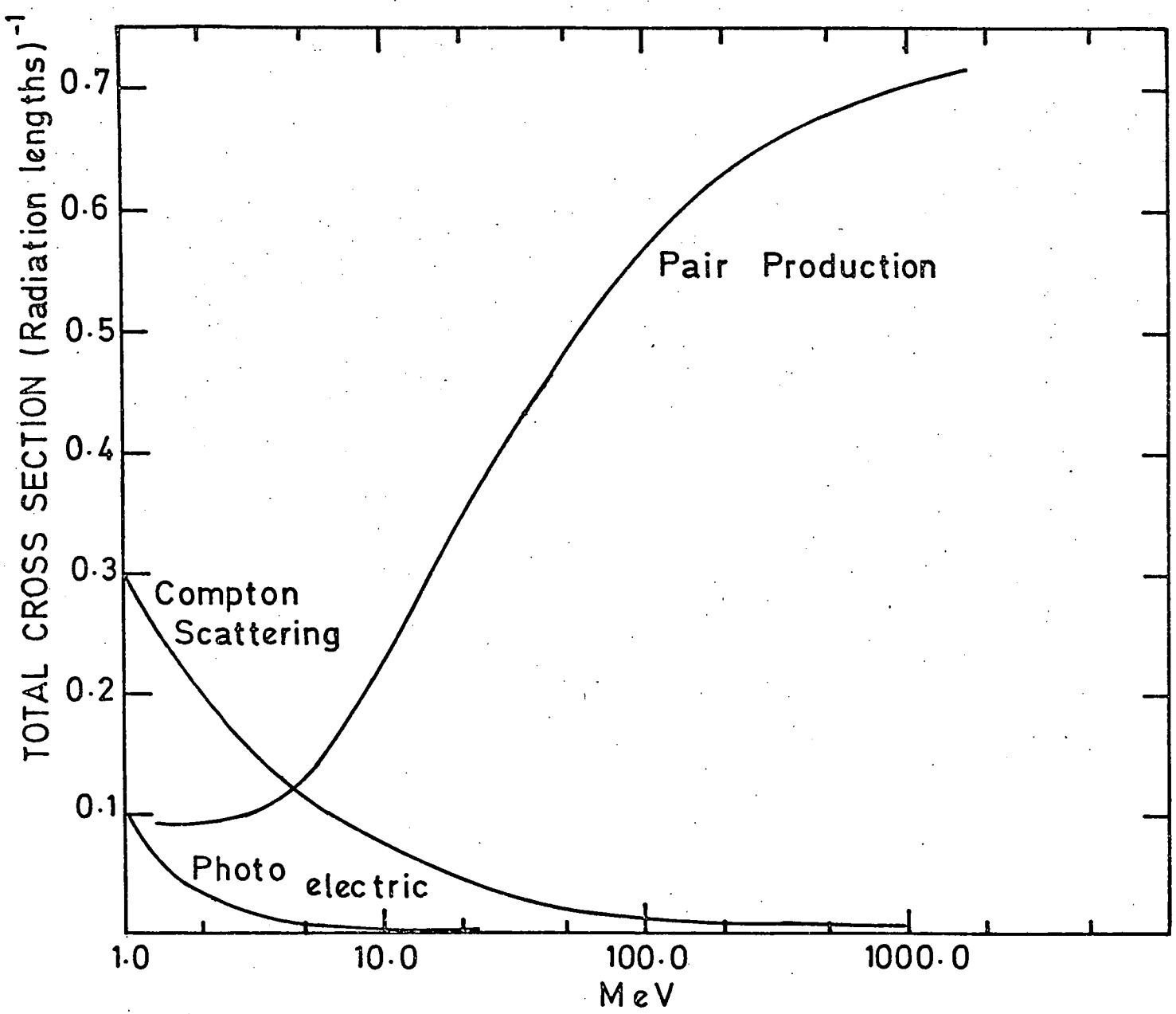

FIGURE 2·1 MAIN INTERACTION PROCESSES

energy photons as it passes through a dense absorber.

(2) PAIR PRODUCTION, for an energy of greater than 1.02 MeV (the rest mass of two electrons) a photon may materialise in a nuclear electromagnetic or electron field in the form of an electron-positron pair.

It is the two above mentioned radiative processes which are primarily responsible for the rapid increase in the number of secondaries, ranging from very low energies to almost that of the primary.

For these secondary electrons positrons and photons of progressively lower energy, further interaction processes, loosely categorised as collision processes, become available. It is by these processes that the shower is absorbed resulting in the characteristic absorption tail of the electromagnetic shower. The primary low energy processes are :

(3) COMPTON EFFECT, whereby an interaction occurs between an atomic electron (regarded as free) and a photon. The photon is not absorbed but is scattered, and proceeds with reduced energy.

(4) PHOTO-ELECTRIC EFFECT, whereby a photon interacts with an atom and is totally absorbed in expelling an electron.

(5) ELASTIC SCATTERING, (Rayleigh, Thompson and Nuclear Resonant). Of these processes, Rayleigh scattering is usually the most important, by which the incident radiation is scattered by the bound electrons, which do not receive sufficient energy to be ejected from the atom.

It has been shown[2,3] that the resultant showers, whether initiated by a high energy electron, positron or photon, differ only slightly and it is primarily by the mechanisms outlined above that the energy of the incident particle is dissipated.

Hence, high energy electromagnetic particles lose most of their energy by radiative processes in the production of high energy secondary electrons, positrons and photons. Photons, in turn, produce e^+ e^- pairs, or are compton scattered, resulting in electrons of similar energy to that

of the initial photon. These electrons produce further photons in turn, initiating more secondaries, but of a progressively lower and lower energy; hence the initial sharp rise in the number of secondaries. Eventually, however, the radiative losses (secondary particle production) cannot compete with the collision losses(absorption of low energy secondaries), and the shower decays away resulting in the long attenuation tail ; the energy of the primary particle being finally dissipated in the excitation and ionisation of the absorber atoms.

To illustrate the profile of the electromagnetic shower, resulting from the above processes, Figure 2.2 shows the results of the Monte Carlo simulations of Messel and Crawford[3]. The shower shape is characterised by the position of the maxima, which is seen to vary with primary energy, and the attenuation coefficient of the shower tail which,for a particular absorber, is invariant with energy. An important property of electromagnetic showers is the linear relationship between the primary energy and the total number of secondaries produced in the shower. This is illustrated in Figure 2.3 and is utilised by all shower detectors in determining the primary energy.

2.3 THEORETICAL AND EXPERIMENTAL SHOWER STUDIES

Much early work has gone into an analytical solution to electromagnetic shower development[4,5,6]. However, even a one dimensional study of shower development, using simple approximations to the physical processes resulted in complex expressions extremely difficult to solve.

The development of the modern computer has allowed the simulation of the shower by the Monte Carlo method, whereby the cross sections of the various physical processes involved in the shower development are represented by probability distributions. Random numbers are used to sample these distributions and hence simulate the shower development. This method,

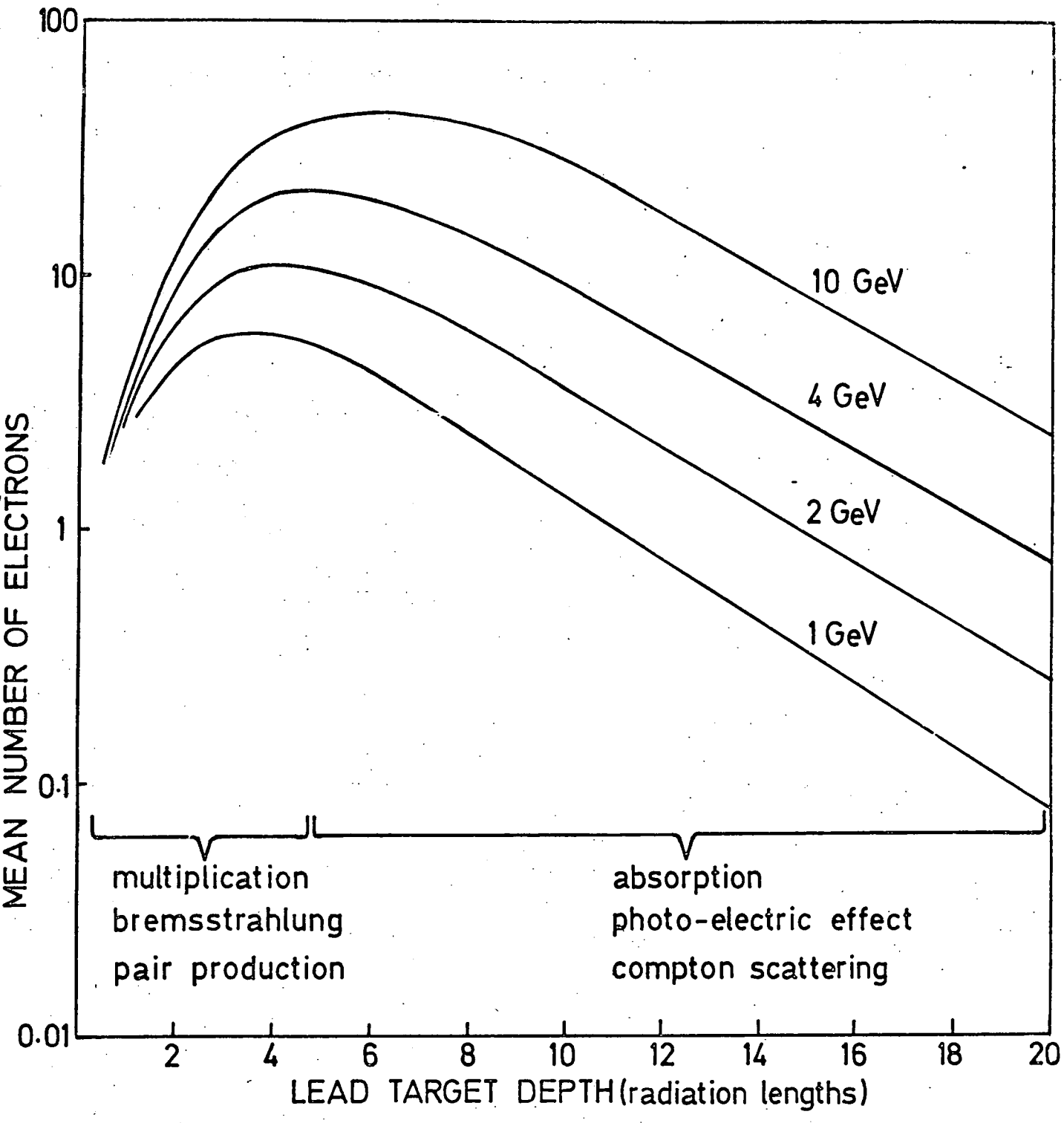

FIGURE 2.2 MEAN NUMBER OF ELECTRONS AS A FUNCTION OF TARGET DEPTH

FIGURE 2.3

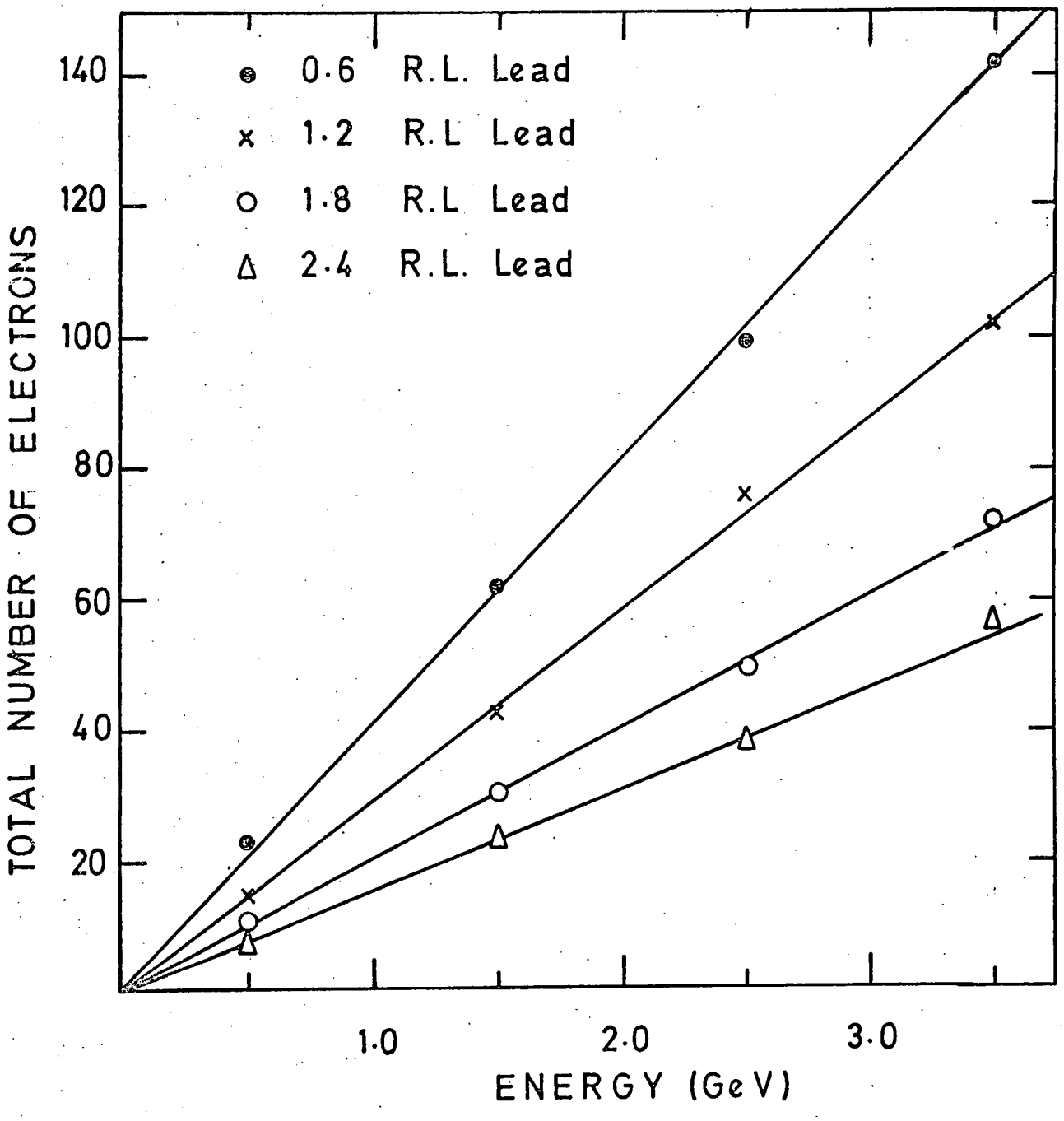

TOTAL NUMBER OF ELECTRONS EXPECTED AS A FUNCTION OF ENERGY FOR VARIOUS ABSORBER THICKNESS

first used by Wilson[7] is now the standard approach to theoretical shower studies[3,8,9,10,11,12].

There have been many experimental studies of electron and photon induced showers, almost all utilising the sampling technique, by which layers of absorber are interspaced with planes of sampling detectors. The major differences in these experiments arises from the type of detector used in sampling the shower, ideally it should have a good multitrack efficiency and spatial resolution for particles incident at a wide range of angles.

Sobers[13] has studied shower development in lead using sampling detectors of scintillator and spark chambers, and has made a comparison of the two methods. Likewise Agrinier[14], Cronin[15] and Bauer[16] have also utilized spark chambers as the sampling elements. Heuch[17] used lucite Cerenkov detectors as the sampling elements whilst studying shower development in lead. Ideally, the presence of the sampling detectors should have little or no effect on the development of the shower. In an attempt to achieve this, Jakeways[18] placed various thicknesses of lead absorber in front of a small scintillator probe which was used to map the resulting shower characteristics. A similar technique was used by Crannel[19] who inserted a small CsI(Tl) detector into a hole in an otherwise solid block of absorber.

In anticipation of the high energies obtainable from the future generation of accelerators, Muller[20] studied electron shower profiles at 15 GeV using a lead-scintillator configuration, and extrapolated his results to 1000 GeV. Lederman[21] used a MWPC placed between a lead absorber and a lead glass Cerenkov to study electron shower development with a view to using the characteristic signature of the electromagnetic shower as part of a hadron trigger.

2.4 ELECTRON, PHOTON DETECTION

There exist many types of detector suitable for electron and photon detection, the choice of detector is principally determined by the energy of the incident radiation and by the type of information (spatial or energy) which the detector is required to give. Detection below about 1 MeV is provided by means of semiconductor Si or Ge detectors[22,23,24], gas proportional devices[22,25] and scintillation detectors[22]. However, the upper limits to the energy detectable by these devices is dictated by the problem of confining the primary radiation and the resultant secondaries within the active volume of the detectors. Above a few MeV use is made of the fact that the number of secondaries produced in the resultant shower is proportional to the primary energy. Detectors in this energy range are made to be sensitive to the number and distribution of the shower secondaries, from which estimates can be made of the energy and trajectory of the incident radiation. These detectors fall into two categories ; the homogeneous type, in which the detecting medium is also the absorber, and the sampling type consisting of absorber interspaced with detecting planes. A brief description of the detectors falling within these two categories will be given since it is with these that the flash tube based detector must be compared.

2.4.1 Homogeneous Total Absorption Detectors

(1) LEAD GLASS CERENKOV[26,27,28,29]. Lead glass is an ideal electromagnetic shower detector, since it has a high Z (nucleus proton number), ensuring the rapid development of the shower, and the transparency of the glass allows almost complete collection of the Cerenkov light emitted by the relativistic charged particles of the electromagnetic shower. In its simplest form the detector consists of a lead glass block, sufficient to contain the shower, to which a photomultiplier tube is optically coupled to record the Cerenkov light. Large arrays are

usually required to obtain sufficient active area and total shower containment. An example is given in Figure 2.4. The modular construction of such arrays allows a degree of spatial resolution, values of $\pm$ 11 mm have been reported[29], however this is only achieved at greatly increased cost and complexity. An important property is the ability to distinguish between electrons/photons and hadrons, allowing its use in trigger systems. An on-line hadron rejection of 1 in 10^4 has been reported[28].

(2) NaI(Tl) CRYSTALS. The most widely used inorganic scintillators are the thallium activated NaI and CsI crystals[22]. A complete assembly consists of a scintillation crystal to which is coupled a photomultiplier tube. Until the work of Hofstadter et al[30,31,32] the detector was limited to energies of less than about 100 MeV; however the production of large single NaI(Tl) crystals has resulted in the containment of electron and photon induced showers of up to 15 GeV, with an energy resolution varying as $1.0\,E^{-\frac{1}{4}}$. As with lead glass the trigger functions are good, however the production of large sensitive areas and extraction of spatial information proves costly.

2.4.2 Sampled Shower Total Absorption Detectors

The general form of the sampled shower detector is shown in Figure 2.4. Assuming the shower to be totally absorbed in the detector and the sampling elements are sensitive to all the shower secondaries passing through or stopping in them, then a $1/\sqrt{E}$ response with energy is expected. If this is the case, then the principal limitation to the resolution comes from sampling fluctuations due to the statistical nature of the showering process, which is always present when the ionisation is not measured throughout the total volume of the absorber. However in practice, it is usually the response of the sampling elements which is the principal limiting factor.

FIGURE 2.4 SOME ELECTRON/PHOTON DETECTORS

a) LEAD GLASS ČERENKOV

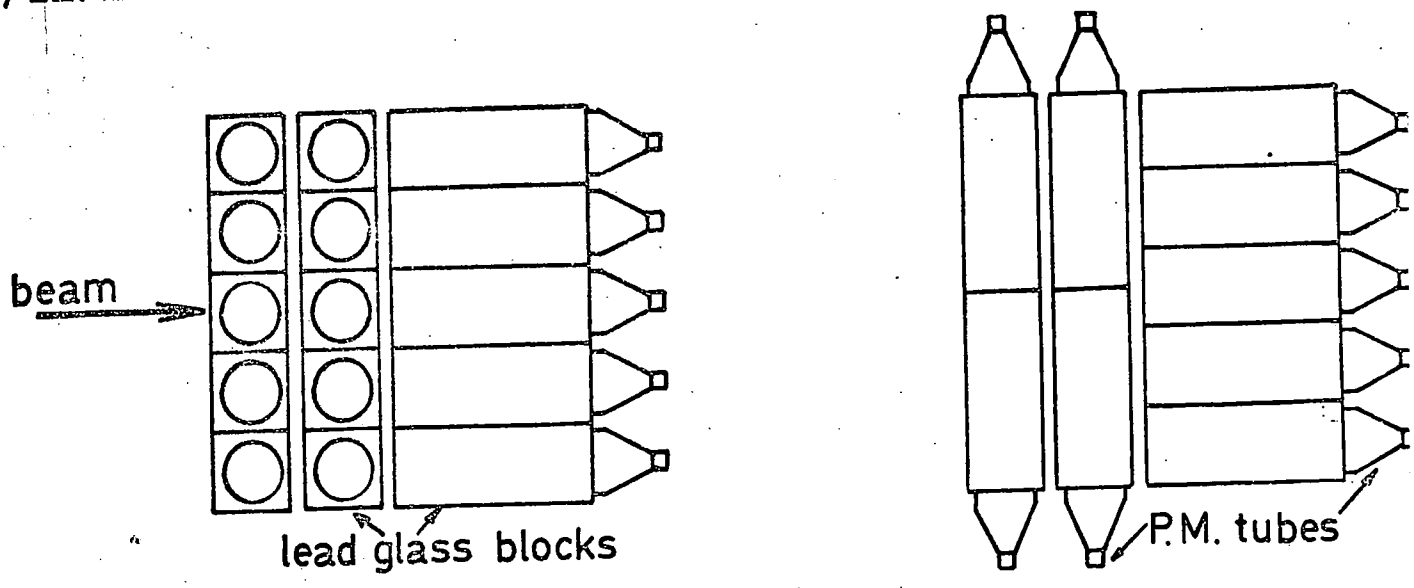

b) SODIUM IODIDE CRYSTAL

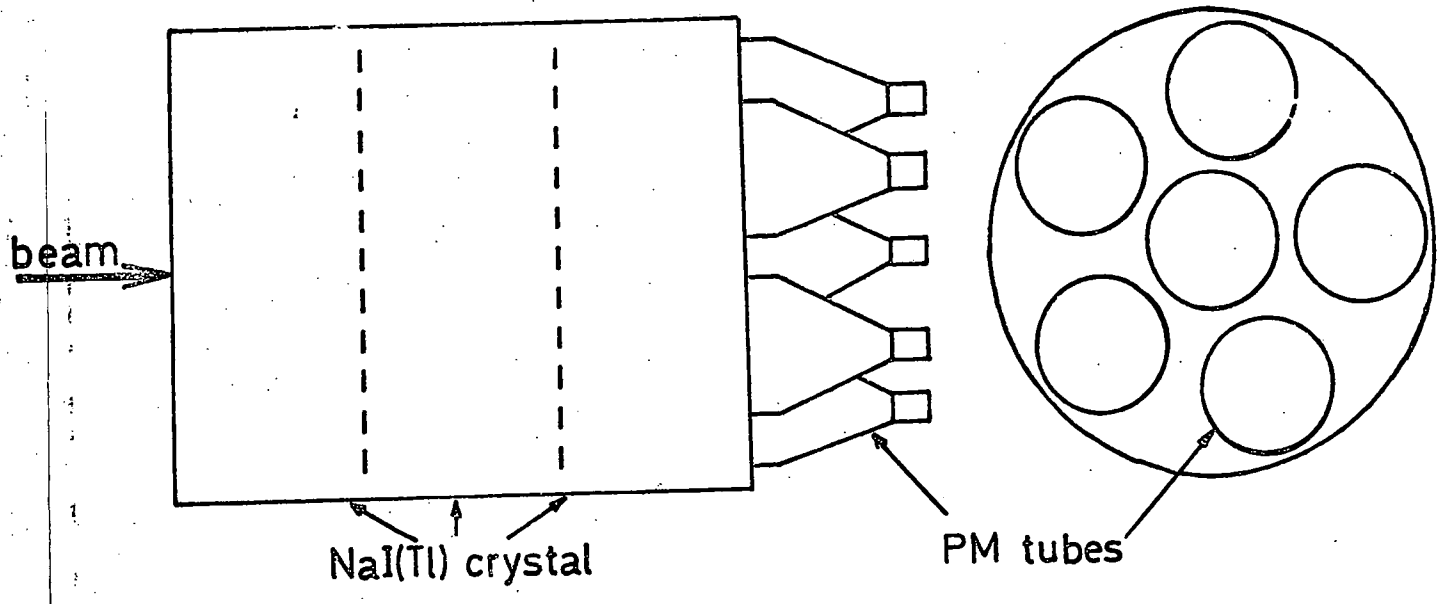

c) SAMPLED SHOWER

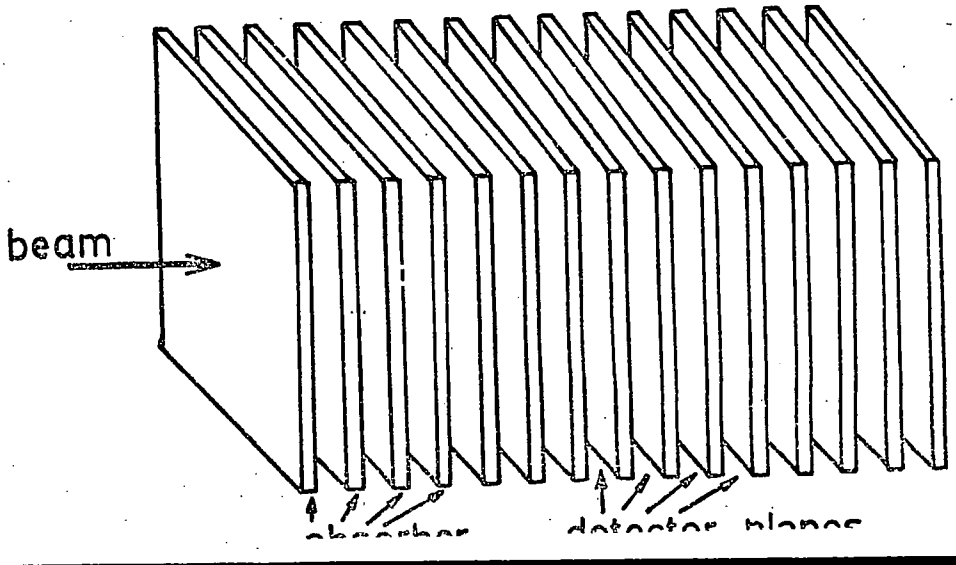

(1) SCINTILLATOR SAMPLING PLANES[33,34,35,36,37]. In this form the sampling planes consist of sheets of scintillator interspaced with sheets of absorber, the light from each scintillator is recorded by a photomultiplier tube, the outputs from which are linearly combined to give a signal which is proportional to the number of shower secondaries. Spatial resolutions of $\pm$ 2 mm have been obtained by replacing the single sheet of scintillator in each sampling plane, by a hodoscope of many scintillator fingers[36].

(2) LUCITE CERENKOV SAMPLING PLANES[38,2]. This detector has a similar configuration to the previous one, except that the detecting elements consist of lucite sheets in which the relativistic charged particles formed in the showering process produce Cerenkov light, which is recorded by a photomultiplier tube, as before.

(3) WIRE CHAMBER SAMPLING PLANES. These detectors consist principally of two types, those using spark chambers[14,16,39,40] and those using MWPC[41] sampling elements. In both cases the number of tracks in each sampling element is recorded and summed to give a measure of the total number of secondaries in the shower, and hence the primary energy. Since there is available a considerable amount of spatial information concerning the shower structure, an estimate of the shower axis and hence the trajectory of the primary can be made.

(4) CHARGE SAMPLING IN LIQUID ARGON[42,43,44,45,46]. This is a relatively new form of detector which consists of sheets of high Z absorber immersed in liquid argon. The alternative sheets of absorber are held at ground and at a high potential such that an electric field exists across the liquid argon. Ionisation produced by the shower secondaries in the argon drift towards the absorber. Recording the quantity of charge by means of charge sensitive amplifiers gives a measure of the total number of secondaries and therefore the energy of the primary.

A spatial resolution of $\pm$ 3mm has been obtained by collecting the charge on individual strips on the absorber.

Table 2.1[47] lists some of the more important properties of the above mentioned detectors. From this table it can be seen that few detectors offer both a reasonable energy and spatial resolution, and of those that do it is at the expense of great cost, complexity and operating difficulties. It is principally these problems which motivated the construction of an electron photon detector with sampling by means of flash tubes, described in the following chapters 3 and 4.

Detector Type	Energy Threshold	Energy Resolution	Spatial Resolution	Trigger Functions	Background Rejection	Ease of Handling
MWPC Sampling	$\sim$ 150 MeV	$\pm 29\%(t/E)^{\frac{1}{2}}$	$\pm$ 3mm	Poor	Poor	Difficult
Pb-Lucite	$\sim$ 150 MeV	$\pm 12\%(t/E)^{\frac{1}{2}}$	$\pm$ 5cm	Good	Fair	Easy
Pb-Plastic Scintillator	$\sim$ 150 MeV	$\pm 10\%(t/E)^{\frac{1}{2}}$	$\pm$ 5cm	Good	Fair	Easy
Pb-Liquid Scintillator	$\sim$ 150 MeV	$\pm 10\%(t/E)^{\frac{1}{2}}$	$\pm$ 5cm	Good	Fair	Difficult
Pb-Liquid Argon	$\sim$ 50 MeV	$\pm 11\%(t/E)^{\frac{1}{2}}$	$\pm$ 5mm	Poor	Poor	Difficult
Pb-Glass	< 20 MeV	$\pm 6\%/E^{\frac{1}{2}}$	$\pm$ 3cm	Good	Good	Easy
NaI Crystal	< 10 MeV	$\pm 1\%/E^{\frac{1}{4}}$	$\pm$ 3cm	Good	Excellent	Moderate

TABLE 2.1 : Typical properties of some electron-photon detectors[47] (t = target thickness)

REFERENCES : CHAPTER TWO

(1) Rossi, B., High Energy Particles, Prentice-Hall Inc.,(1952).

(2) McFarlane, W.K., Rothe, K.W., Wadlinger,A.E., Nuc.Inst: Meth., 91 (1971) 85.

(3) Messel, H., Crawford,D.F., Electron-Photon Shower Distribution Function, Pergamon Press (1970).

(4) Rossi, B., Greisen, K., Rev. Mod.Phys. 13 (1941) 249.

(5) Synder,H.S., Phys.Rev. 76 (1949) 1563.

(6) Nishimura,J., Kamata,K., Prog.Theor.Phys.Suppl.6 (1958) 93.

(7) Wilson,R., Phys.Rev. 86 (1958) 261.

(8) Barocelli,A., Nuc.Inst: Meth., 118 (1974) 445.

(9) Zerby,C.D., Moran,H.S., J.Appl.Phys.,Vol.34, No.8(1963)2445.

(10) Penzias,J.,Acta Physica Austriaca 43 (1975) 249.

(11) Longo,E., Sestili, I., Nucl.Inst. Meth. 128 (1975) 283.

(12) Volkel,V., Internal Report DESY, 65/6 (1965).

(13) Sobers,D., Nuc.Inst.Meth.109 (1973) 29.

(14) Agrinier,B., et al. Nuc.Inst.Meth. 88 (1970) 109.

(15) Cronin,J., Rev.Sc.Inst. 33 (1962) 946.

(16) Bauer, A., et al., International Symposium on Electron Photon Interactions, Hamburg (1965) 401.

(17) Heusch, C., Nuc.Inst.Meth. 29 (1964) 125.

(18) Jakeways, R., Nuc.Inst.Meth. 84 (1970) 79.

(19) Crannel,C., Phys. Rev. 161 (1976) 310.

(20) Muller, D., Phys. Rev. 5 (1972) 2677.

(21) Lederman, L., Nuc.Inst.Meth. 129 (1975) 65.

(22) England,J.B.A., Techniques in Nuclear Structure Physics Part 1 (London : MacMillan) p 1 - 130.

(23) McKay,K.G., Phys. Rev. 84 (1951) 829.

(24) Friedland, S.S., Nucleonics 18 (1960) 2.

(25) Curran,S.C., Wilson, W.H., Alpha, Beta, Gamma Ray Spectroscopy Vol. 1 (Amsterdam, North Holland) 303 - 344.

REFERENCES Continued : CHAPTER TWO

(26) Beale,J.S., et al. Nuc.Inst.Meth. 117 (1974) 501.

(27) Siemann, R.H., et al. Nuc.Inst.Meth. 129 (1975) 427.

(28) Appel, J.A., et al. Nuc.Inst.Meth. 127 (1975) 495.

(29) Barber, D., et al. A 480 Channel Lead Glass Cerenkov Detector, Daresbury Lab. submitted to Nuc.Inst.Meth. (1977).

(30) Hofstadter, et al. Nature 221 (1969) 228.

(31) Hughes, E.B., et al, IEEE, Nuc.Sci. 19 No. 3, 126.

(32) Hughes,E.B., et al, IEEE, Nuc.Sci. 17 No.3, 14.

(33) Backenstoss, G., Nuc.Inst.Meth. 21 (1963) 155.

(34) Zichichi, A., International Conf.on Instrumentation for H.E.P., Frascati, May 1973.

(35) Bohmer, V., et al, Nuc.Inst.Meth. 122 (1974) 313.

(36) Bashnin, B., et al, Nuc.Inst. Meth. 120 (1974) 391.

(37) Knauer, J.P., Nuc.Inst. Meth. 129 (1975) 91.

(38) Heusch, C.A. Nuc.Inst.Meth. 29 (1964) 125.

(39) Basile, M., Nuc. Inst. Meth. 101 (1972) 433.

(40) Breskin, A., Nuc.Inst.Meth. 135 (1976) 415.

(41) Katsura, T., Nuc.Inst.Meth. 105 (1972) 245.

(42) Knies, G., Nuc. Inst.Meth. 120 (1974) 1.

(43) Engler, J., Nuc.Inst.Meth. 120 (1974) 157.

(44) Willis, W., Nucl.Inst.Meth. 120 (1974) 221.

(45) Hitlin, D., Nucl.Inst.Meth. 137 (1976) 225.

(46) Cerri. C., Nucl.Inst.Meth. 141 (1977) 207.

(47) Atac. M., Proc. Calorimeter Workshop, FNAL, (1975) 57.

CHAPTER THREE

AN ELECTRON-PHOTON DETECTOR EMPLOYING HIGH PRESSURE FLASH TUBES

3.1 INTRODUCTION

The detector to be described in this chapter was designed and built as a consequence of experience gained operating a prototype detector in a positron beam [1,2]. The object of this prototype detector was to evaluate the performance of flash tubes, with short sensitive and recovery times, in an accelerator environment, and to investigate the potential of a flash tube assembly as an electromagnetic shower detector. The results of these investigations were encouraging, no adverse effects due to the high background radiation were encountered, spatial and energy resolutions of $\pm$ 1 cm and 48% respectively, were obtained, also no deterioration in the resolution at event rates of 50 sec^{-1} was noticeable.

The design of the detector could clearly be improved in many respects, the sensitive volume being insufficient to ensure total shower containment at high energies, and the use of large diameter flash tubes resulted in poor multitrack efficiency. In order to evaluate the true potential of this type of detector, an improved device, with increased sensitive volume, utilising small diameter, high pressure flash tubes, was constructed. The design and operation of the detector is described below.

3.2 CHARACTERISTICS OF HIGH PRESSURE FLASH TUBES

Extensive studies of the characteristics of the flash tubes used in this detector have been made by other workers [2,3,4]. These characteristics have considerable influence on the design of the detector, and therefore a brief summary will be given here.

The flash tubes were constructed of low resistance JENA 16B glass [5] to reduce the effect of induced electric fields. Each tube was coated with a white enamel paint to prevent photons from one discharging tube penetrating into the gaseous volume of adjacent tubes, thereby causing spurious ignitions. The principal features of the tubes are given in Table 3.1.

TABLE 3.1 : Principal Features of the Flash Tubes

Tube Length (cm)	Diameter		Glass Type	Pressure (ATM)	Gas Composition (%)	Recovery Time (ms)	Sensitive Time (μs)
	Internal (mm)	External (mm)					
50	∿ 8	8.2-8.8	JENA 16B	2.2	70 Ne, 30 He +2 CH_4	0.6	2.0

The parameters of the high voltage pulse used to fire the flash tubes are given in Table 3.2. It has been found that the performance of the high pressure flash tubes is more sensitive to variations of these parameters, than are the low pressure tubes [3,6].

TABLE 3.2 : Parameters of the High Voltage Pulse

Peak Electric Field Strength ($kV\ Cm^{-1}$)	Rise Time. T_r (ns)	Pulse Width, T_L (RC Decay Time) (μs)	Pulse Delay, T_D (ns)
9.5 - 10.0	50 - 70	3 - 5	200

The effect of variation of these parameters has some bearing upon the design tolerances of the flash tube assemblies (e.g. electrode separation-applied field), and are given below.

3.2.1 Factors Influencing Efficiency

(a) Pulse Magnitude : Figure 3.1(a) shows the variation of the layer efficiency as a function of the applied field for a number of rise times[3]. For Tr = 70 ns, the plateau region occurs at approximately 9.5 kV Cm^{-1}, the layer efficiency of 88% at this field value, representing an internal efficiency of almost 100%. For applied fields in excess of 10.0 kV Cm^{-1}, spurious flashing occurs, and is seen to increase with increasing field. Therefore, efficient operation requires fields of between 9.5 and 10.0 kV Cm^{-1}.

(b) Pulse Rise Time : The dependence of layer efficiency upon rise time is clearly seen from Figure 3.1(b) for two values of applied field[3].

(c) Pulse Length : The variation of layer efficiency with pulse width (RC decay constant) is shown in Figure 3.2[3]. It can be seen that for efficient operation, pulse lengths in excess of 3 μs are required. However this data was taken at a relatively slow rate (1 event min^{-1}), which allows the induced electric field, caused by charges adhering to the tube walls, to decay away. At event rates higher than this, the effect of the induced fieldbecomes apparent. Since a long pulse will sweep more charge to the tube walls, it is desirable to maintain the pulse length as short as possible, if it is wished to operate at high event rates. For this reason the pulse length was restricted to between 3 and 5 μs.

3.2.2 Factors Influencing the Digitisation Pulse

Information as to whether a tube has discharged or not is obtained by means of a small probe in contact with the face of the flash tube, as shown in Figure 3.3[7]. If the tube does not flash, then any pulse appearing across the resistor R is due to electrical pickup, and may be eliminated by inserting the digitisation probe inside a screening aluminium

FIGURE 3·1(a) EFFICIENCY AS A FUNCTION OF PEAK APPLIED FIELD FOR SEVERAL RISE TIME VALUES

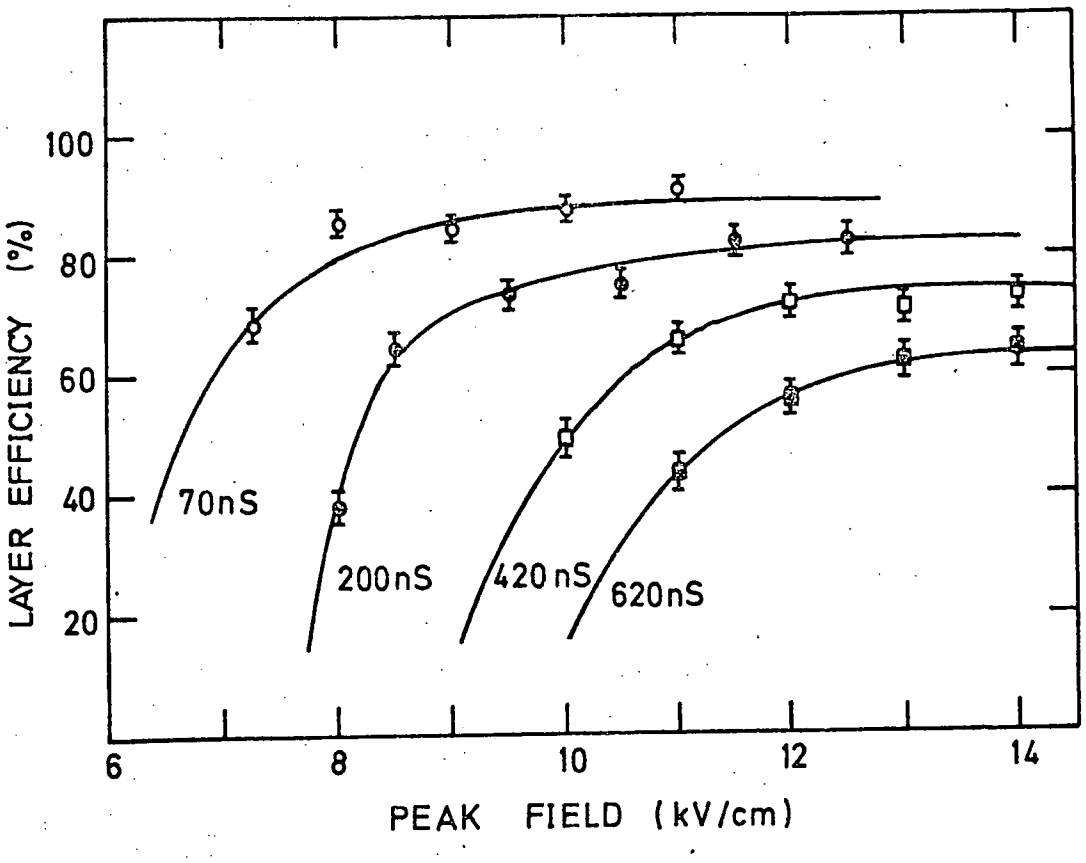

FIGURE 3·1(b) EFFICIENCY AS A FUNCTION OF RISE TIME FOR TWO APPLIED HT FIELDS

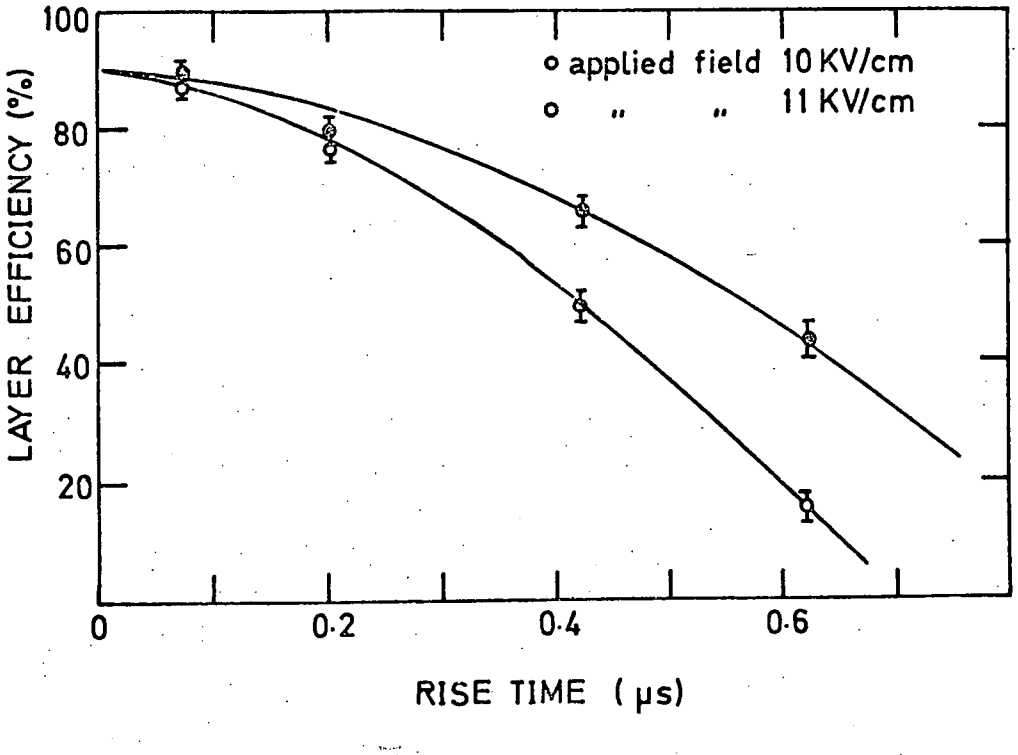

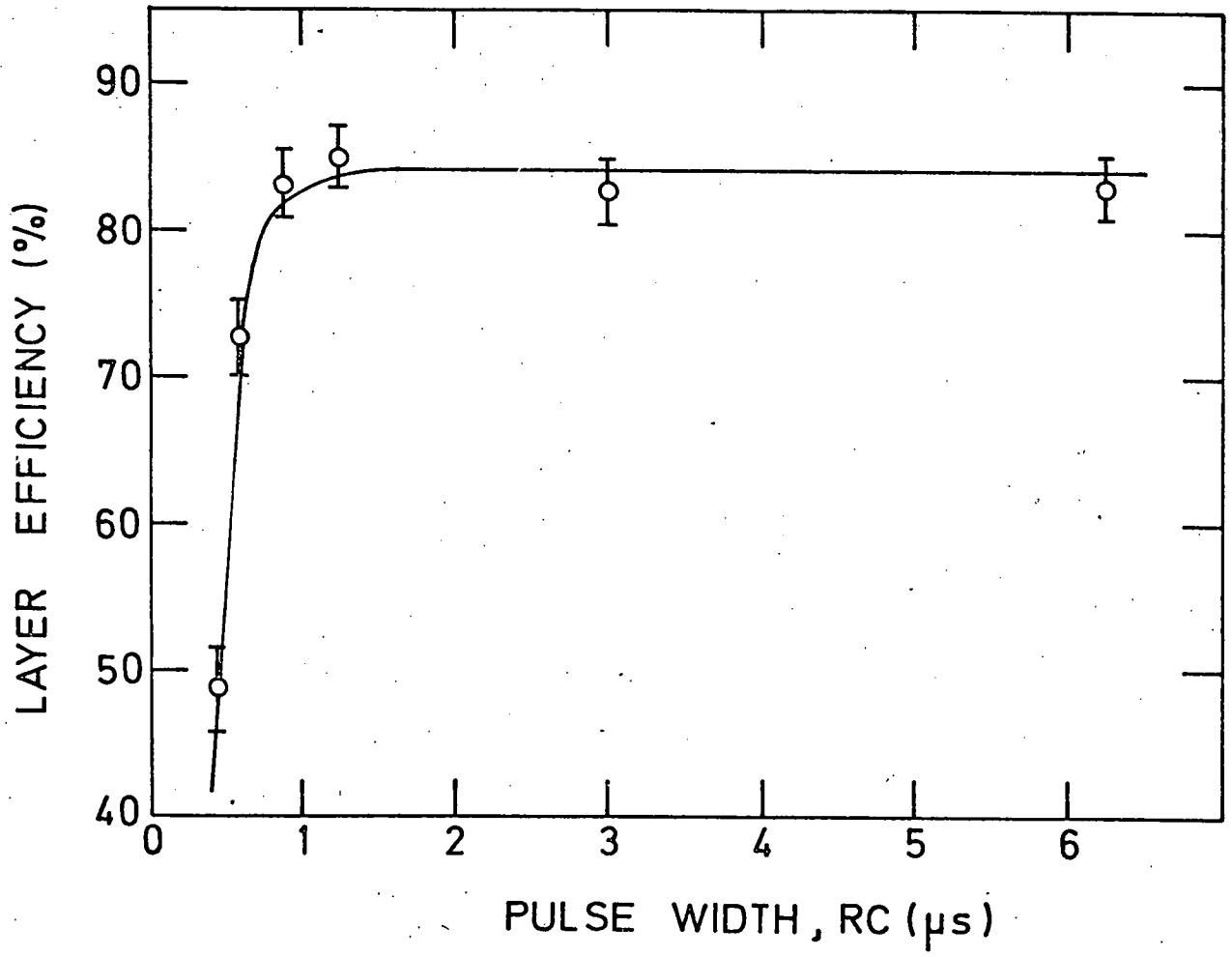

FIGURE 3.2 LAYER EFFICIENCY AS A FUNCTION OF HT PULSE WIDTH

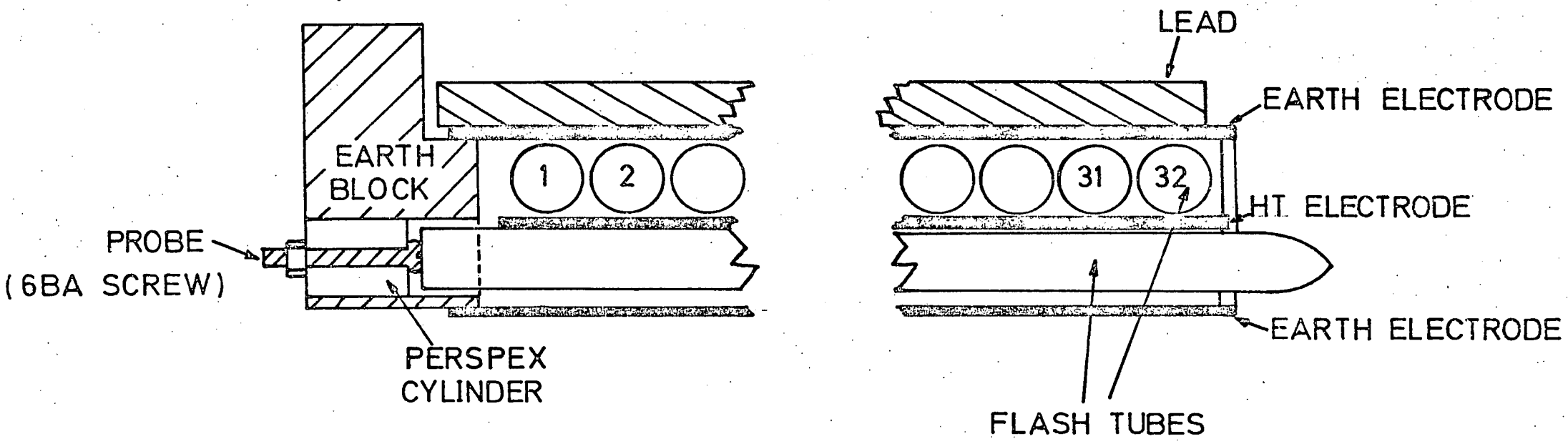

FIGURE 3.3 SECTION THROUGH A MODULE SHOWING DIGITISATION PROBE ARRANGEMENT

block. If the tube flashes a voltage pulse appears across the resistance R due to a capacitive coupling between the probe and the HT electrode via the plasma in the tube, an equivalent circuit for the mechanism is shown in Figure 3.4[3]. It is required that the pulse from the probe is of sufficient magnitude to set an IC latch (threshold approximately 4 v) which formed part of the readout memory (see section 3.3). The following factors are found to significantly effect the digitisation pulse height.

(a) Dependence of Pulse Height on Peak Applied Field : Figure 3.5(a)[3] shows the variation of digitisation pulse height with peak applied field for two digitisation probe diameters. The two slopes are due to the two different effective capacitances of the probe arrangements. The slope of the larger diameter probe being greater due to the larger capacitive coupling of the probe.

(b) Dependence of Pulse Height on HT Pulse Length : The variation of digitisation pulse height with the length of the applied HT pulse is shown in Figure 3.5(b)[3]. According to the theory of operation of the digitisation probe[7], the digitisation pulse height will depend upon the magnitude of the applied HT pulse at the time of formation of the plasma inside the tube. The digitisation pulse height is seen to increase rapidly with the length of the applied HT pulse. However, it should be borne in mind that the results were obtained at a low event rate. An increase in event rate will result in a lower effective applied field and hence a smaller digitisation pulse height.

(c) Variation of Pulse Height with Probe Resistance R: Figure 3.6(a)[3] shows the dependence of the digitisation pulse height with probe resistance. This behaviour can be understood by reference to the equivalent circuits shown in Figure 3.4. C_e is the equivalent capacitance of the probe - HT electrode arrangement at the time of formation of the plasma. C_s represents the stray capacitance of the associated

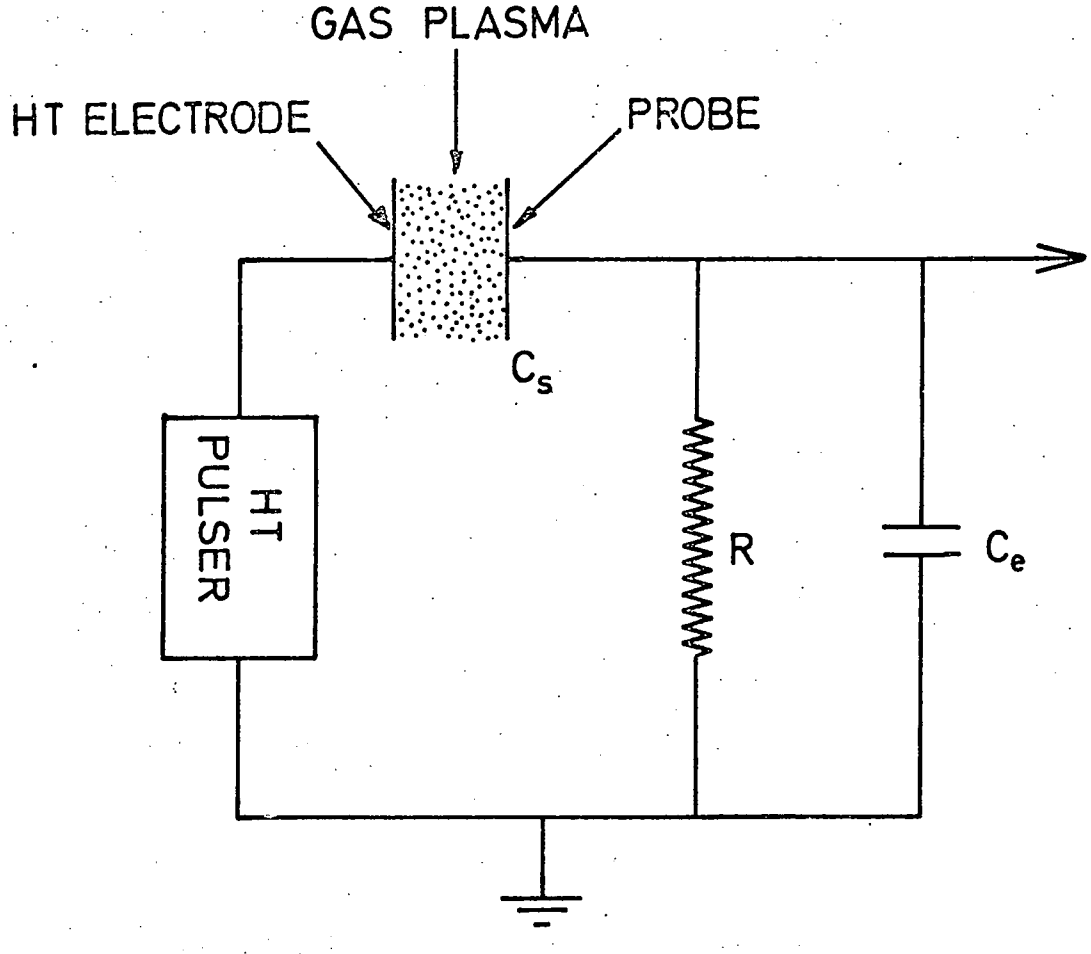

FIGURE 3.4 EQUIVALENT CIRCUIT OF THE DIGITISATION PROBE ARRANGEMENT

FIGURE 3.5(a) DIGITISATION PULSE HEIGHT AS A FUNCTION OF APPLIED HIGH VOLTAGE PULSE HEIGHT

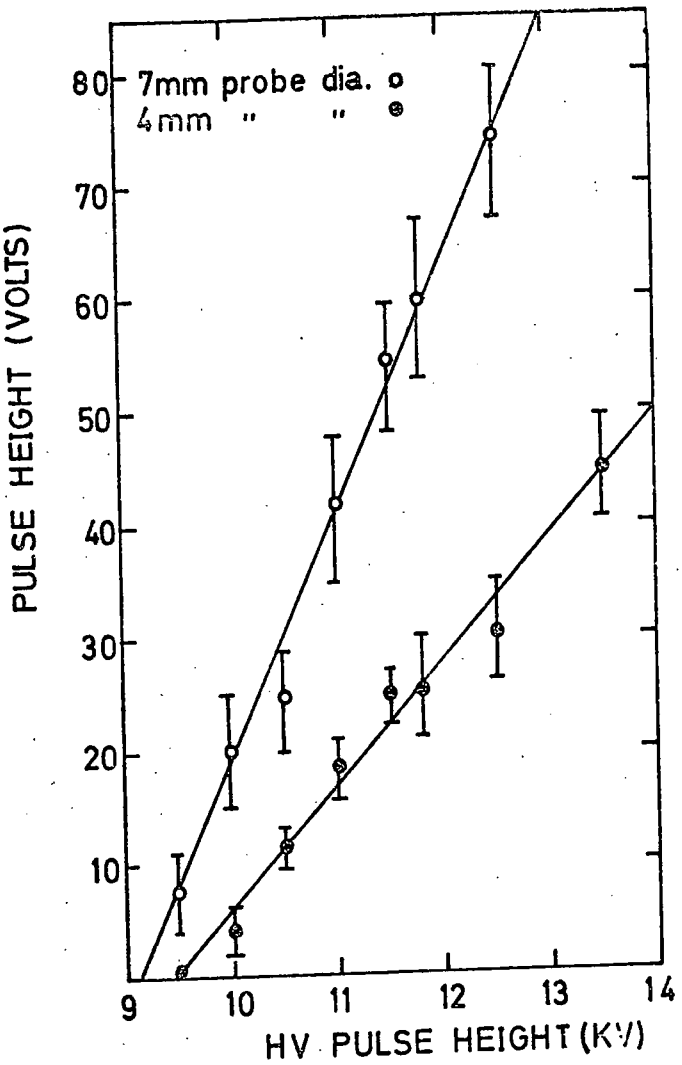

FIGURE 3.5(b) DIGITISATION PULSE HEIGHT AS A FUNCTION OF APPLIED HIGH VOLTAGE PULSE LENGTH

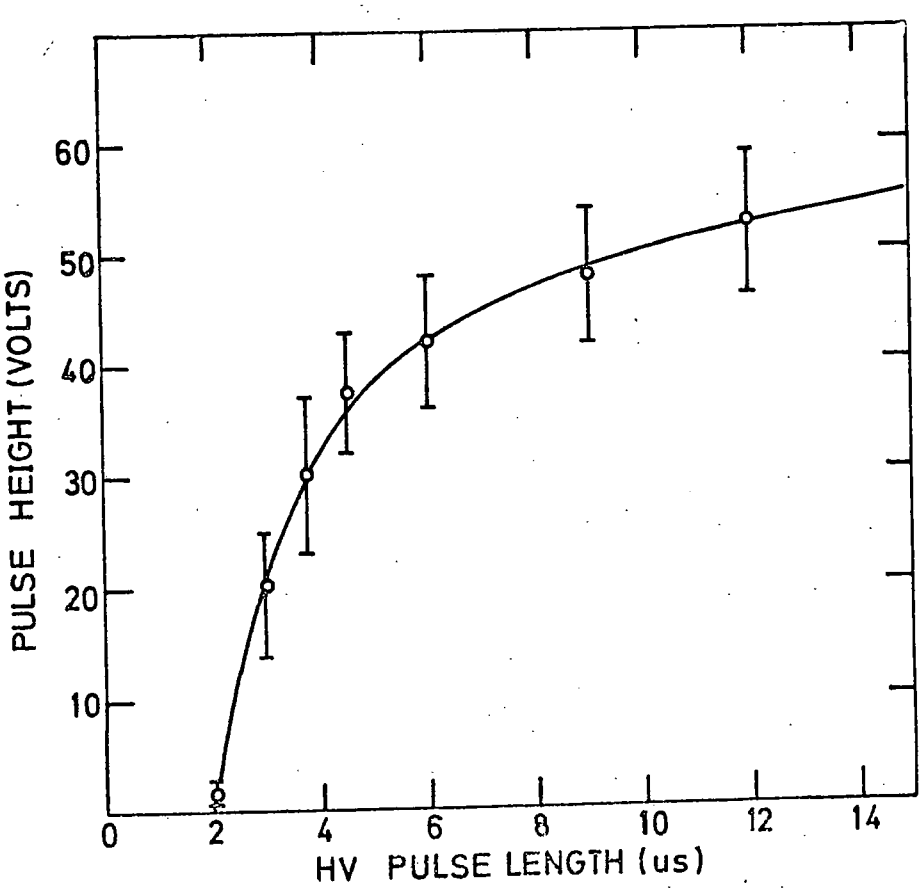

FIGURE 3.6(a) DIGITISATION PULSE HEIGHT AS A FUNCTION OF PROBE RESISTANCE

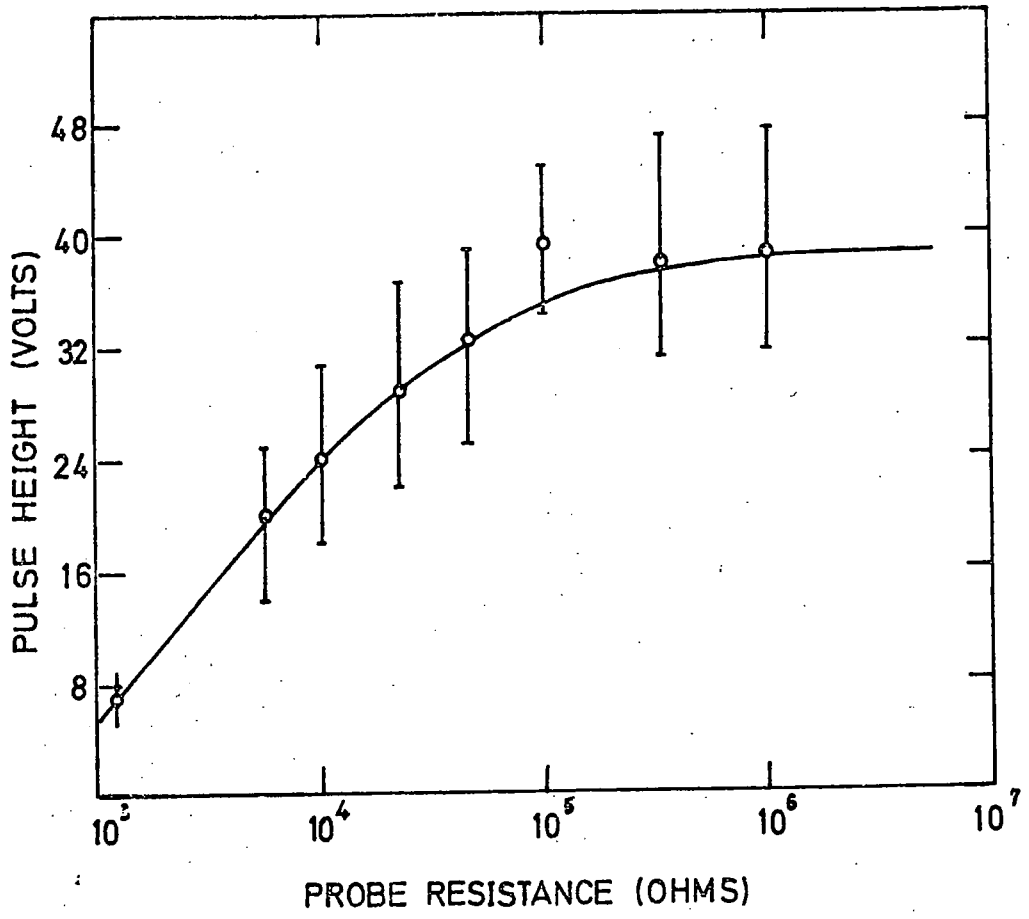

FIGURE 3.6(b) DIGITISATION PULSE HEIGHT AS A FUNCTION OF HT ELECTRODE-TUBE SEPARATION

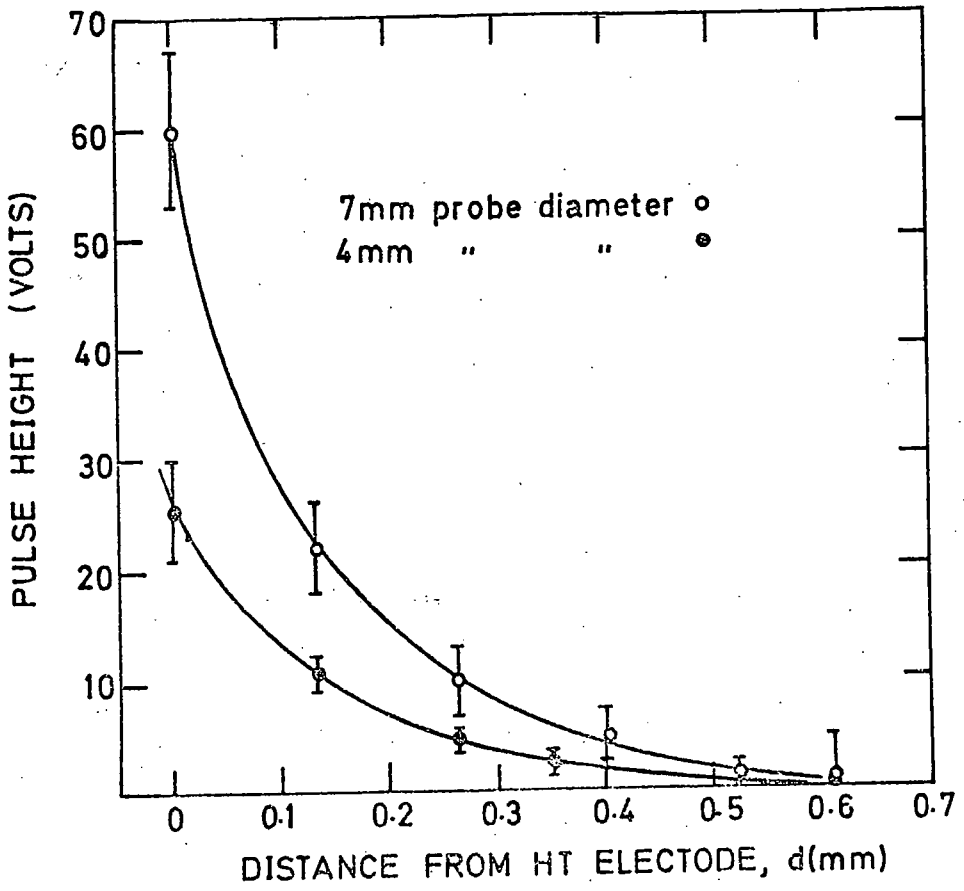

circuitry. The digitisation pulse height is seen to increase with R until the impedance of C_s makes any further increase in R ineffective.

(d) Dependence of Pulse Height with Separation Between the Flash Tube and the HT Electrode : This dependence is shown, for two probe sizes, in Figure 3.6(b)[3]. It can be seen that a separation as small as 0.1 mm has a considerable effect. As yet no satisfactory explanation has been found, however the approximate $1/d^2$ (where d is the distance between the HT electrode and the flash tube wall) dependence of the pulse height may give some indication of the physical process involved.

(e) Dependence of Pulse Height upon Flashing Rate : The variation of digitisation pulse height with flashing rate is shown in Figure 3.7(a)[4]; a decrease in pulse height of a factor of 4 occurring when the flashing rate is increased from 0.5 to 1.0 events sec^{-1}. This decrease is caused by the induced electric field, resulting from charges from the previous discharge, adhering to the inner wall of the tube. The direction of this field is such that it opposes the applied HT field, resulting in a lower effective HT field[5]. It can be seen from Figure 3.7(b)[4] that the digitisation pulse height from a tube flashing at a constant high rate may be increased by increasing the applied HT field. However, this does not offer a simple solution for an array of flash tubes where the flashing rate is expected to vary across the array. This would result in an excessively high applied HT field for those tubes which flash at a lower rate, resulting in spurious ignitions.

3.2.3 Recovery and Sensitive Times

The recovery and sensitive times of a flash tube are of particular importance if it is required that the tube operates successfully in a high background radiation and at high event rates, such as may be experienced with a machine based experiment. The sensitive and recovery times of neon-helium filled tubes, doped with methane, have been extensively

FIGURE 3·7(a) DIGITISATION PULSE HEIGHT AS A FUNCTION OF EVENT RATE

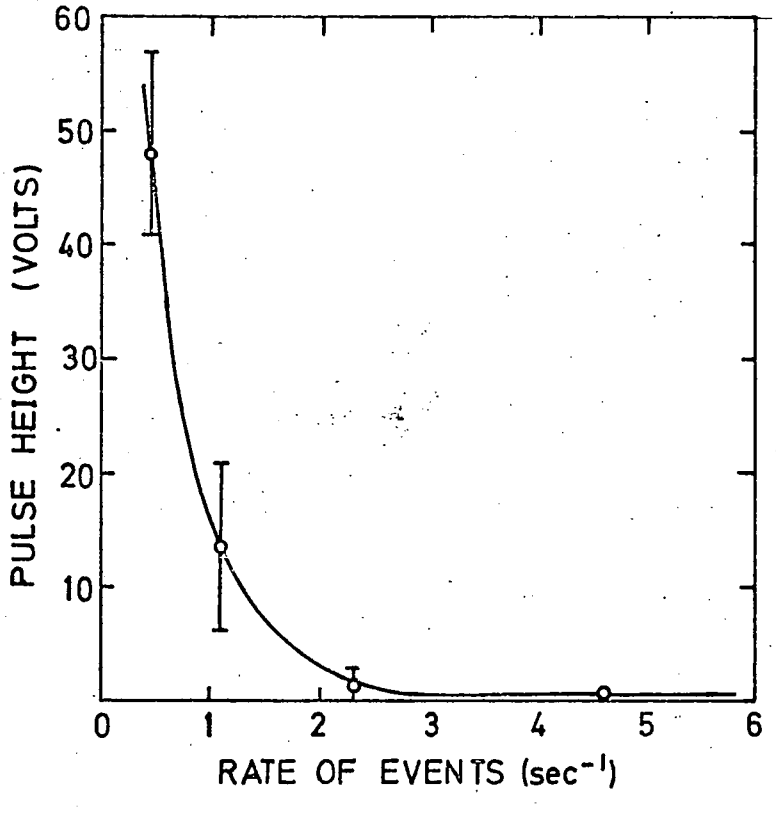

FIGURE 3·7(b) DIGITISATION PULSE HEIGHT AS A FUNCTION OF APPLIED HIGH VOLTAGE FIELD

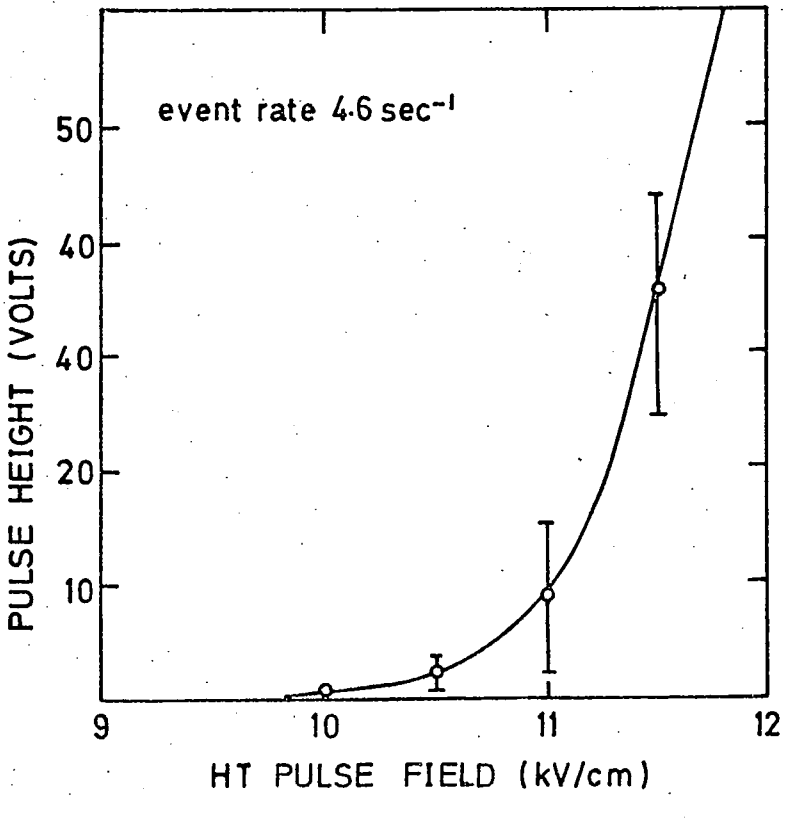

studied by other workers[1,2]. Their results for the high pressure tubes used in the present detector are summarised below.

(a) Sensitive Time : The sensitive time is defined as the delay required between the passage of the particle and the application of the HT pulse for the internal efficiency to fall to 50%, this represents a value of approximately 45% in terms of the layer efficiency for the tubes used in the present detector. A short sensitive time is obtained by applying a square wave clearing field of frequency 100 Hz, peak to peak voltage of approximately 100 v. This ensures that the primary ionisation left by a charged particle is rapidly swept from the gas volume. Figure 3.8(a) shows the relationship between layer efficiency and delay in application of the HT pulse, for the tubes used in the present detector; it can be seen that the sensitive time is approximately 2.0 μs.

(b) Recovery Time : The recovery time is defined as that time delay, after a tube has flashed, for the probability of re-ignition on application of a second pulse, to fall to 50%. Short recovery times have been obtained by the addition of small quantities of molecular gas, eg. O_2, CO_2, CH_4,[2,10] to the neon-helium. The recovery time for the tubes used in the present detector can be seen from Figure 3.8(b) to be 0.6 ms.

3.3 CONSTRUCTION OF DETECTOR

A general description of the detector is given, followed by more detailed accounts of the principal features of the detector.

The detector is of the sampled shower type and is shown schematically in Figure 3.9 and by the photograph in Figure 3.10. Twelve identical detector planes were used, 0.6, 1.2 and 1.8 radiation length sheets of lead may be inserted between each plane. Eleven of these detector planes were used in sampling the electromagnetic shower, the twelfth positioned at the front of the detector was used to determine the point of entry, of

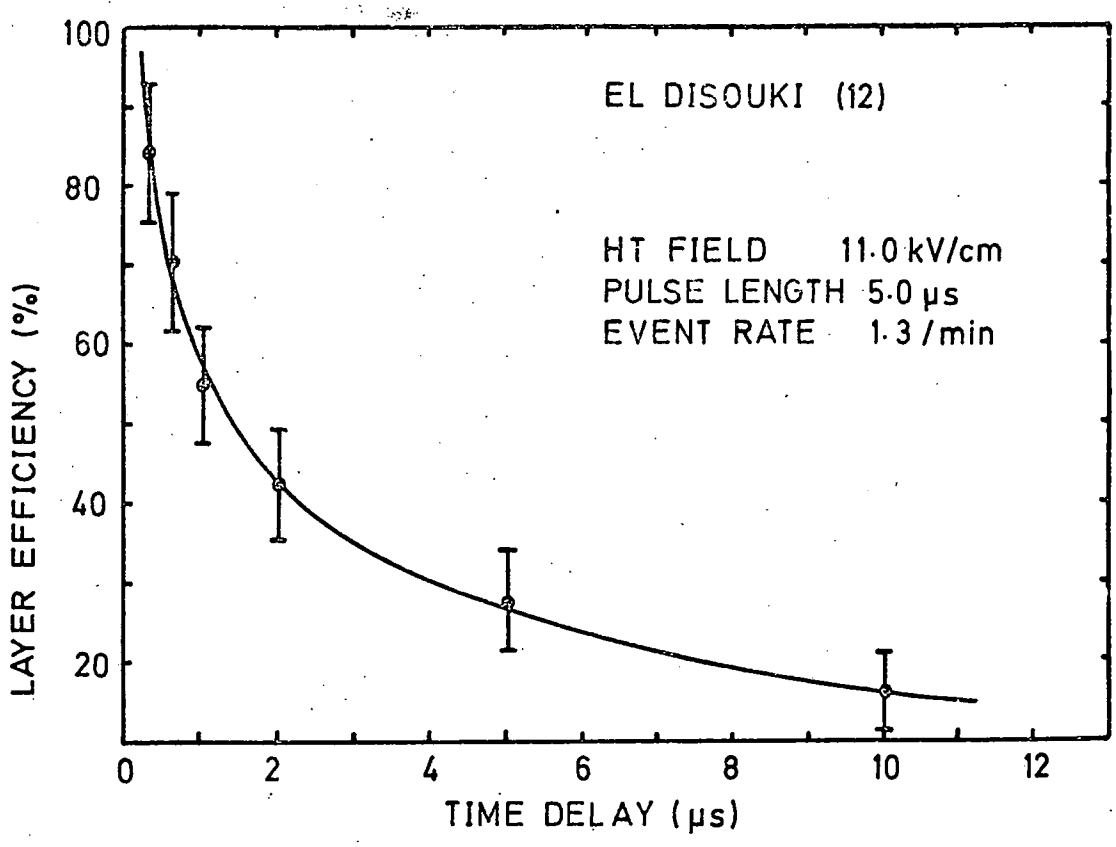

FIGURE 3.8a LAYER EFFICIENCY AS A FUNCTION OF DELAY

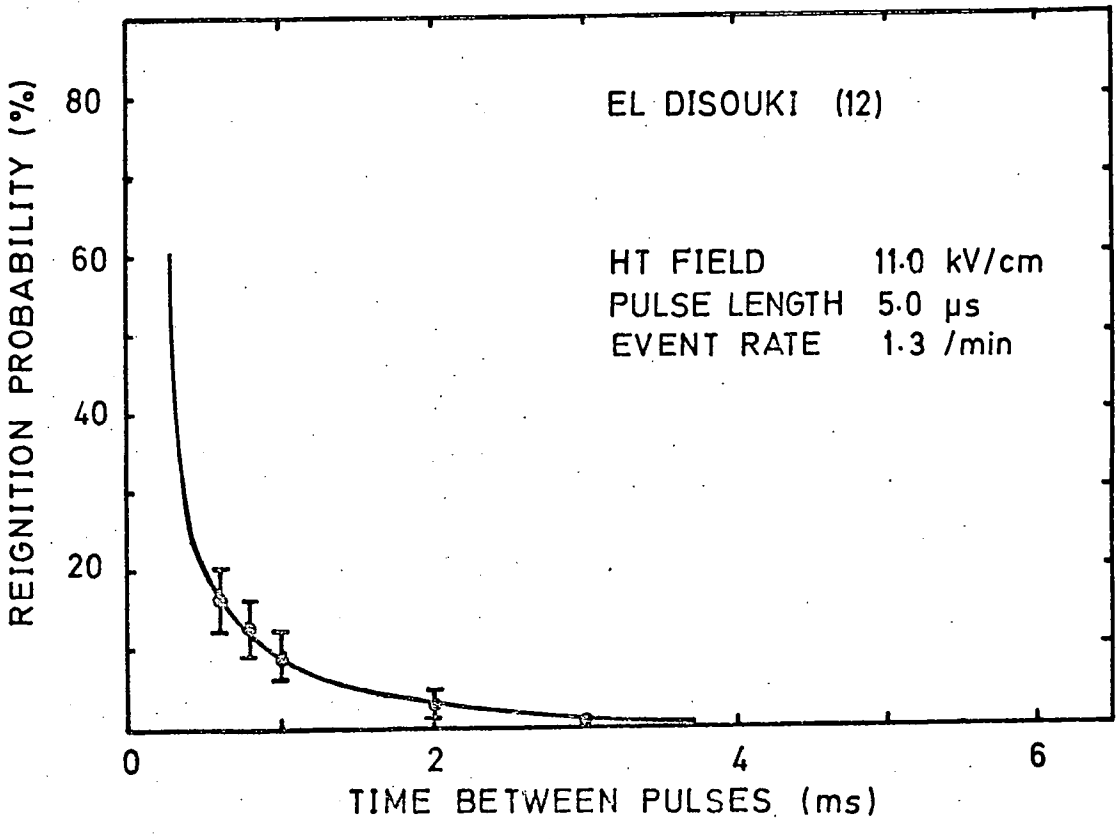

FIGURE 3.8b REIGNITION PROBABILITY AS A FUNCTION OF TIME BETWEEN HT PULSES

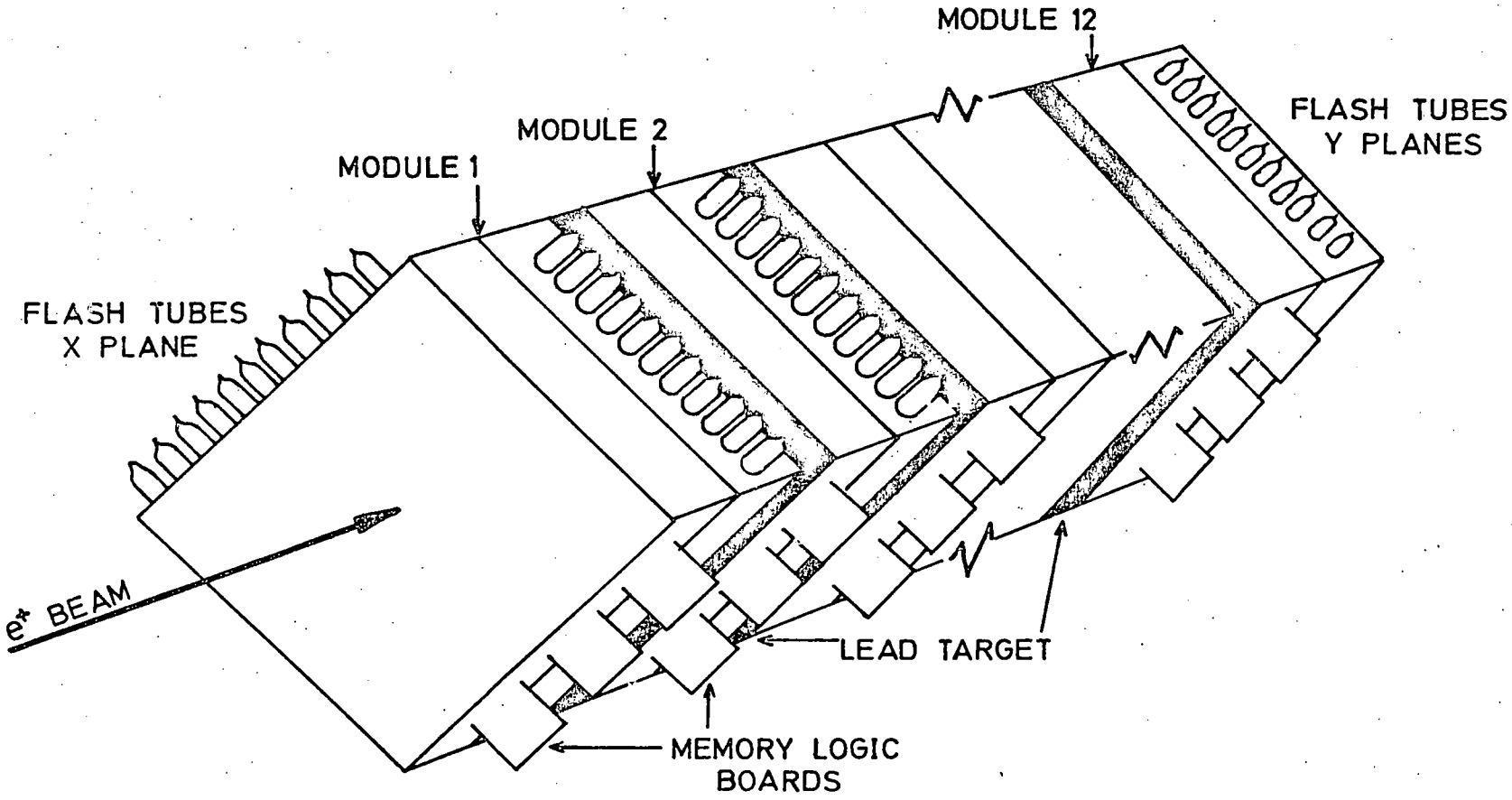

FIGURE 3.9 SCHEMATIC DIAGRAM OF THE HIGH PRESSURE FLASH TUBE CHAMBER

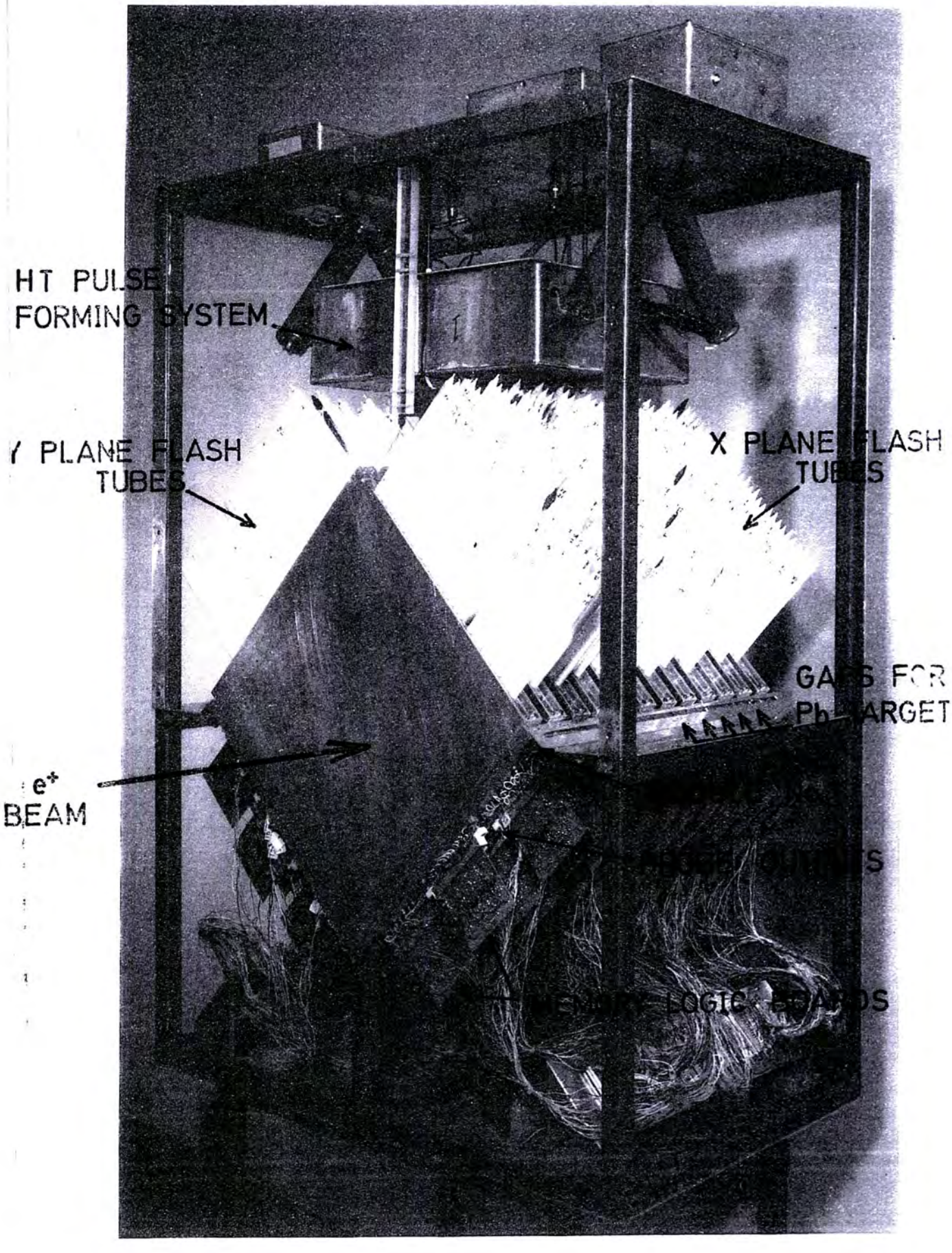

FIGURE 3.10 THE FLASH TUBE CHAMBER WITH THE SIDE PANELS REMOVED

the primary positron, into the detector, hence no lead absorber was placed in front of this detector plane. Each detector plane contained two layers of 32 flash tubes, positioned orthogonally such that they would provide X-Y co-ordinates of the incident radiation. Information was extracted from the tubes by means of digitisation probes, the output pulse from a probe being recorded by a TTL memory logic, which in turn was interrogated by the main data handling system. The flash tubes were fired by applying a simple RC generated pulse to the HT electrode. To prevent electrical interference from this pulsing system, the steel framework which supported the flash tube assembly and pulsing system, was clad in aluminium sheet.

3.3.1 Shower Sampling Module

The detector contained twelve identical detector planes, eleven of which were used to sample the shower. Each of these modules contained two parallel planes of 32 tubes, the axes of which were positioned orthogonally. The two planes of flash tubes shared a common HT electrode, which was accurately positioned by means of perspex spacers. Since the region of the HT plateau where the tubes could be efficiently operated was only 1 Kv Cm^{-1} wide, a variation of 1 mm in the positioning of the HT electrode results in a change of approximately 1 kV Cm^{-1} in the field strength. It is, therefore, essential that the HT electrode be maintained in precise alignment with the earth electrodes. These earth electrodes were formed by the two outer faces of the module. Their separation was maintained by the side members and the digitisation block as shown in Figure 3.3.

It is essential that the positions of the flash tubes be known accurately, and that they be positioned as closely as possible, resulting in a high layer efficiency. This was achieved by means of accurately machined holes in the digitisation block, and by corresponding holes

in the opposing side member, as shown in Figure 3.3. The diameter of the holes was 9.3 mm and the distance between their centres 9.5 mm, resulting in a layer efficiency of approximately 88% over an area of 30.4 cm x 30.4 cm.

The digitisation probes, which were 6 BA pan head brass screws, were located in the digitisation block by means of perspex spacers. To increase the digitisation probe pickup and hence the digitisation pulse height, 7 mm diameter aluminium foil discs were glued to the plane ends of the flash tubes.

The data acquisition system required that the information provided by the digitisation probes should be temporarily stored, prior to being read by a computer. This was achieved by providing each digitisation probe with a TTL set-reset latch. This latch, normally in a state representing logical '1', is set to logical '0' by the digitisation pulse obtained from the discharging tube. In this manner the information regardin whether a tube flashed or not is permanently recorded by the state of its associated latch. When this information is no longer required, the latch may be returned to logical '1' by means of a reset pulse. The memory logic for one flash tube is shown in Figure 3.11.

The memory logic circuits are mounted upon printed circuit boards, each one containing two sextuple set-reset latches (type 74118) and one dual four input positive NAND buffer (type 7440), to give a 12 bit storage register. Figure 3.12 shows the circuit diagram of one such 12 bit register A total of 72, 12 bit storage registers are required to service the 768 flash tubes contained in the detector. These boards were mounted in 32-way edge connectors, fixed to the undersides of the digitisation blocks.

As explained in section 3.2.2., it is essential that the HT electrode was maintained in contact with the flash tube wall. This is a considerable problem since the outside diameter of the tube may vary by up to $\pm$ 0.4 mm.

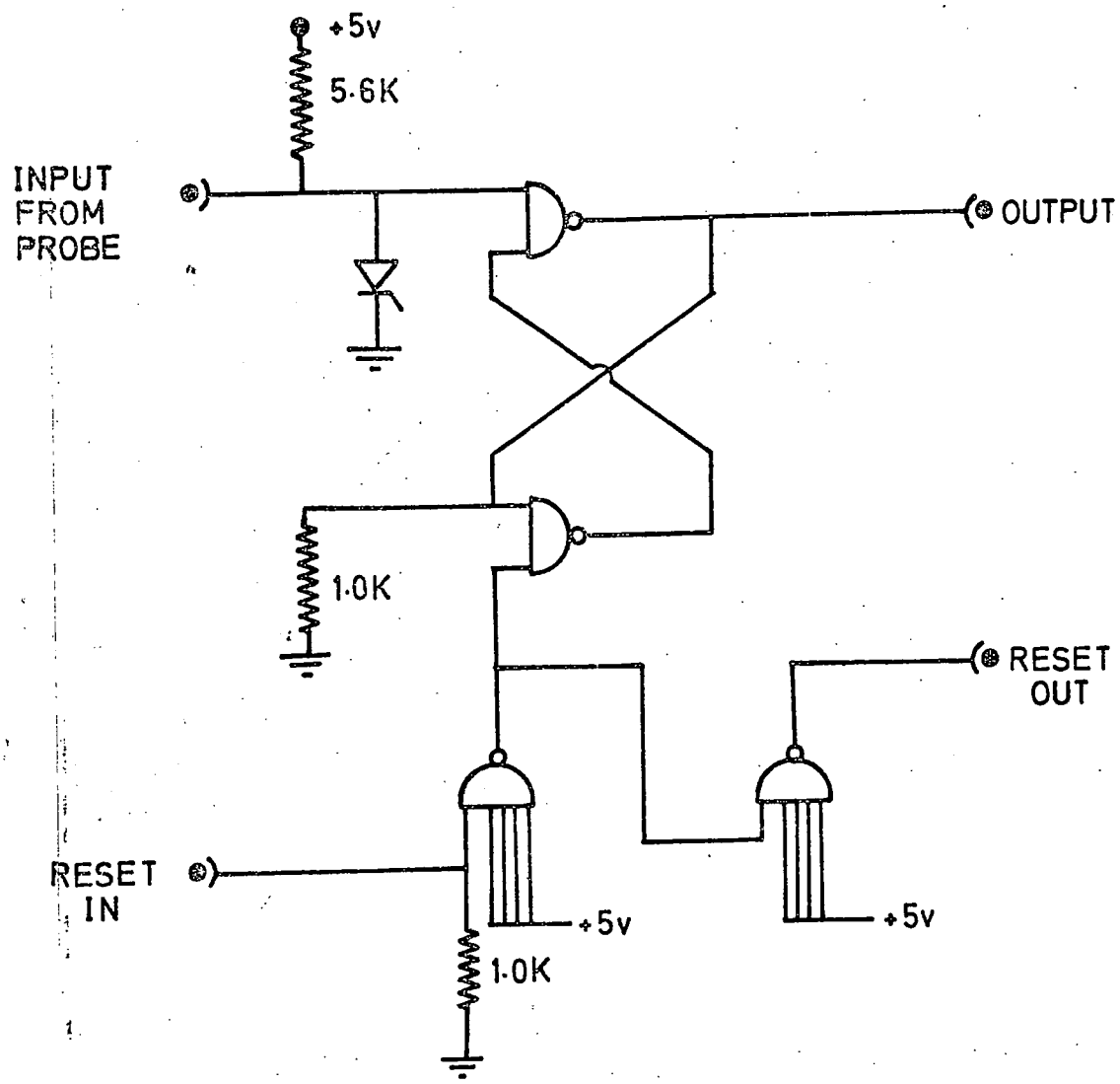

FIGURE 3.11 MEMORY LOGIC FOR ONE FLASH TUBE

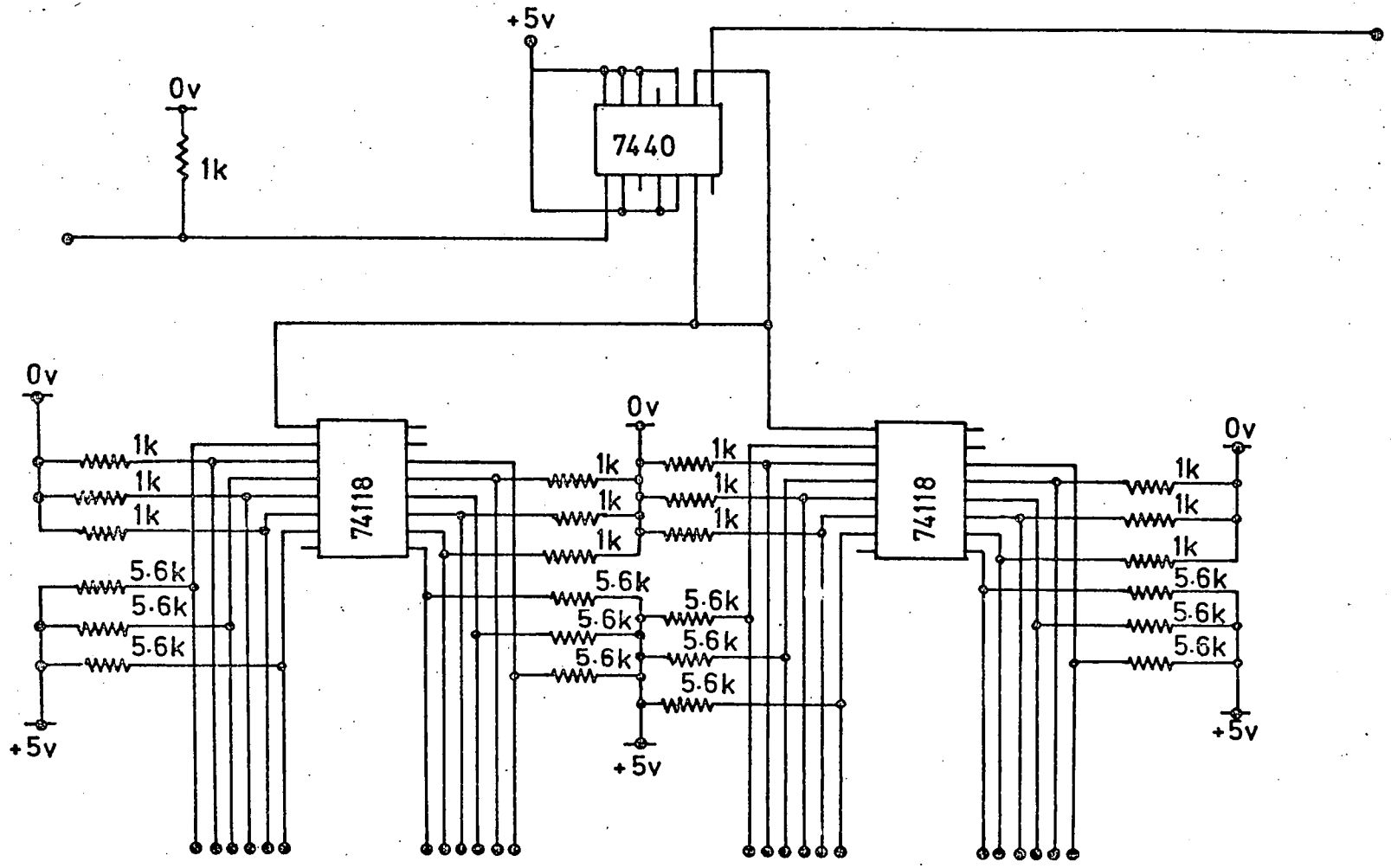

FIGURE 3.12 A 12 BIT INPUT REGISTER

Contact was maintained by means of a strip of folded aluminium foil, attached to both faces of the HT electrode, which expanded against the flash tubes.

The assembled modules were located in the main detector frame, such that the tube axes were orientated to 45^{o} to the vertical, thus the weight of each tube assured a constant contact between the plane face of the flash tube and its digitisation probe. Each digitisation block was provided with a machined aluminium ledge, which, when the modules were inserted in the detector frame, provided a support for the inserted lead absorber.

The choice of a modular system allowed the removal of a complete sampling plane plus its associated electronics without the need of dismantling the entire detector.

3.4 THE HIGH VOLTAGE PULSING AND CLEARING FIELD SYSTEM

The HT pulse used to fire the flash tubes is of a simple RC decay type. This is obtained by charging a high voltage capacitor, C_1, to a voltage V_o, and then by means of a fast switching device, discharging it to ground via a resistor R_1. The flash tube arrays, of capacitance C_2 are connected in parallel with R_1, and the resulting pulse, applied to the HT electrode decays exponentially in the manner

$$V = -V_o \exp\ (-t/R(C_1 + C_2)) .$$

The pulsing circuit is shown in Figure 3.13. Six 3000 pf, 20 Kv capacitors were used, each capacitor supplying two modules via a 850 Ω resistor. Fast switching of the capacitor to ground was provided by means of a hydrogen thyratron (English electric type CX.1157) capable of switching up to 20 Kv into modules of at least 10,000 pf with a rise

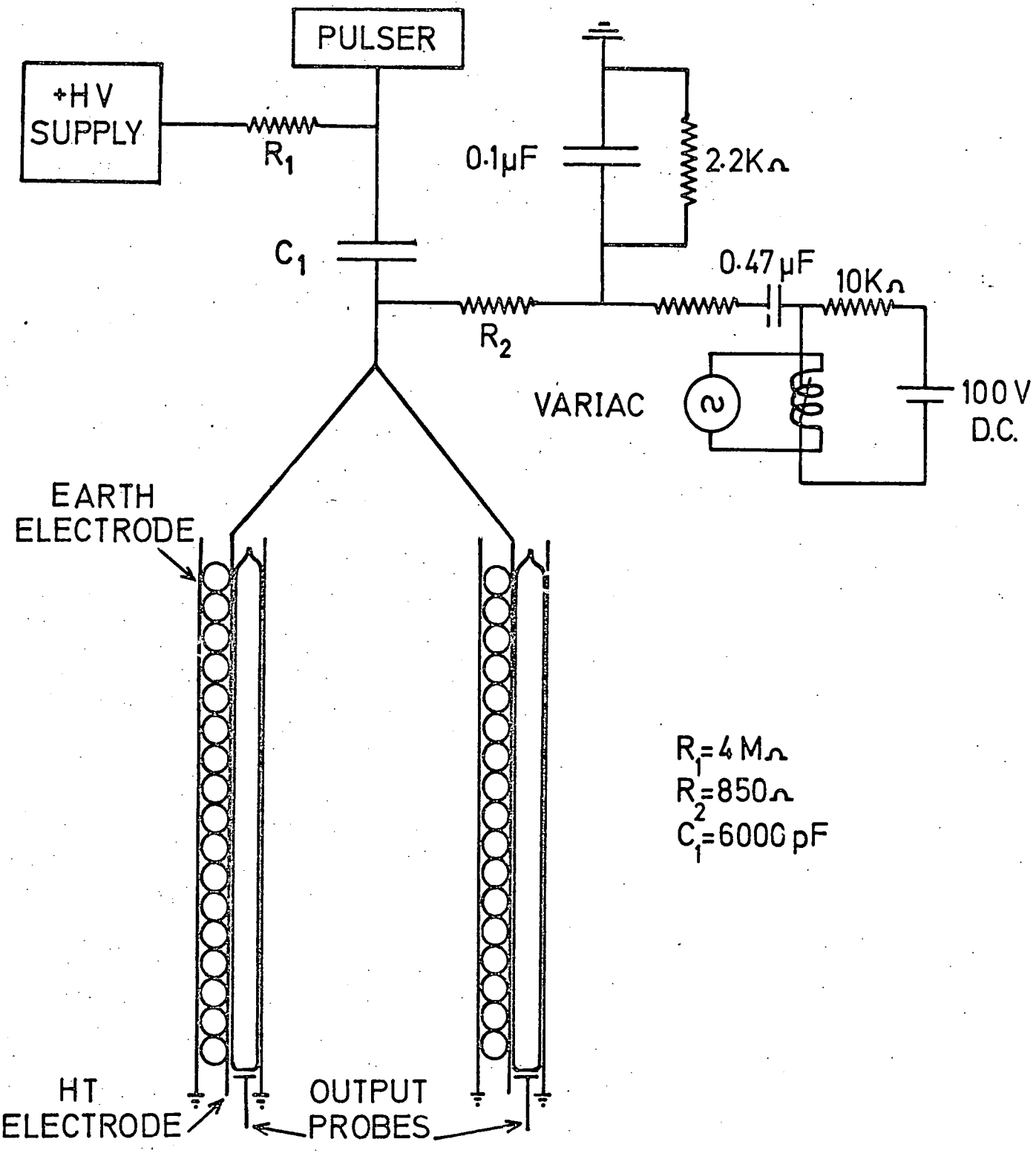

FIGURE 3·13 THE HIGH VOLTAGE PULSING AND APPLIED CLEARING FIELD ARRANGEMENT

time of 40 ns. Due to the high electrical noise levels associated with this type of switching system, the whole assembly was placed in a screening box on top of the detector, as seen in Figure 3.10. The characteristics of the HT pulse formed in this manner are given in Table 2.

In order to obtain a short sensitive time, a 100 Hz, square wave pulse, of variable magnitude was applied in the manner shown in Figure 3.13.

3.5 DATA ACQUISITION

As explained in section 2.2, the resultant high energy electromagnetic showers, whether initiated by an electron, positron or gamma ray, are essentially identical, assuming the primary energy to be the same. For this reason it was convenient to evaluate the detectors performance by use of a positron beam.

3.5.1 The Positron Beamline

The detector was evaluated using the e^+ testbeam facility of the 5.2 GeV Electron Synchrotron at the Daresbury Laboratory [11]. The main elements of the beamline are shown in Figure 3.14. The beamline operates on the double conversion principle. Photons are produced by interaction of the accelerated electron beam with an internal machine target of tungsten. These photons are scrubbed of charged particles by means of a permanent magnet and collimator slit. The resultant photon beam is then converted into electron-positron pairs by interaction with a copper target. Positrons of the desired momentum are then selected by means of a variable bending magnet and a collimator.

By this means a beam of energy from 200 MeV up to the maximum operating energy of the machine was obtainable. The momentum spread was approximately $\pm 1\%$ and the beam size on emerging into the experimental area is 20 mm x 40 mm. The maximum angular divergence of the beam is $\pm 2^{o}$.

The test beam may be operated in two modes, parasitically or by

FIGURE 3.14 THE POSITRON BEAM LINE

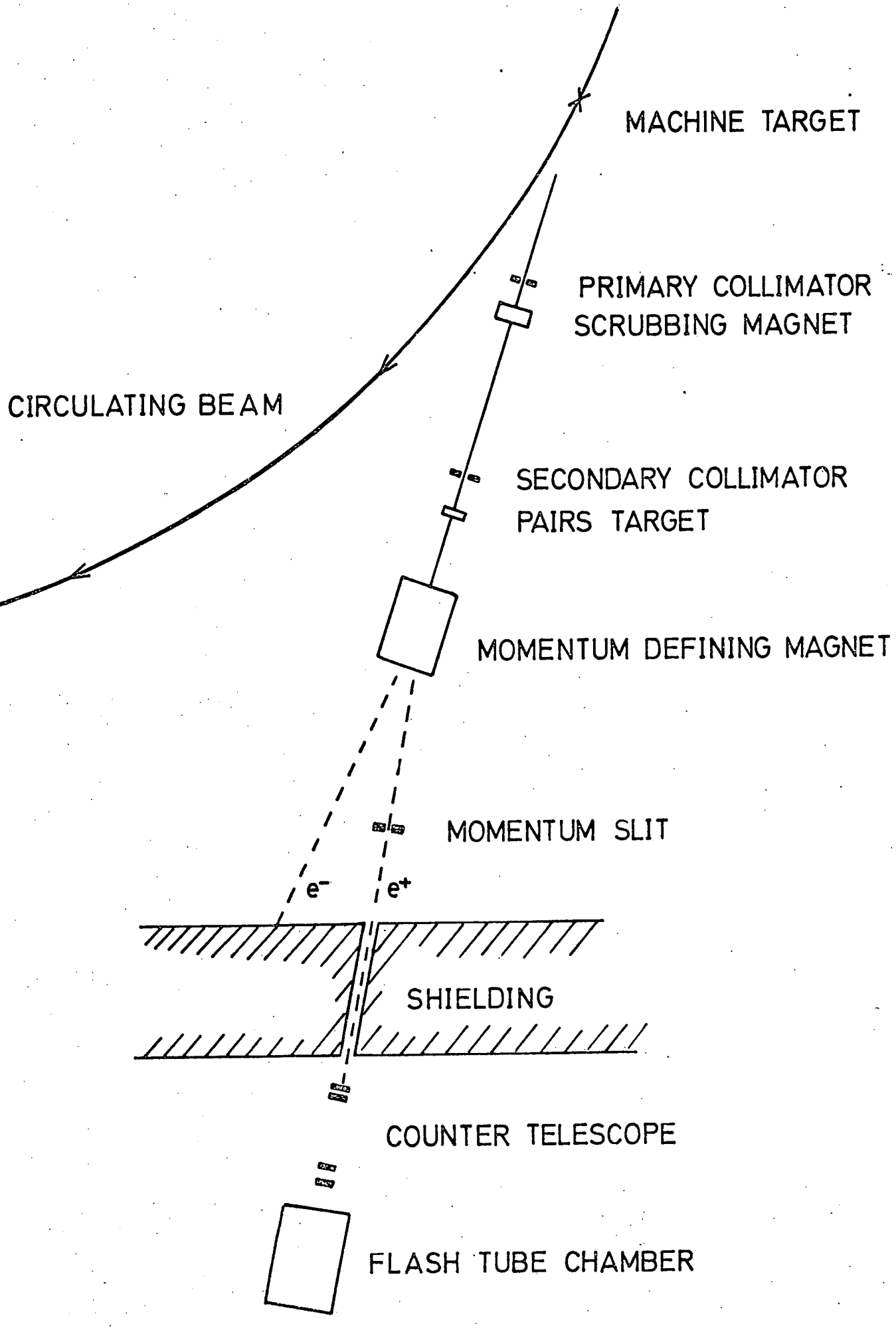

means of a beam bump. The parasitic mode relied on the interaction of electrons, scattered from the main circulating beam by other targeting stations in the synchrotron, with the tungsten target. The beam bump mode utilises a pulsed magnet, to perturb the circulating beam into the machine target. The detector was tested using the latter extraction system. Two lengths of beam bump were available, 0.6 and 1.0 ms. The latter being necessary to extract beam at the highest momentum values. A beam was accelerated in the synchrotron every 19 ms ; which resulted in a maximum extraction frequency of approximately 50 sec^{-1}. However, since the action of the beam bump usually disturbed the beam conditions of other users, extraction was restricted to every 60th acceleration cycle whilst using the 1 ms bump. For higher rates the short bump was used, however it was not possible to extract electrons above 2.0 GeV using this bump, hence all high rate data was restricted to positrons of momenta 1.5 GeV and less.

The maximum positron flux of the testbeam depended principally upon the operational conditions of the accelerator and the momentum of the positrons required. Extraction was "tuned" for a particular momentum by adjusting the position of the beam bump with respect to the start of the acceleration cycle which was located by a timing pulse received at a minimum field of the NINA magnets. The flux was controlled by adjusting the magnitude of the beam bump and the position of the machine target with respect to the beam orbit. By this means the flux was maintained at approximately 50 positrons per extraction, located within a 1 ms "window" centred in time about the maxima of the beam bump.

The resultant positrons were bunched, which reflected the nature of the accelerated electron beam from which they were obtained. It is essential that particles within these bunches are not separated by less than 2 μs (the sensitive time of the detector) since this would result in multiple tracks occurring in the detector.

The maximum rate at which the detector can be operated in theory is determined by the recovery time of 0.6 ms. This should allow event rates of up to 1 KHz. The normal extraction modes mentioned above allow a maximum frequency of 50 Hz, extracting on consecutive cycles, or a minimum frequency of 500 Hz, extracting within a 2 ms beam spill. This leaves the range of 50 Hz to 500 Hz unobtainable. Should it be required to operate the detector within this frequency range, it was proposed to use both the parasitic and the bump modes of extraction. The first particle being extracted via the bump mode, and at the same time a delayed gate is triggered allowing a second parasitically produced particle to be accepted by the system. By adjusting the gate delay, frequencies between 50 and 500 Hz may be obtained.

3.5.2 Trigger Logic and Data Handling

A positron produced in the manner described above was selected by means of a fourfold coincidence of the scintillations $S_1 \rightarrow S_4$ shown in Figure 3.15. It was also required that this coincidence should fall within a 1.0 ms wide "window", timed with respect to the start of the acceleration cycle, to cover the period of beam extraction. This would ensure that all coincidences resulted from genuine extracted particles.

Upon receiving a satisfactory coincidence, a trigger was sent to the HT pulsing system, and the logic paralysed against receiving further coincidences. Information as to whether a tube flashed or not was temporarily stored within the TTL memory logic. After a delay of 10 ms, which allowed the effects of the H.T. pulse to pass, the state of the 768 latches was read out in parallel by way of 6 132-way cables, into 3 256 bit CAMAC input registers, and hence into the 8K memory of a PDP 11 computer, which controlled the data acquisition program. Having been read, the latches were reset by a + 5V level from a CAMAC output level unit. The system was then in a state where it could receive another

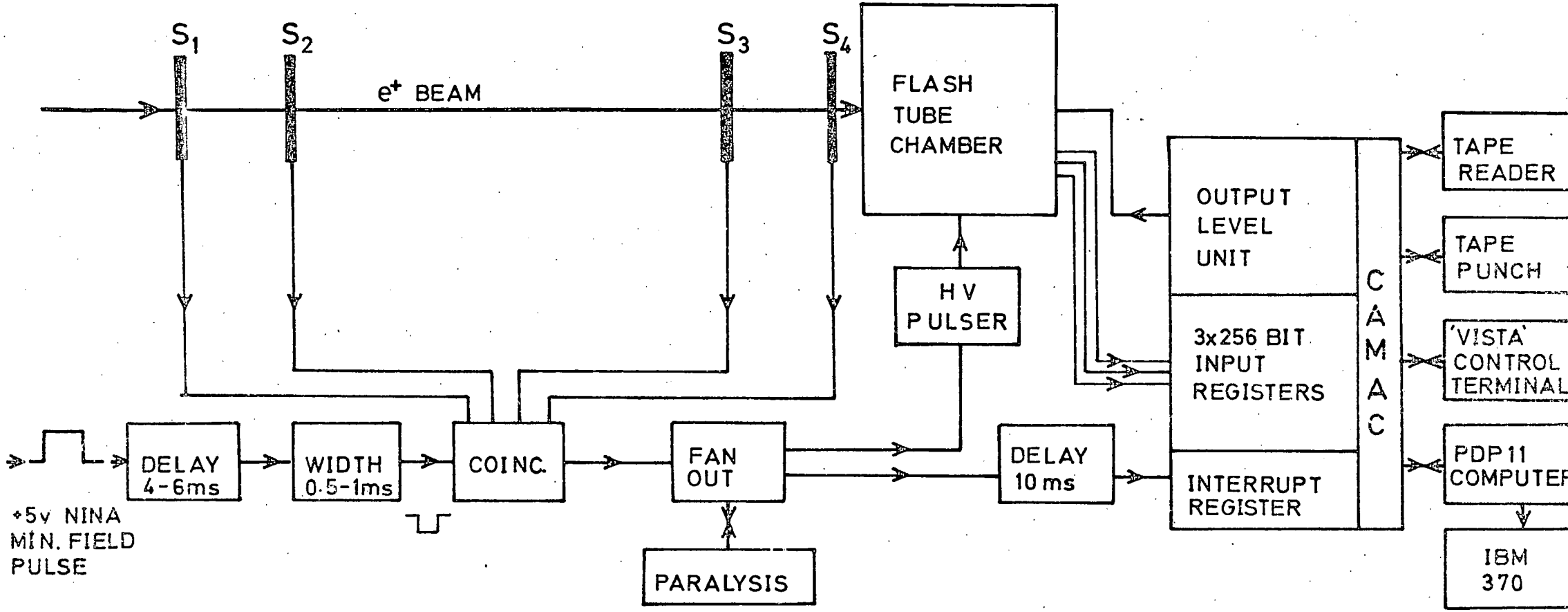

FIGURE 3.15 THE DATA ACQUISITION SYSTEM

event, and the paralysis was removed from the trigger logic. Upon a second event being buffered within the PDP 11, the buffer was cleared by writing its contents to disc in the main IBM 370, and subsequently to tape. This completed one cycle of the data acquisition program which is summarised in Figure 3.16.

The decision to send pairs instead of individual events down the data link, was determined by the possible need to operate the detector at rates of 1 KHz. The data link buffer of the IBM 370 was unable to handle the 48 16 bit words arriving every 1 ms. This was overcome by sending 2 events in one block, every 20 ms (the cycle time of the accelerator), to the link buffer. This then means that the data taking rate is only restricted by the speed of the CAMAC system and the cycle time of the PDP 11 computer program. For this reason the acquisition program was written in assembler language, giving a program cycle time of less than 1 ms.

The facility also existed to display individual events, during operation of the detector, on the vista control terminal. Some examples of typical events obtained in this manner are given in Figure 3.17.

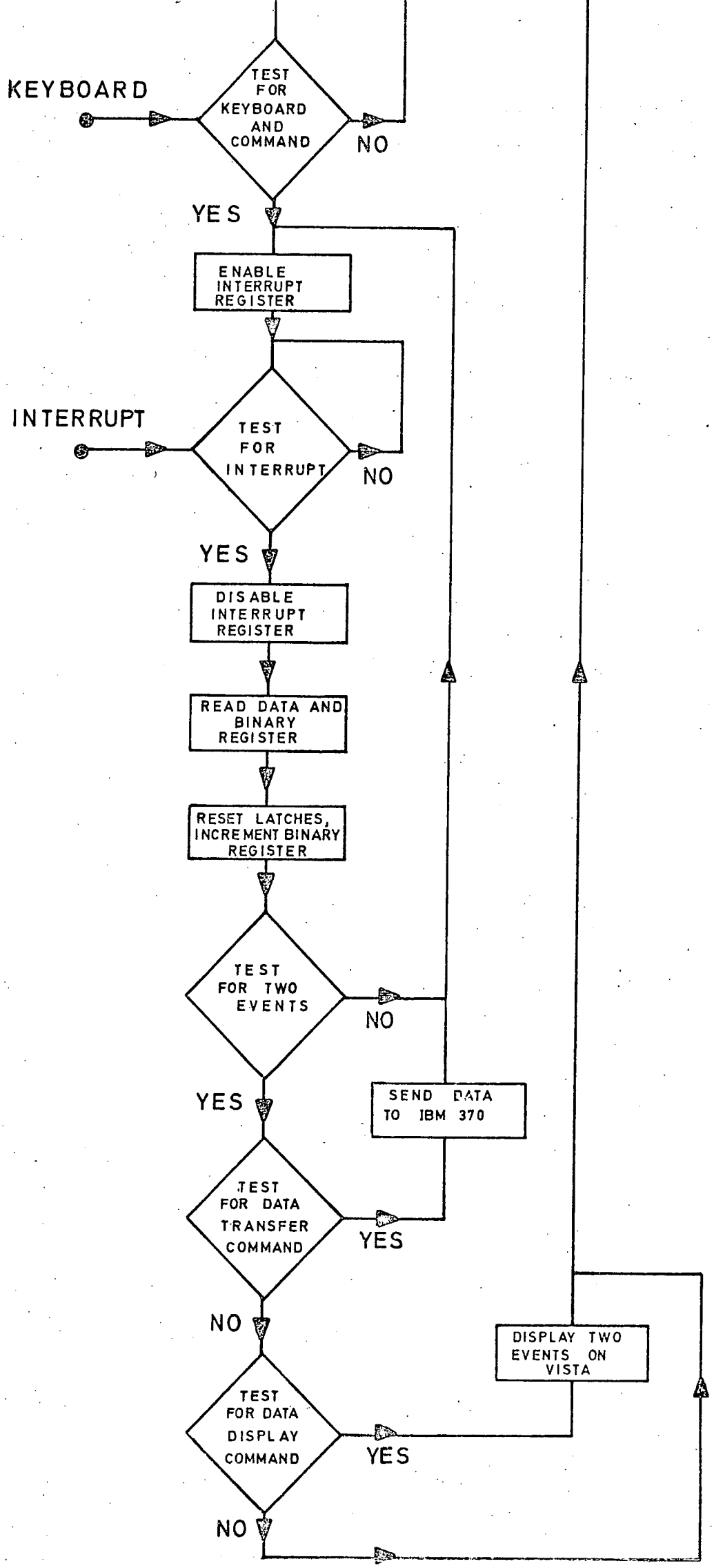

FIGURE 3.16 FLOW DIAGRAM OF THE DATA ACQUISITION PROGRAM

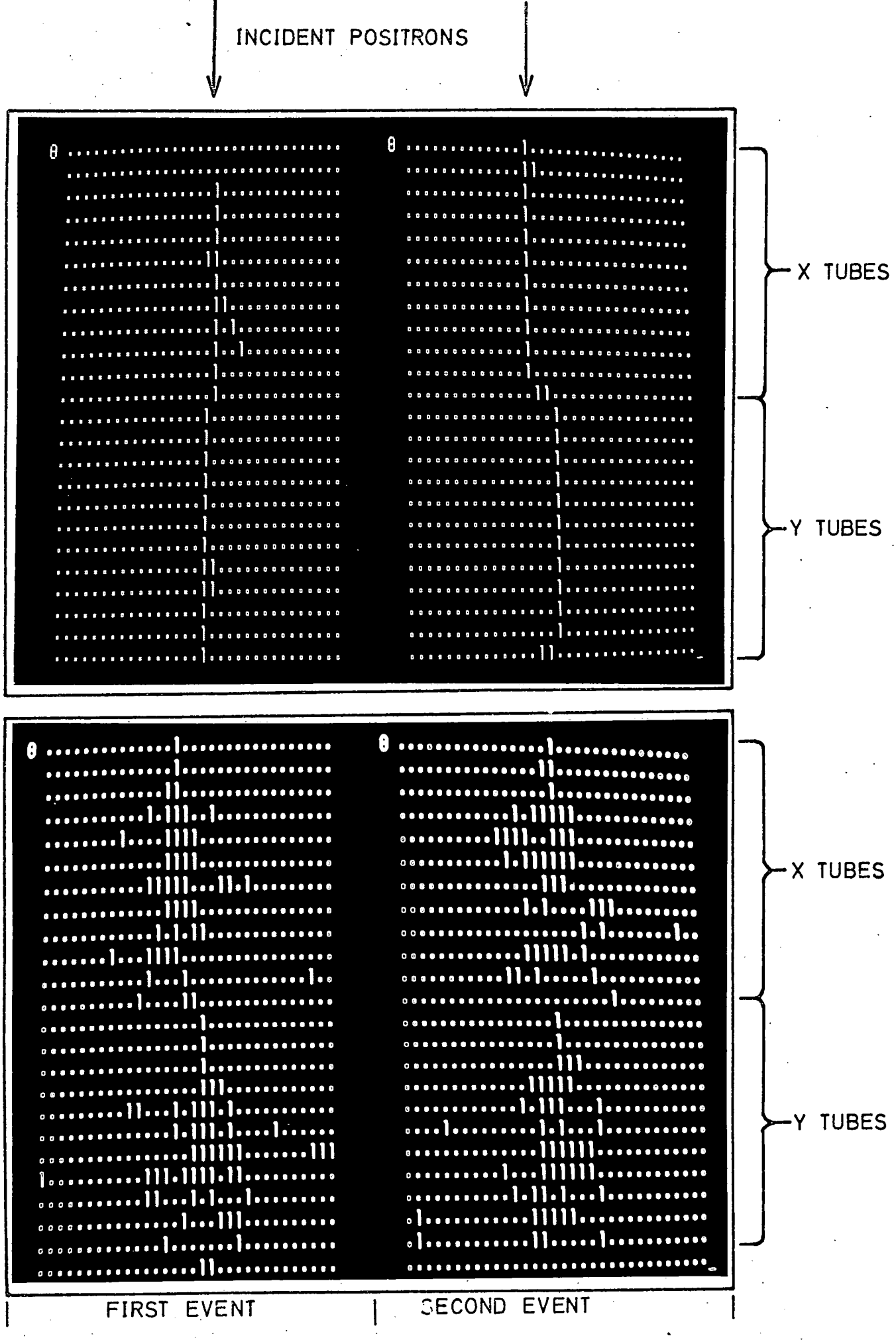

GURE 3·17 POSITRON TRACKS AND SHOWERS AS SEEN ON VISUAL DISPLAY SCREEN

REFERENCES : CHAPTER THREE

(1) Chaney, J.E., Breare, J.M., Nucl.Inst. Meth., 124, (1975) 61

(2) Chaney, J.E., Ph.D Thesis, University of Durham (1974)

(3) Breare, J.M., Nandi, B.C., Tait, I.D., Nucl.Inst.Meth., 133, (1976) 415

(4) Breare, J.M., Nandi, B.C., Tait, I.D., Nucl.Inst.Meth., 136, (1976) 517

(5) Breare, J.M., et al. International Conference on Instrumentation for HEP, Frascati, (1973) 221

(6) Coxell, H., Wolfendale, A.W., Proc.Phys. Soc., 75, (1960) 378

(7) Ayre, C.A. Thompson, M.G. Nucl.Inst., Meth., 69, (1969) 106

(8) Breare, J.M., et al, International Conference on Instrumentation for HEP, Frascati (1973) 218

(9) Brosco, G., Conversi, M., Giovannini, M., Nucl. Inst. Meth., 111, (1973) 477

(10) Breare, J.M., et al, International Conference on Instrumentation for HEP, Frascati, (1973) 215

(11) Aitken, T.W., (1970) Daresbury Laboratory Report, DNPL/TM 70

CHAPTER FOUR

INVESTIGATION OF THE PERFORMANCE OF THE HIGH PRESSURE FLASH TUBE CHAMBER AS AN ELECTROMAGNETIC SHOWER DETECTOR

4.1 INTRODUCTION

As explained in chapter 2, high energy electron-photon detection utilises the resultant electromagnetic shower to obtain information concerning the primary particle. Two important properties of the electromagnetic shower, which may be used to provide energy and spatial information are [1,2,3] :

(1) The number of secondaries produced in the shower is linearly related to the primary energy.

(2) The axis of the electromagnetic shower is on average located along the trajectory of the primary particle.

The developing electromagnetic shower is subject to fluctuations, and since the shower is only sampled at fixed intervals, the effect of these fluctuations is likely to be enhanced. Furthermore the sampling elements may not exhibit a uniform response with energy, to the changing characteristics of the shower at the sampling plane (i.e. changing density of secondaryparticles). For these reasons, all detectors operating on the shower sampling principle must be calibrated in a well defined mono-energetic beam.

Ideally, the sampling elements should record precisely the number and distribution of the secondary particles crossing the sampling plane, in which case the errors of measurement of the shower, are due solely to the statistical fluctuations in the shower development, and the frequency

at which it is sampled. By comparison of the shower parameters obtained from the sampling elements, with those predicted by theory, for various energies, it can be determined if the sampling elements respond uniformly with the changing shower characteristics.

A comparison will therefore be made between the theoretically predicted shower and that observed in the detector, before presenting the results of the spatial and energy resolution of the detector.

4.2 ELECTROMAGNETIC SHOWER PARAMETERS AS RECORDED BY THE DETECTOR

Positron initiated electromagnetic showers were studied using the detector, in the energy range 0.5 to 4.0 GeV, data being taken at 0.5 GeV intervals. 0.6, 1.2 and 1.8 radiation lengths of lead target were available for insertion between the sampling planes. Approximately 2000 positron initiated showers were recorded for each combination of energy and target thickness, the sampling planes providing information as to the number and distribution of the shower secondaries. It was found that for a given energy the information provided by the sampling planes using the different thickness of lead target, differed only slightly, and hence the data obtained at a particular energy for the three thickness of target, were combined to give the number and distribution of the shower secondaries as a function of target depth.

Some principal features which characterise the electromagnetic shower are its overall shape, or transition curve, the position of the shower maxima and the attenuation coefficient of the shower tail. A comparison of these parameters as obtained from the detector, with the prediction of theory, will provide information as to how the detector responds to the changing characteristics of the electromagnetic shower

for various energies.

(1) TRANSITION CURVE : This curve describes the number of shower secondaries as a function of target depth. The transition curve obtained from the detector is shown in Figure 4.1. The full line represents the Monte Carlo simulations of Messel and Crawford [1], using an electron cut off value of 2.0 MeV. The broken line represents the experimental results obtained from the detector by taking the mean number of flashed tubes in a particular layer, which gives a measure of the number of ionising particles crossing that layer. It can be seen that the discrepancy between theory and experimental becomes considerable with increasing primary energy. This is a direct result of the flash tubes inability to distinguish between one or more than one particle traversing its volume, resulting in an increasing error in the estimation of the number of shower secondaries as the shower density increases.

Correction can be made to the data, accounting for the finite space resolution of the flash tube and its layer efficiency, using the following relationship [31], assuming a uniform distribution of secondaries incident on the layer of tubes

$$K = \frac{\ln\left(1-\bar{M}/M_o\right)}{\ln\left(1-\mu/M_o\right)}$$

where K = number of shower secondaries crossing the detector plane.

μ = layer efficiency.

M_o = number of tubes contained within the shower section.

$\bar{M}$ = mean number of tubes igniting in the layer.

The derivation of this expression is given in Appendix I. The data corrected using this expression is given by the dotted curve in

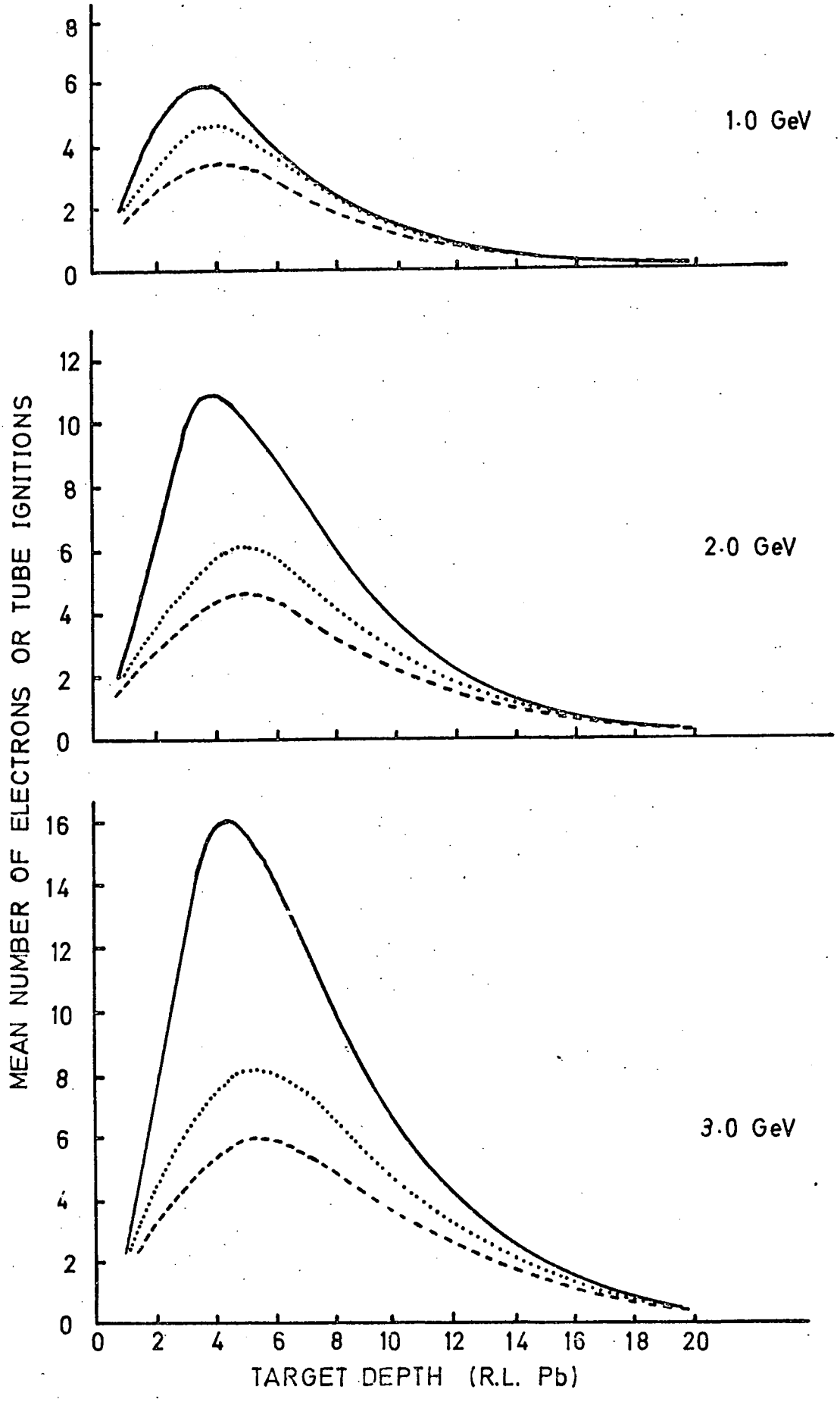

FIGURE 4·1 SHOWER TRANSITION CURVES IN LEAD

Figure 4.1. It can be seen that at low energies the correction is a close approximation to the theoretical transition curve, particularly beyond the shower maxima. The discrepancy around the shower maxima, which increases with primary energy is due to the assumption of a uniform distribution of shower secondaries no longer being valid.

The manner in which the primary energy is measured, requires that the shower is totally contained within the detector. It can be seen from Figure 4.1, that using 1.8 radiation lengths of target between each module (representing a total thickness of 19.8 radiation lengths), that the shower is almost totally contained. However, using 0.6 and 1.2 radiation lengths of target (6.6 and 13.2 radiation lengths total thickness respectively) it can be seen that a considerable portion of the shower is lost from the rear of the detector.

The deviations from theory mentioned above will be seen to be of considerable importance regarding the performance of the detector, especially with respect to the energy measurement.

(2) POSITION OF SHOWER MAXIMA : Theory predicts that the position of the shower maxima (defined as the depth of absorber at which the probability of finding an electron is greatest), should be linearly related to the logarithm of the primary energy. The results obtained from the detector are shown in Figure 4.2, along with the theoretical[1,4,5,6,7] and experimental[8,9,10,11] results of previous workers. It can be seen that the results are in good agreement with the experiment of Jakeways and Calder[8] (see section 2.3) and the theory of Nagel[5]. However, disagreement between experiment and theory increases with increasing energy.

(3) ATTENUATION COEFFICIENT : It is the photon attenuation which is responsible for the characteristic tail of the electromagnetic shower,

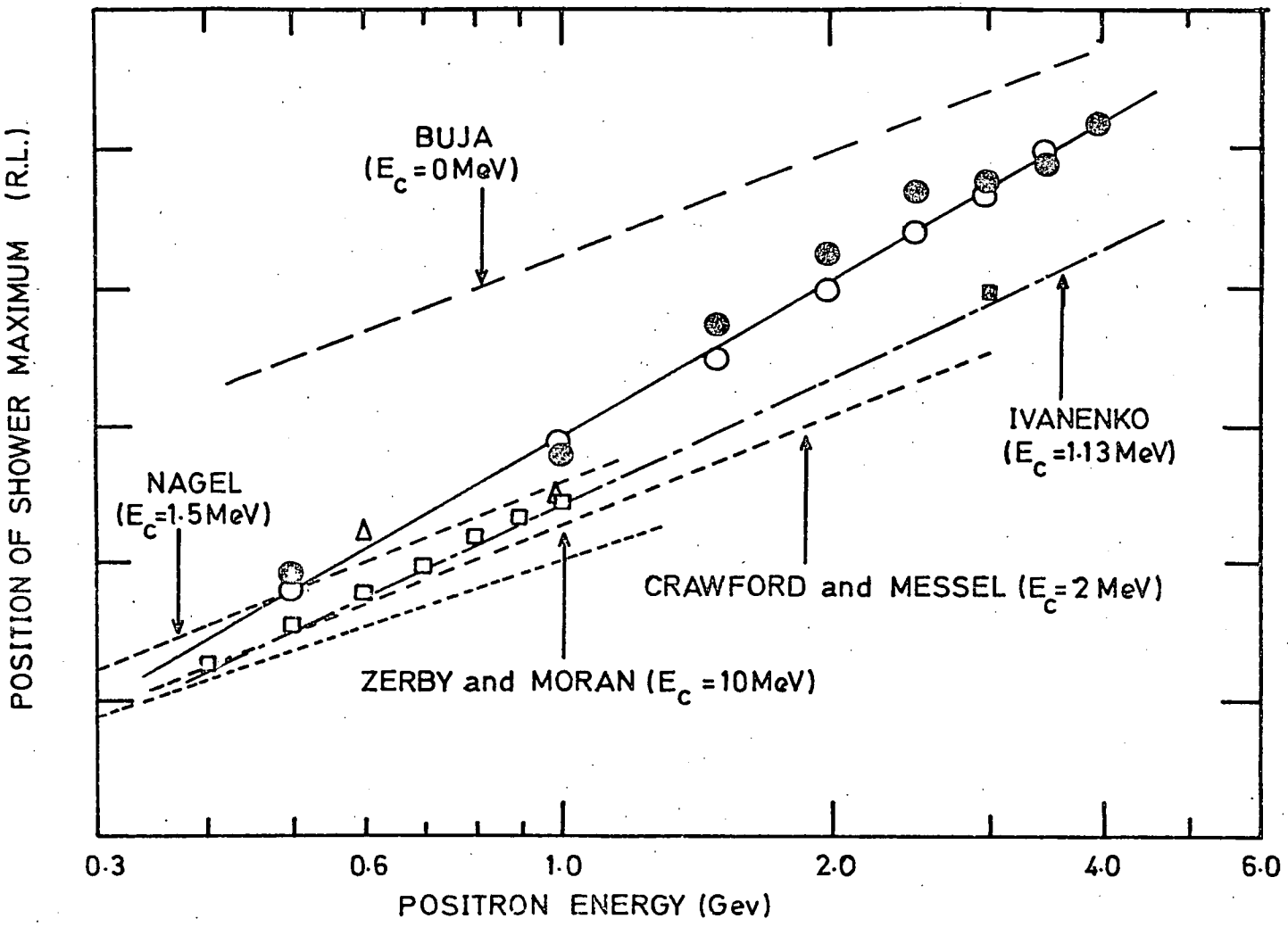

KEY: ○ PRESENT EXPERIMENT, ◉ JAKEWAYS and CALDER, □ HEUSCH and PRESCOTT, ■ BACKENENSTOSS et al, Δ YUDA et al.
E_c = ELECTRON CUT-OFF ENERGY

FIGURE 4·2 COMPARISON OF THE POSITION OF THE SHOWER MAXIMUM WITH THE THEORETICAL AND EXPERIMENTAL RESULTS OF PREVIOUS WORKERS

since most particle production results from pair production occuring by photon interaction. Photons of low energy are unlikely to contribute to further particle production and are absorbed from the shower, resulting in the attenuation of the number of secondaries with target depth beyond the shower maximum. This attenuation is described by the relationship $Ae^{-\lambda t}$, where t is target depth, A is a constant and λ is the fractional rate of decrease of the tail of the transition curve. The variation of the photon attenuation coefficient is shown in Figure 4.3 (a)[12], giving a minimum value of 0.27 R.L.$^{-1}$ at 4 MeV. This is expected to be lower if the effect of the compton recoil photons are considered. Figure 4.3(b)[13] shows the attenuation coefficient as a function of energy, obtained from the detector. The average value of 0.24 R.L.$^{-1}$ agrees well with the above mentioned work, although there is considerable disagreement with the results of Messel and Crawford[1], who obtained a value of 0.33.

From the considerations above, it appears that the most significant problem is due to the inability of the flash tube to distinguish between one or more particles traversing its sensitive volume, and that this will be most apparent in the energy measurement of the detector.

4.3 MEASUREMENT OF PRIMARY PARTICLE ENERGY

Theoretical considerations[1,2] show that the number of secondary ionising particles produced in a shower is linearly related to the primary energy. Since the number of flash tubes igniting gives a measure of the total number of secondary particles contained in the shower, this figure may be used to find the energy of the primary particle.

Data was taken at energies of 0.5 to 3.5 GeV, using 0.6, 1.2 and 1.8 radiation lengths of lead target between the modules. Approximately 2000 positron induced showers were recorded for each combination of target

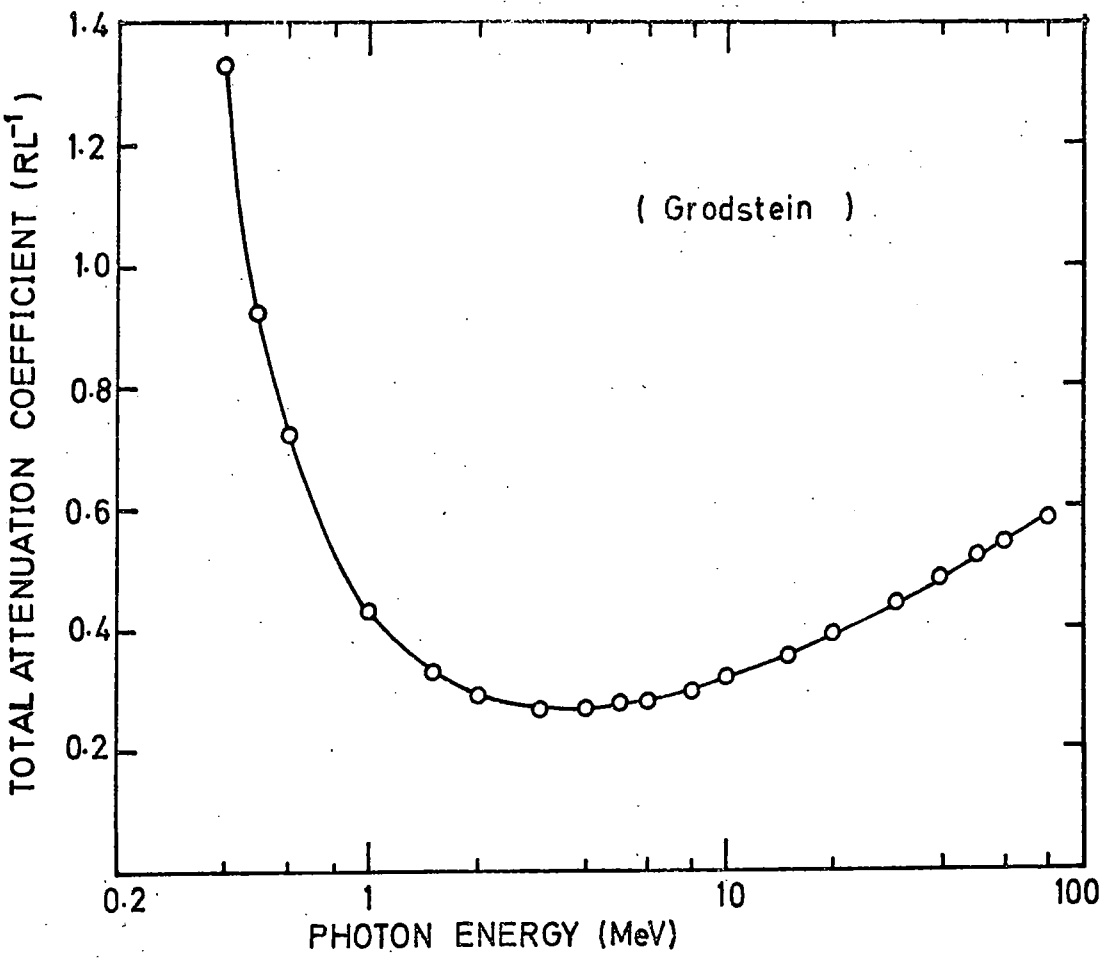

FIGURE 4·3(a) TOTAL ATTENUATION COEFFICIENT AS A FUNCTION OF PHOTON ENERGY

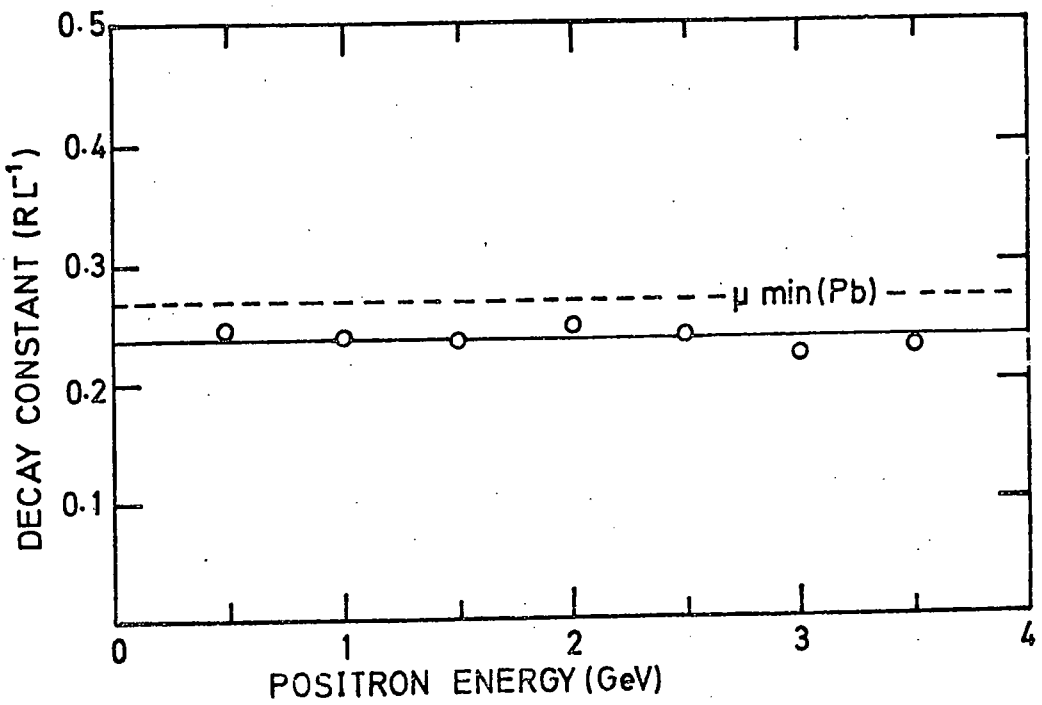

FIGURE 4·3(b) DECAY CONSTANT OF SHOWER TAIL AS A FUNCTION OF POSITRON ENERGY

thickness and primary energy. The frequency distribution of the number of tube ignitions obtained for various primary energies and target thickness is shown in Figure 4.4. Curves showing the number of flash tube ignitions as a function of primary energy are shown in Figure 4.5. It can be seen, particularly for high primary energy and thin target, that the curves deviate considerably from the linear relationship expected from theory[1,2]. The principal causes of this deviation are listed below.;

(1) Failure to contain the whole shower within the detector. Figure 4.6 shows the number of flash tube ignitions for each module for 3 primary energies using 0.6 and 1.8 radiation lengths of lead target. It can be seen that the shower is almost completely contained for all energies using 1.8 radiation lengths of lead. However, using 0.6 radiation lengths, a considerable fraction of the total shower escapes from the rear of the detector. The lateral losses are, however, insignificant compared to the longitudinal loss, as can be seen from Figure 4.7, which shows the lateral shower profiles obtained from each sampling plane for 3.0 GeV primary energy and 0.6 radiation lengths of target.

(2) Inability to distinguish between one or more ionising particles passing through the sensitive volume of a flash tube. The secondary particles constituting the shower are produced on average within a narrow core, whose axis represents the axis of the shower. As the primary energy increases, the shower density near the axis is such that the probability of more than one particle passing through a tube is greatly increased. This is clearly shown by Figure 4.1, where the greatest deviation between theory and experiment occurs at the position of the shower maximum.

(3) Effect of internal clearing fields upon the efficiency of the flash tube[14,15,16,17,18,19]. Internal clearing fields become significant

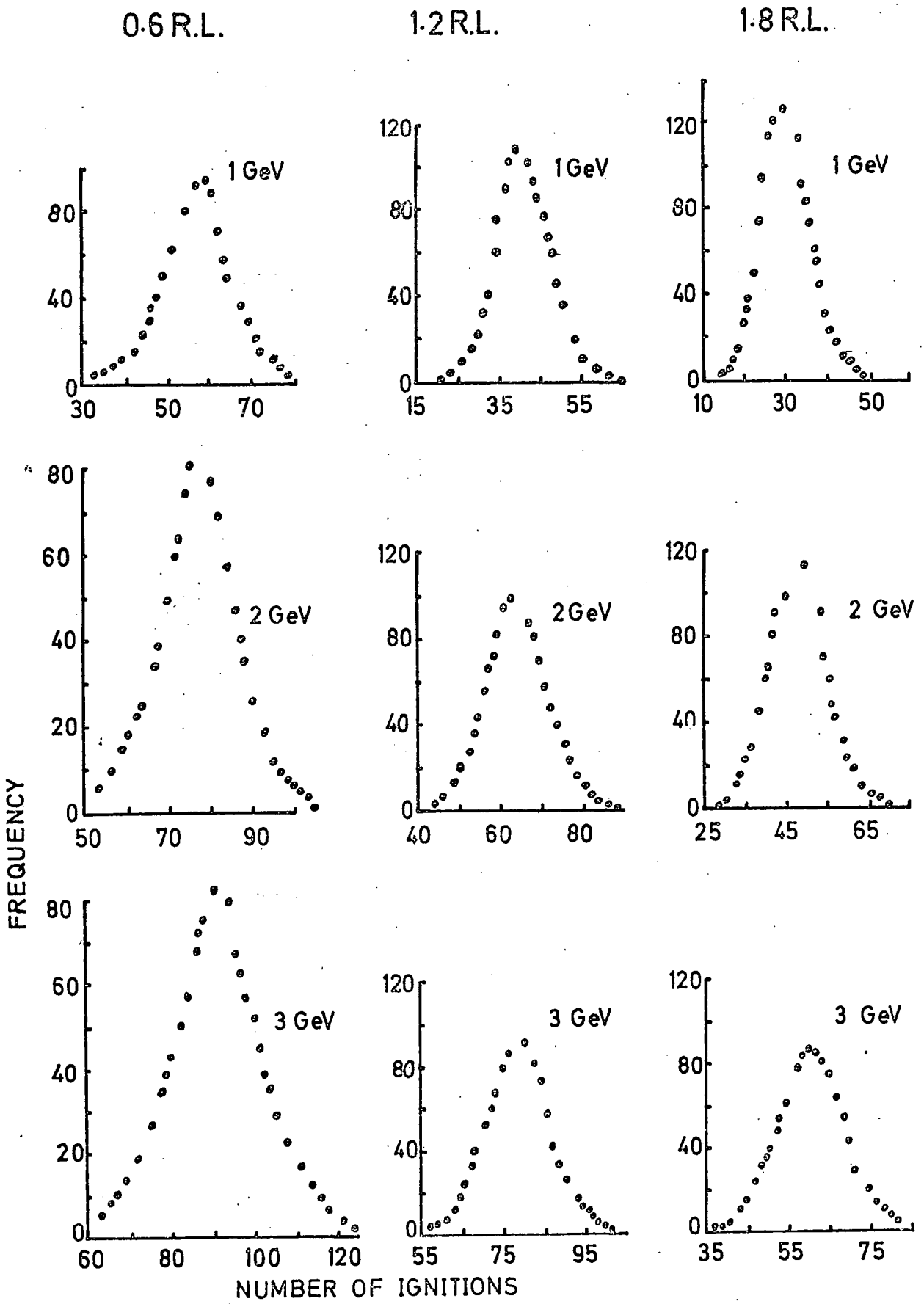

FIGURE 4.4 FREQUENCY DISTRIBUTION OF THE TOTAL NUMBER OF TUBE IGNITIONS FOR VARIOUS COMBINATIONS OF ENERGY AND TARGET

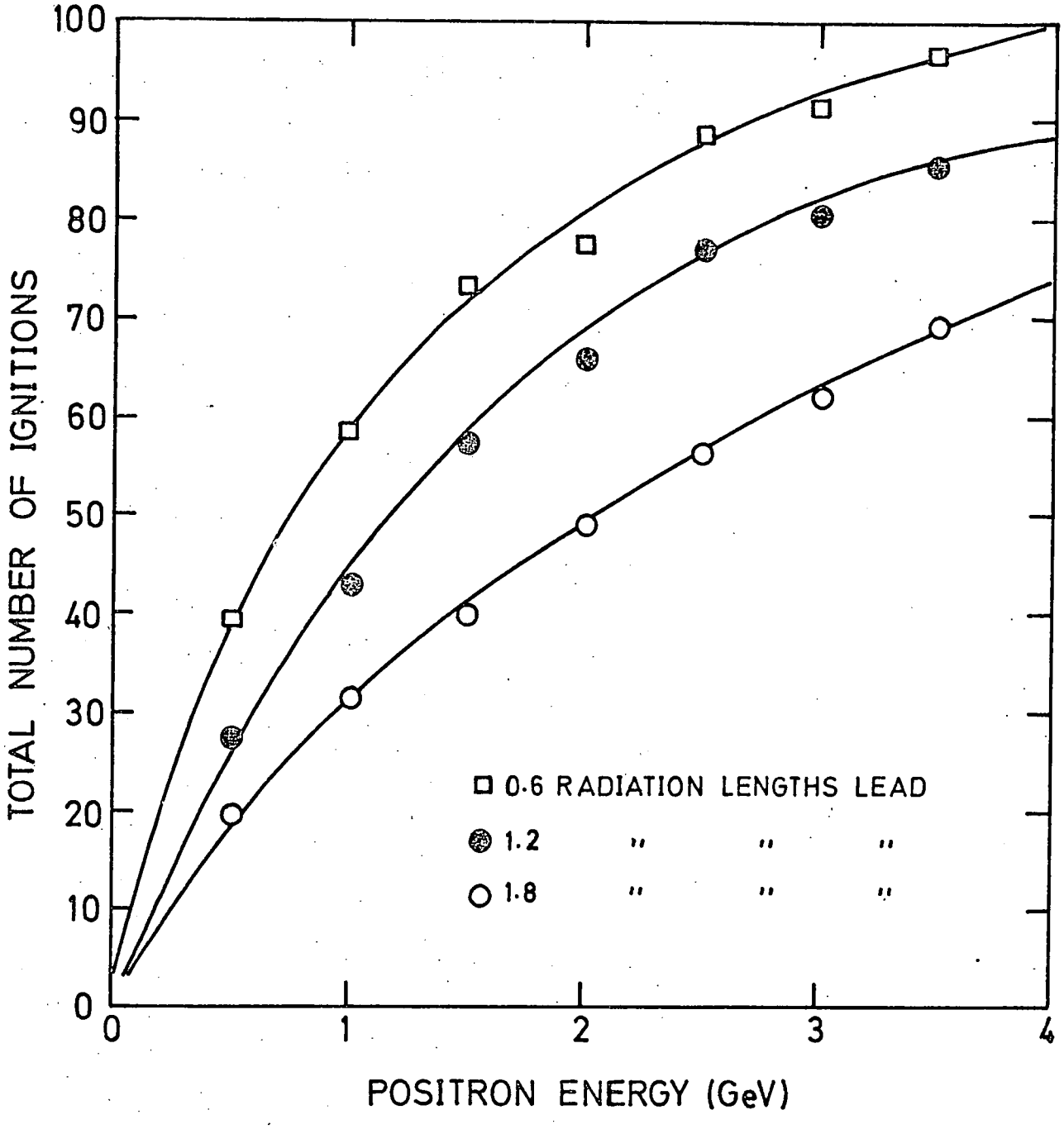

FIGURE 4·5 MEAN TOTAL NUMBER OF TUBE IGNITIONS AS A FUNCTION OF POSITRON ENERGY

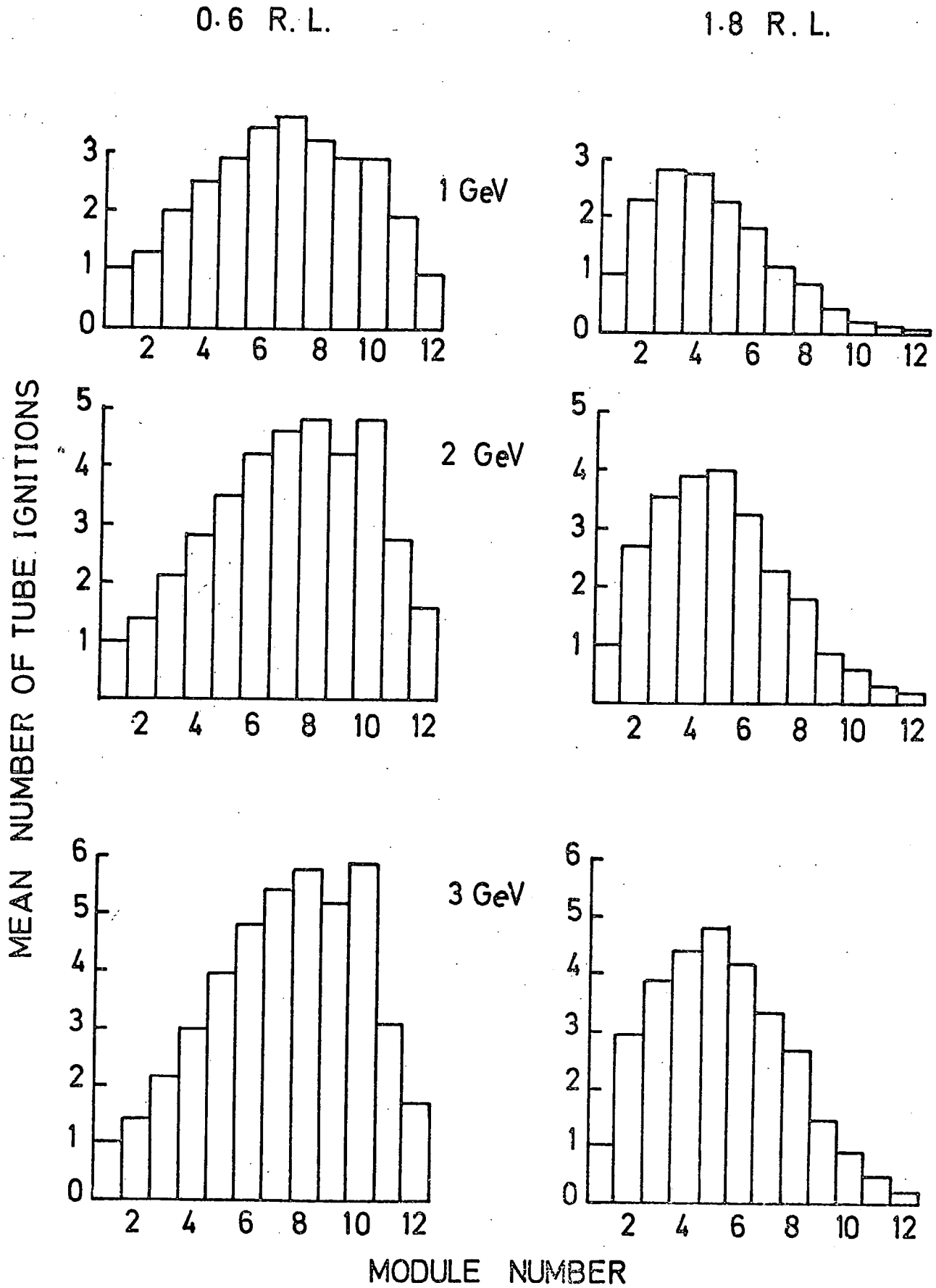

FIGURE 4·6 AVERAGE NUMBER OF IGNITIONS IN EACH MODULE FOR VARIOUS ENERGY AND TARGET COMBINATIONS

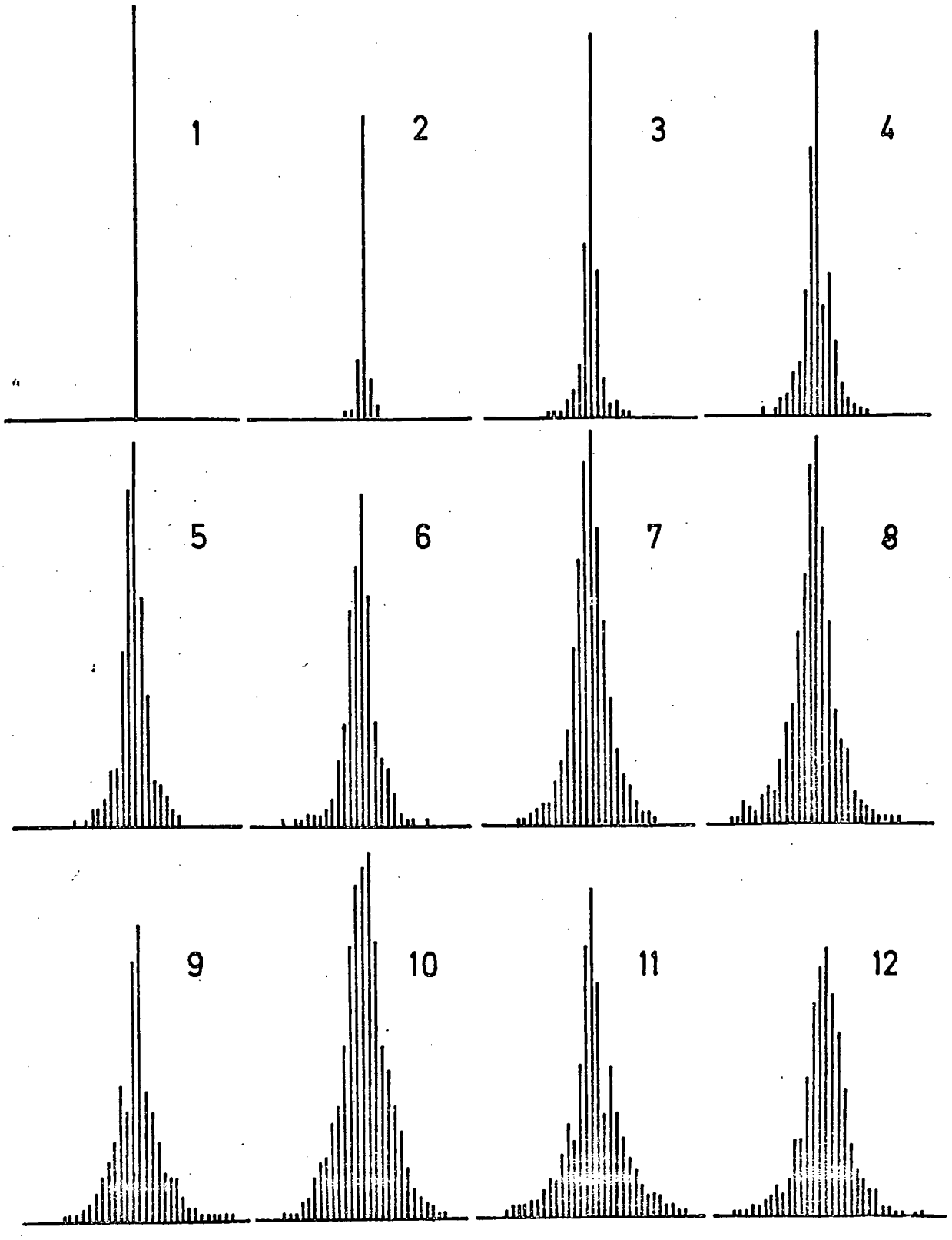

FIGURE 4.7 LATERAL DISTRIBUTION OF SHOWER SECONDARIES IN 12 MODULES FOR 3 GeV PRIMARY ENERGY AND 0.6 RADIATION LENGTH THICK TARGET

if the flash tubes are operated at high rate. The internal field of a flash tube has been shown to influence the performance of an adjacent tube, and since the number of tube ignitions increases with energy, the effect is energy dependent.

The non-linearity seen in Figure 4.5, due to failure to contain the shower, may be corrected for by use of the data taken using 1.8 radiation lengths of lead. The number of tubes igniting beyond target depths of 6.6 and 13.2 radiation lengths may be found by summing the number of expected tube ignitions at 0.6 and 1.2 radiation length intervals respectively, to obtain the number of tubes expected to have ignited had the shower been totally contained.

A correction factor for the decrease in efficiency caused by internal clearing fields has been found in the following manner for each combination of target thickness and primary energy. The efficiencies of the modules were recorded for single particles and the results plotted as efficiency as a function of the number of tube ignitions per minute. Similar data was taken using showers, the number of ignitions in a module per minute being recorded and the efficiency found from the plot of efficiency versus event rate. The correction factor is then the ratio of the expected efficiency at low rate and the observed efficiency at high flashing rate.

The mean total number of tube ignitions corrected for longitudinal losses and inefficiency at various energies for 0.6 and 1.2 radiation lengths of target are shown in Figure 4.8. It can be seen that the non-linearity is considerably reduced, and the remaining deviation is principally due to more than one electron passing through an individual flash tube. Table 4.1 shows the overall sensitivity of the detector to the number of secondary particles. This was obtained by comparing the number of observed

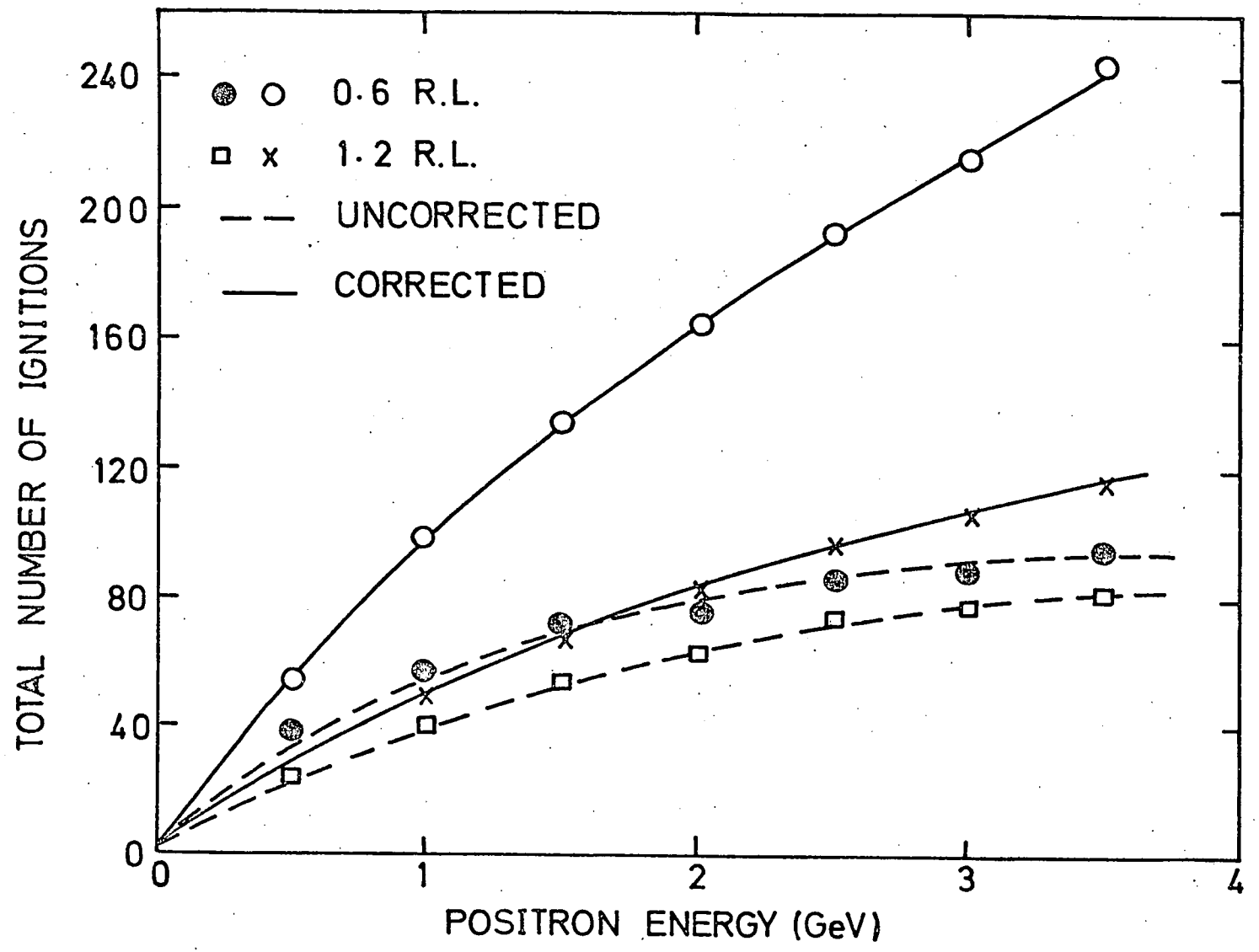

FIGURE 4·8 MEAN TOTAL NUMBER OF TUBE IGNITIONS CORRECTED FOR LONGITUDINAL LOSSES AND INEFFICIENCY

particles with the number predicted by theory, for an energy detection threshold of 2 MeV. It can be seen that the sensitivity decreases as the total number of electrons produced increase.

TABLE 4.1 : Individual Electron Sensitivity at Different Energies

Energy (GeV)	Radiation Lengths	Average Total Number of Electrons (Theory)	Average Total Number of Observed Tube Ignitions (Uncorrected)	Average Total Number of Tube Ignitions (Corrected for Efficiency, Loss)	Sensitivity % (Corrected)
0.5	0.6	26.5	20.0	21.0	79
1.5	0.6	68.0	36.5	39.5	58
2.5	0.6	102.8	44.0	50.5	49
3.5	0.6	143.3	48.2	57.0	40
0.5	1.8	11.2	9.8	10.0	89
1.5	1.8	32.0	20.0	20.5	64
2.5	1.8	55.7	28.5	30.0	54
3.5	1.8	81.9	34.7	36.8	45

4.4 ENERGY RESOLUTION

The energy resolution of the detector may be expressed as dE/E and was obtained from the following relationship,

$$\frac{dE}{E} = \frac{N}{E} \cdot \frac{dN}{N} \cdot 1\Big/\frac{dN}{dE}$$

where : $\frac{dN}{dE}$ is the gradient of the curve in Figure 4.5 for a particular value of E

dN is the FWHM of the frequency distribution of tube ignitions (see Figure 4.4)

N is the mean number of tube ignitions

E is the energy of the primary particle.

The energy resolution obtained using 0.6, 1.2 and 1.8 radiation lengths of lead target is shown in Figure 4.9. Because the number of secondaries in a shower is linearly related to the primary energy E, the resolution is expected to improve as $1/\sqrt{E}$. The experimental points obtained using 1.8 radiation lengths of lead are found to fit the relationship

$$R = \frac{41.6}{\sqrt{E}} + 24.5$$

where R is the resolution (FWHM) expressed as a percentage, and E is the primary energy in GeV. For low primary energies the resolution is considerably improved by using 0.6 and 1.2 radiation lengths. However, as the primary energy is increased, the effects of the escaping shower and high secondary densities becomes apparent and the resolutions deviate from the expected $1/\sqrt{E}$ improvement and eventually cross the curve obtained using 1.8 radiation lengths of lead.

4.5 DETERMINATION OF TRAJECTORY OF THE PRIMARY PARTICLE

The secondary particles constituting the electromagnetic shower are on average symmetrically distributed around the projection of the trajectory of the primary particle. Use can be made of this to determine the position of the primary particle. The development of an electromagnetic shower is subject to fluctuations in density and distribution of the secondary particles, which introduces a considerable uncertainty in the

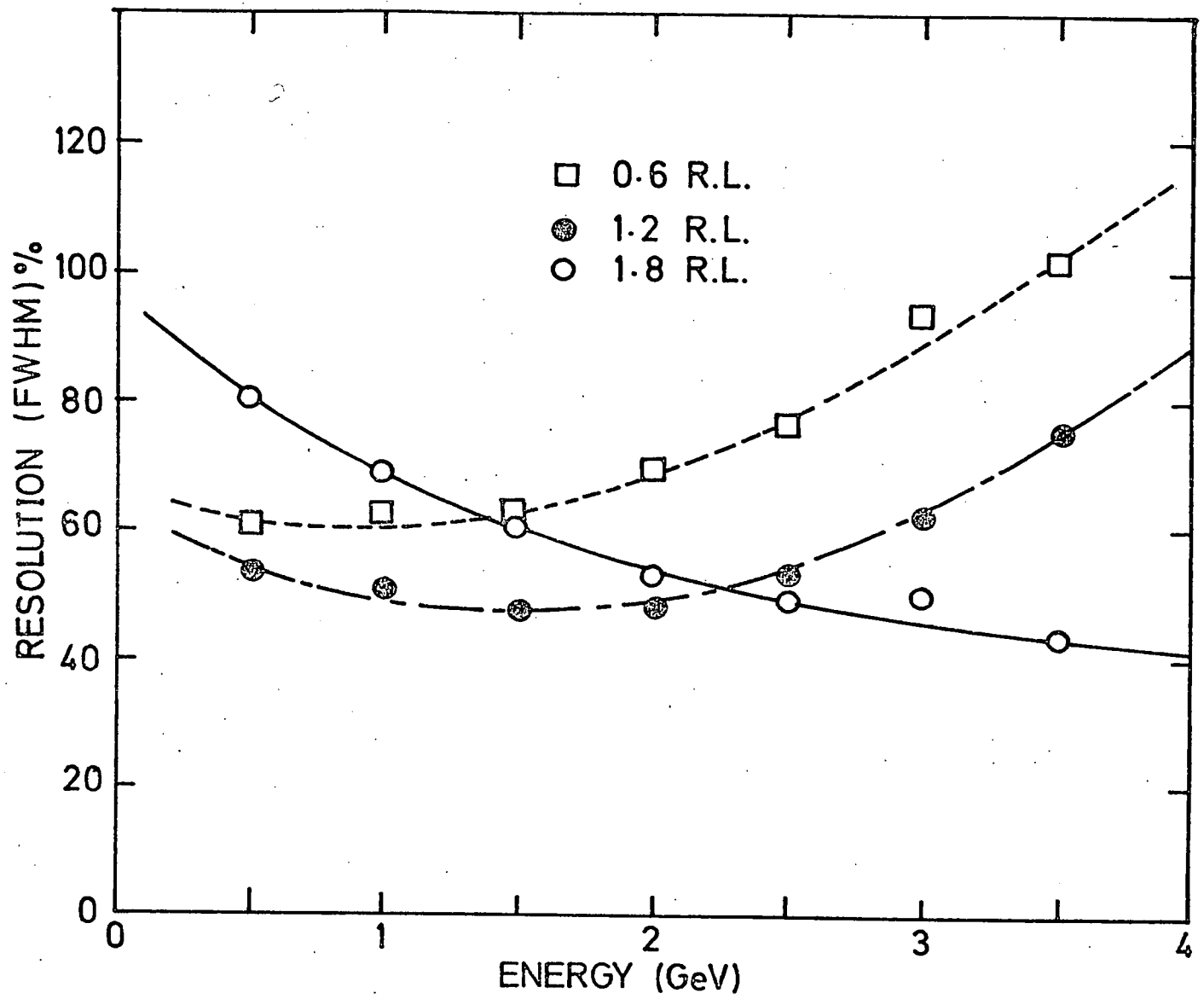

FIGURE 4·9 ENERGY RESOLUTION AS A FUNCTION OF ENERGY, DATA UNCORRECTED FOR LONGITUDINAL LEAKAGE AND INEFFICIENCY

determination of the shower axis. For this reason a statistical method[20] has been employed in locating the shower axis, which takes into consideration the fluctuations in the development of individual showers.

4.5.1 Location of Shower Axis

An initial estimate of the shower axis was made, in which no account was taken of the fluctuations occuring in the developing shower. This initial estimate made use of the fact that the shower developed with approximately circular symmetry around the shower axis. The "centre of gravity" of the lateral shower section in each sampling plane was found by calculating the geometric mean of the distribution of the flashed tubes, using the following expression

$$\bar{Y}_i = \sum_{j=1}^{32} \frac{Y_{ij}}{N_i} \qquad (1)$$

where $\bar{Y}_i$ is the co-ordinate of the shower centre in the i^{th} module

Y_{ij} is the co-ordinate of the j^{th} ignited tube in the i^{th} module

N_i is the total number of ignitions in the i^{th} module.

To these centroids, a straight line representing the first estimate of the shower axis, is fitted using the least squares method.

As explained in section 3.3, the point of entry of the primary positron into the detector was located by means of a single flashed tube in each layer of the first module, and to avoid ambiguity only events satisfying this criteria were accepted for analysis. The deviation of the point of intersection of the calculated shower axis in the 1st sheet of lead target, from the position defined by the ignited tubes in the 1st module, is referred to as the "apex deviation of the shower." It must

be remembered that such a deviation carries an inherent error of $\pm$ 4 mm (a tube radius). This definition of the apex deviation is illustrated in Figure 4.10.

As pointed out, this initial estimate of the shower axis makes no allowance for the fluctuations, caused by multiple coulomb scattering and absorption, which occur in the developing shower. The effect of these fluctuations can be seen in Figure 4.6, which shows the mean distribution of ignited tubes in each module, obtained from 820 events. Although these sections were obtained for specific energy and target configurations, they may be taken as typical examples of sections through the developing shower. The initial spike is associated with the primary positron, however, this rapidly disappears as the distributions broaden due to scattering and absorption, as the shower develops in the detector.

Shower secondaries, located at the sides and rear of the shower are subject to greater fluctuations in density and position, and therefore less reliance, when calculating the shower axis, can be placed on the data they provide, than on that provided by particles found at the front and core of the shower. Allowance was made for these fluctuations by weighting the flashed tubes according to their position in the shower as defined by the initial estimate of the shower axis. The flashed tubes are weighted in the lateral and longitudinal direction in the following manner.

LATERAL WEIGHTING: The distribution of the flashed tubes in each sampling plane may be represented by a function of the Gaussian form[20], and since the spread of the distribution gives a measure of the reliability of the data, it may be used in calculating the lateral weighting factors for the flashed tubes in the module. The weighting factor W_{ij} for the

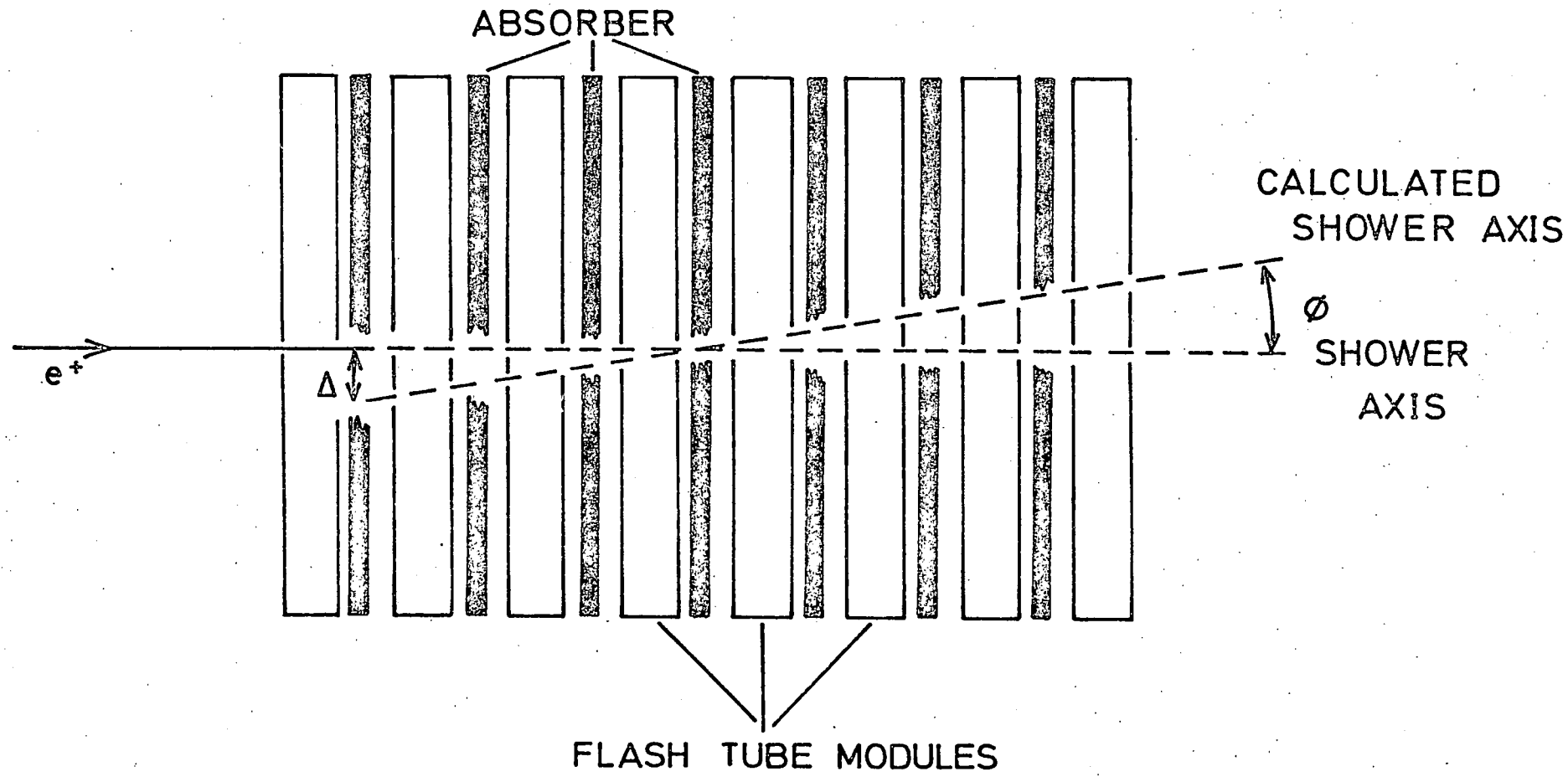

FIGURE 4.10 APEX DEVIATION (Δ) AND SHOWER AXIS ANGLE (Ø)

j^{th} tube in the i^{th} module is given by

$$W_{ij}(Y_{ij}) = \exp(-q^2_{ij}) \quad (2)$$

where

$$q_{ij} = \frac{(Y_{ij} - Y_i)\cos\phi}{K_i \sigma_i} \quad (3)$$

and Y_{ij} is the distance of the j^{th} tube in the i^{th} module, from the base of the module.

Y_i is the distance of the shower axis in the i^{th} module from the base of the module.

σ_i is the quantity representing the spread of the shower in the i^{th} module.

K_i is the fitting parameter for the i^{th} module.

ϕ is the angle between the shower axis and the plane of the module.

The parameters listed above are illustrated in Figure 4.11.

Since the incident positrons were restricted to $\phi = 0 \pm 2^{o}$, then ϕ can be considered as small and equation (3) can be rewritten as,

$$q_{ij} = \frac{Y_{ij} - Y_i}{K_i \sigma_i} \quad (4)$$

The width of the shower section in each module is characterised by the standard deviation σ_i. The standard deviations obtained for 3 primary energies and two target thickness are shown in Figure 4.12. The gradual increase in width due to multiple scattering and absorption can be seen, although the increase in width with depth is seen to be approximately the same for all 3 primary energies. A fitting factor, K_i, was chosen such

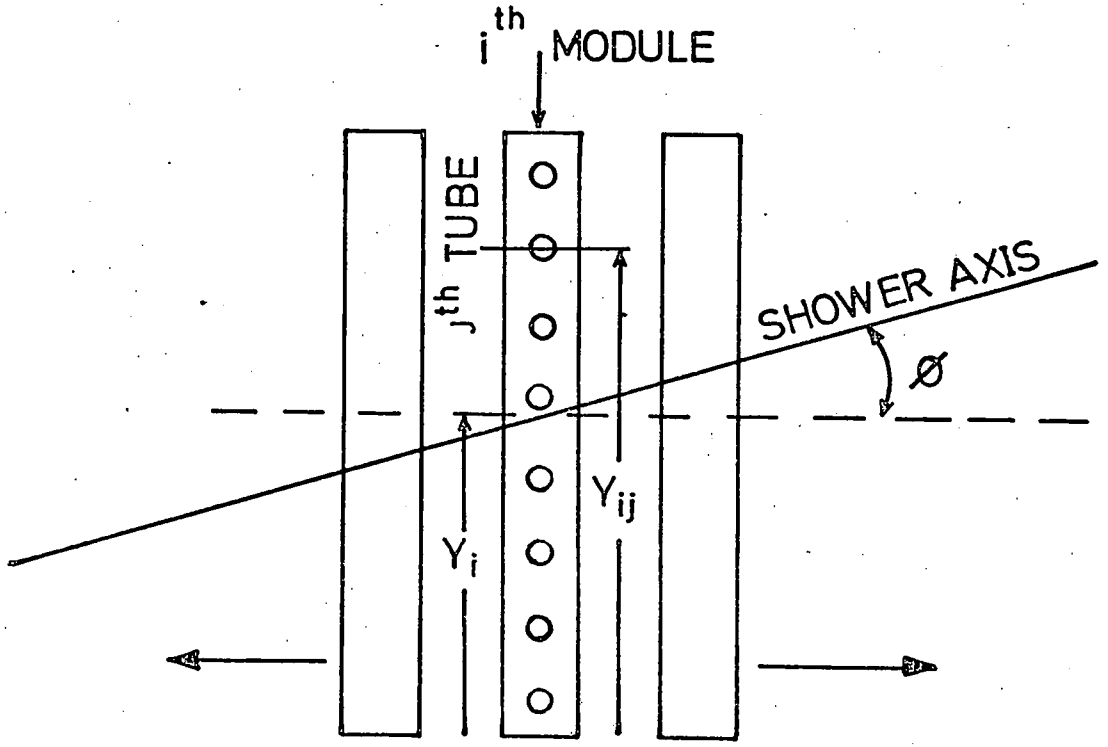

FIGURE 4.11 PARAMETERS USED IN THE ANALYSIS

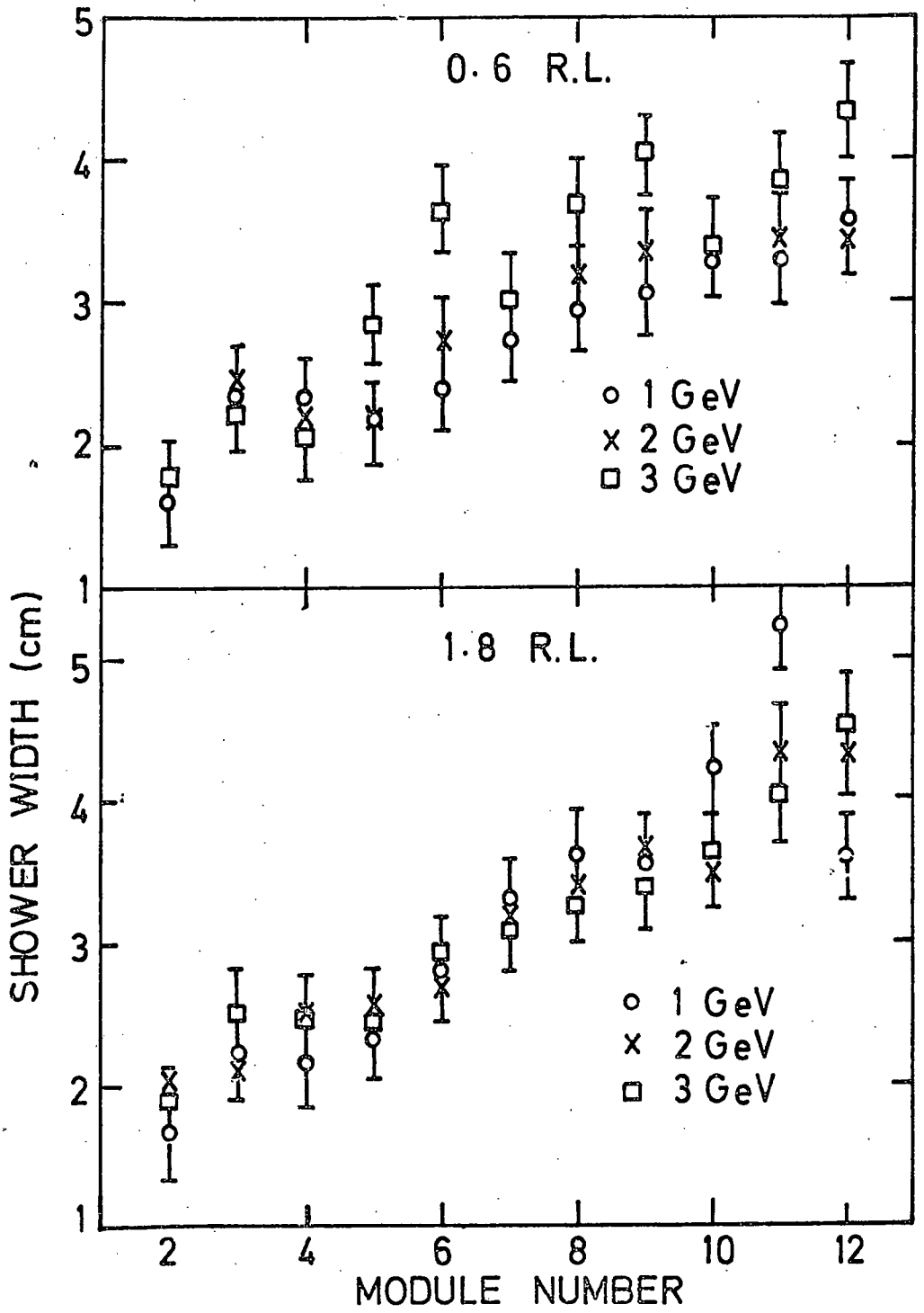

FIGURE 4·12 SHOWER WIDTH (STANDARD DEVIATION OF SHOWER PROFILE) AS A FUNCTION OF DEPTH

that the Gaussian weighting function, W_{ij} in equation (2) was a close approximation to the observed profile. The value of K_i was found to vary from module to module, and also depended upon the primary energy and target thickness. An average value, obtained from the values of K_i under various combinations of energy and target, of 3.5, was used in the final analysis. It was found that the estimation of the shower axis was not critically dependent on the value of K_i, and therefore the error incurred by using an average value of K_i was small.

LONGITUDINAL WEIGHTING : A longitudinal weighting factor was required which took account of the increasing fluctuations of the shower with target depth. Two weighting factors were tried, $1/L_i$, where L_i is the depth of target traversed before the i^{th} module, and $1/\sigma_i$, where σ_i is the standard deviation of the distribution of flashed tubes in the i^{th} module. The standard deviations of the distribution of the apex deviations, obtained using various powers of these weighting factors, is shown in Table 4.2. It can be seen that the weighting factor $1/\sigma^2$ gives the best results for both X and Y planes, and hence $1/\sigma^2$ was chosen as the longitudinal weighting factor.

TABLE 4.2 : Standard Deviation of the Apex Deviation Using Different Weighting Factors

Longitudinal Weighting Factor	Standard Deviation (mm)	
	X Plane	Y Plane
$1/\sigma_i$	8.8	11.5
$\{1/\sigma_i\}^2$	7.4	11.1
$\{1/\sigma_i\}^3$	6.8	11.7
$\{1/\sigma_i\}^4$	7.6	12.4
$1/L_i$	7.8	12.1
$\{1/L_i\}^2$	9.3	16.1
$\{1/L_i\}^3$	12.0	19.3

This result is not surprising since the value of σ_i is unique to each module, and best describes the shower fluctuations observed by the particular module.

Using the weighting factors described above, and employing equations 1,2 and 4, an improved estimate of the shower axis was made by means of a weighted iterative fit in the following manner. Having made the simple first estimate of the shower axis using equation 1, lateral weighting factors for the flashed tubes in each module were calculated, and used in obtaining the weighted centroids of the shower. A straight line was fitted to these new weighted shower centres, using a least squares method which incorporated the longitudinal weighting factors. A further set of weighting factors was then calculated with respect to the new shower axis and the whole process repeated to obtain a second weighted estimate of the shower axis.

This iterative process was continued until the differences in successive values of the apex deviation converged to a constant value, usually after about 5 interactions.

4.5.2 Spatial Resolution of the Detector

The apex deviations were obtained in the manner just described, for some 1400 events, for each combination of target thickness and primary energy. Examples of the resulting distributions of apex deviations are shown in Figure 4.13, for two primary energies. The spatial resolution is defined as the width of the distribution containing 76% of the data. In the case of the distribution of apex deviations, which approximated to a Gaussian distribution, this is equivalent to the full width at half maximum height of the distribution. Figure 4.14 shows the spatial resolution for various absorbers calculated using the above criteria and making allowance for the uncertainty of $\pm$ 4 mm in the location of the

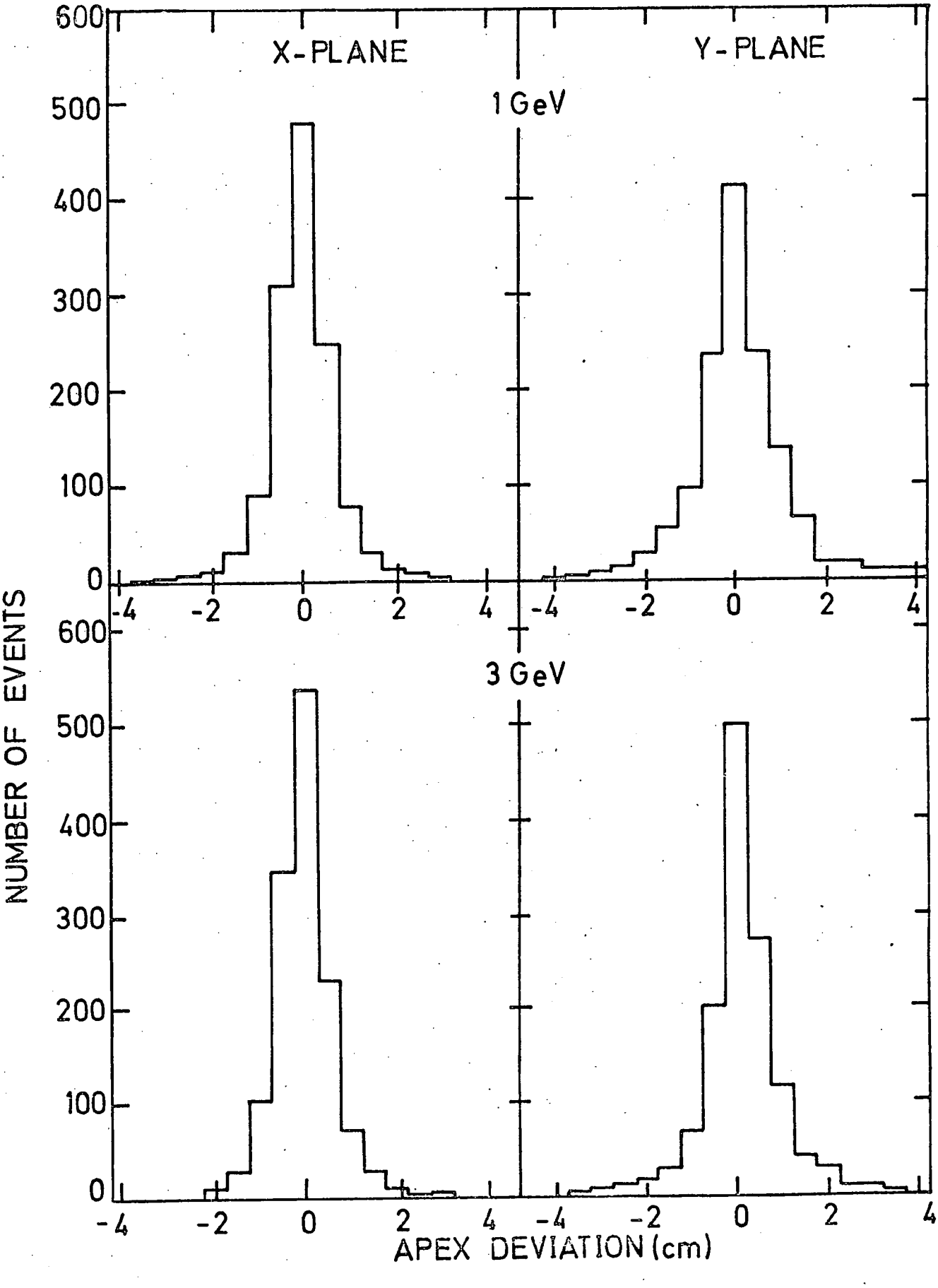

FIGURE 4.13 FREQUENCY DISTRIBUTION OF APEX DEVIATION
1.2 R.L. LEAD TARGET BETWEEN MODULES

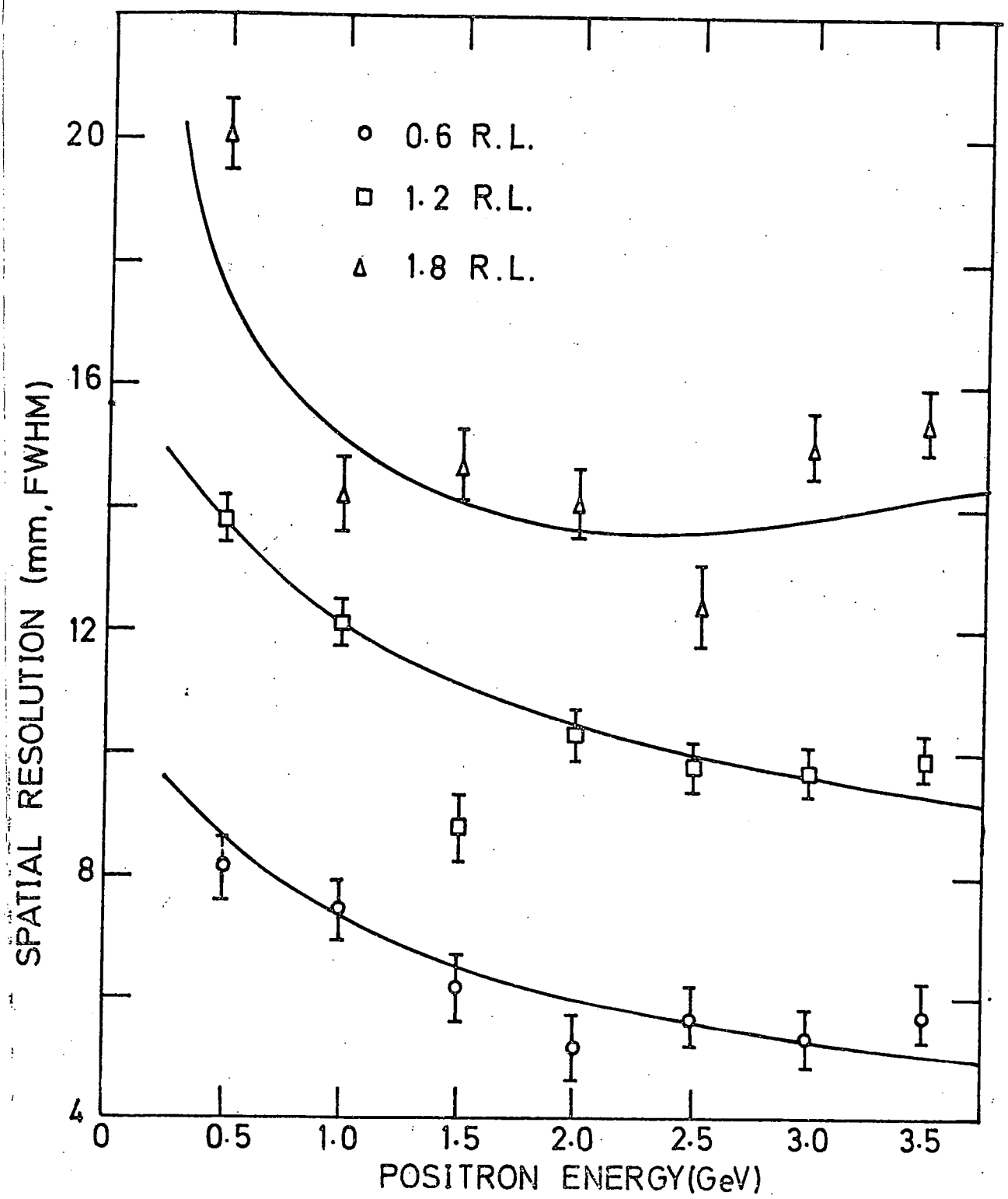

FIGURE 4·14 SPATIAL RESOLUTION OF THE CHAMBER AS A FUNCTION OF POSITRON ENERGY. DATA FROM Y PLANES

primary positron in the first module. The spatial resolution is seen to improve as the primary energy increases and the target thickness decreases. The best resolution obtained is approximately $\pm$ 5 mm(FWHM) for 3.5 GeV positrons, using 0.6 radiation lengths of lead target between the modules.

4.5.3 Angular Resolution of the Detector

Having obtained the equation of the weighted shower axis as described in 4.5.1, it is then possible to calculate the angle of the shower axis to the normal of the detector planes, for each event. The distributions of the shower axis angles for two primary energies is shown in Figure 4.15. The angular resolution of the chamber was defined in the same manner as the spatial resolution, as the FWHM of the distribution of the angular deviations of the shower axis from the normal.

The flash tube chamber was arranged in the beam, such that the positrons were incident normally upon the centre of the plane of the first module. However, the positron beam was only defined to $\pm 2^{\circ}$ and this uncertainty must be allowed for in the calculation of the angular resolution. Figure 4.16 shows the angular resolution, corrected for the uncertainty of $\pm 2^{\circ}$, for various target thickness. It can be seen that the angular resolution steadily improves for all target thickness, with increasing energy, until approximately 2.0 GeV, after which it plateaus. The best resolution obtained is approximately $\pm 4^{\circ}$, (FWHM), beyond 2.0 GeV, using 0.6 radiation lengths of lead.

4.6 PERFORMANCE OF THE DETECTOR AT HIGH EVENT RATES

When a flash tube discharges the charge produced is swept by the applied high voltage field to the walls of the tube, where they

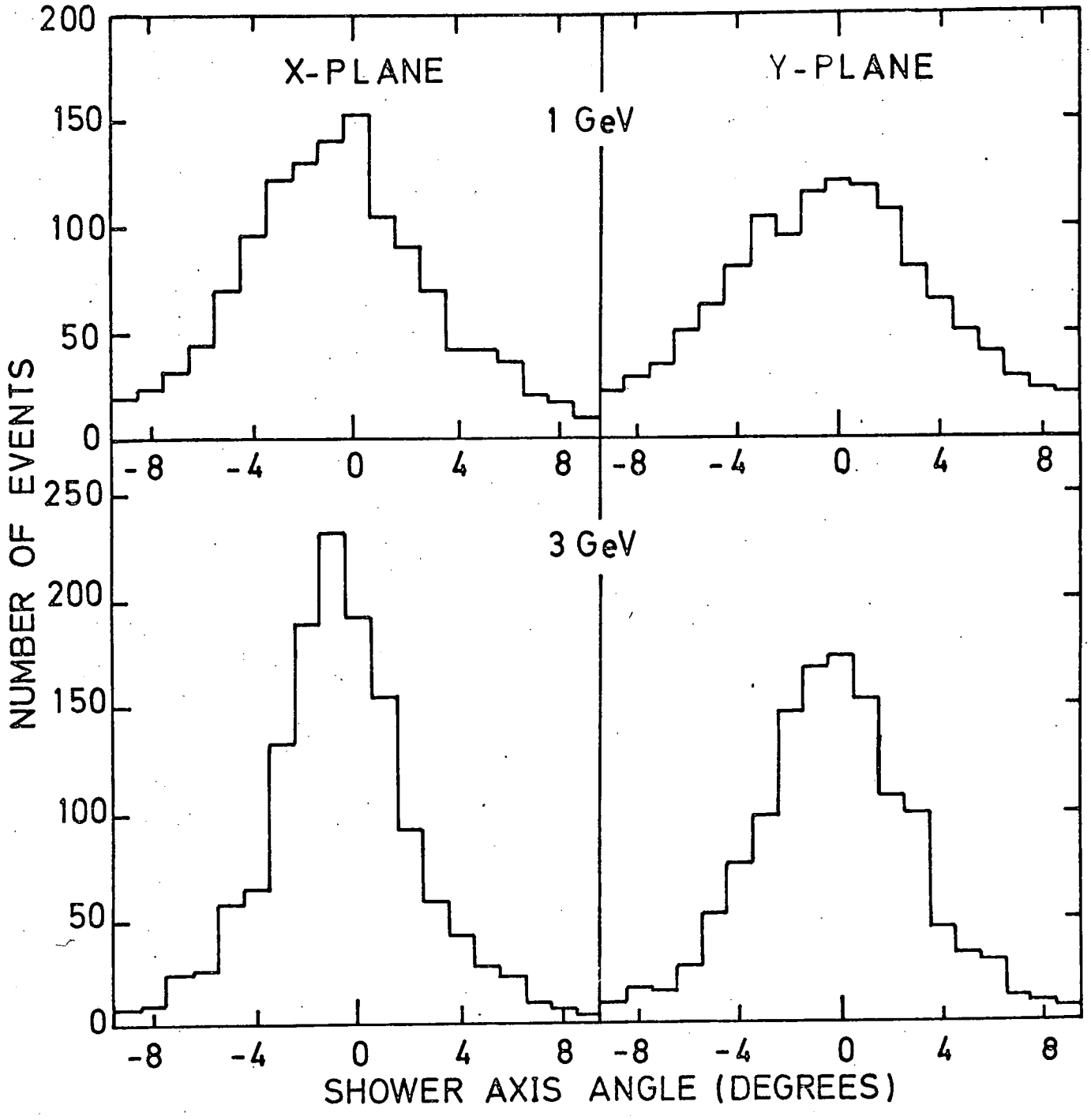

FIGURE 4.15 FREQUENCY DISTRIBUTION OF SHOWER AXIS ANGLE, 1.2 R.L. LEAD BETWEEN MODULES

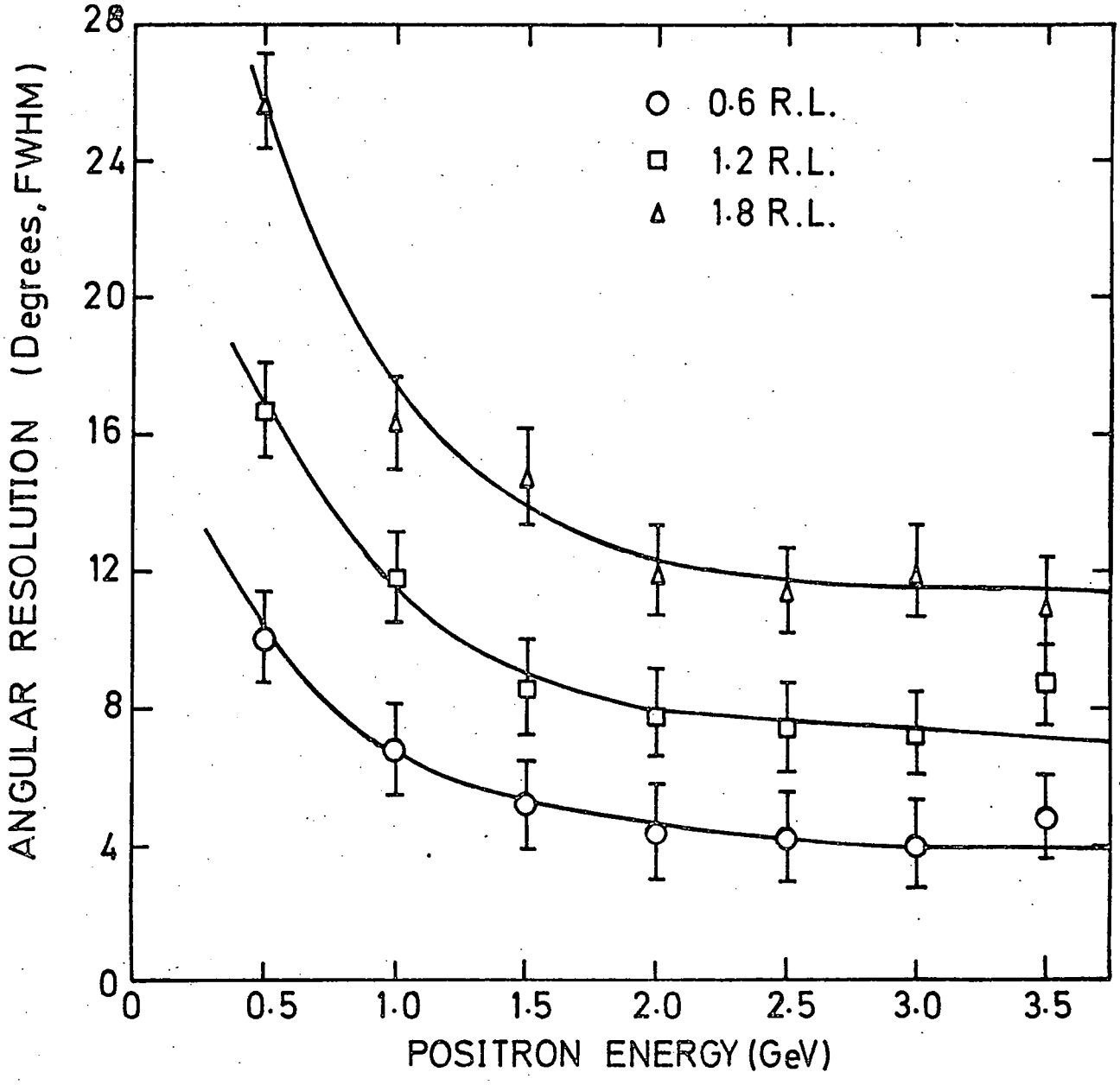

FIGURE 4.16 ANGULAR RESOLUTION OF THE CHAMBER AS A FUNCTION OF POSITRON ENERGY. DATA FROM Y PLANES

will adhere. The presence of these charges on the walls of the flash tube results in an electric field across the gas volume, the direction of which is such that it opposes any subsequently applied H.T. pulse, and results in a lower effective applied field. These charges recombine by migration under the influence of their own field, across the tube walls. The field due to these charges is observed to decay exponentially, with a time constant which depends upon the intrinsic capacitance and resistivity of the flash tube[15], and upon the polarity of the applied H.T. pulse[21]. The later dependence upon the polarity of the H.T. pulse is not understood, but results in two distinct decay constants, 0.6 seconds for a positive pulse and 27.7 seconds for a negative pulse. Figure 4.17 shows this decay of the internal fields for the high pressure tubes used in the present experiment.

As the event rate is increased, so the time between successive ignitions in which the internal field may decay, decreases. This results in a reduction of the effective applied field and hence the digitisation pulse height. The variation of pulse height with flashing rate for the high pressure tubes used in the present experiment is shown in Figure 4.18. Should the pulse height fall below the threshold required to set the memory logic latches (approximately 4 V), the tubes will appear inefficient. The average layer efficiency of the detector as a function of event rate is given in Figure 4.19, it can be seen that the layer efficiency falls by 13% when the event rate is increased from 0.2 to 1.0 event sec^{-1}. This rate dependence of the efficiency is unacceptable, especially with respect to the manner in which the energy measurements are made.

4.7 REDUCTION OF INTERNAL FIELDS

Two approaches are available for reduction of the internal clearing

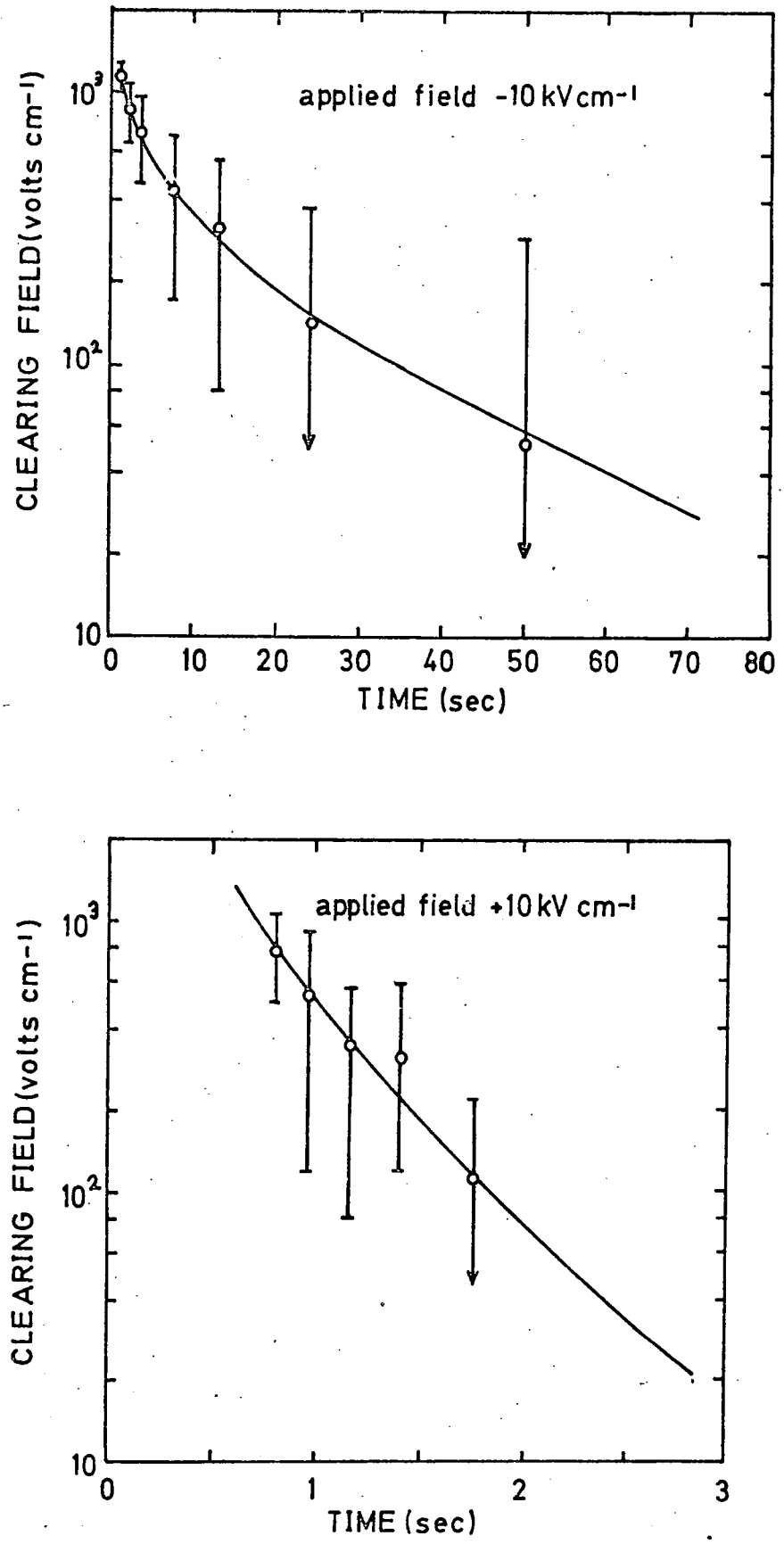

FIGURE 4.17 DECAY OF INTERNAL CLEARING FIELD WITH TIME FOR POSITIVE AND NEGATIVE APPLIED HT FIELDS

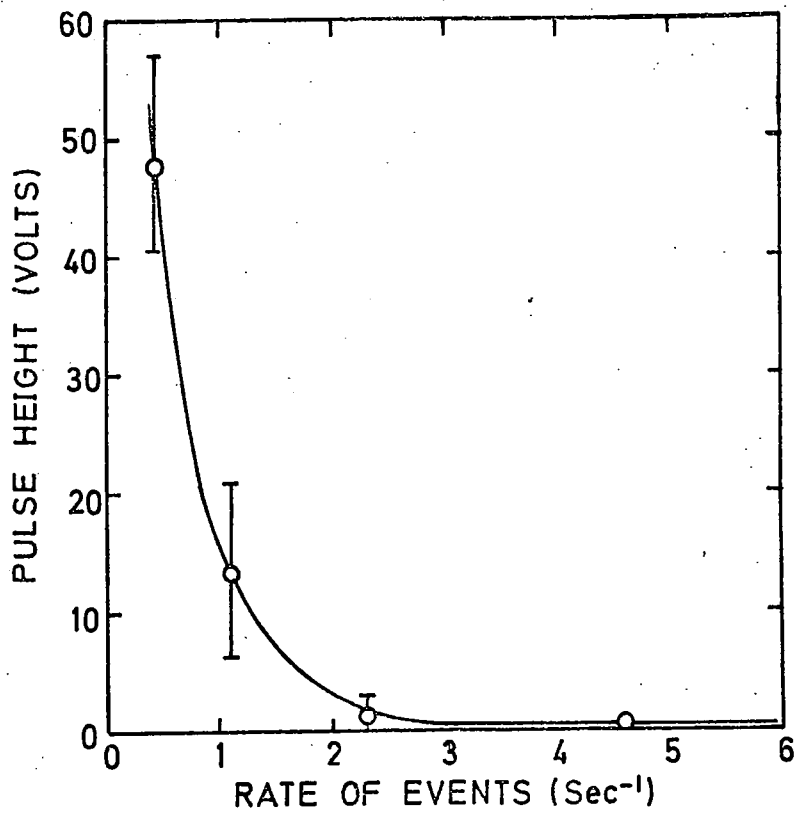

FIGURE 4.18 DIGITISATION PULSE HEIGHT AS A FUNCTION OF EVENT RATE. HT PULSE FIELD -10kV/cm, LENGTH 4.5 μs

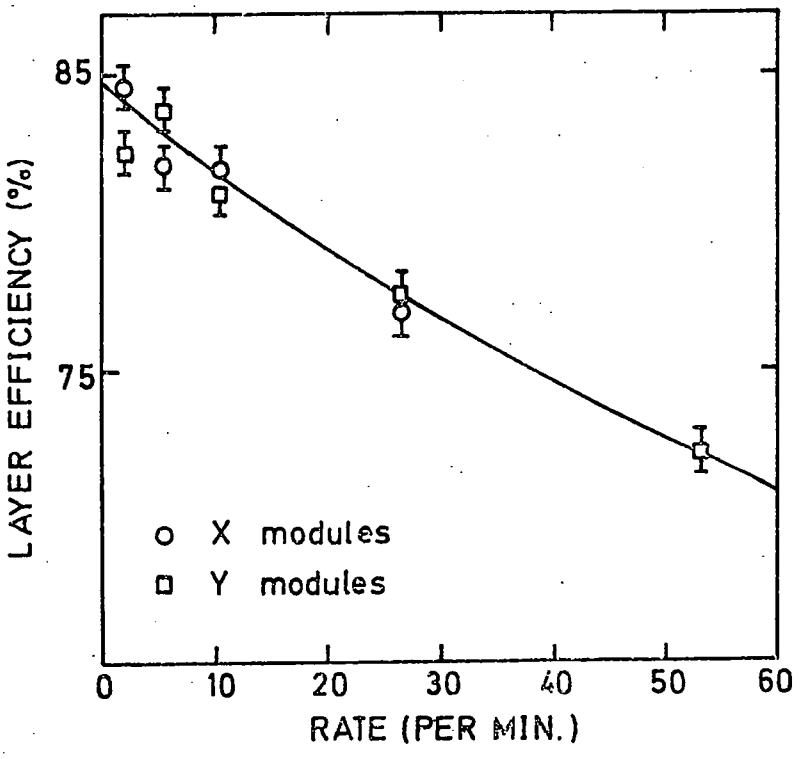

FIGURE 4.19 LAYER EFFICIENCY AS A FUNCTION OF RATE OF CHAMBER OPERATION

field, either reducing the amount of charge deposited on the walls, or alternatively increasing the rate of recombination of charge around the tube walls. The latter solution requires the reduction of the surface resistance of the glass by some surface treatment method. Since this would require the fabrication of a complete set of treated tubes, the former solution appeared more attractive. Two methods of reducing the amount of charge deposited on the tube walls were tried and are described below.

4.7.1 Use of Alternate Polarity H.T.Pulses

By the use of alternative polarity pulses it was hoped that the charges deposited on the tube walls during one discharge would be neutralised by the charges of opposite polarity deposited during a subsequent discharge using an applied H.T. field of the opposite polarity. To test this hypothesis, a series of laboratory experiments were conducted on a single high pressure tube using a RU-106 source[21]. Figure 4.20 shows the variation of the mean digitisation pulse height with rate of flashing for alternate polarity applied fields of 10 kV cm^{-1}. It can be seen that neither the negative or the positive digitisation pulse height falls appreciably up to event rates of 1.6 events sec^{-1}. Figure 4.21 shows the standard deviation of the pulse height as a function of flashing rate. It can be seen that the standard deviation of the pulse height increases considerably with event rate. This is caused by the tube failing to flash every time the H.T. pulse is applied. Failure to fire consecutively results in a smaller digitisation pulse, since the internal field is not neutralised. Should the tube fire consecutively, then the effective applied field will be enhanced by the internal field resulting from the previous discharge, thus yielding a greater digitisation pulse height.

An alternate polarity pulsing system was built for the flash

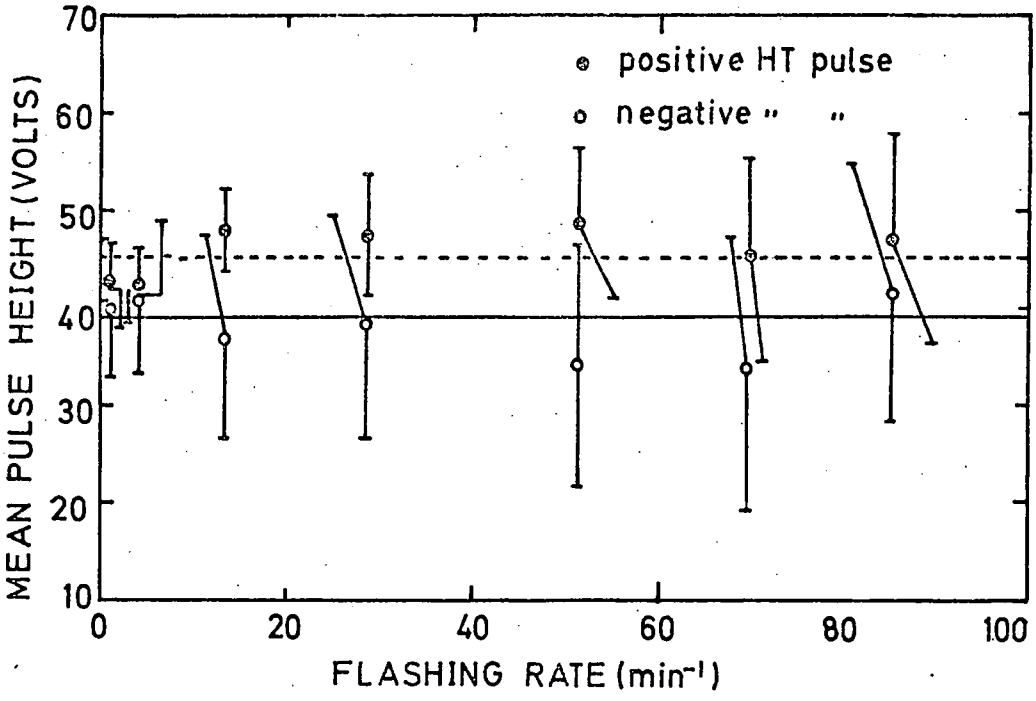

FIGURE 4.20 VARIATION OF MEAN DIGITISATION PULSE HEIGHT WITH FLASHING RATE FOR ALTERNATE POLARITY APPLIED FIELDS OF 10kV/cm

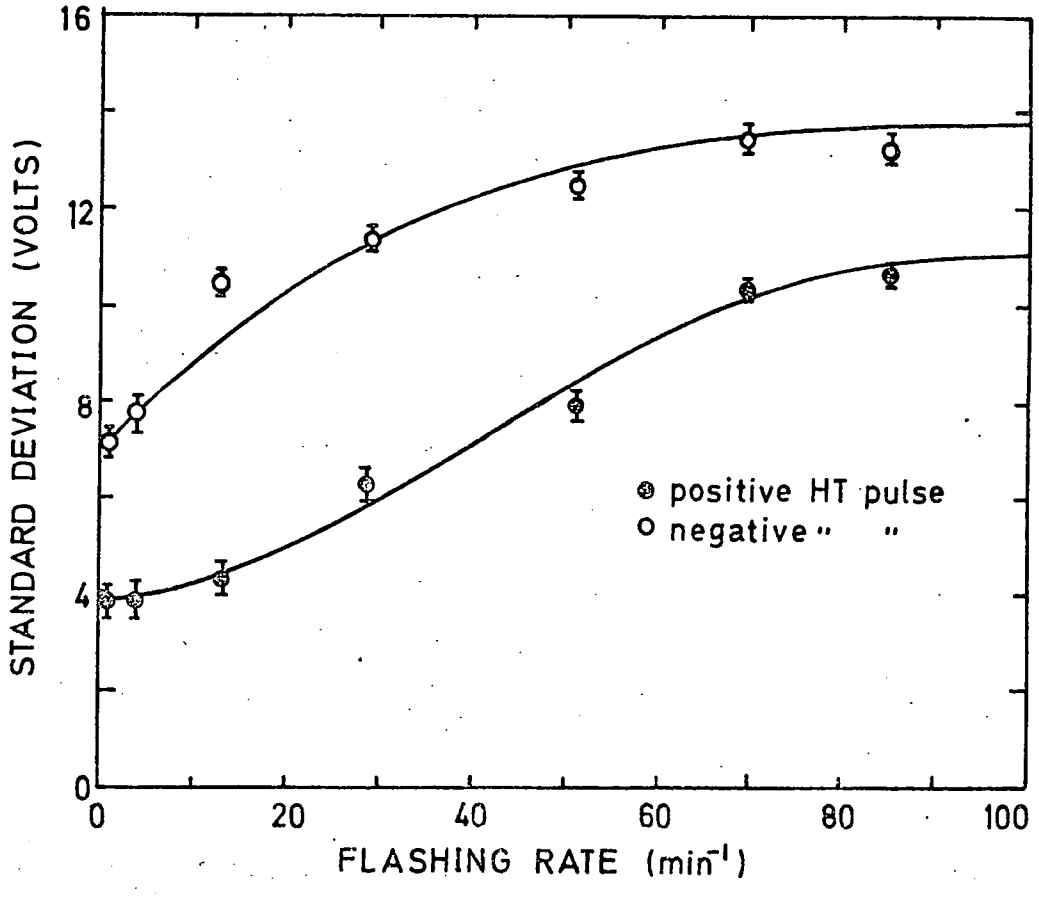

FIGURE 4.21 STANDARD DEVIATION OF PULSE HEIGHT DISTRIBUTION AS A FUNCTION OF FLASHING RATE

tube chamber and tested in the positron beam. However, it was found that at event rates in excess of 1 event sec^{-1}, the modules exhibited both inefficiency and spuriousness.

This was clearly due to the effective applied field falling outside the limits set for efficient operation of the tube due to the effects mentioned above. Since the plateau region of the applied field, in which the tubes could be successfully operated, lay between 10.0 and 10.5 kV cm^{-1} (see section 3.2.1) it was obviously too narrow to allow the use of an alternate polarity pulsing system, which resulted in a wide range of effective applied fields.

4.7.2 Use of Oscillating H.T. Pulses

It has been shown that the long tail associated with the normal RC type pulse has a considerable influence upon the quantity of charge swept to the tube walls[22]. Reduction of the pulse decay time results in less charge being deposited on the walls, but is limited by the minimum pulse length required for efficient operation of the tube. An oscillating HT pulse was therefore chosen since it is relatively easy to produce, and the reversal of the field direction would result in charges of both signs being deposited on a particular area of the tube wall, thereby neutralising one another.

An oscillating pulse was obtained by insertion of a 3 mH inductance in the high voltage network, as shown in Figure 4.22 (b). A variety of damping resistors, of between 47 and 424 Ω could also be included, to adjust the length and magnitude of the pulse train. Examples of the pulse shapes obtained are shown in Figure 4.22 (a). It was found from a study of layer efficiency with event rate, that the pulse shape obtained using 94 Ω damping gave the best results. However, inefficiency was still present, as can be seen from Figure 4.23 which shows the mean total number of tube

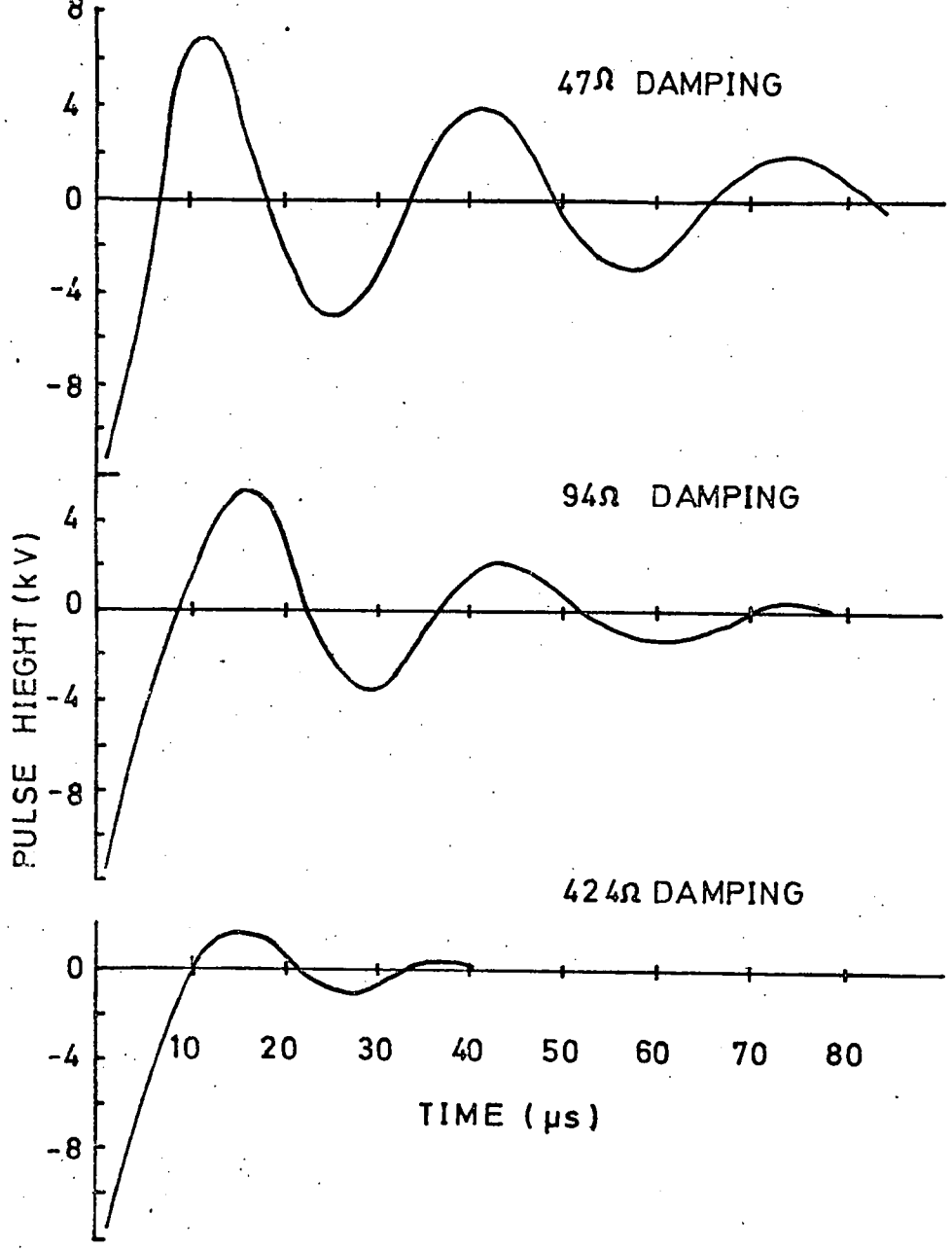

FIGURE 4·22(a) HIGH VOLTAGE PULSE SHAPES

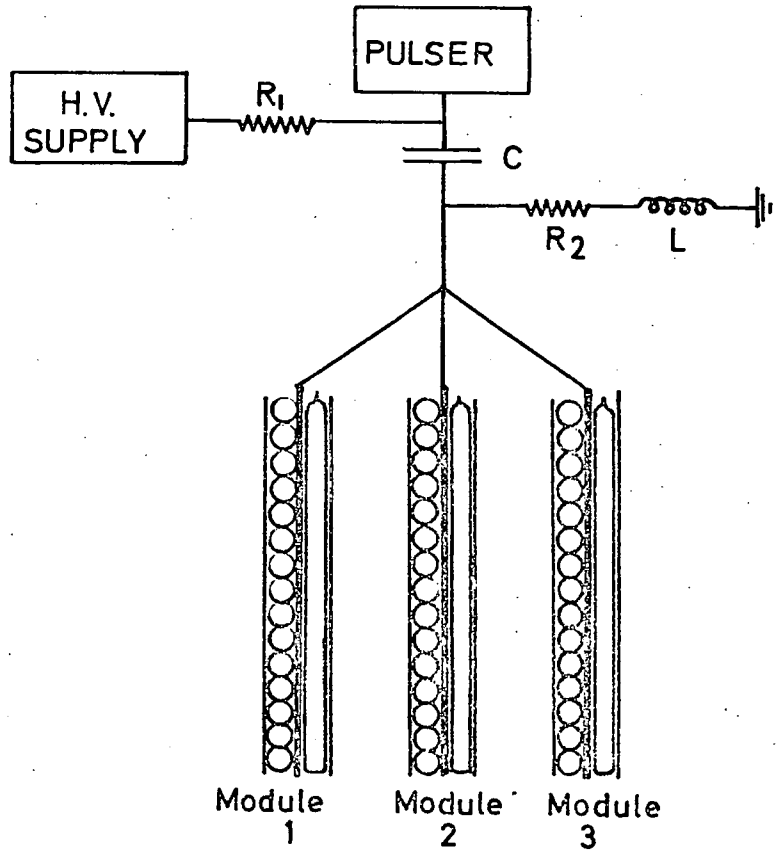

R =1·0 MΩ
L=3 MH

R = 47- 424Ω Damping Resistor
C = 3000 pf

FIGURE 4·22(b) HIGH VOLTAGE PULSE FORMING CIRCUIT

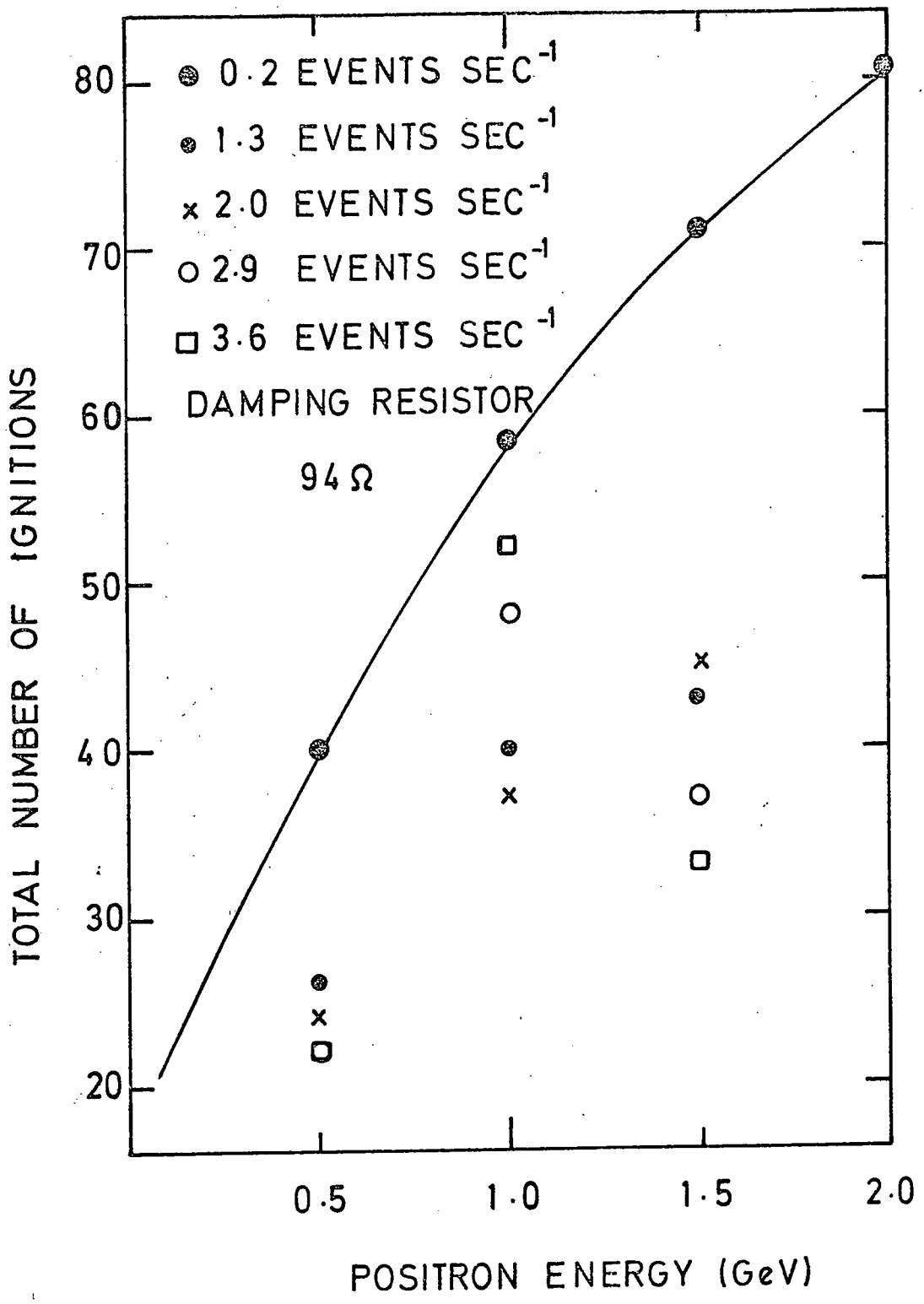

FIGURE 4·23 MEAN TOTAL NUMBER OF TUBE IGNITION AS A FUNCTION OF ENERGY FOR A NUMBER OF RATES

ignitions as a function of energy for a number of rates. The dependence of efficiency upon event rate, would invalidate the method used to determine the primary energy for event rates varying above about 1 event sec^{-1}.

The onset of inefficiency and spuriousness can be clearly seen from Figure 4.24, which shows the lateral shower sections obtained for rates of 1.3 and 7.5 events sec^{-1}. These distributions should be compared to those in Figure 4.7 which were obtained at an event rate of 0.1 events sec^{-1}.

4.8 CONCLUSIONS

It has been shown that high pressure neon-helium flash tubes, doped with methane can operate successfully in an acceleration type environment. Tests conducted with an electromagnetic shower detector using planes of flash tubes as the sampling elements showed that such a detector can offer a competitive degree of both spatial and energy resolution. A comparison of the energy resolution of the flash tube chamber, using 1.2 and 1.8 radiation lengths of lead target, with other shower detectors, is made in Figure 4.25. It can be seen that for primary energies of 1 GeV and below, the resolution is as good as, or better, than that offered by the more complex wire chambers, or plastic scintillator sampling devices. However, at higher energies the resolution deteriorates using 1.2 radiation lengths of lead, due to high shower density and poor containment.

Although a detector operating on the shower sampling principle cannot attain the energy resolutions associated with the homogeneous type of detector, such as lead glass or NaI, it must be remembered that to attain spatial resolutions of the order of $\pm$ 5mm (FWHM) as was achieved with the flash tube chamber, results in both complex and costly devices.

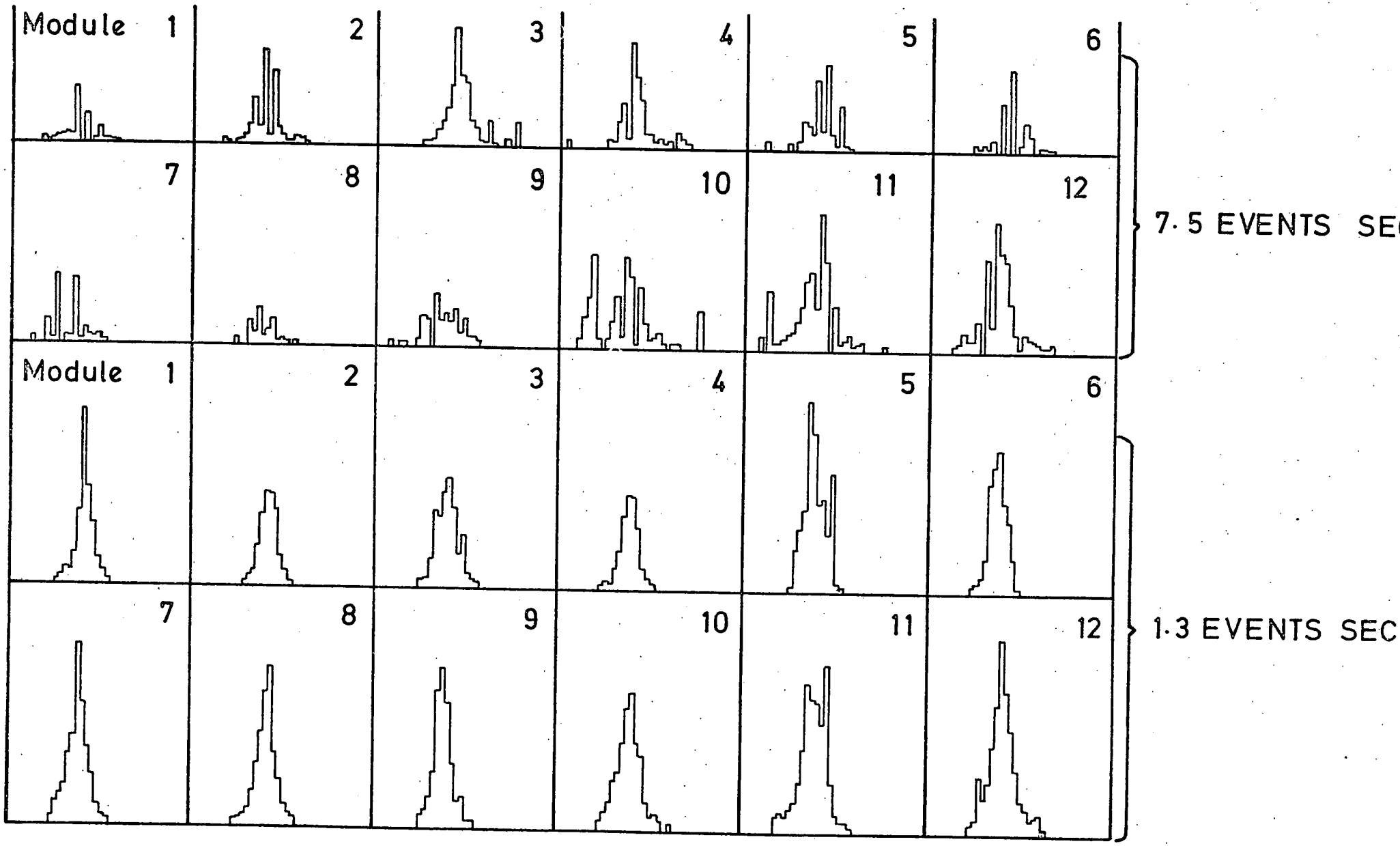

FIGURE 4.24 LATERAL SHOWER SECTIONS FOR 2 RATES

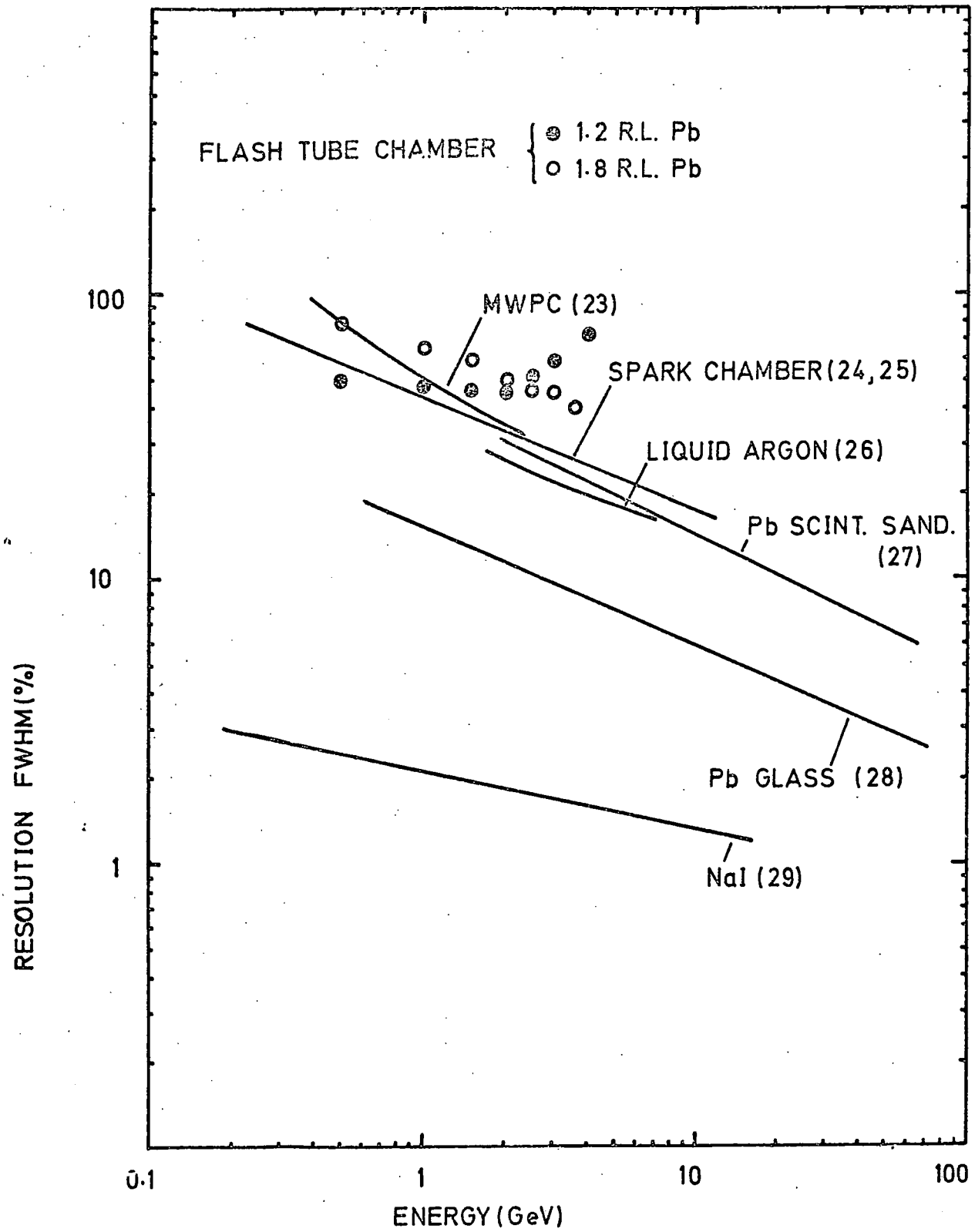

FIGURE 4·25 COMPARISON OF THE ENERGY RESOLUTIONS OF SOME CURRENT FORMS OF ELECTROMAGNETIC SHOWER DETECTORS WITH THAT OBTAINED USING THE HIGH PRESSURE FLASH TUBE CHAMBER

Furthermore, it is possible to achieve large sensitive areas using flash tube arrays (the cost per tube being independent of its length), which is not generally the case with the other detectors illustrated in Figure 4.25.

It appears, therefore, that flash tubes can fulfill the requirement for a simple inexpensive large area electron-photon detector offering a reasonable degree of both spatial and energy resolution for use on acceleration based experiments. However, the restriction to event rates of less than 1 event sec^{-1}, due to internal fields, will limit the possible applications of the detector. Simple solutions to the problem, in the form of modified pulsing systems, failed to reduce the internal fields, and it appears that it is necessary to reduce the surface resistance of the glass by some surface treatment to reduce the internal fields. Earlier attempts at reducing the surface resistance by a coating of stannic oxide had proved unsuccessful[22], resulting in spurious flashing. Other surface treatments were not tried since it was felt that this would greatly increase the cost of the detector.

It has been previously shown that large diameter, low pressure methane doped flash tubes, can be operated at event rates of 50 events sec^{-1}, without deterioration due to internal fields[30]. It was decided, therefore, to build a detector using these large diameter tubes. To overcome the insensitivity due to the large diameter of the tubes, it was decided to use two layers of tubes, with staggered centres, for each X and Y detecting plane. To locate the position of the incident positron, a system of drift chambers was used, thus eliminating the large uncertainty ($\pm$ a tube radius) which arose when defining the apex deviation in the high pressure flash tube chamber. The construction, operation and performance of this detector is described in the following chapter.

REFERENCES: CHAPTER FOUR

(1) Messel H., Crawford D.F., Electron Photon Shower Distribution Function, Pergamon Press, New York (1970).

(2) Volkel V., Internal Report, DESY, 67/16, (1967).

(3) Rossi B., High Energy Particles, Prentice-Hall Inc., (1952).

(4) Zerby C.D., Moran H.S., J. Appl.Phys. 34, (1963), 2445.

(5) Nagel H., Z. Phys. 186, (1965), 319.

(6) Buja Z., Acta. Phys. Polon., 24 (1963), 381.

(7) Ivanenko I.P., Sanosudov B.E., J.Nucl. Phys., (USSR), 5,(1967),622.

(8) Jakeways R., Calder I.R., Nucl. Inst.Meth. 84, (1970), 79.

(9) Heusch C.A., Prescott C.Y., Phys. Rev., 135, (1964), B 772.

(10) Backenstoss G., et al., Nucl.Inst.Meth., 21, (1963), 155.

(11) Yuda T., et al., Nuovo Cinento, 65, (1970), 205.

(12) Grodstein G.W., Nat. Bur. Stds. Circular, 583, (1975).

(13) Greisen K., Phys. Rev., 75, (1949), 1071.

(14) Breare J.M., Nandi B.C., Tait I.D., Nucl. Inst. Meth., 136, (1976) 517.

(15) Breare J.M., Doe P.J., Nucl. Inst.Meth. 133, (1976), 247.

(16) Breare J.M., et al., Int.,Conf.on Inst. High Energy Physics, Frascati, (1973), 221.

(17) Holroyd F.W., Breare J.M., Nucl. Inst. Meth., 100, (1972), 429.

(18) Ferguson H., Rastin B.C., Nucl.Inst. Meth., 96, (1971), 405.

(19) Ashton F., et al., Lettere al Nuovo Cinento, Vol.2, No.14, (1971),707

(20) Franzinetti G., Gerber H.J., CERN Report NPA 64 - 10, (1964).

(21) Breare J.M., Nandi B.C., Tait I.D., Nucl.Inst. Meth., 138 (1976),457.

(22) Holroyd F.W., Ph.D. Thesis, Durham University, (1971).

(23) Katsura T., et al., Nucl.Inst. Meth., 105 (1972), 245.

(24) Allkofer O.C., et al., Internal Report. University of Kiel, Germany (1973).

(25) Bauer A., Proc. Int. Conf. Electron and Photon Interactions at High Energies, Hamburg, (1965), 401.

(26) Engler J., et al., Nucl.Inst.Meth., 120 (1974), 157.

(27) Knauer J.P., Yount D.E., Nucl.Inst.Meth., 129, (1975), 91.

(28) Appel J.A., et al., Nucl.Inst.Meth., 127 (1975) 495.

(29) Hofstadter R., Proc. Int: Conf.Inst. for High Energy Physics, Frascati, (1973), 362.

(30) Chaney J.E., Breare J.M., Tait I.D., Nucl. Inst. Meth., 125, (1975), 189.

(31) Brosco G., Thesis, University of Rome, (1972).

CHAPTER FIVE

AN ELECTRON-PHOTON SHOWER DETECTOR EMPLOYING LOW PRESSURE FLASH TUBES

5.1 INTRODUCTION

It has been shown in Chapter 4 that it is possible to construct a relatively simple, inexpensive shower detector using planes of flash tubes as the sampling elements offering a useful degree of both spatial and energy resolution. However, the applications of this detector to accelerator based experiments will be limited unless the maximum event rate can be raised above the present ceiling of less than 1 sec^{-1}.

Large diameter, low pressure flash tubes, have been shown to operate successfully at event rates of 50 sec^{-1} (1), without any detectable deterioration in their performance. The use of large diameter flash tubes results in a degradation of the detectors ability to resolve individual particles in dense showers, which will be of particular significance regarding the energy measurement. An improvement may be achieved by the use of two staggered layers of flash tubes for each sampling plane. This, and other improvements were incorporated in the detector described below, which would enable it to operate at event rates of at least 50 sec^{-1} yet still maintain the useful resolution obtained from the high pressure flash tube chamber.

5.2 DESIGN AND CONSTRUCTION OF THE DETECTOR

The shower detector consisted of eleven sampling modules, interspaced with gaps, in which various types and thickness of target material could be inserted. For these series of tests, 0.6, 1.2, 1.8 and 2.4 radiation lengths of lead and 0.5 radiation lengths of iron were used.

Each sampling plane contained four layers of 16 tubes per layer, arranged in two orthogonal sets of two staggered layers, so as to provide X and Y co-ordinates of the distribution of shower secondaries across the sampling plane. This resulted in a sensitive area of 32 cm square. A section through a sampling module is shown in Figure 5.1. The characteristics of the tubes used in the detector are given in Table 5.1. Some means must be provided to prevent photons from one flashing tube from causing an adjacent tube to flash. Previously, with the large diameter tubes, this had been achieved by sleeving the tubes in thin black plastic[1]. To accommodate this additional material the distance between tube centres must be increased, resulting in a lower layer efficiency. The tubes of the present detector were, therefore, coated in a thin layer of black enamel paint.

TABLE 5.1: Flash Tube Characteristics

Diameter (mm) Internal	Diameter (mm) External	Length (mm)	Pressure (Torr)	Glass Type	Gas Composition	Sensitive Time (μs)	Recovery Time (ms)
16	18	500	600	Soda	70% Ne 30% He +1% CH_4	3.0	7.0

Although it has been shown that painting the tube reduces the conductivity of the outer surface and enhances the effect of the internal fields[2], it was considered that this would have little effect upon the tube's performance under the anticipated operating conditions.

To determine the position of entry of the incident particle into the detector, and hence the true apex of the resulting shower, two independent

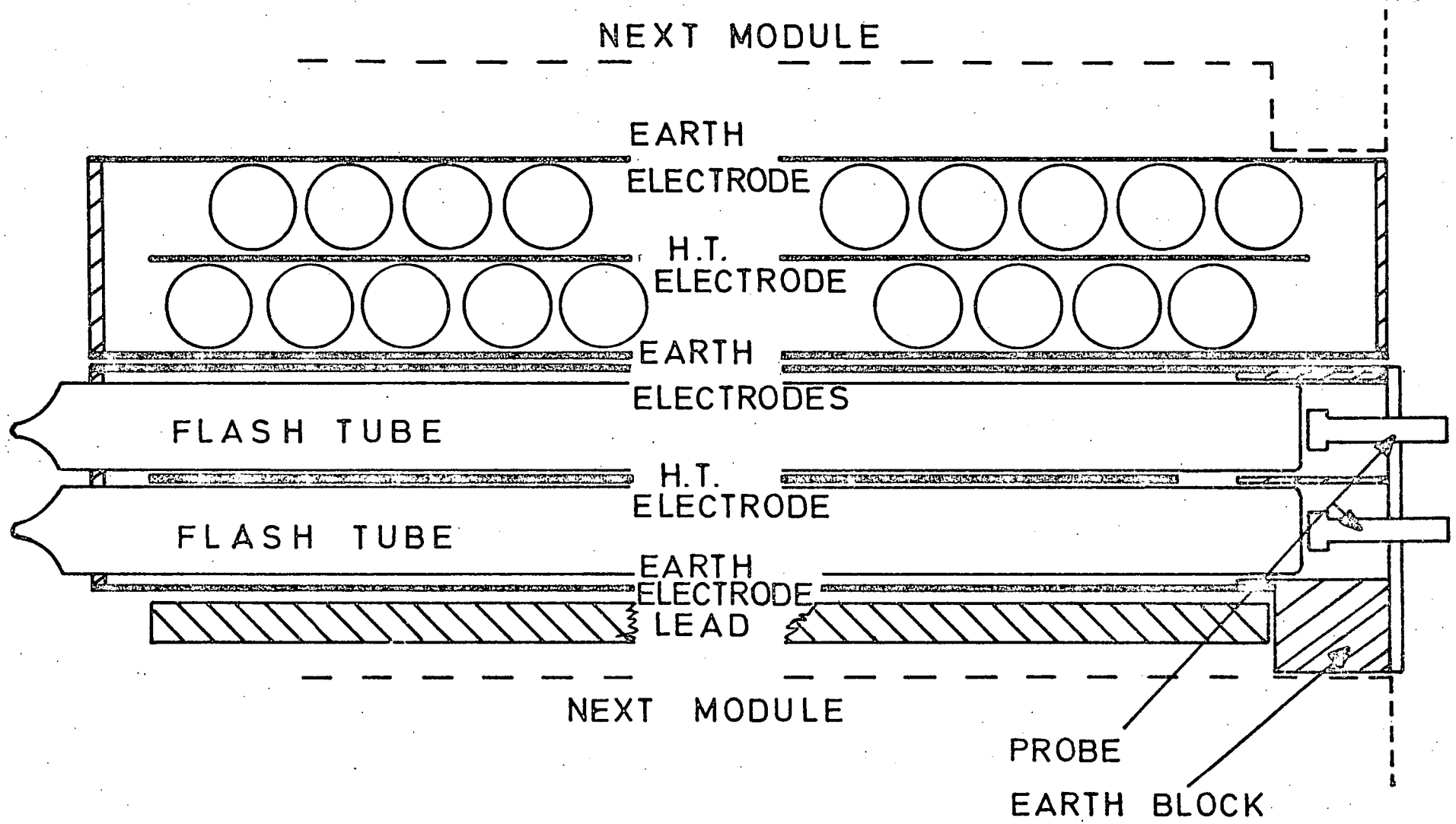

FIGURE 5.1 A SAMPLING PLANE

systems were adopted which represented a considerable improvement upon the method used in the high pressure chamber, and are described below.

(1) Eight layers of flash tubes, of the type described in Table 5.1, containing eight tubes per layer, arranged in two orthogonal sets of four staggered layers, were placed immediately in front of the first layer of target material, where the apex of the shower is located. These layers of flash tubes are referred to as the apex planes. The total sensitive area of the apex planes amounted to 16 cm square. Since it is necessary to define single tracks in these apex planes, the probability of showering must be kept to a minimum. All apex plane electrodes were manufactured from 1 mm aluminium sheet, as opposed to the 2 mm sheet used in the shower modules. The total amount of inert material amounted to 0.28 radiation lengths in the apex modules.

(2) Six drift chambers, each containing two drift cells, were arranged in 3 sets of two orthogonal layers, to resolve the left-right ambiguity and provide X-Y co-ordinates for the incident particle. The drift length of 26 mm resulted in a detection area of 130 mm x 130 mm, but due to the staggered configuration the area in which tracks could be uniquely defined was 78 mm x 78 mm.

The drift chambers were of a novel design[3], the cathode wires being etched on each side of a copper coated printed circuit board. The etched field wires on each side of the board being orthogonal, such that adjacent chambers (one in the X and one in the Y plane) share the same board, resulting in a low mass, simple configuration which reduces the likelihood of scattering. The total amount of inert material amounted to 0.05 radiation lengths.

It was intended not only to utilise the spatial information provided

by these chambers, but also to investigate their performance under the more convenient conditions of a particle beam, (as opposed to a radio active source). Hence the geometry of the system of chambers was not optimised solely for the requirements of the shower detector, (the chambers being closely stacked resulting in a poor lever arm and hence angular resolution).

The assembly of drift chambers was mounted immediately in front of the apex planes as shown schematically in Figure 5.2 and the photograph in Figure 5.3. The performance of the drift chambers and apex planes, and the manner in which their spatial information was employed is given in section 5.7.2.

The whole assembly of shower modules, apex planes and drift chambers, shown schematically in Figure 5.2., was supported in a steel framework, clad in aluminium sheet to prevent electrical interference from the high voltage pulsing system. The complete detector system, minus the aluminium sides is shown in Figure 5.3.

5.3 ELECTRONIC CIRCUITS, TRIGGER LOGIC AND DATA ACQUISITION SYSTEM

5.3.1 H.T.Pulsing and Clearing Field System

The flash tubes were fired by means of a high voltage pulse, of the RC decay type, applied to the HT electrode. This pulse was formed by the circuit shown in Figure 5.4, the switching was achieved by means of a hydrogen thyratron (English Electric CX 1157). The characteristics of the RC pulse are given in Table 5.2, and refer to the pulse used whilst taking data at a low event rate. For other operating conditions the pulse was changed accordingly.

FIGURE 5.2 SCHEMATIC VIEW OF ASSEMBLED DETECTOR

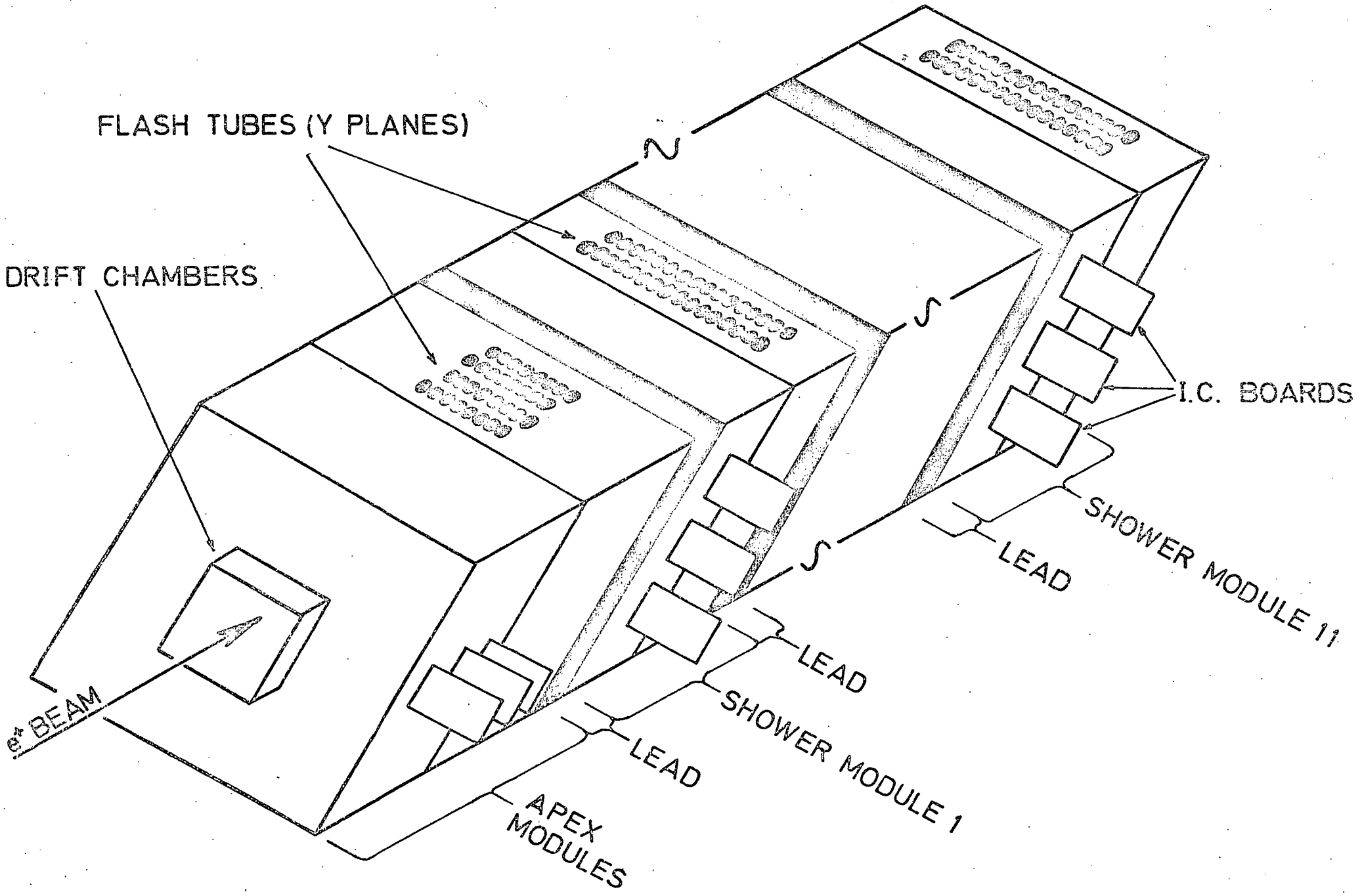

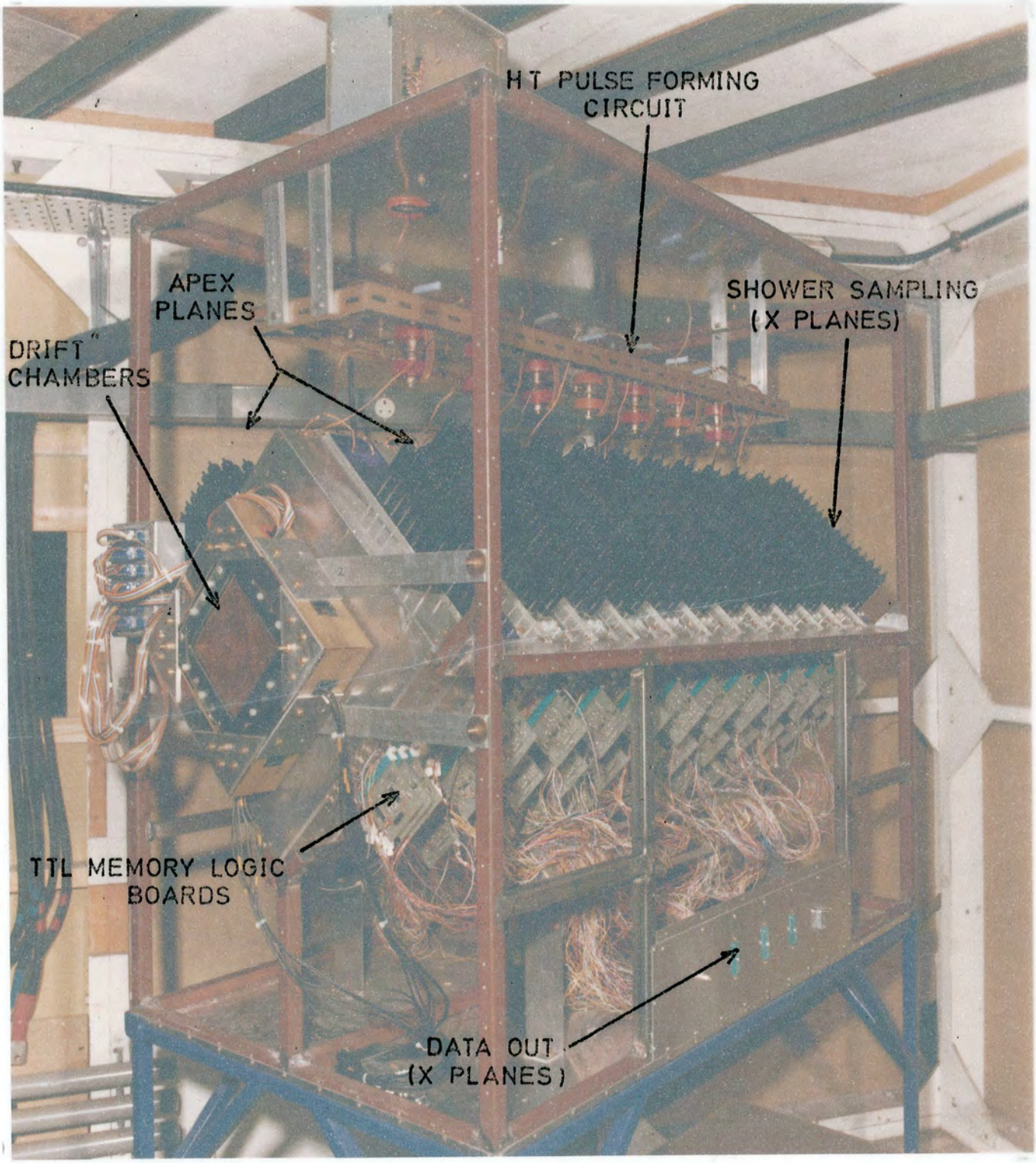

FIGURE 5.3 ASSEMBLED DETECTOR WITH SIDE PANELS REMOVED

PHOTO DNPH

TABLE 5.2 : Characteristics of the High Voltage Pulse

Peak Field (kV/Cm)	Decay Constant (μs)	Rise Time (ns)	Delay (ns)
4.75	2.0	80	400

Since the number and type of module supplied by each 6000 pf capacitor, shown in Figure 5.4, varied, it was necessary to incorporate a damping resistor to ensure that the pulse characteristics were identical for each module. Without this damping resistor a large spike and excessive ringing of the HT pulse occurred in some modules.

To ensure a short sensitive time, a square wave clearing field of frequency 100 Hz, magnitude $\pm$ 30 V/Cm was applied as shown in Figure 5.4.

5.3.2 Output Digitisation

A flashed tube was recorded by means of a digitisation probe[4]. This probe consisted of a brass M6 screw, whose head was placed in contact with the plane end of the flash tube. Figure 5.5 shows the dependence of the digitisation pulse height upon the applied field for 3 probe sizes, at an event rate of 50 sec^{-1}. It can be seen that for the particular probe size (11 mm) and applied field (4.75 kV/Cm) chosen, the digitisation pulse height obtained across the 5.6 kΩ input impedance of the TTL memory logic remains well above the threshold of 4 V required to set the latches.

As with the detector employing high pressure flash tubes, the data acquisition system required that the information concerning whether a tube

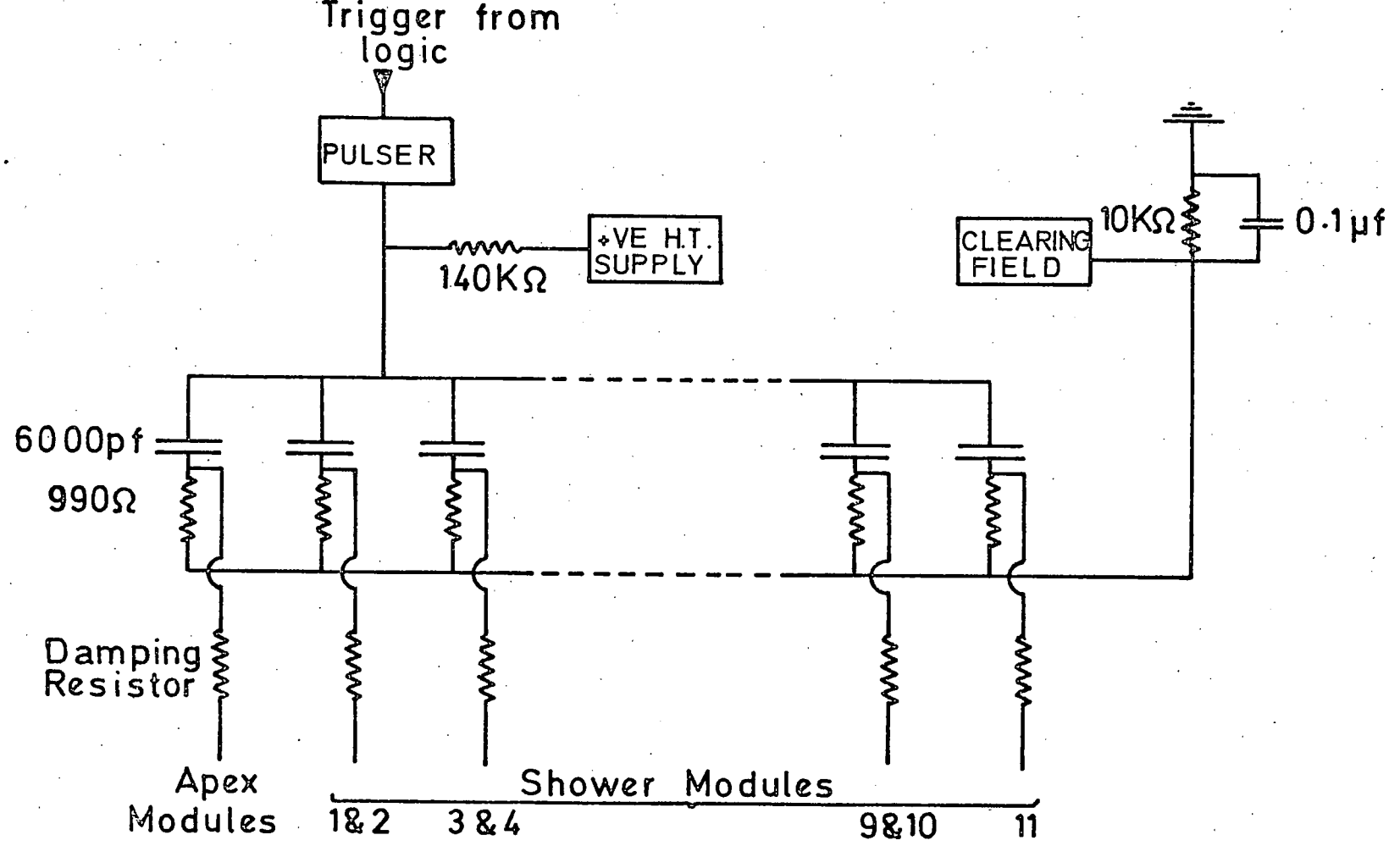

FIGURE 5.4 HIGH VOLTAGE PULSING AND CLEARING FIELD CIRCUITS

FIGURE 5.5 Variation of pulse height with applied field for 3 disc sizes

Flashing rate 50/sec

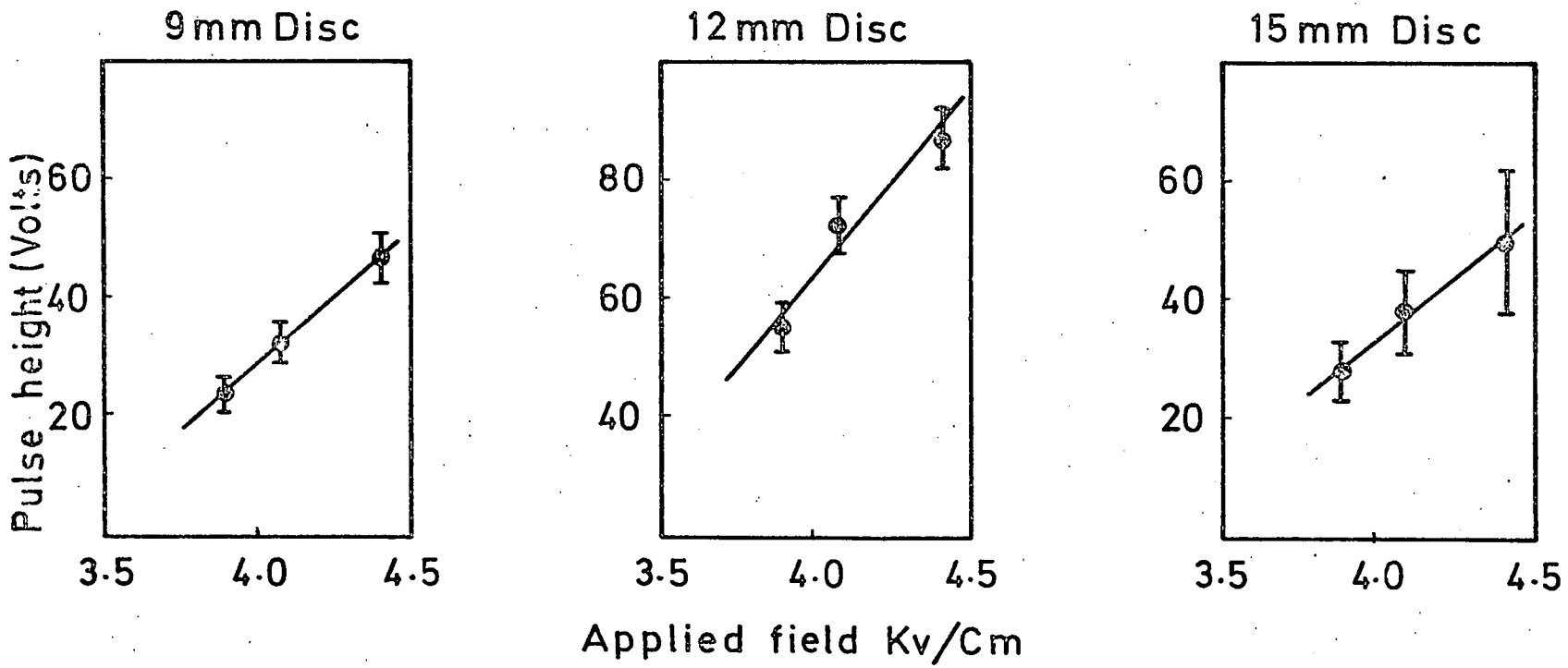

flashed or not should be temporarily stored before processing by the on-line computer. This was achieved by means of TTL latches as described in 3.3.1. The latches required to service the 64 tubes of each sampling module were mounted on 6 printed circuit boards, as seen in the photograph in Figure 5.3.

5.3.3 Trigger Logic and Data Acquisition System

As with the previous detector tests were conducted using the NINA electron synchrotron test beam facility at the Daresbury Laboratory, as a source of mono-energetic positrons. The trigger logic and data acquisition system is shown in Figure 5.6. The complete cycle of the data acquisition system for one event is described below.

(1) A NINA minimum field pulse is received at the time of injection. After a delay, determined by the energy at which it is wished to extract the positrons, a "window" of 2 ms is set. Should a coincidence of the scintillations $S_1 \rightarrow S_4$ occur within this window, it is taken as evidence that a positron of known energy has passed into the detector.

(2) The interrupt register in CAMAC is disabled against receiving further information.

(3) A start pulse is sent to the drift chamber T.D.C's.

(4) A trigger is sent to the high voltage pulsing system, approximately 400 ns has passed since the initial coincidence was received.

(5) After a delay of approximately 10 μs, to allow the high voltage pulse and its effects to die away, the status of the latches is read via 6 x 132 way cables by 3 x 256 bit CAMAC input registers into the PDP 11-05 computer where it is temporarily buffered, along with the TDC data.

(6) The digitisation latches are reset and the TDC's cleared in readiness for the next event.

TRIGGER LOGIC AND DATA AQUISITION

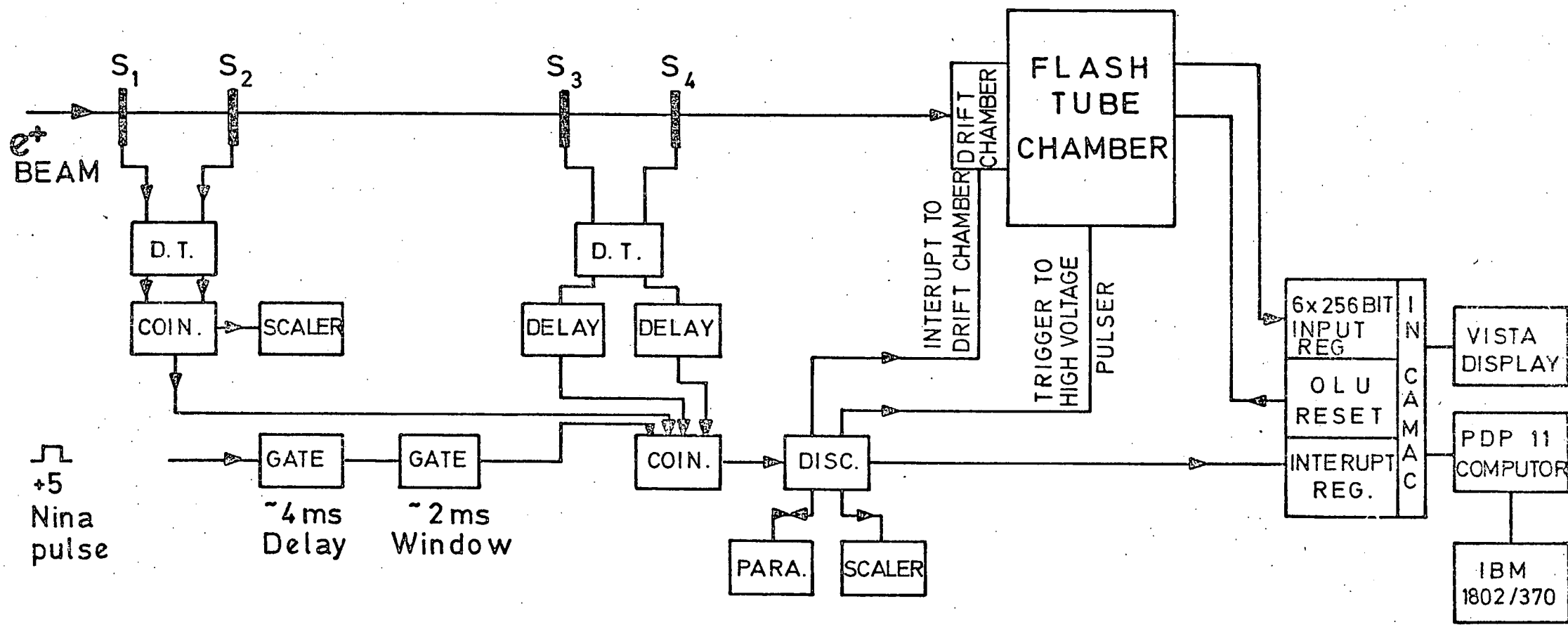

FIGURE 5.6

(7) The data for the event is sent down the data link, where it is stored on disc in the IBM 370 computer.

(8) The paralysis is removed from the interrupt register, ready for the next event.

The program controlling the above sequence of events was written in a language called CATY[5], which is primarily designed for testing CAMAC systems. Although it is a simple and convenient language for this purpose, it is rather slow for data acquisition requirements. Because of this, although the detector may be operating at a high event rate, the speed at which the computer is able to "process" events is determined by the cycle time of the program. For example, although the maximum rate at which the chamber was operated was 50 events sec^{-1}, the rate at which the program could handle data was 30 events sec^{-1}. This meant that the computer ignored 40% of the available events, however no bias could exist at to which events were written to disc, and the data was unaffected statistically.

5.4 OPERATION OF THE DETECTOR IN THE POSITRON BEAM

Before the detectors performance as a shower counter could be ascertained it is first necessary to determine the fundamental requirements such as field strength, rise times etc., necessary to ensure efficient operation of the flash tubes. Also, all spurious and inefficient tubes must be replaced and a check made of the sensitive and recovery times of the flash tubes. This setting up of the detector in the positron beamline is described below.

5.4.1 HT Plateau and Module Efficiencies

The most convenient way in which to determine the efficiency of the detector is to remove the lead target and measure the ability to detect straight through single particle tracks. The efficiency of the i^{th} layer

being given by

$$\sigma_i = \frac{\text{total number of ignitions in } i^{th} \text{ layer}}{\text{Total number of events}}$$

However, the amount of inert material in the detector is approximately 2.4 radiation lengths and therefore the probability of a particle passing through the detector, without initiating a shower,is small. Once a shower has occurred the probability of finding a flashed tube in subsequent layers is greatly increased, resulting in an artificially high estimate of the efficiency of that module. This can be seen in Figure 5.7, where the efficiency of the modules is seen to rise towards the rear of the detector. To overcome this problem, it was decided to take the 64 tubes of the apex planes in which the probability of showering is much reduced, as a representative sample of the total 768 tubes.

In this manner the HT plateau shown in Figure 5.8 was obtained, and a field of 4.75 kV/Cm was chosen for efficient operation.

Plots of the beam profile at each sampling plane, obtained for a large number of events (approximately 2000), revealed the presence of spurious or inefficient tubes by way of spikes or holes in an otherwise smooth distribution. These defective tubes were replaced.

5.4.2 Determination of Sensitive Time

The sensitive time is defined as that time between the passage of a particle through a flash tube and the application of the HT pulse, for which the internal efficiency falls to 50%. For the tubes used in the present experiment this represents a layer efficiency of approximately 40%.

By means of a gate generator, a variable delay could be introduced between the fourfold coincidence and the triggering of the high voltage pulse. For each delay approximately 1000 events were taken at a rate

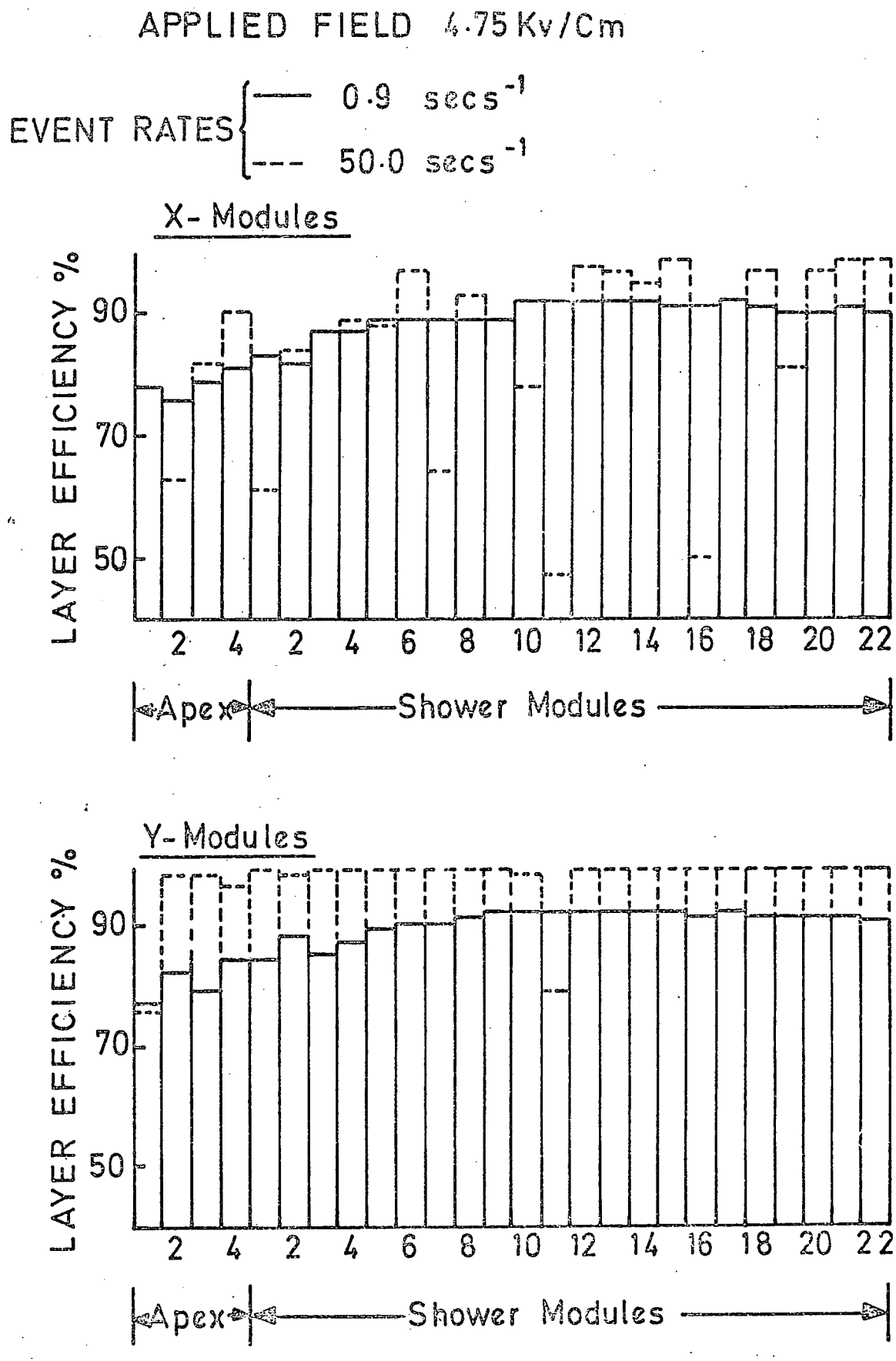

FIGURE 5.7 LAYER EFFICIENCY FOR MODULES FOR 2 RATES

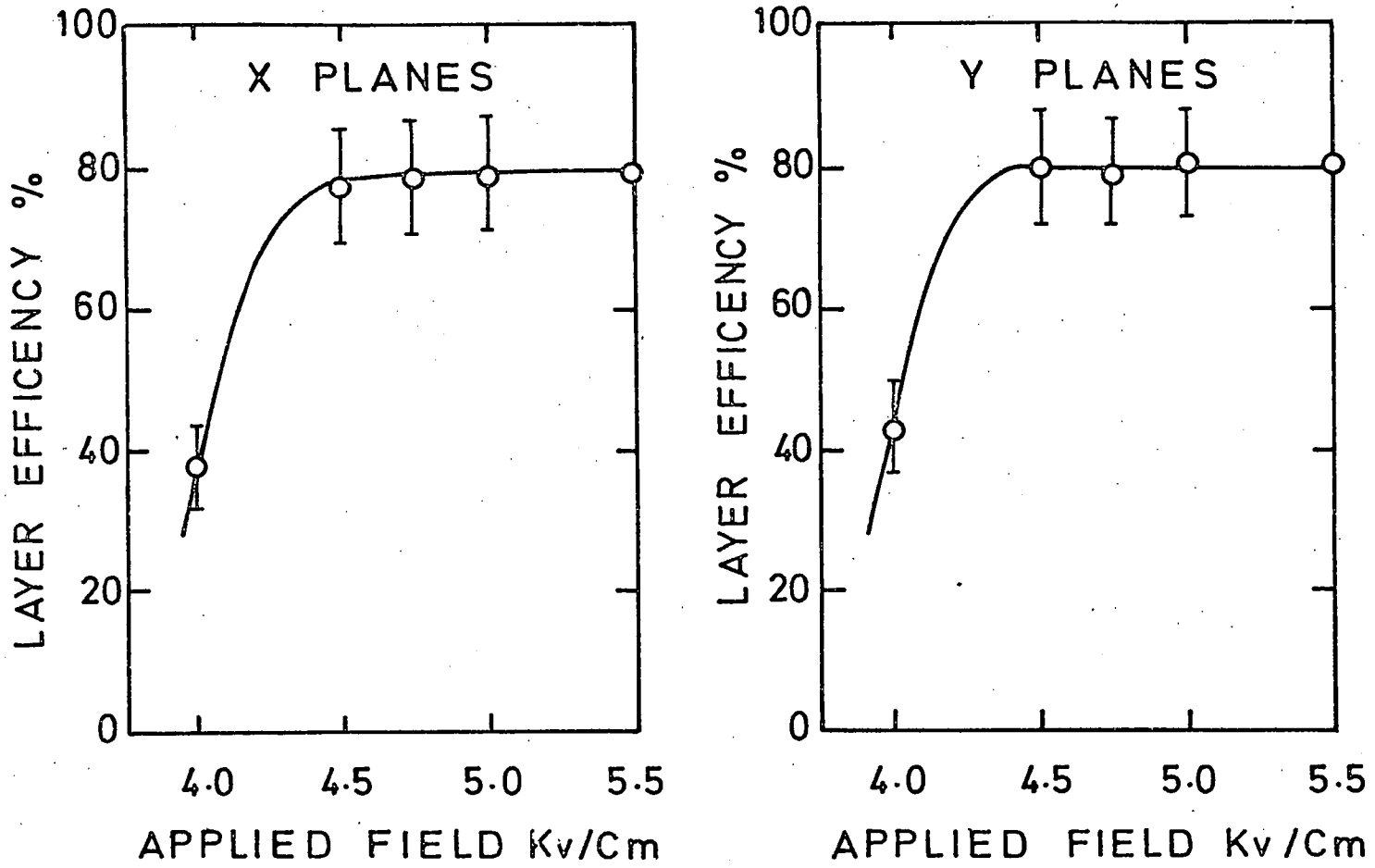

FIGURE 5.8 LAYER EFFICIENCY AS A FUNCTION OF APPLIED FIELD

of 10 events min^{-1}. The results are shown in Figure 5.9, and by the above definition a sensitive time of 3.0 μs is obtained. This is in good agreement with the results of other workers.

During these tests a square wave clearing field of frequency 100 Hz, magnitude ± 30 V/Cm was applied across the tubes.

5.4.3 Determination of Recovery Time

The recovery time is defined as that period of time necessary between the flashing of the tube and the application of a second high voltage pulse, for the probability of spurious reignition to fall to 50%.

A simple program was written using CATY and is outlined in Figure 5.10. Due to the speed of the CATY program, and the short time interval between successive HT pulses, it was only possible to handle limited quantities of data,for this reason only the behaviour of the X planes was studied.

Because of the short time delays between the first and second pulse, care had to be taken to ensure that the output of the power supply, at the time of applying the second pulse, did not fall below the value required to ensure efficient operation of the tubes. The output of the power supply was matched to the pulse forming network by insertion of a series resistor in the charging line. The optimum value of this resistor was found empirically to be 138 kΩ.

The detector was operated at an event rate of 10 min^{-1}, and a minimum of 100 events recorded for each value of delay between the 1st and 2nd HT pulse. The results are given in Figure 5.11, giving a recovery time of 7 ms, a factor of 12 greater than that of the earlier workers[1].

The method used here to determine the recovery time is considered superior to that used for previous measurements[6], since it allows the

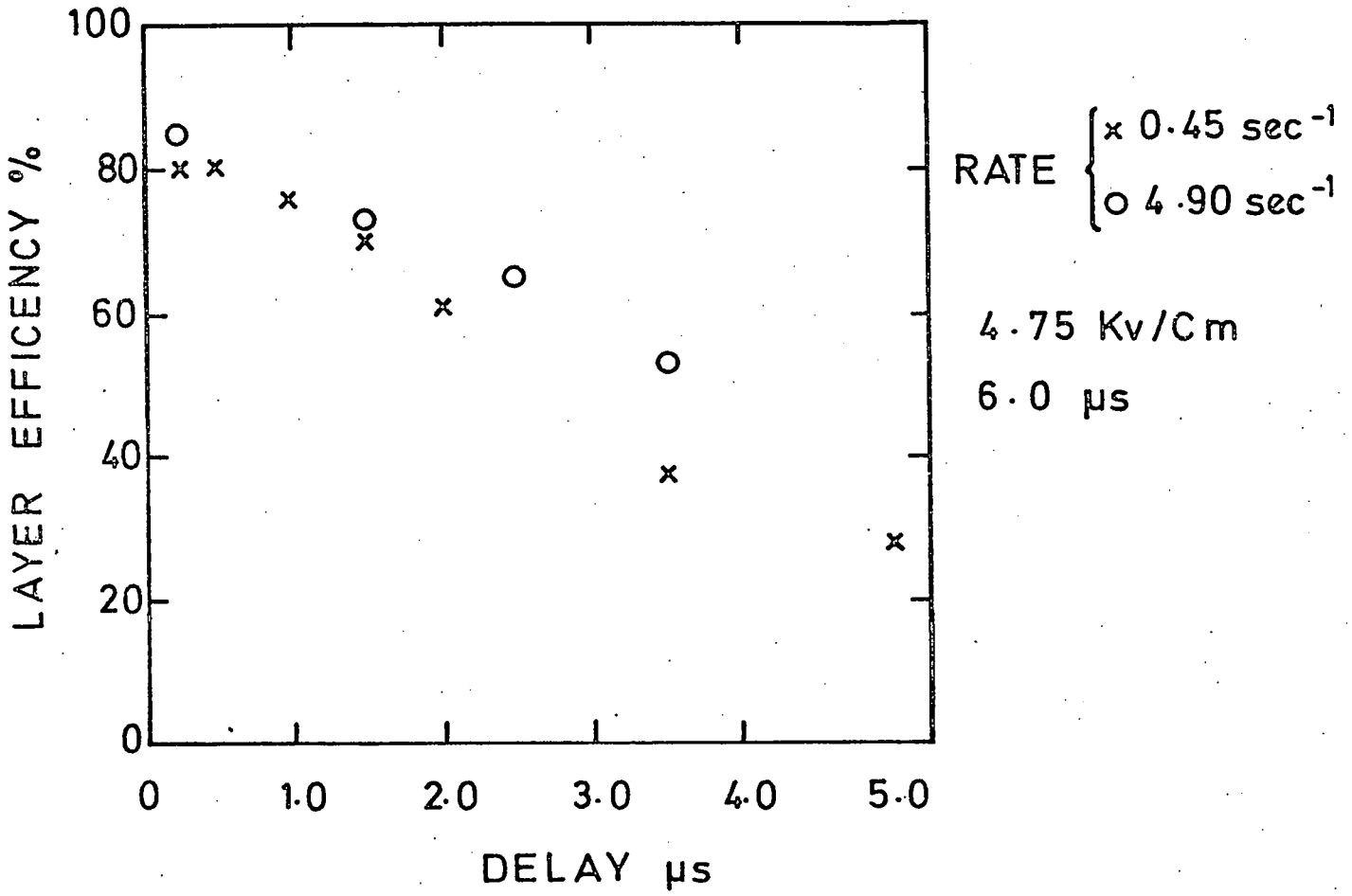

FIGURE 5.9 SENSITIVE TIME FOR 2 RATES

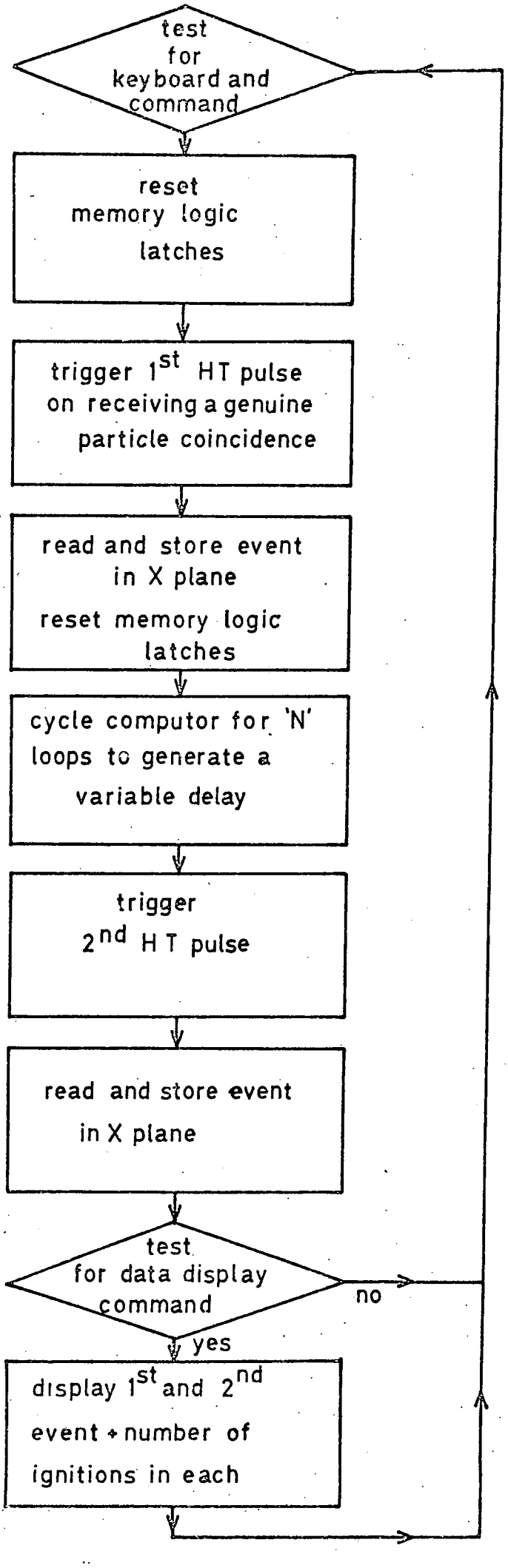

FIGURE 5.10 FLOW DIAGRAM OF THE PROGRAM USED IN THE DETERMINATION OF THE RECOVERY TIME

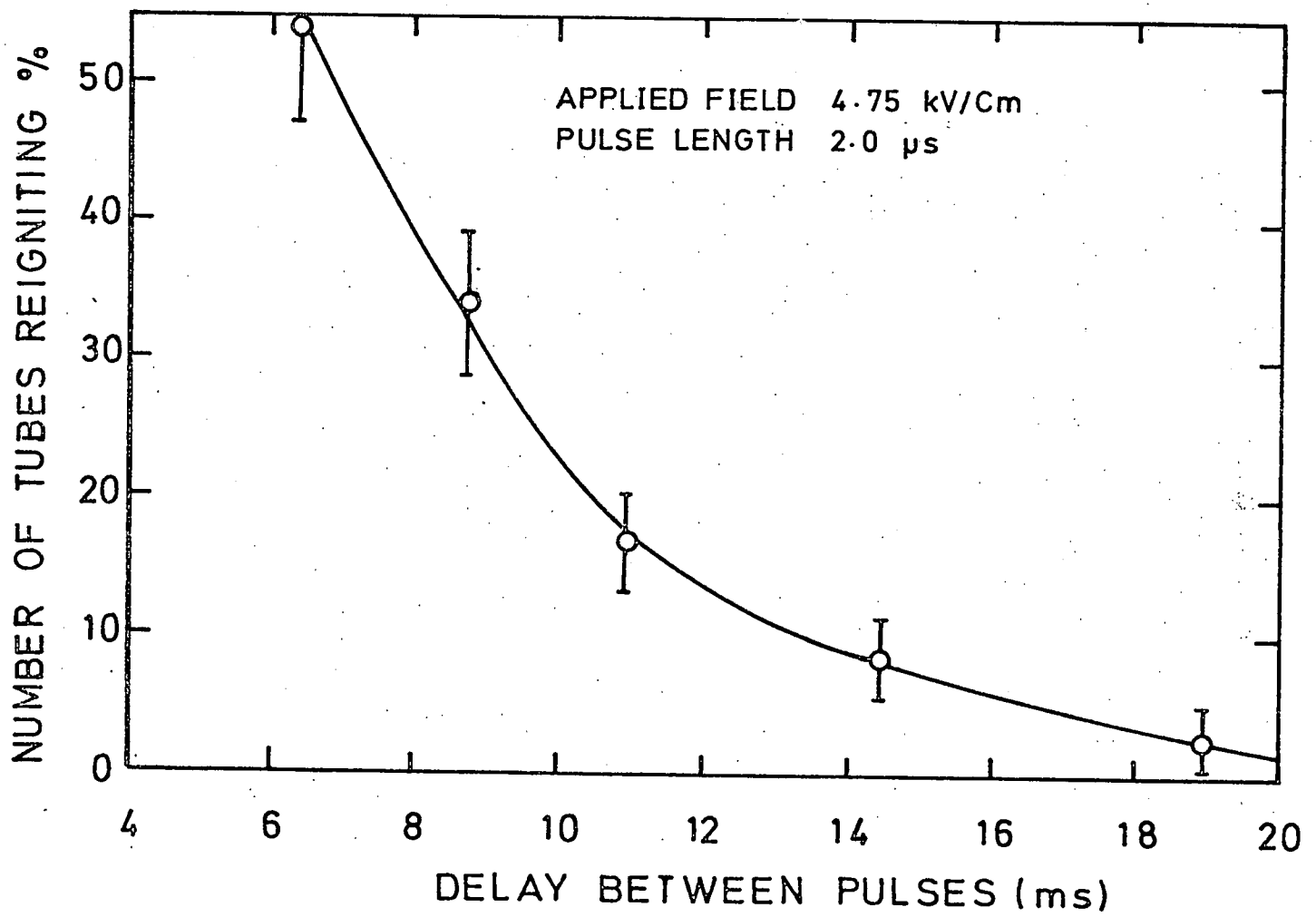

FIGURE 5.11 RECOVERY TIME AT AN EVENT RATE OF 10 min^{-1}

study of reignition patterns of individual events, and those events where an ionising particle passed through the detector immediately before, or during the application of the 2nd HT pulse may be easily identified and rejected.

5.5 ELECTROMAGNETIC SHOWER PARAMETERS RECORDED BY THE DETECTOR

As explained in section 4.2, a comparison of the major parameters of the electromagnetic shower recorded by the detector, with those predicted by theory, can be of assistance in understanding the behaviour of the detector since both the energy and spatial measurements rely on a uniform response to charges in both the number and the distribution of the shower secondaries.

Shower data was taken using positrons in the energy range 0.5 to 3.5 GeV, 0.6, 1.2, 1.8 and 2.4 radiation lengths of lead, and 0.5 radiation lengths of iron being used as target material. For each energy-target configuration approximately 2000 events were taken at a rate of 10 events min^{-1}. The principal parameters relating to the number and distribution of the shower secondaries are the transition curve, the position of the shower maxima and the attenuation coefficient of the shower tail.

Figure 5.12 shows both the experimental and theoretical transition curves ; obtained for 3 primary energies in lead. The theoretical curves are obtained from the Monte Carlo simulations of Messel and Crawford[7] for a threshold level of 2 MeV. The data from the detector has been presented in two forms. Firstly, the average number of flash tube ignitions in a single layer of tubes has been plotted as a function of target thickness preceeding the layer. The discrepancy between theory and experiment is a factor of approximately 2 worse than that occurring with high pressure tubes,

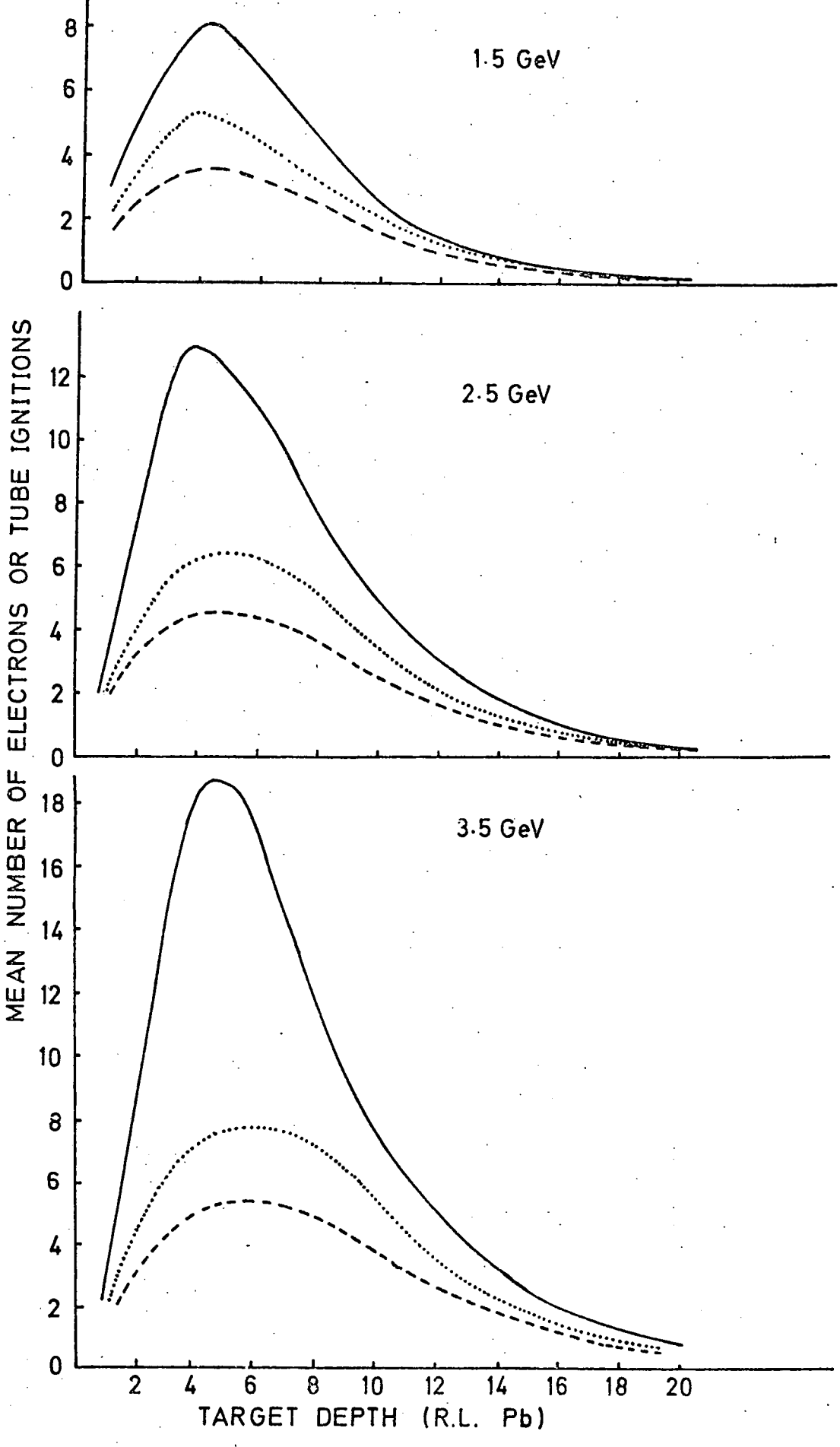

- - - - - PRESENT EXPERIMENT

..... CORRECTED DATA

——— THEORY

FIGURE 5·12 SHOWER TRANSITION CURVES IN LEAD

which reflects the inability with increasing diameter to resolve individual particles in dense showers. The dotted curve represents the data corrected for this finite spatial resolution. The relationship used to correct the data (see Appendix 1), assumes a uniform flux crossing the layer of tubes. It can be seen from the deviation between theory and the corrected data that only at large target depths and low primary energy does this assumption start to become valid.

The position of the shower maximum, defined as the target depth at which the probability of finding a secondary is greatest, is shown in Figure 5.13. It can be seen that the results obtained using lead target agree with the theory at low energies but deviate towards greater target depth with increasing energy. This again is due to the dependence of the flash tubes ability to resolve individual particles, upon the particle density, which, coupled with the fact that the shower secondaries lie on average within a cone, results in the peak number of tube ignitions, (which is a function not only of the number of particles, but also their density) occurring at greater target depth. The experimental results of Backenstoss et al[8], obtained using scintillator sampling in iron are included in Figure 5.13 for comparison with the data obtained from the present detector using iron target. The positions of the shower maxima for various primary energies in lead and iron are given in Table **5.3**.

TABLE 5.3 : Shower Maxima and Attenuation Coefficients

Energy (GeV)	Position of Shower Maxima (R.L.)		Attenuation Coefficient ($R.L^{-1}$)	
	Lead	Iron	Lead	Iron
0.5	2.6 ± 0.3	1.7 ± 0.1	0.27	0.40
1.5	4.2 ± 0.4	3.3 ± 0.3	0.26	0.30
2.5	5.0 ± 0.4	4.2 ± 0.3	0.24	0.30
3.5	5.4 ± 0.4	5.0 ± 0.4	0.24	0.29

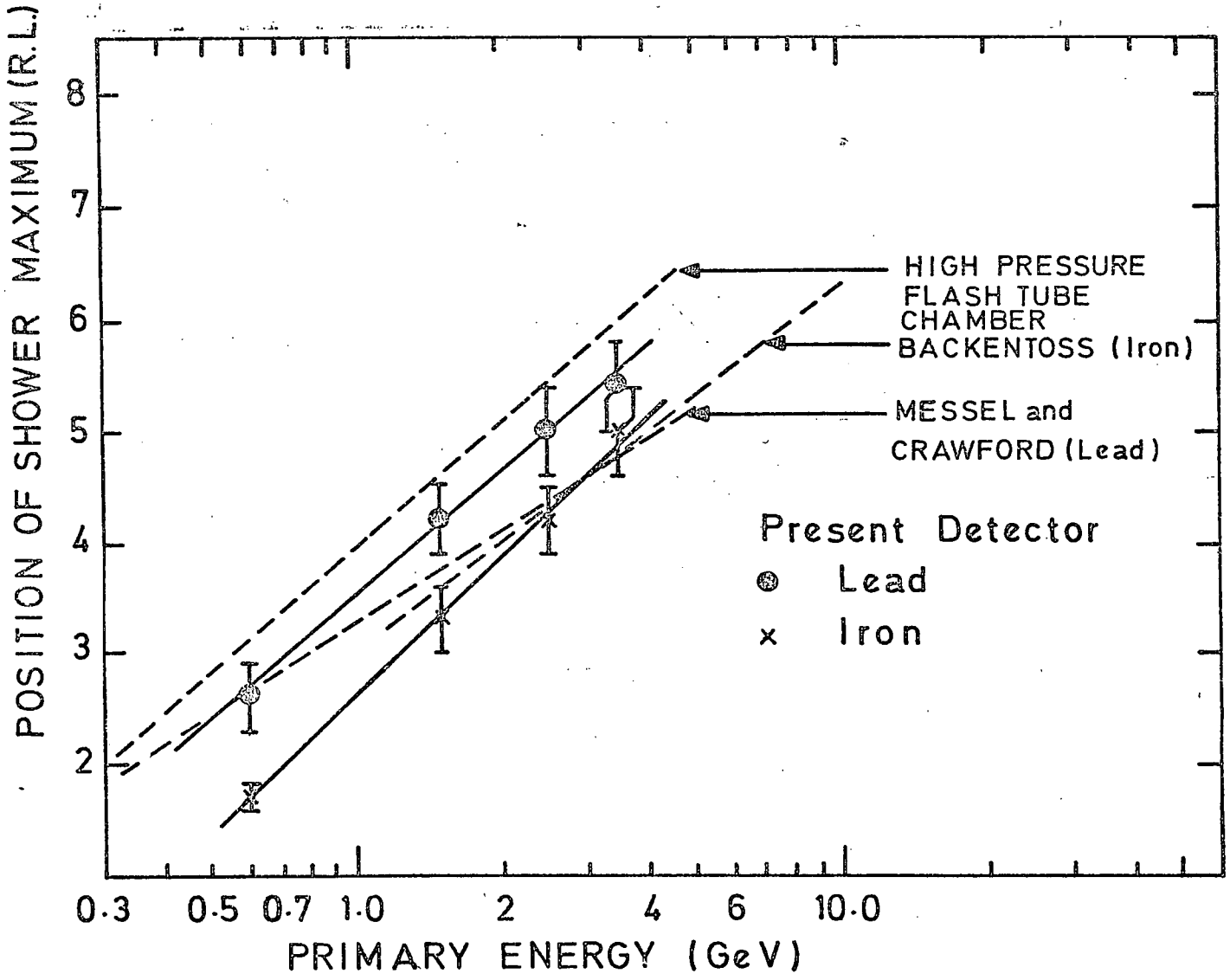

FIGURE 5·13 POSITION OF SHOWER MAXIMUM AS A FUNCTION OF ENERGY

Also given in Table 5.3 are the attenuation coefficients obtained for various energies in lead and iron by means of a least squares fit to the data points beyond the shower maximum. The decrease of the attenuation coefficient with increasing energy again results from the poor resolving powers of the flash tubes. However, the values of the attenuation coefficient at 0.5 GeV, where the effect of particle density is not excessive, are in good agreement with the values given by Siegbahn[9] of 0.27 and 0.42 R.L.$^{-1}$ for lead and iron respectively.

5.6 ENERGY MEASUREMENT

The primary energy is determined in the same manner as for the previous detector, the mean number of flashed tubes being taken as a measure of the number of shower secondaries, which is proportional to the primary energy. The number of flashed tubes may deviate considerably from the number of secondary particles in the shower, due to failure to contain the shower within the volume of the detector and the inability of the flash tube to resolve individual particles in dense showers as shown in section 5.5. These defects result in an under-estimation of the number of secondaries with increasing energy.

An indication of the longitudinal shower loss using 0.6, 1.2 and 1.8 radiation lengths of lead is given in Figure 5.14. It can be seen that even at 0.5 GeV, using 0.6 R.L. lead, a considerable portion of the shower escapes from the rear of the detector. Containment can be assured by the use of thicker target, 1.8 R.L. lead almost completely contains a 3.5 GeV shower. However, the use of thicker target results in greater statistical fluctuations in the number of shower secondaries, and therefore may not necessarily mean an improved resolution. Losses also occur in the lateral direction, but are small compared to the longitudinal loss, as can

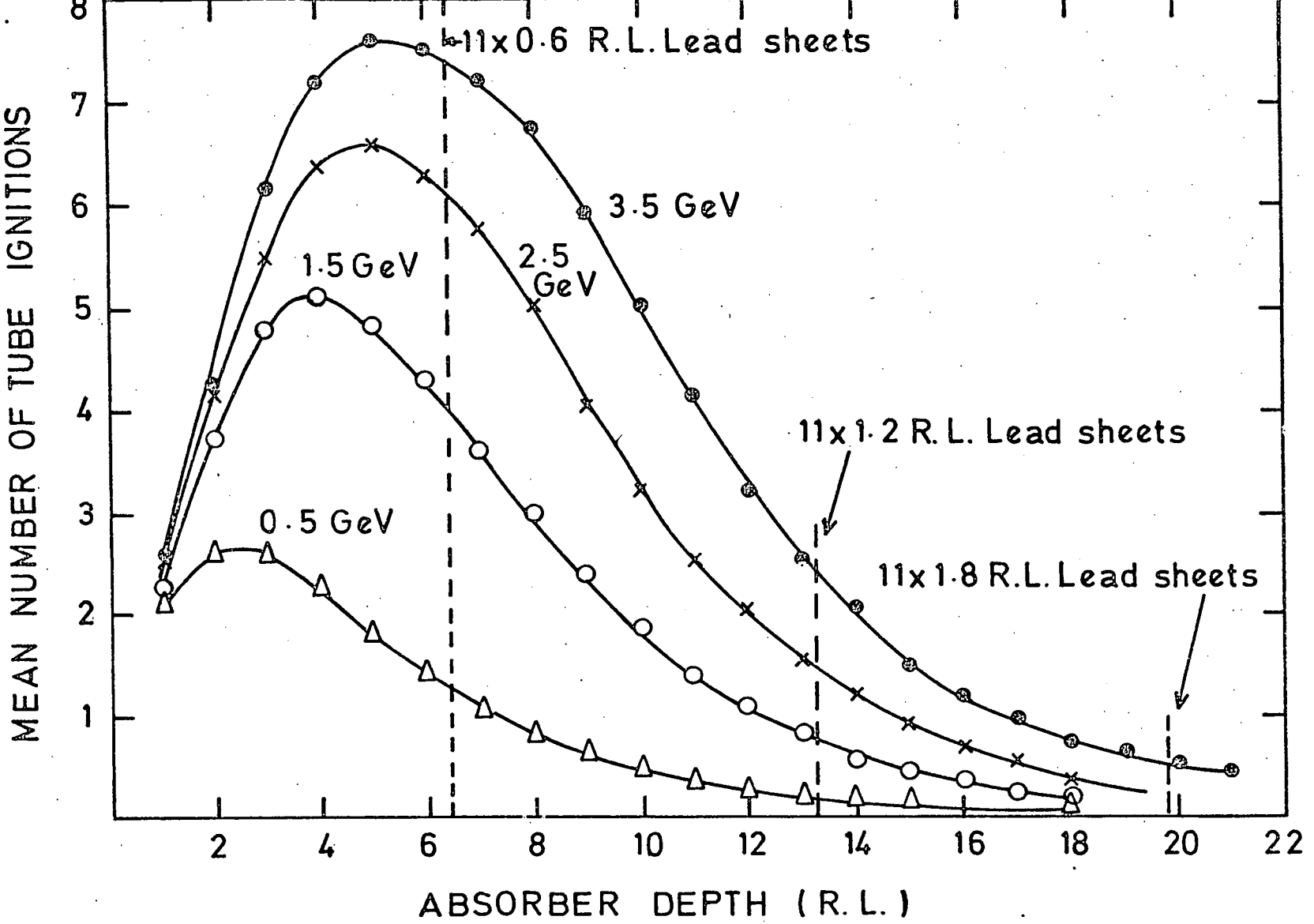

FIGURE 5·14 LONGITUDINAL SHOWER SHAPES AND TOTAL ABSORBER THICKNESS USING 0·6, 1·2 AND 1·8 R.L. LEAD

be seen from Figure 5.15, which shows the shower shapes obtained at 3.5 GeV using 0.6 R.L. lead target, the worse energy-target configuration as regards shower containment. Table 5.4 shows the percentage of shower contained within the detector for various target thickness and energy. The number of tube ignitions as a function of energy corrected for shower loss gives a closer approximation to the linear relationship predicted by theory.

TABLE 5.4: Percentage of Longitudinal Shower Leakage

Target (R.L.pb)	Energy (GeV)	Number of Tube Ignitions	Percentage of Shower Contained	Number of Ignitions Corrected for Loss
0.6	0.5	25.5	76.8	32.2
	1.5	56.0	69.3	80.8
	2.5	75.7	56.3	134.4
	3.5	89.9	48.8	184.2
1.2	0.5	40.3	96.0	41.9
	1.5	67.1	93.9	71.5
	2.5	97.4	92.4	105.4
	3.5	123.2	89.8	137.2

The remaining deviation from linearity is primarily due to the poor individual electron sensitivity of the large diameter tubes. The sensitivity of a single layer of flash tubes at various target depths and primary energy is shown in Table 5.5. The inverse relationship between sensitivity and the number of particles crossing the layer can be clearly seen. The sensitivity falling to a minimum at the target depth corresponding to the position of the shower maxima.

The choice of two staggered layers of tubes for the X and Y sampling elements eliminates the insensitive volume due to the thickness

TABLE 5.5 : Individual Electron Sensitivity of a Layer of Flash Tubes as a Function of Energy For Various Target Thickness

Target Thickness R.L. Pb	Target Depth R.L. Pb	Individual Electron Sensitivity (%)			
		0.5 GeV	1.5 GeV	2.5 GeV	3.5 GeV
	1.0	98.1	91.2	90.7	80.3
	1.8	84.2	69.1	61.6	54.9
	2.6	76.7	61.7	48.0	40.6
	3.4	68.0	52.6	43.5	26.1
	4.2	67.1	48.6	40.5	33.4
0.6	5.0	66.5	51.4	45.4	38.2
	5.8	64.6	51.1	44.3	34.1
	6.6	61.6	53.6	51.5	40.7
	7.4	57.1	53.6	51.6	40.8
	8.2	53.2	52.8	50.8	42.6
	9.2	57.1	50.9	52.7	42.7
	2.2	81.7	73.1	66.1	62.7
	4.2	71.5	57.2	40.0	35.6
	6.2	75.4	53.8	44.1	34.1
	8.2	74.4	59.6	49.3	35.5
	10.2	69.6	65.7	58.1	35.0
1.8	12.2	68.4	71.6	66.7	47.7
	14.2	64.7	70.1	65.9	48.3
	16.2	46.9	67.9	65.8	50.7
	18.2	44.6	63.6	60.2	50.0
	20.2	50.0	61.7	49.3	48.6
	22.2	44.6	60.0	50.0	52.1

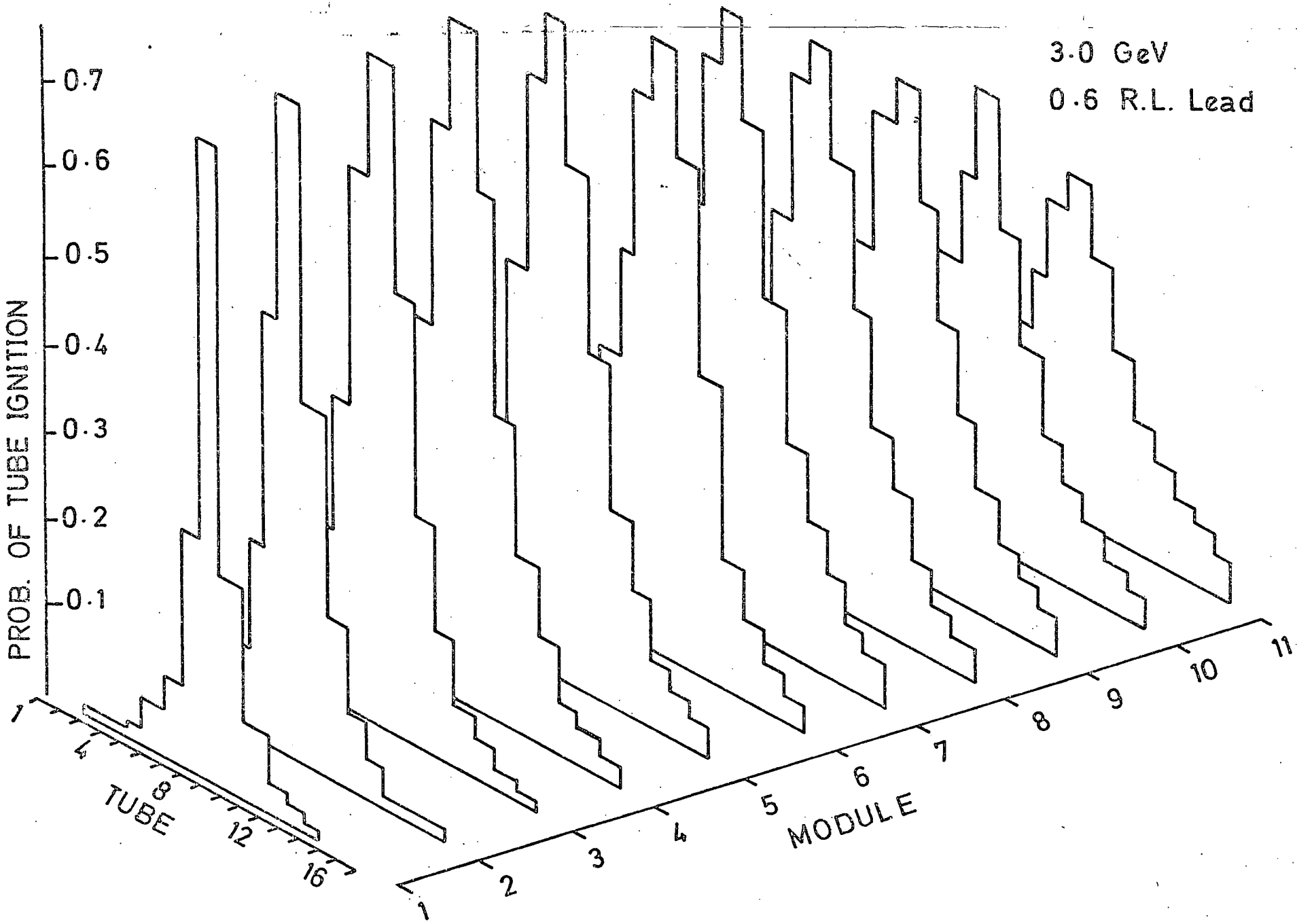

FIGURE 5·15 SHOWER DEVELOPMENT WITHIN DETECTOR

of the tube walls that occurs with a single layer of tubes. However, since the sensitive volumes of the two layers overlap, a situation may arise, particularly at low secondary particle density, where the number of flashed tubes is an overestimate of the number of secondary particles. Assuming a uniform flux, the worst possible overestimate, from pure geometrical considerations, is by a factor of 1.6. Further consideration to this problem is given in Appendix 1.

5.6.1 Energy Resolution

Since the number of tube ignitions does not remain proportional to the number of shower secondaries, and hence the primary energy, it is not possible to use the FWHM of the frequency distribution of ignited tubes as a measure of the energy resolution of the detector. The energy resolution, $^{dE}/_{E}$, was calculated using the following expression, which took account of this lack of proportionality

$$\frac{dE}{E} = \frac{N}{E} \cdot \frac{dN}{N} \cdot \frac{1}{dN/dE}$$

where : $\frac{dN}{dE}$ is the gradient of the curve, shown in Figure 5.16, of the mean number of tube ignitions as a function of energy E

dN is the FWHM of the frequency distribution of the number of tube ignitions for a particular E. Examples of these distributions are given in Figure 5.17

N is the mean number of tube ignitions for a particular E

E is the primary energy in GeV

The resolutions obtained using this relationship, for various primary energy and target are given in Table 5.6 and shown in Figure 5.18. The resolution of the detector is, in theory, expected to improve as $^{1}/\sqrt{E}$,

TABLE 5.6 : Energy Resolution Using One and Two Layers of Flash Tubes

Target Thickness (R.L.Pb)	Primary Energy (GeV)	Resolution (%)		Target Thickness (R.L.Pb)	Primary Energy (GeV)	Resolution (%)	
		2 Layers	1 Layer			2 Layers	1 Layer
0.6	0.5	57.7	63.0	1.8	0.5	72.0	70.0
	1.0	37.7	48.0		1.0	56.2	62.0
	1.5	33.3	48.0		1.5	53.7	59.0
	2.0	35.6	45.0		2.0	50.8	62.0
	2.5	37.5	55.0		2.5	46.0	64.0
	3.0	34.3	67.0		3.0	44.5	64.0
	3.5	38.7	96.0		3.5	44.3	76.0
1.2	0.5	44.9	70.0	2.4	0.5	85.3	94.0
	1.0	40.8	51.0		1.0	68.8	79.0
	1.5	41.3	52.0		1.5	53.7	66.0
	2.0	40.7	47.0		2.0	48.9	59.0
	2.5	42.2	51.0		2.5	48.8	63.0
	3.0	42.1	53.0		3.0	45.4	73.0
	3.5	40.2	68.0		3.5	46.6	64.0

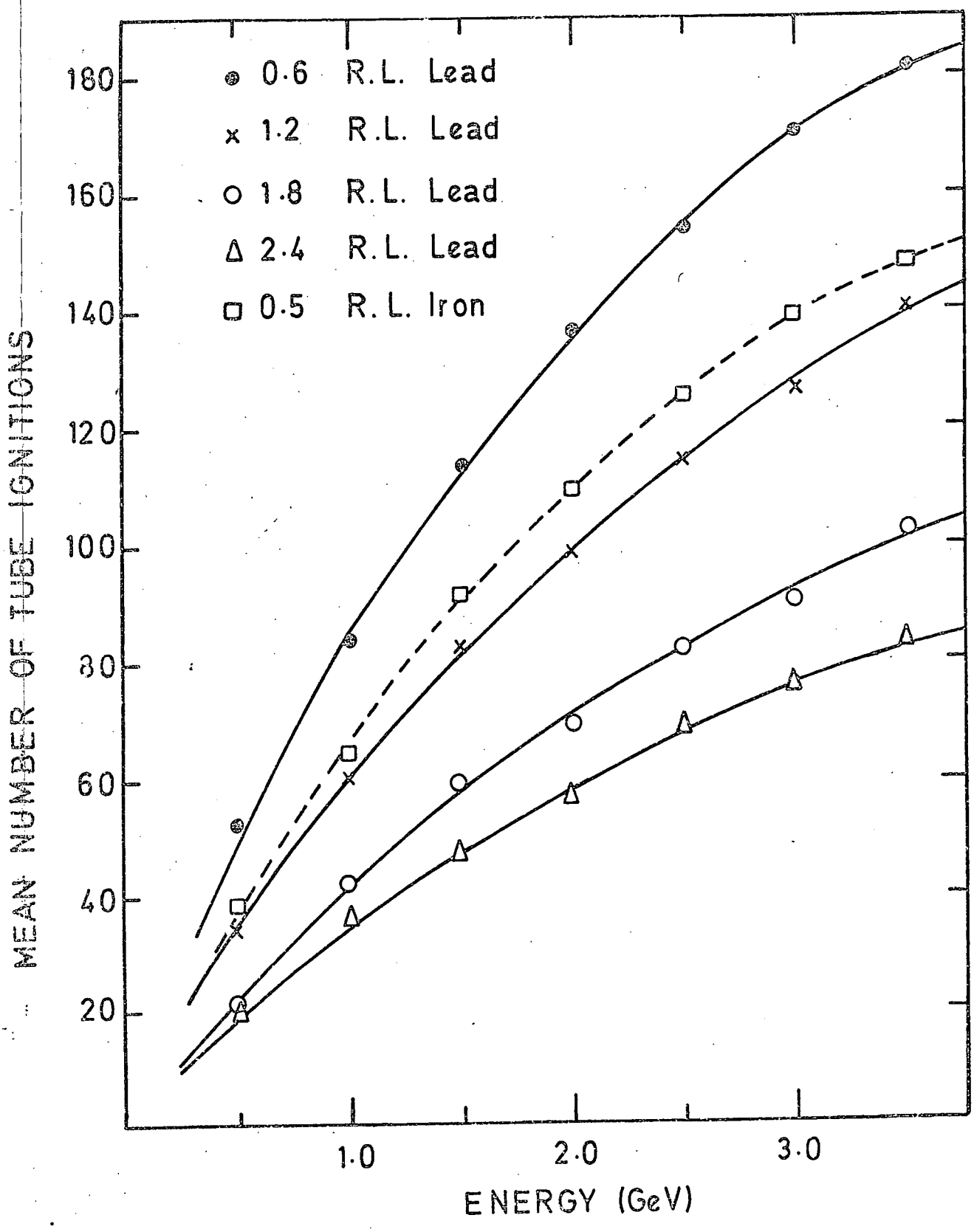

FIGURE 5.16 NUMBER OF TUBE IGNITIONS AS A FUNCTION OF ENERGY FOR VARIOUS TARGET THICKNESS (CORRECTED FOR LONGITUDINAL LOSS)

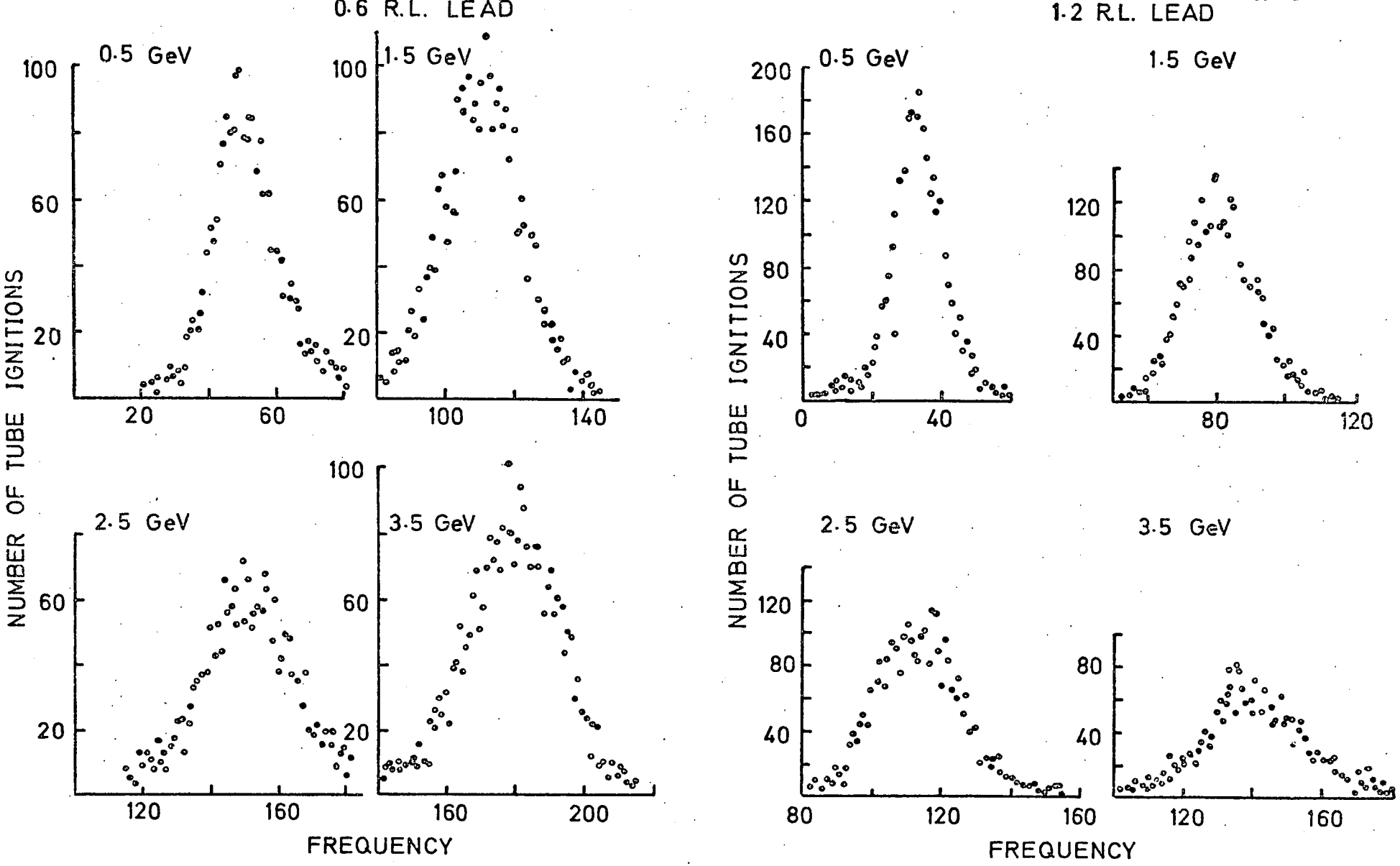

FIGURE 5.17 FREQUENCY DISTRIBUTION OF THE NUMBER OF TUBE IGNITIONS FOR TWO THICKNESS OF LEAD TARGET AND VARIOUS ENERGIES

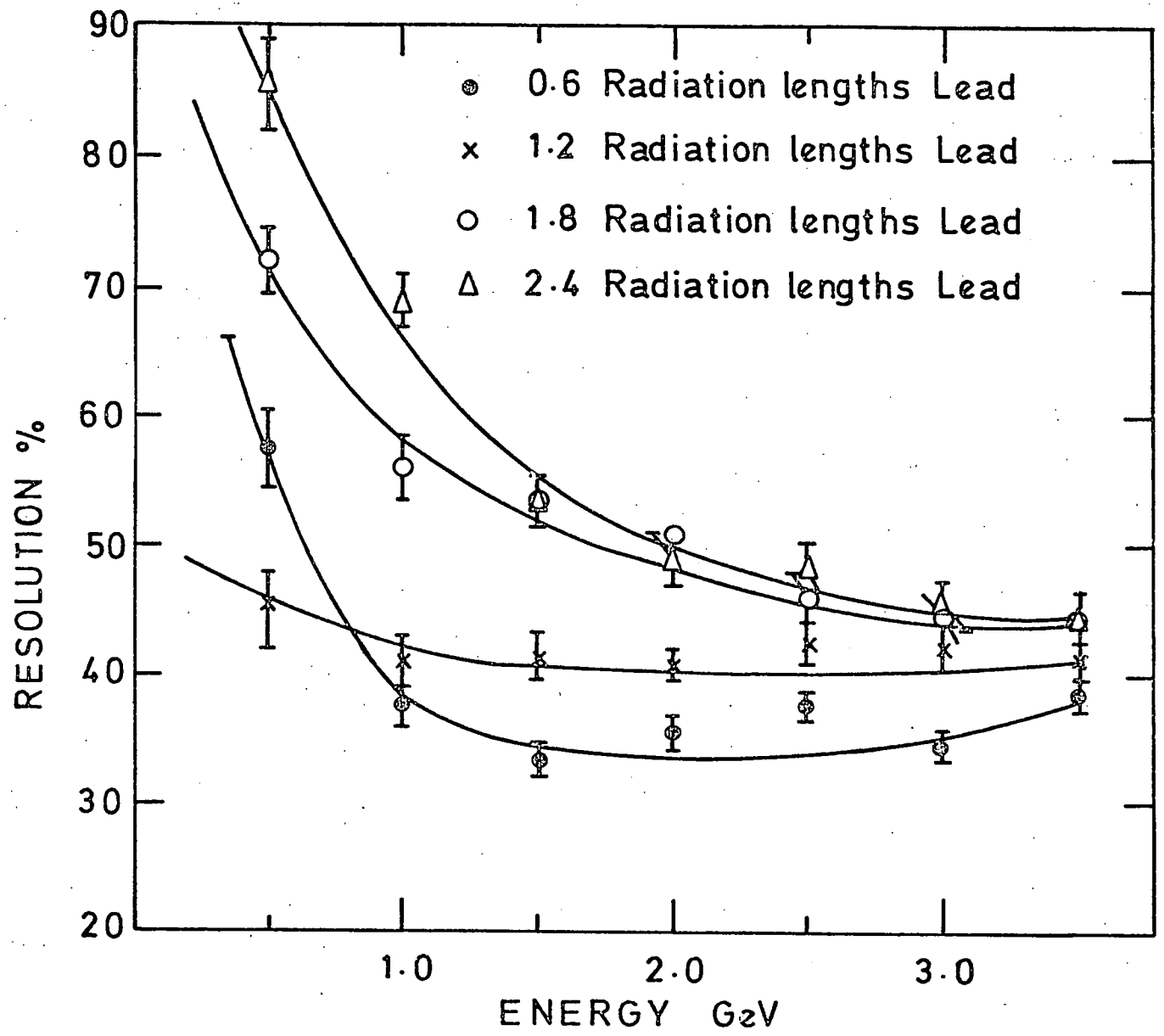

FIGURE 5.18 ENERGY RESOLUTION AS A FUNCTION OF ENERGY

and the experimental points obtained using 1.8 and 2.4 radiation lengths of lead target, are found to fit the relationships

$$R = 19.2 + 42.1/\sqrt{E}$$

$$R = 32.5 + 25.8/\sqrt{E}$$

respectively, where R is the resolution (%) and E is the primary energy (GeV).

At low energies, the resolution is seen to improve using 0.6 and 1.2 radiation length lead, however the resolution rapidly deviates from the expected $1/\sqrt{E}$ improvement due to leakage and individual electron sensitivity. A best resolution of approximately 35% was obtained at 2.0 GeV using 0.6 radiation lengths of lead.

The improvement in energy resolution resulting from using 2 layers of staggered tubes can be seen from Table5.6 which show the resolution calculated using one layer of tubes only. The change in resolution should be governed by the $1/\sqrt{2}$ improvement of dN/N obtained using two layers of tubes. In practice, however, the resolution deviates from this expected $1/\sqrt{2}$ improvement at high and low energies, due to the differing response of the 1 and 2 layer configurations to the changing parameters of the shower.

5.7 SPATIAL AND ANGULAR RESOLUTION

The technique used to determine the spatial and angular resolution of the detector is almost identical to that employed with the high pressure flash tube chamber. Use is made of the fact that, subject to statistical fluctuations, the shower of secondaries is uniformly distributed radially around the extension of the trajectory of the incident positron. Thus if the longitudinal axis of the shower is found it may be projected forward to find the initial point of interaction of the primary,called the shower apex

The deviation of the shower apex from an accurate measurement of the position of the primary particle, obtained from the drift chamber assembly is then determined. The FWHM of the frequency distribution of these deviations, for a large number of events, is then used as a measure of the spatial resolution. The angular deviation of the calculated shower axis from the normally incident primary is obtained from the equation of the shower axis. The FWHM of the frequency distribution of these angular deviations gives a measure of the angular resolution.

5.7.1 Fitting the Shower Axis

Each sampling plane of flash tubes will give a lateral section through the shower. The shower sections shown in Figure 5.19 may be taken as typical sections. The centre of gravity of the shower section for an individual event is found by calculating the geometric mean of the distribution, using the following expression

$$\bar{Y}_i = \sum_{i=1}^{16} \frac{Y_{ij}}{Y_i} \qquad (1)$$

where $\bar{Y}_i$ = is the co-ordinate of the centre of gravity of the shower in the i^{th} module

Y_{ij} = is the co-ordinate of the j^{th} ignited tube in the i^{th} module

n_i = is the total number of tube ignitions in the i^{th} module.

To the 22 shower centroids obtained for each X and Y plane, a straight line is fitted using the least squares method, and a first estimate of the shower axis is obtained. This initial estimate of the axis takes no account of the statistical fluctuations to which the developing shower is subject, and which results in the information in the head and core of the

FIGURE 5·19 LATERAL SHOWER SHAPES

PRIMARY ENERGY 0·5 GeV

ABSORBER 0·6 RADIATION LENGTH Pb

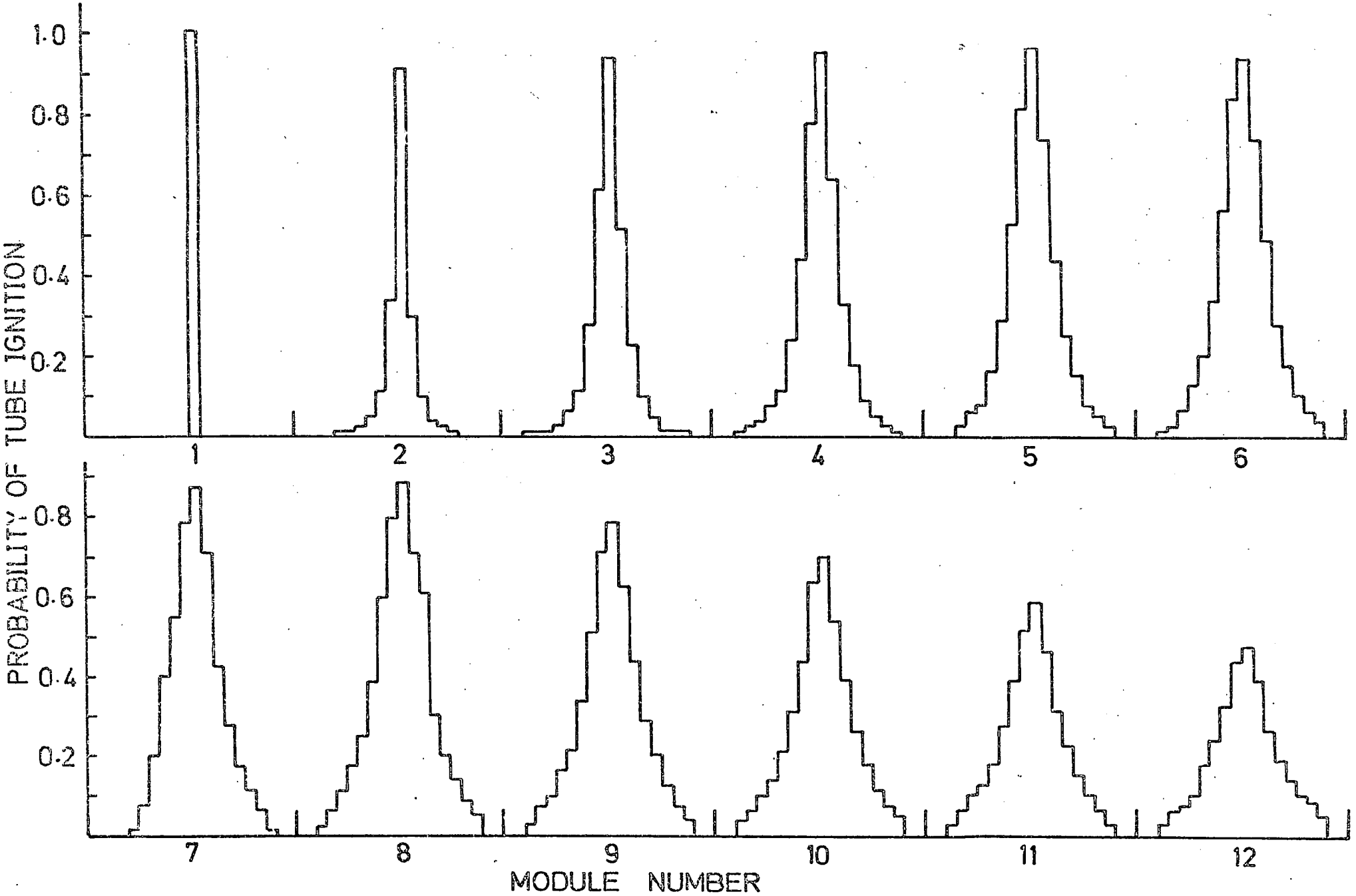

shower being more reliable than that of the tail and sides. To account for these fluctuations the data is weighted in the lateral and longitudinal directions according to the position, with respect to the initial estimate of the shower axis from which the data originated.

In calculating the lateral weighting factor, use is made of the approximate gaussian form of the distribution of flashed tubes, as can be seen in Figure 5.19. The lateral weighting factor for the J^{th} tube in the i^{th} module is given by the following relationship

$$W_{ij}(Y_{ij}) = \exp(-q_{ij}^2) \tag{2}$$

where $$q_{ij} = \frac{Y_{ij} - Y_i \cos\phi}{\sigma_i} \tag{3}$$

and Y_{ij} = is the distance of the j^{th} tube in the i^{th} module from some fixed reference point

Y_i = is the distance of the shower axis from the same reference point used in the definition of Y_{ij}

ϕ = is the angle between the shower axis and the perpendicular to the plane of the modules

σ_i = is the standard deviation of the shower in the i^{th} module

since $\phi \leq 2^{o}$, equation (3) can be written as

$$q_{ij} = \frac{Y_{ij} - Y_i}{\sigma_i} \tag{4}$$

The data was weighted in the longitudinal direction according to $1/\sigma_i$, where σ_i is the standard deviation of the distribution of ignited tubes

in the i^{th} module, and best represents the fluctuations in density and position of the shower secondaries at that plane. The variation of the standard deviation of the shower profile with depth is given in Figure 5.20, for two target thickness and 3 primary energies. It can be seen that there is no appreciable variation of shower width with energy.

The shower axis was fitted using an iterative process which incorporated the lateral and longitudinal weighting factors. Having first obtained the unweighted initial estimate of the shower axis by means of a least squares fit to the shower centroids, obtained using equation (1), a new set of shower centres, laterally weighted with respect to the initial shower axis , are calculated. To these new shower centres an improved estimate of the shower axis is obtained by means of a least squares fit, incorporating the longitudinal weighting factor $1/\sigma_i$. New weighted shower centres are calculated with respect to the improved estimate of the axis, and the process continued. Upon completion of each iterative loop the values of the shower axis angle ϕ and the intercept of the axis with a defined reference plane (situated in the drift chambers) was recorded. The iterative process was continued until the value of the intercept and ϕ converged to approximately constant value, which usually occurred after 5 iterative loops.

5.7.2 Determination of the Position of the Primary Particle

Having calculated from the shower data the trajectory of the primary positron, it is then necessary to refer this calculated position to a more accurate estimate of the primary trajectory. Previously, in the case of the high pressure flash tube chamber this had been achieved by two orthogonally positioned layers of tubes, placed immediately in front of the first layer of target material. This situation was improved upon,

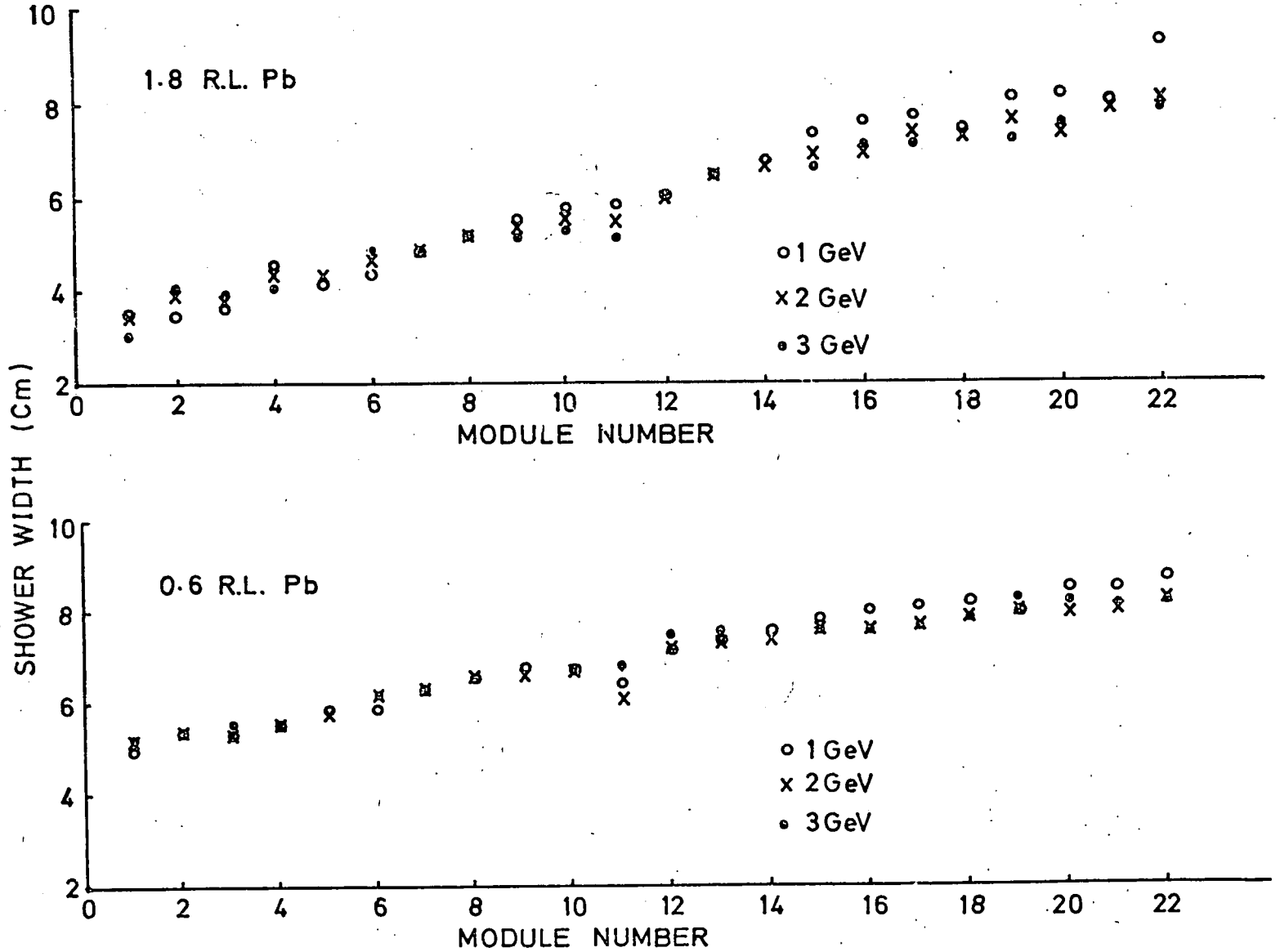

FIGURE 5·20 SHOWER WIDTHS (STANDARD DEVIATION OF SHOWER PROFILE) AS A FUNCTION OF DEPTH

in the present detector by employing systems of drift chambers and staggered layers of flash tubes.

The assembly of drift chambers and flash tubes, is shown for one plane by Figure 5.21. The drift chambers, designed by A.R.Hedge at Durham, were of a printed cathode type, the cathode wires being etched on each side of a copper coated printed circuit board. The etched field wires on each side of the board being orthogonal, such that adjacent chambers (one in the X and one in the Y plane) share the same board, resulting in a simple low mass configuraton which reduces the likelihood of scattering. The use of 3 staggered layers, as shown in Figure 5.21, overcomes the left-right ambiguity, which with a drift length of 26 mm provided a sensitive area of 78 mm x 78 mm over which the primary position may be defined uniquely.

It was necessary not only to use the drift chambers to provide information concerning the position of the primary, but also to determine the spatial resolution of the chambers using the particle beam. The geometric requirements of these two aims were conflicting, the shower detector requiring the drift chambers to be well separated to provide the maximum lever arm, whereas the spatial resolution measurements required the chambers to be closely stacked to avoid the surveying problems associated with a widely spaced system. The latter system was adopted, and a spatial resolution of $\pm$ 0.25 mm was recorded, although the angular resolution of the system ($\pm$ 2^{o}) was poor.

To avoid total dependence upon the drift chambers, the performance of which was uncertain prior to conducting the tests, a system of 8 staggered layers of flash tubes, arranged in two orthogonal sets of 4 staggered layers, were employed. These were referred to as the apex planes, one of which can be seen in Figure 5.21. The positron beam, incident upon this array of flash tubes was restrained by the trigger scintillators to a divergence of $\pm$ 2^{o}, and therefore only a limited number

FIGURE 5-21

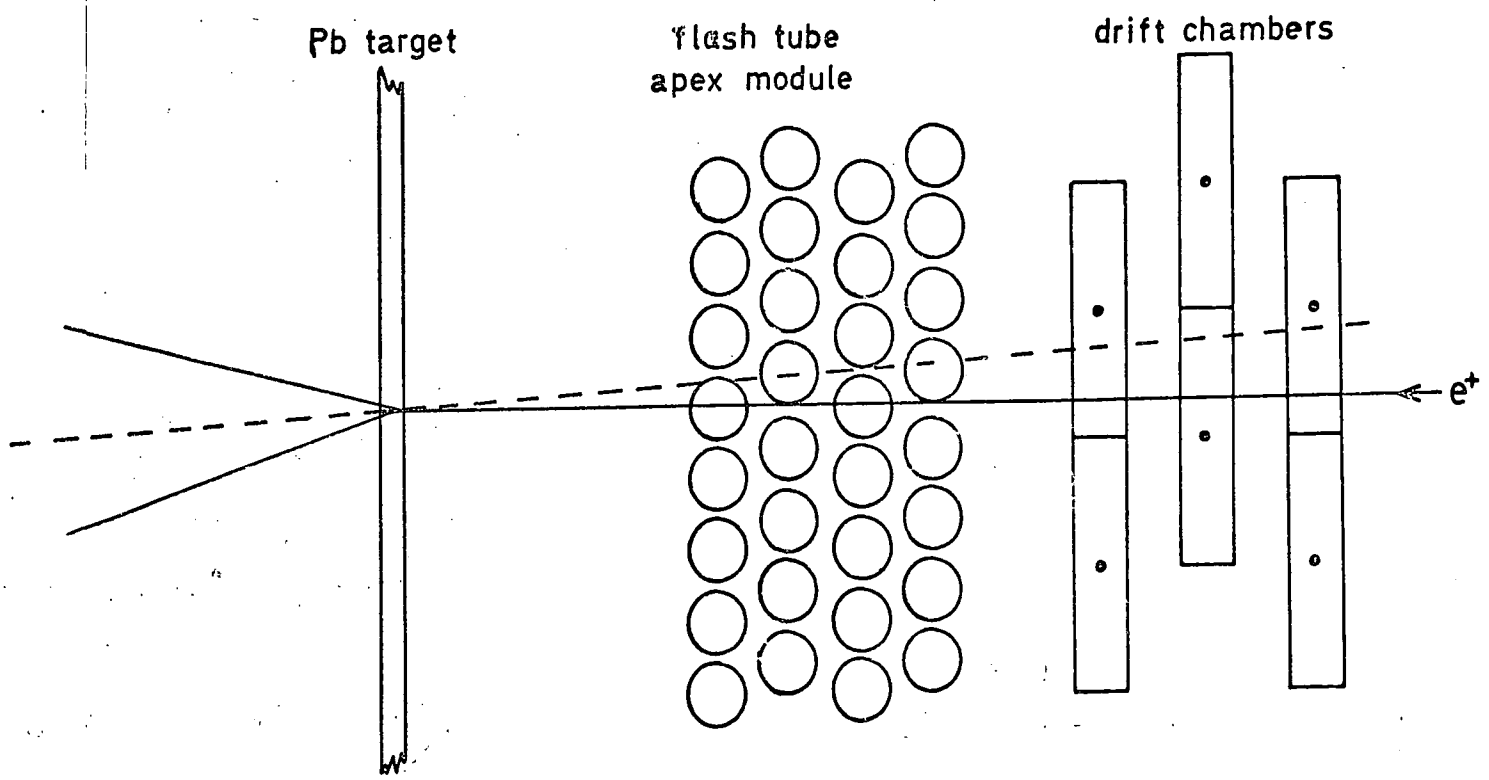

DRIFT CHAMBER AND APEX MODULE CONFIGURATION

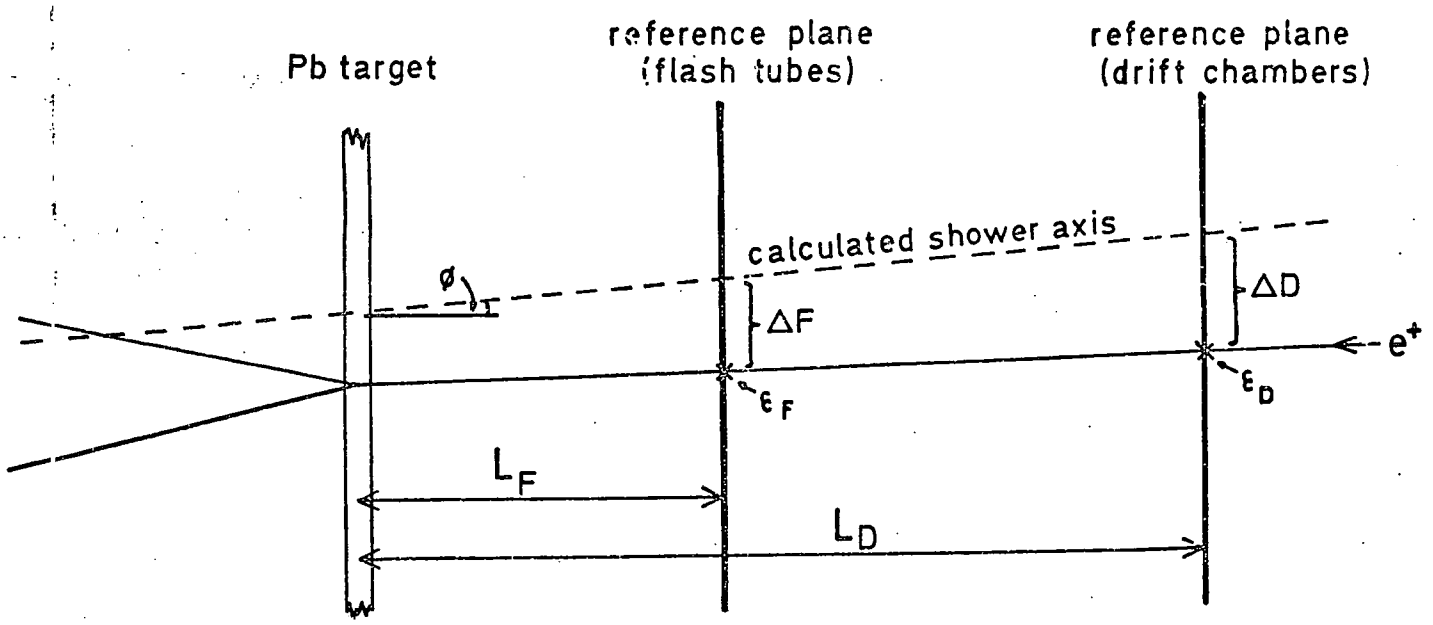

DEVIATION OF THE CALCULATED SHOWER AXIS, ΔD, ΔS

of patterns of tube ignitions can occur in the apex planes. These 12 patterns are given in Figure 5.22 along with their associated spatial error.

To each of these detector systems a reference plane was assigned, as shown in Figure 5.21. The point of intersection of the calculated shower axis with these planes is then determined and the deviations ΔD and ΔF for the drift chambers and apex planes respectively obtained. Ideally, since the flash tube and drift chamber assemblies have a poor angular resolution, the plane in which the deviation of the shower axis is recorded should be located as close as possible to the first sheet of target material in which the shower apex is situated, in which case it might be expected that Δ_F would represent a more accurate measure of the true spatial resolution. However, the large error, ε_F associated with the flash tube assembly results in the deviation Δ_D, with its smaller error ε_D, yielding a better estimate of the true spatial resolution of the shower counter, although the plane in which Δ_D is measured is further removed from the target sheet. For this reason the spatial resolution of the shower counter is defined with respect to the drift chamber array.

5.7.3 Spatial Resolution

The spatial resolution of the shower detector was defined as the FWHM of the frequency distributions of the deviations Δ_D. Distributions of Δ_D were obtained for approximately 3000 events, for each combination of energy and target. Examples of these distributions are given in Figures 5.23 and 5.24 for 1.0 and 3.0 GeV, using 1.2 R.L. lead.

The dependence of the spatial resolution upon the primary energy and target thickness is given in Figures 5.25 and 5.26. The spatial resolution is seen to improve rapidly with increasing energy for all target thickness, up to approximately 2.0 GeV, after which it plateaus. This

FIGURE 5.22 EVENT SELECTION IN THE APEX PLANES

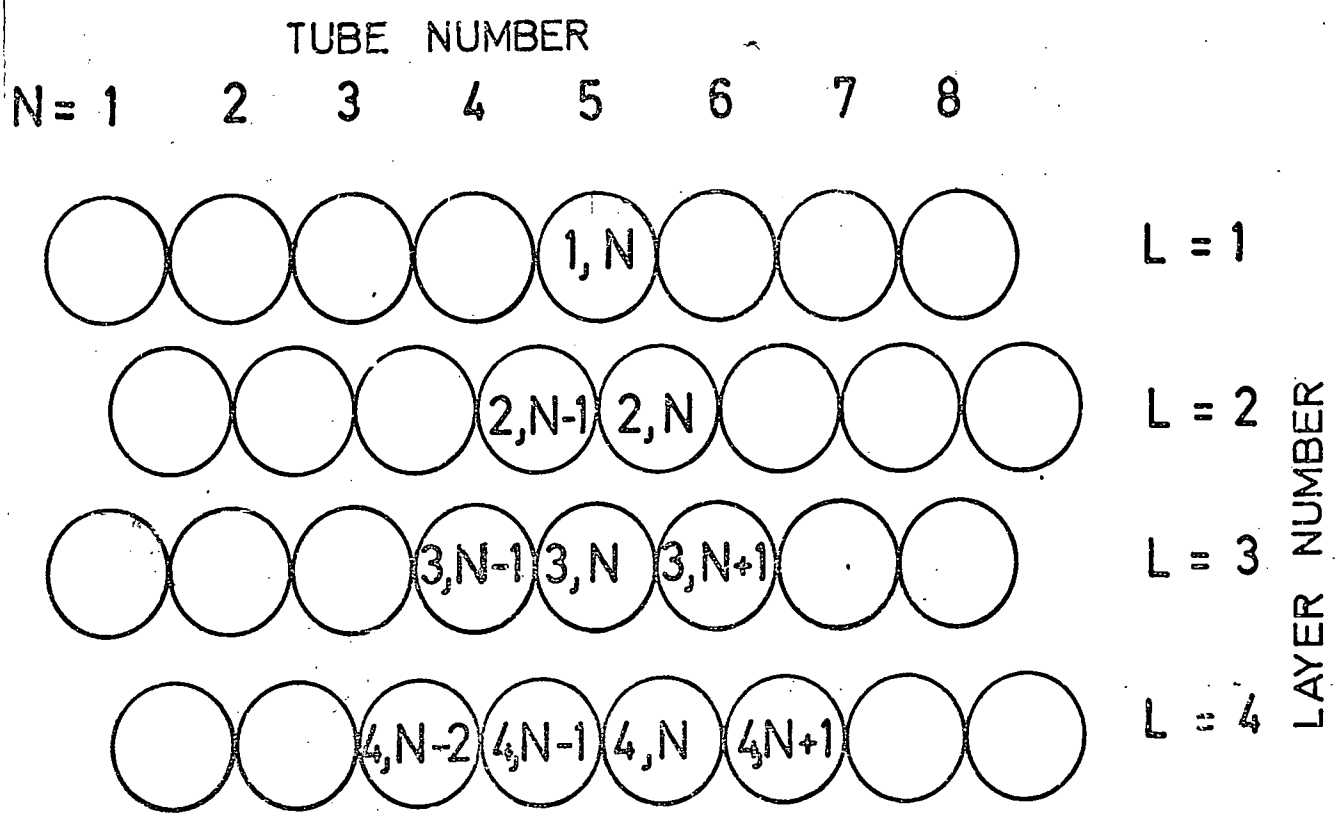

ACCEPTABLE COMBINATIONS

	COMBINATIONS	Error (mm) X Plane	Error (mm) Y Plane
1	(1,N) = 1, (2,N)=0, (2,N+1)=0, (3,N)=1, (4,N)=1	1	3
2	(1,N) = 1, (2,N-1)=1, (3,N)=1, (4,N)=0, (4,N+1)=0	1	2
3	(1,N)=1, (2,N)=1, (3,N)=1, (4,N)=0, (4,N+1)=0	1	2
4	(1,N)=1, (2,N-1)=1, (3,N)=0, (3,N-1)=0, (4,N-1)=1	4	3
5	(1,N)=1, (2,N)=1, (3,N-1)=0, (3,N)=0, (4,N)=1	3	4
6	(1,N)=1, (2,N)=1, (3,N)=1, (4,N)=1	3	4
7	(1,N)=1, (2,N-1)=1, (3,N)=1 (4,N-1)=1	4	4
8	(1,N)=0, (2,N)=0, (2,N-1)=0, (3,N)=1, (4,N-1)=1	2	1
9	(1,N)=0, (1,N+1)=0, (2,N)=1, (3,N)=1, (3,N+1)=0, (4,N)=1	2	1
10	(1,N-1)=0, (1,N)=0, (2,N-1)=1, (3,N-1)=0, (3,N)=0, (4,N-1)=1	3	1
11	(1,N)=1, (2,N-1)=0, (2,N)=0, (3,N)=1, (4,N)=1	4	3
12	(1,N)=1, (2,N-1)=0, (2,N)=0, (3,N)=1, (4,N-1)=1	4	3

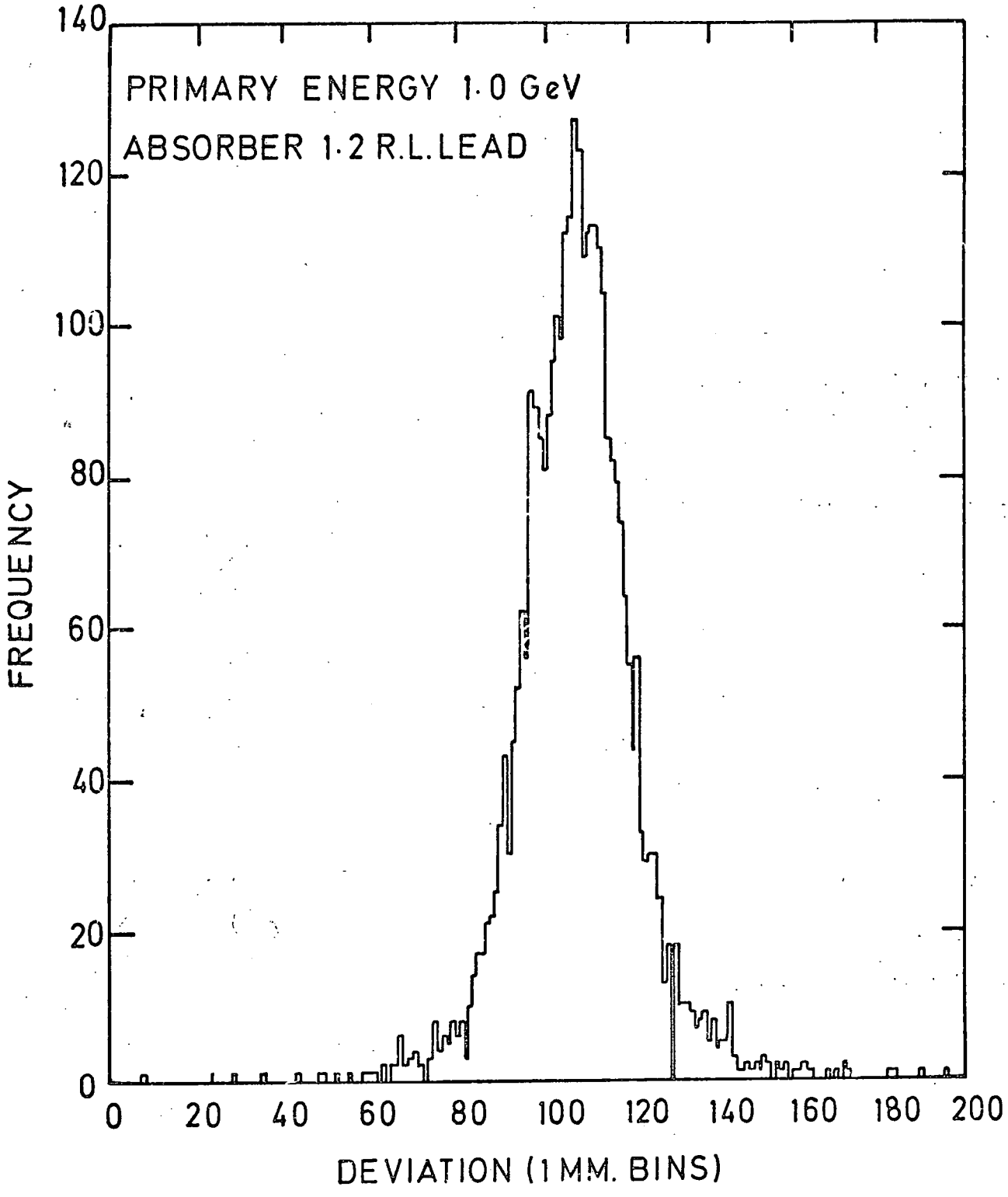

FIGURE 5·23 DEVIATION BETWEEN DRIFT CHAMBER CO-ORDS AND EXTRAPOLATED COMBINED SHOWER CO-ORDS (X PLANE)

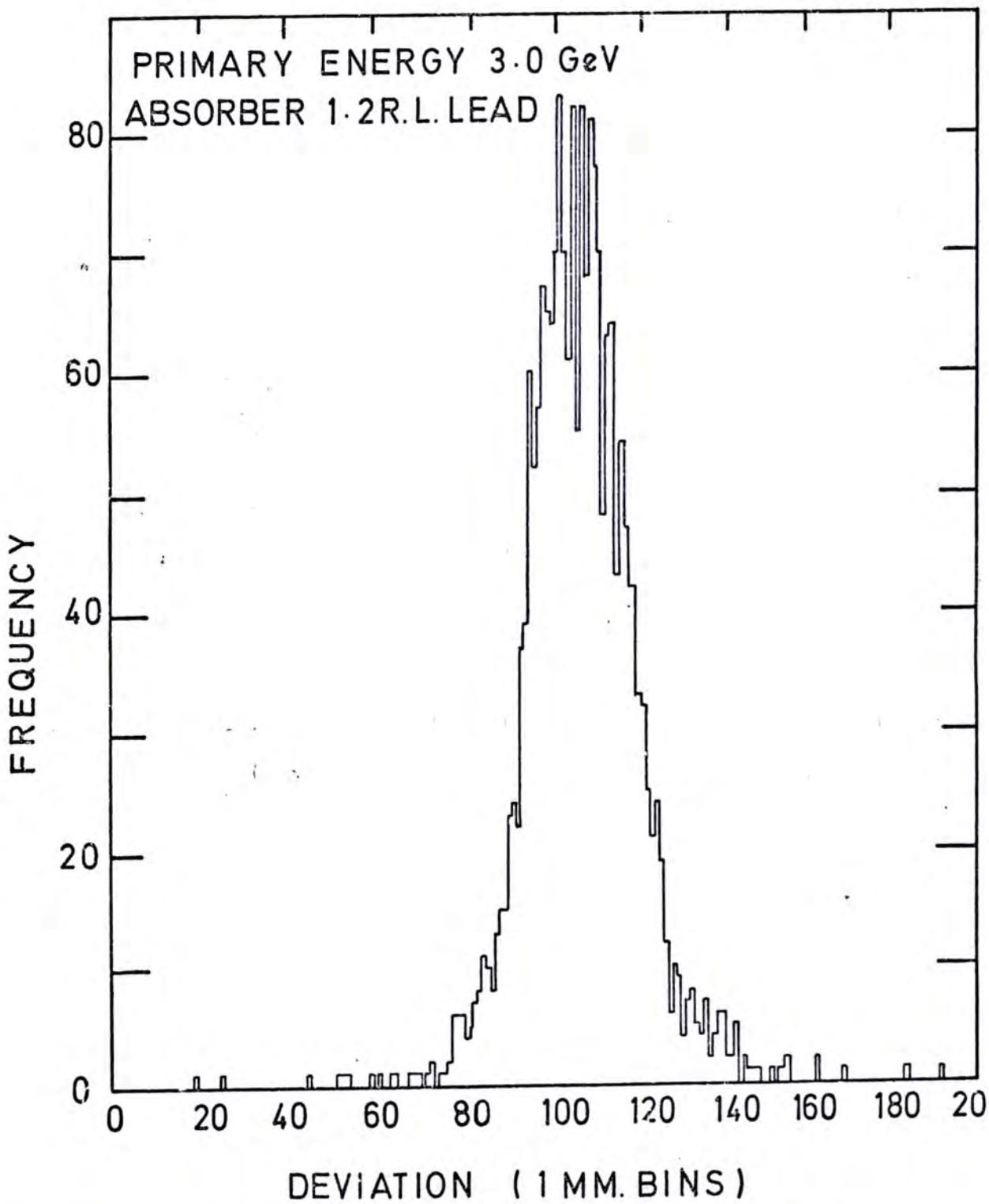

FIGURE 5.24 DEVIATION BETWEEN DRIFT CHAMBER CO-ORDS AND EXTRAPOLATED COMBINED SHOWER CO-ORDS (X PLANE)

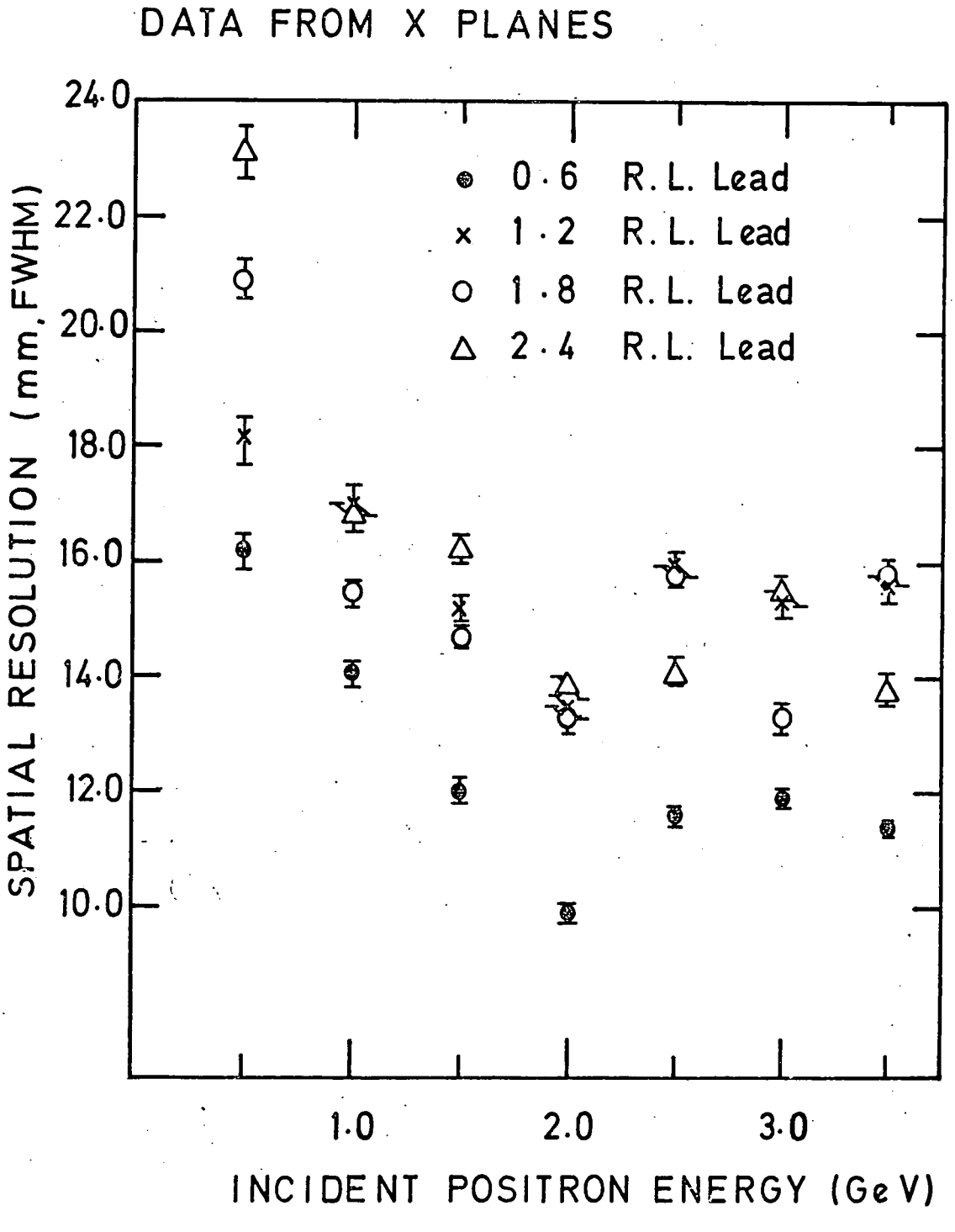

FIGURE 5.25 SPATIAL RESOLUTION AS A FUNCTION OF ENERGY

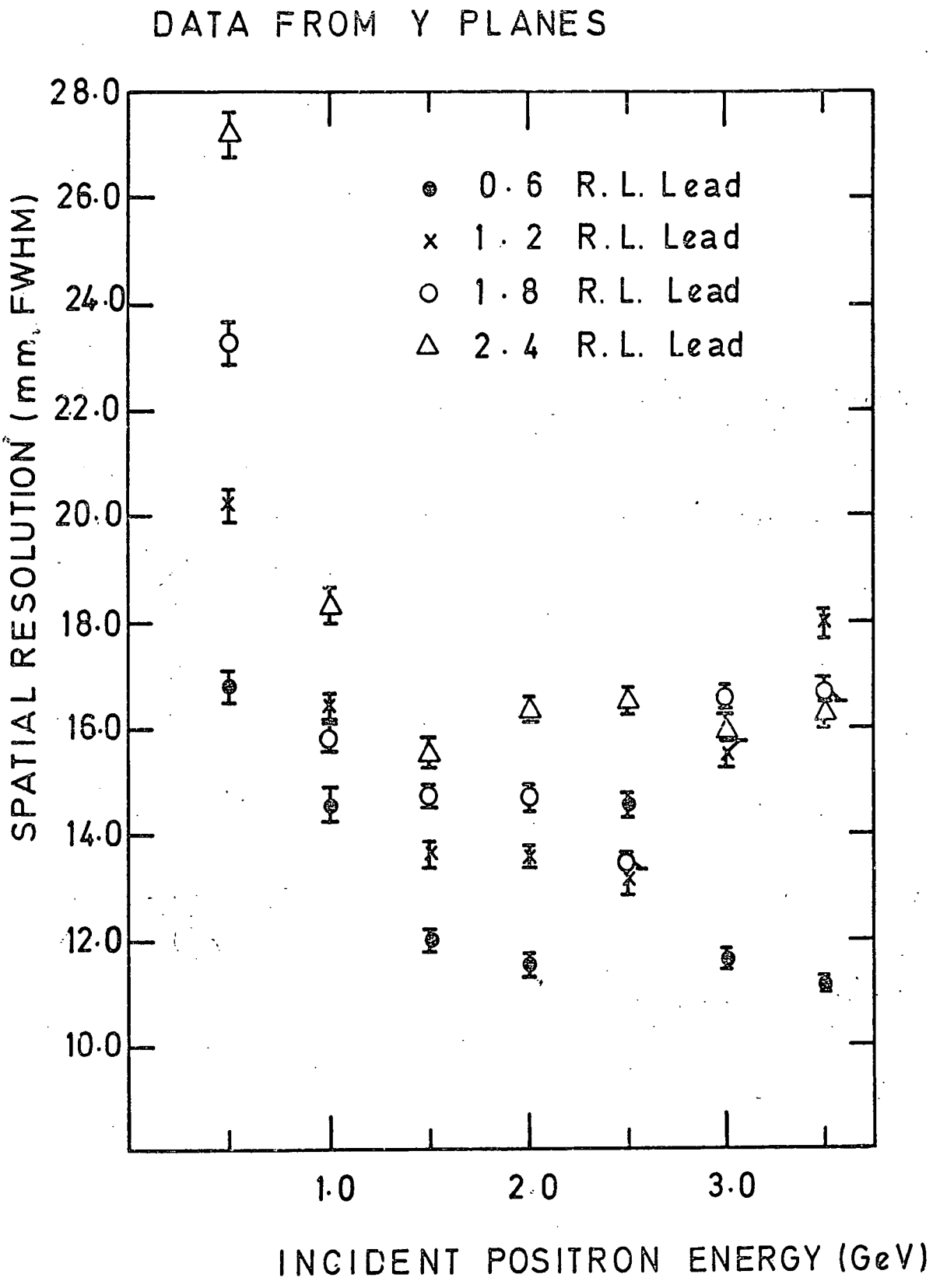

FIGURE 5·26 SPATIAL RESOLUTION AS A FUNCTION OF ENERGY

plateauing is thought to be due to the poor individual electron sensitivity of the flash tubes. Hence, although the density of particles, and therefore the information obtainable near the core of the shower increases with primary energy, the number of flashing tubes remains approximately the same resulting in no further improvement of the resolution. A best resolution of approximately 11 mm (FWHM) was obtained using 0.6 R.L. lead target, for energies of 2.0 GeV and above.

The improvement obtained using two sampling layers of tubes can be seen from Table 5.7 which shows the spatial resolutions obtained using one and two layers of tubes in each sampling plane. It can be seen that in all cases the resolution is improved, however the improvement is by less than the factor $1/\sqrt{2}$ which may be expected by sampling the shower twice.

Unlike the energy resolution, the spatial resolution is expected to be less sensitive to the shower escaping from the rear of the detector. To investigate this dependence the analysis programme was run on 3 sets of data, 0.6, 1.2 and 1.8 radiation lengths of lead at 3.5 GeV. In the analysis the rearmost modules were successively "masked" so as to contribute no information to the fitting routine. The results are given in Table 5.8 and Figure 5.27. It can be seen that beyond 60% shower containment, very little improvement is obtained. This is due to the relatively slight contribution of the rearmost modules to the fitting routine owing to the uncertainty associated with the data obtained from the rear of the shower. This dependence of resolution upon containment may be of importance in designing a detector for a specific requirement.

5.7.4 Angular Resolution

In calculating the angular resolution the assumption is made that the primary positrons are all incident normally upon the first sampling plane of the shower detector. This is not strictly true, since the

TABLE 5.7 : Spatial and Angular Resolution using One and Two Layers of Flash Tubes

Target R.L.Pb	Energy GeV	Spatial Resolution (mm). 1 Layer	2 Layers	Angular Resolution (deg) 1 Layer	2 Layers
	0.5	18.3	16.2	4.8	4.1
	1.0	16.5	14.1	3.0	2.6
	1.5	14.4	12.0	2.6	2.3
0.6	2.0	14.3	9.8	2.2	2.0
	2.5	13.8	11.6	2.6	2.5
	3.0	14.4	11.8	2.2	1.9
	3.5	13.3	11.3	2.0	1.8
	0.5	20.2	20.2	7.4	6.1
	1.0	18.6	16.4	4.5	3.8
	1.5	14.9	13.6	3.9	3.2
1.2	2.0	16.3	13.6	3.4	2.9
	2.5	15.5	13.1	3.2	2.8
	3.0	15.0	15.5	3.5	2.9
	3.5	18.5	17.9	3.6	3.1
	0.5	28.8	27.2	13.1	10.5
	1.0	19.9	18.3	9.1	7.4
	1.5	17.0	15.5	7.2	5.9
1.8	2.0	20.5	16.4	6.8	5.3
	2.5	17.8	16.5	6.2	5.1
	3.0	17.7	15.9	6.0	4.8
	3.5	16.7	16.2	5.2	4.2

TABLE 5.8 : Dependence of Spatial and Angular Resolution Upon Shower Containment.

Absorber Thickness (RL)	Number of Modules used in Analysis	Percentage of Shower Contained Within Detector	Spatial Resolution (mm)		Angular Resolution (Deg.)	
			X Planes	Y Planes	X Planes	Y Planes
0.6 Radiation Lengths Lead 3.5 GeV	11	77.6	11.35	11.11	1.79	1.83
	10	72.3	11.17	11.26	1.97	1.87
	9	66.1	11.24	11.40	1.83	1.93
	8	58.8	11.45	11.50	1.91	2.04
	7	50.2	11.74	11.71	2.04	2.25
	6	40.6	12.10	12.71	2.19	2.59
	5	30.7	12.42	14.66	2.67	3.03
	4	20.8	13.70	14.34	3.34	3.98
	3	12.0	16.54	15.77	5.03	5.60
	2	5.4	20.15	17.47	9.26	10.08
1.2 Radiation Lengths Lead 3.5 GeV	11	97.5	15.57	17.97	2.97	3.10
	10	95.0	15.47	18.39	2.98	3.20
	9	90.2	15.50	18.33	3.06	3.26
	8	88.5	15.61	17.96	3.09	3.36
	7	83.0	15.67	17.92	3.19	3.42
	6	75.0	15.60	18.14	3.35	3.50
	5	65.0	15.71	18.39	3.55	3.69
	4	51.0	15.76	18.85	4.04	4.52
	3	33.0	17.49	20.41	5.35	6.07
	2	16.0	21.35	20.79	9.31	10.45
1.8 Radiation Lengths Lead 3.5 GeV	11	100.0	15.18	16.56	3.29	3.84
	10	99.7	14.91	16.63	3.34	3.94
	9	98.5	15.63	16.43	3.51	3.98
	8	97.5	15.45	16.09	3.54	4.13
	7	95.0	15.53	16.02	3.63	4.22
	6	91.0	14.64	16.33	3.67	4.35
	5	84.0	14.94	16.52	3.70	4.49
	4	72.0	16.02	15.58	4.08	4.77
	3	55.0	17.46	16.56	5.19	6.14
	2	31.0	21.61	17.55	9.10	9.85

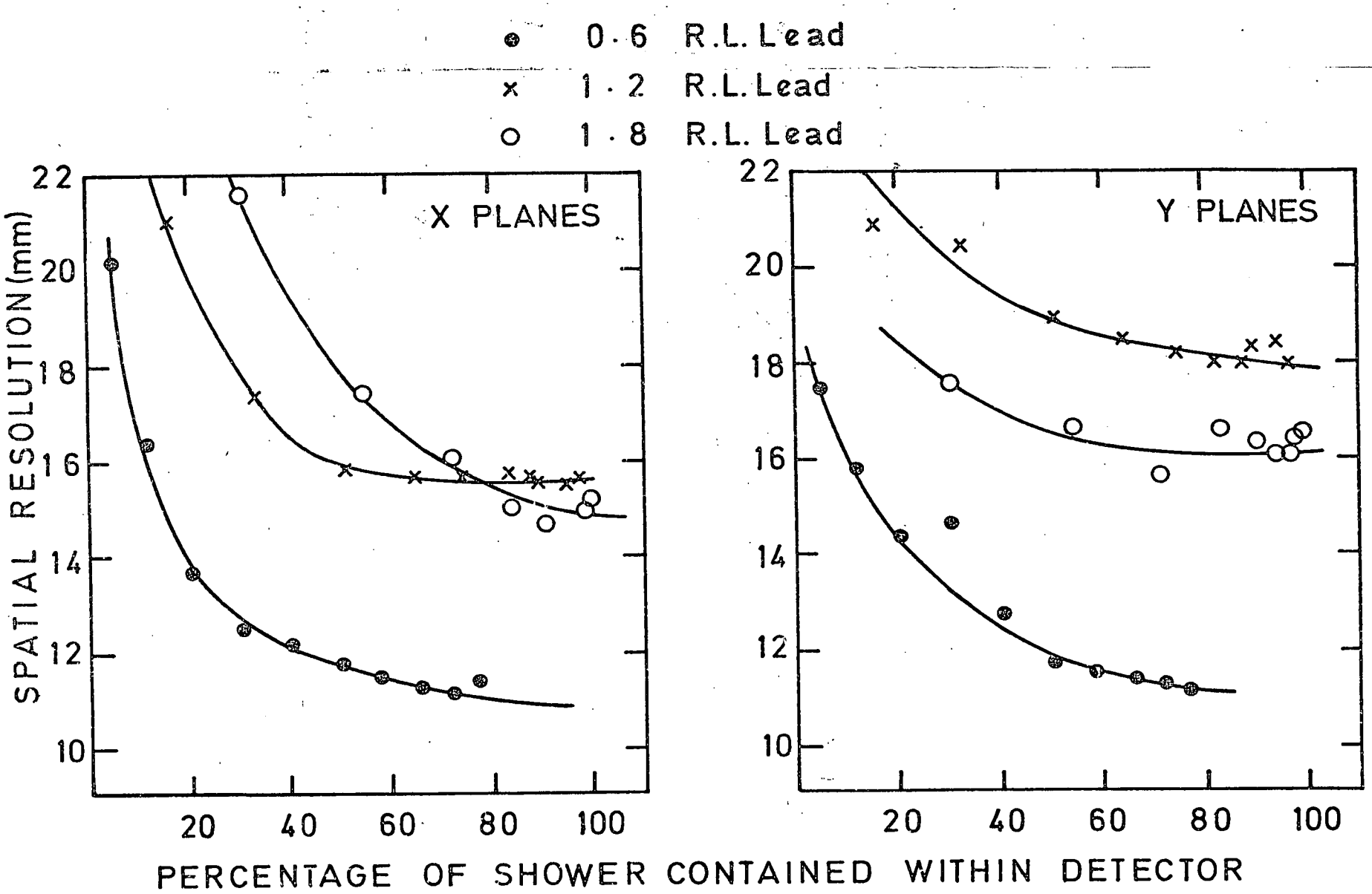

FIGURE 5·27 SPATIAL RESOLUTION AS A FUNCTION OF PERCENTAGE OF SHOWER CONTAINED WITHIN DETECTOR (PRIMARY ENERGY 3·5 GeV)

scintillator telescope only restricts the primary positrons to within $\pm 2^{\circ}$ of the normal. Having obtained the equation of the calculated shower axis, the angular deviation of the shower axis from the normal is calculated. The FWHM of the frequency distribution of these angular deviations for some 3000 events is defined as the angular resolution. Distributions were obtained for all combinations of target and primary energy, examples of typical distributions obtained are given in Figure 5.28. The dependence of the angular resolution upon primary energy and target thickness is shown in Figure 5.29; the data has been corrected for the $\pm 2^{\circ}$ uncertainty in the beam angle. The behaviour is very similar to that of the spatial resolution, the resolution plateauing beyond 2.0 GeV, due to the individual electron sensitivity of the tubes. A best angular resolution of 2° (FWHM) is obtained beyond 2.0 GeV using 0.6 R.L. lead.

The effect of using one and two layers of flash tubes in a sampling plane is shown in Table 5.7 as with the spatial resolution an improvement is obtained using two sampling layers, although less than the factor $1/\sqrt{2}$ which may be expected.

From Figure 5.30 and Table 5.8, it can be seen that containment beyond 60% results in little improvement of the angular resolution in agreement with the behaviour of the spatial resolution.

5.8 OPERATION OF THE DETECTOR AT HIGH EVENT RATES

One of the problems which prevented the operation of the high pressure flash tube chamber at high rates was the decrease of the digitisation pulse height with increasing event rate, such that it fell below the 4 V threshold required to set the memory logic latches. This is due to the presence of induced fields which oppose the applied HT pulse, resulting in a fall in efficiency of the tube. Tests conducted upon the low pressure

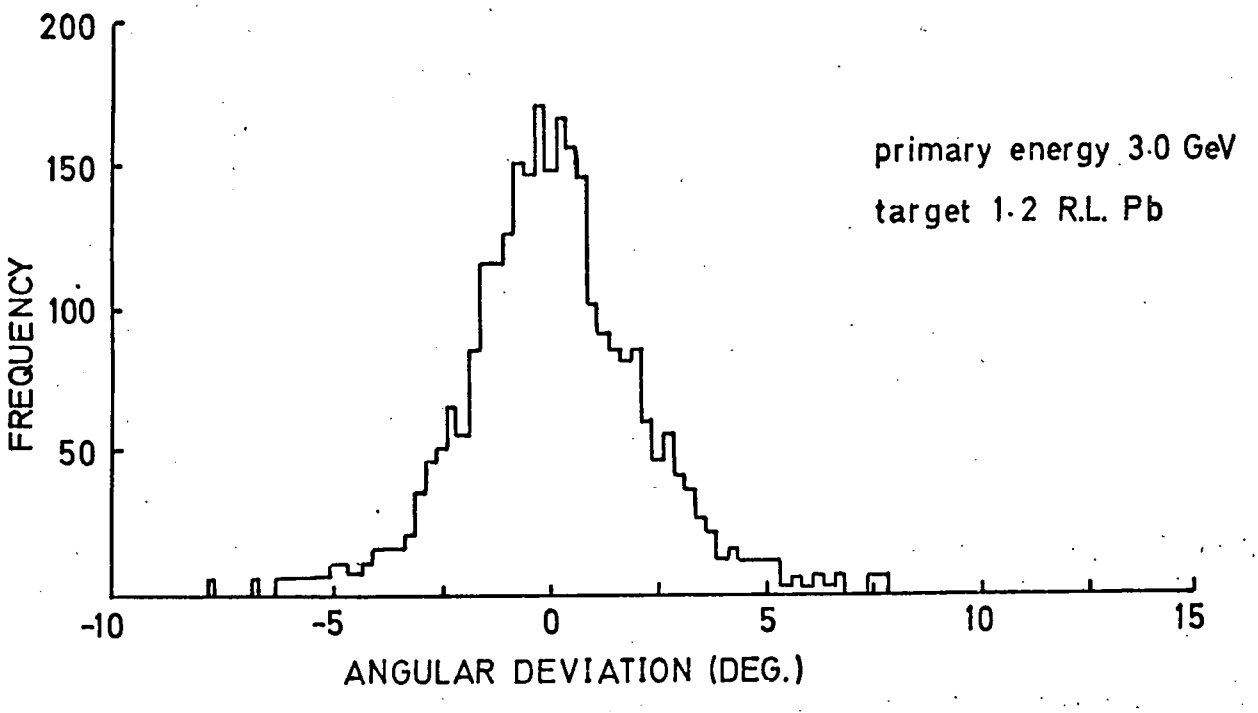

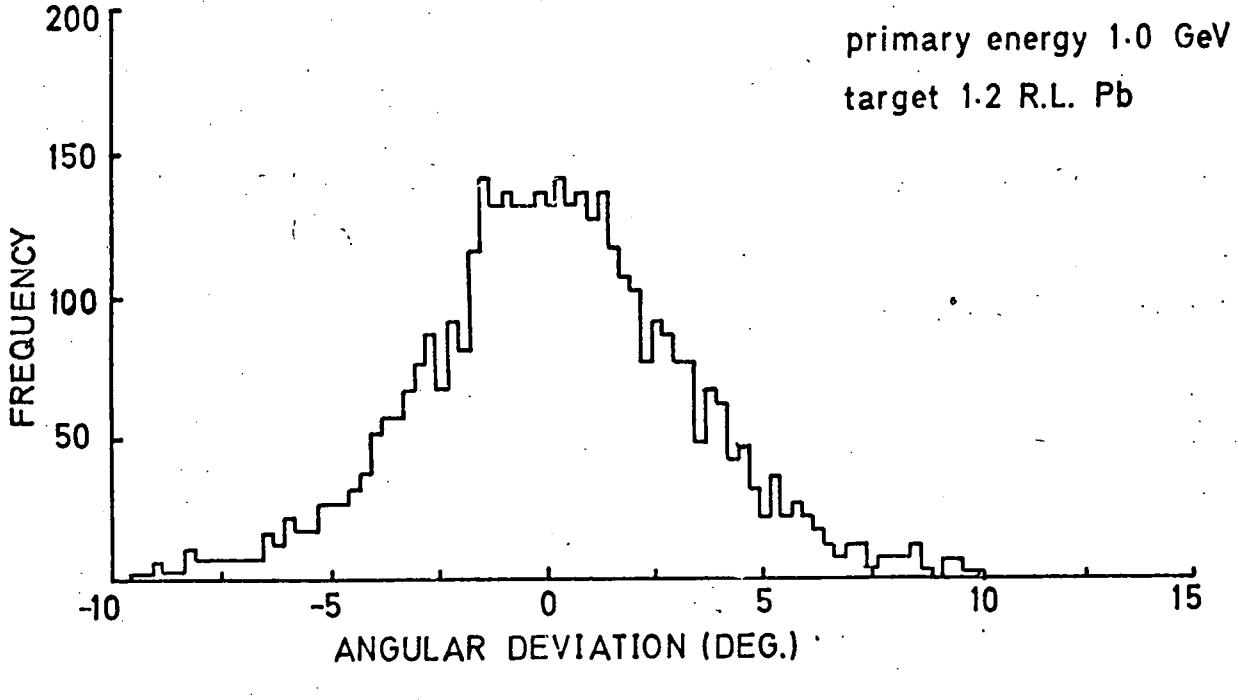

FIGURE 5.28 ANGULAR DEVIATION OF SHOWER AXIS FROM NORMAL INCIDENCE

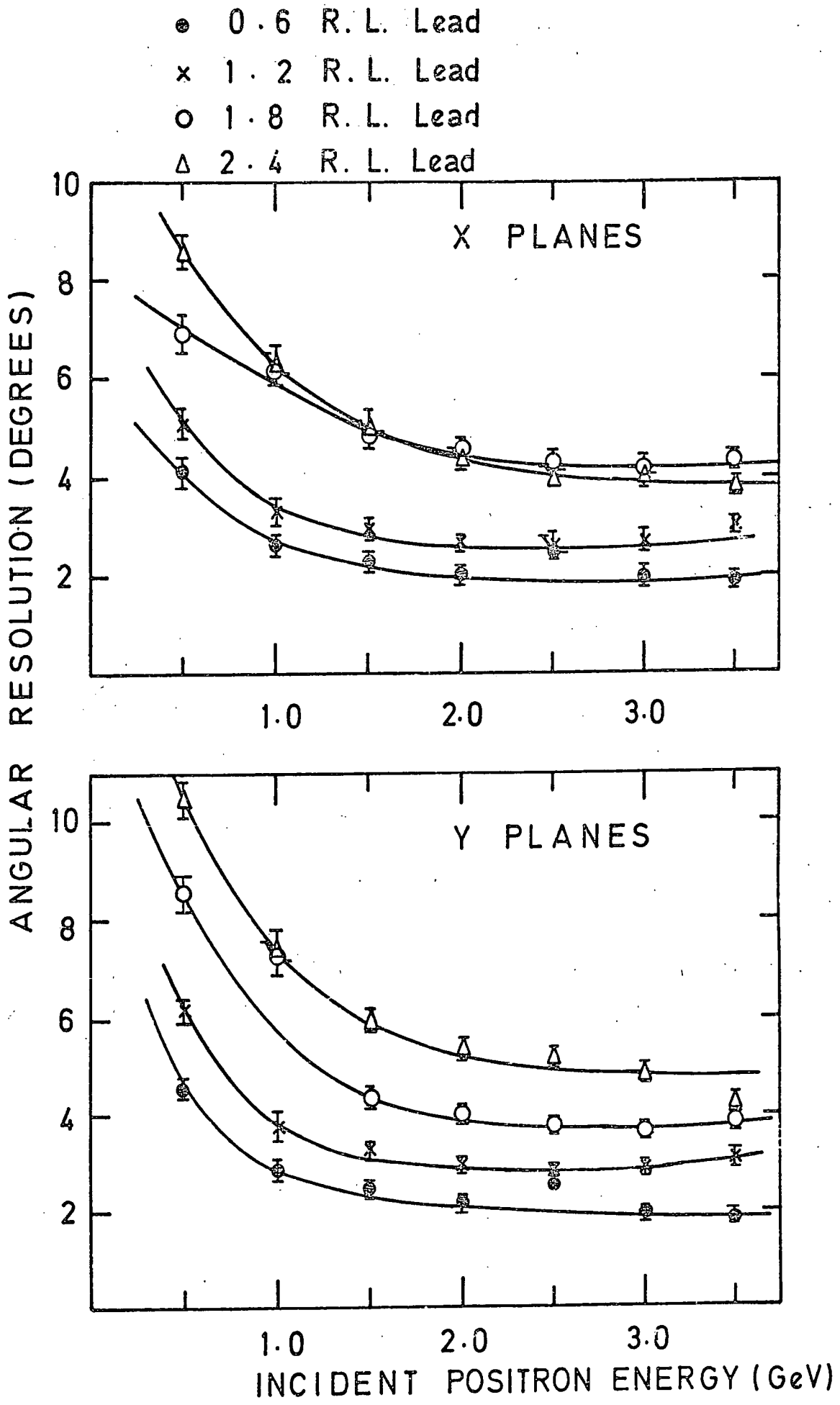

FIGURE 5·29 ANGULAR RESOLUTION AS A FUNCTION OF ENERGY

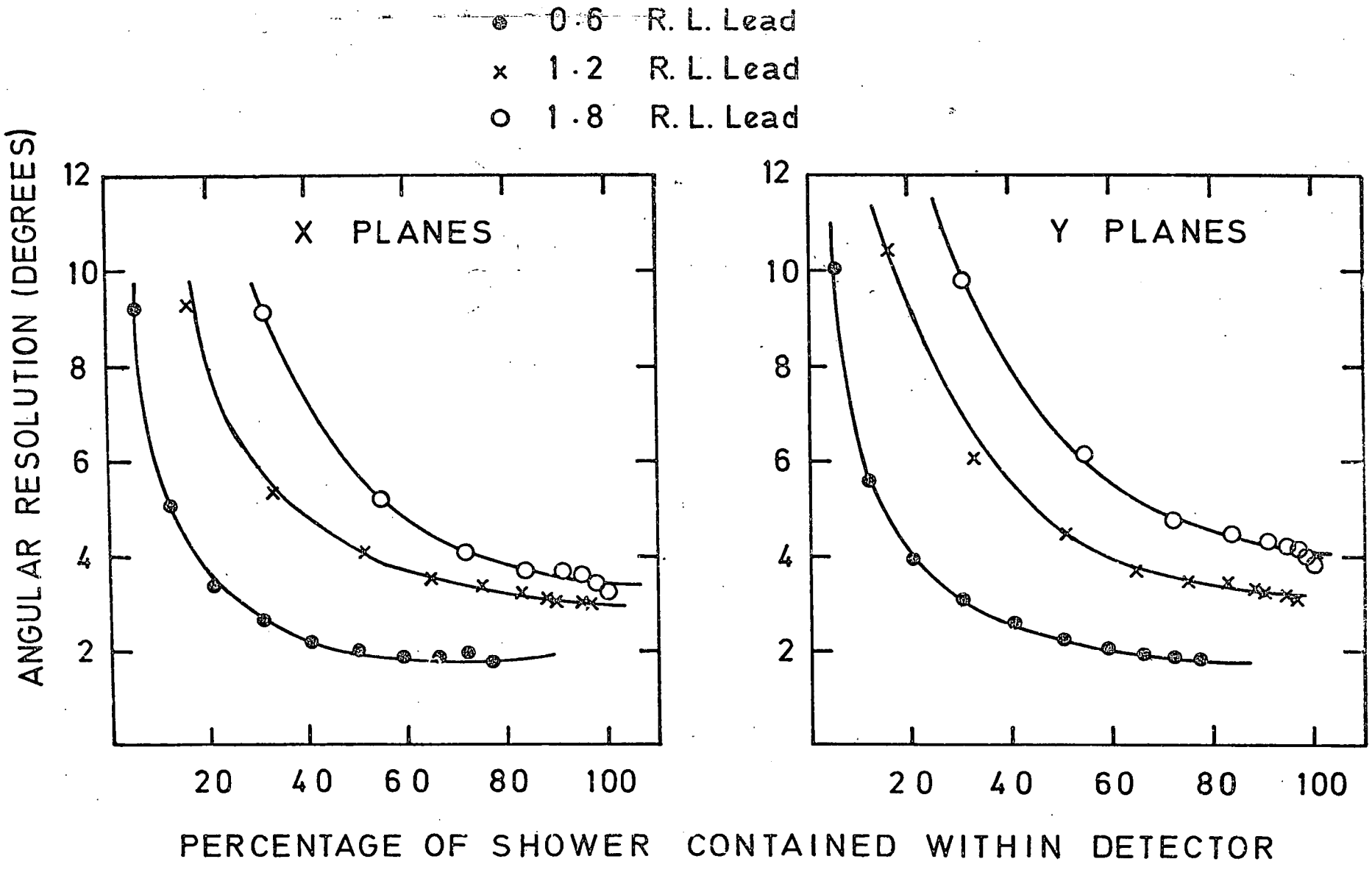

FIGURE 5.30 ANGULAR RESOLUTION AS A FUNCTION OF PERCENTAGE OF SHOWER CONTAINED WITHIN DETECTOR

flash tubes using a RU 106 source, at an event rate of 50 sec^{-1}, showed that even for applied fields as low as 3.75 kV/Cm, the digitisation pulse height remains well above the threshold required to set the memory logic latches, as can be seen in Figure 5.5.

If the detector is to operate successfully in an environment of high background radiation at a high event rate, it is necessary that the efficiency, sensitive and recovery times, are unaffected by operation at high rates. The behaviour of these quantities with changing event rates were investigated and the results given below.

5.8.1 Effect of Rate on Efficiency

In the manner described in section 5.4.1, efficiency measurements were carried out for a number of event rates up to 50 sec^{-1}.

Since it is known that the effect of the induced field increases rapidly with rate, it was decided to operate the detector further above the knee of the high voltage plateau, ensuring that the opposing induced field did not result in too premature a fall in the efficiency. Also, since the magnitude of the induced field depends upon the length of the high voltage pulse[10], the measurements were repeated for two pulse lengths. Figure 5.31 shows the averaged efficiencies for the X and Y modules for two applied pulse lengths. It can be seen that there is a distinct difference in the behaviour of the X and Y modules. For both pulse lengths the Y modules rapidly become spurious above an event rate of 10 sec^{-1}. However, for the 2 μs pulse, the efficiencies of the X planes after an initial increase in spuriousness begins to fall, presumably by the backing off of the applied field by the induced field. The use of the longer high voltage pulse causes the X planes to behave in a similar manner to the Y planes, becoming progressively more spurious with event rate. It is clear from these results that the large diameter flash tubes are unexpectedly sensitive to the effect of induced fields, behaving in a manner similar to that of the high pressure tubes.

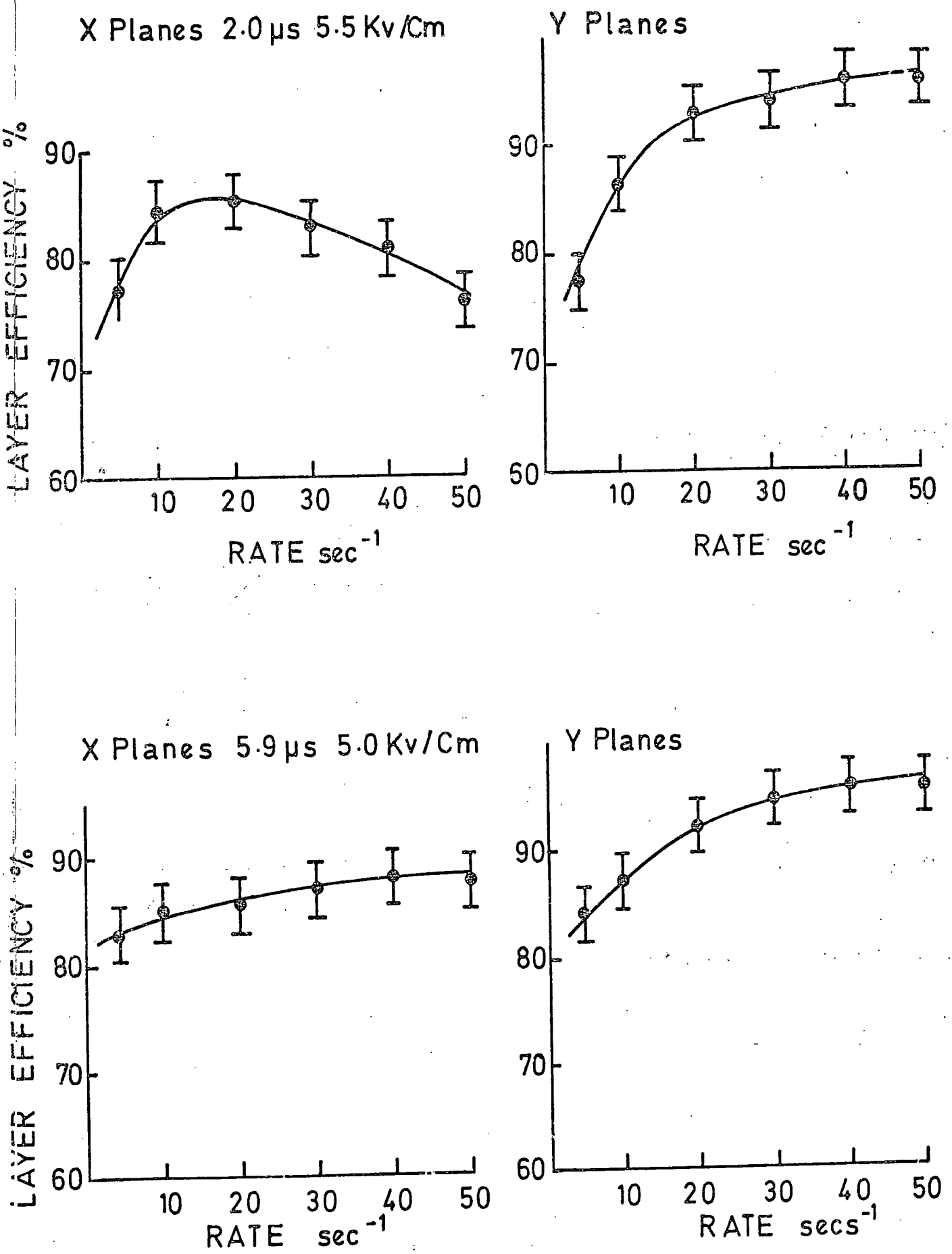

FIGURE 5·31 EFFICIENCY AS A FUNCTION OF RATE FOR 2 PULSE LENGTHS

Figure 5.7, which shows the response of the individual modules at event rates of 0.9 and 50 events sec^{-1}, using a pulse of 4.75 kV/Cm of duration 2 μs, exhibits the same striking difference between the X and Y planes. The Y planes, almost without exception, become totally spurious at high rates, however the X planes fall into two distinct categories, one spurious and one inefficient.

This behaviour is clearly due to fields caused by charge deposited upon the inner walls of the flash tube, however an explanation of the difference in behaviour of the X and Y planes is difficult. Care was taken to ensure no preferential positioning of a particular tube production batch within the detector, further, exchanging the X and Y tubes produced no change in the behaviour of the modules indicating that the cause is associated with some difference in the X and Y modules. Adjacent X and Y planes shared the same high voltage pulse source, hence any fault in the pulse forming network would cause a similar response in adjacent X-Y planes; this was not observed, also the pulse shapes in adjacent X-Y modules were seen to be identical. A difference in the electrode separation will result in a change in the applied field, 1 mm difference corresponding to approximately 0.5 kV/Cm charge in field strength. All shower modules were manufactured to the same tolerances and were essentially identical. However, since the X and Y modules were manufactured in two separate production batches, it is possible that such a variation did exist.

5.8.2 Effect of Rate on Sensitive Time

The sensitive time was measured in the same manner as described in section 5.4.2, for two event rates of 0.5 and 5 events sec^{-1}. The results are shown in Figure 5.9. During data acquisition, a 100 Hz, $\pm$ 30 V square wave clearing field was applied across the tubes. It can be seen that a factor of 10 increase in event rate produces a 40% increase

in sensitive time.

The sensitive time of the flash tube is determined by the ability of the primary ionisation to remain free within the volume of the gas. This is influenced by a number of factors, principally recombination and drift, under the influence of fields to the tube walls. It is expected that due to the increased induced field across the flash tube at high rates, the loss of primary ionisation due to drifting to the tube walls would also increase, resulting in a reduction of the sensitive time. Since the reverse tendency is observed it is suggested that the increase in apparent sensitive time is not due to the primary ionisation remaining in the gas volume, but due to a secondary charge production mechanism, resulting from the presence of the high induced fields.

5.8.3 Effect of Rate on Recovery Time

The recovery time was measured for 5 rates between 1 and 20 events sec^{-1} with an applied field of 4.75 kV/Cm, length 2 μs, using the technique described in section 5.4.3. The results are shown in Figure 5.32. After a steep initial rise the curve plateaus and starts to fall. The reason for this fall is thought to be due to the reduction of the effective applied H.T. field by the induced field. Although care was taken to ensure that the 2nd applied pulse would produce a field of 4.75 kV/Cm, to ensure a normal efficiency, the effective applied field was far less. For example, assuming a decay constant of 3.0 sec for the induced field and assuming an applied field of 4.75 kV/Cm, the strength of the induced field, after 50 ms (corresponding to the period associated with an event rate of 20 sec^{-1}) will be approximately 1.1 kV/Cm giving an effective applied field of 3.65 kV/Cm, which is below the field strength required for maximum efficiency. This calculation is only intended to illustrate the problem which is more complex involving a dynamic equilibrium of many factors.

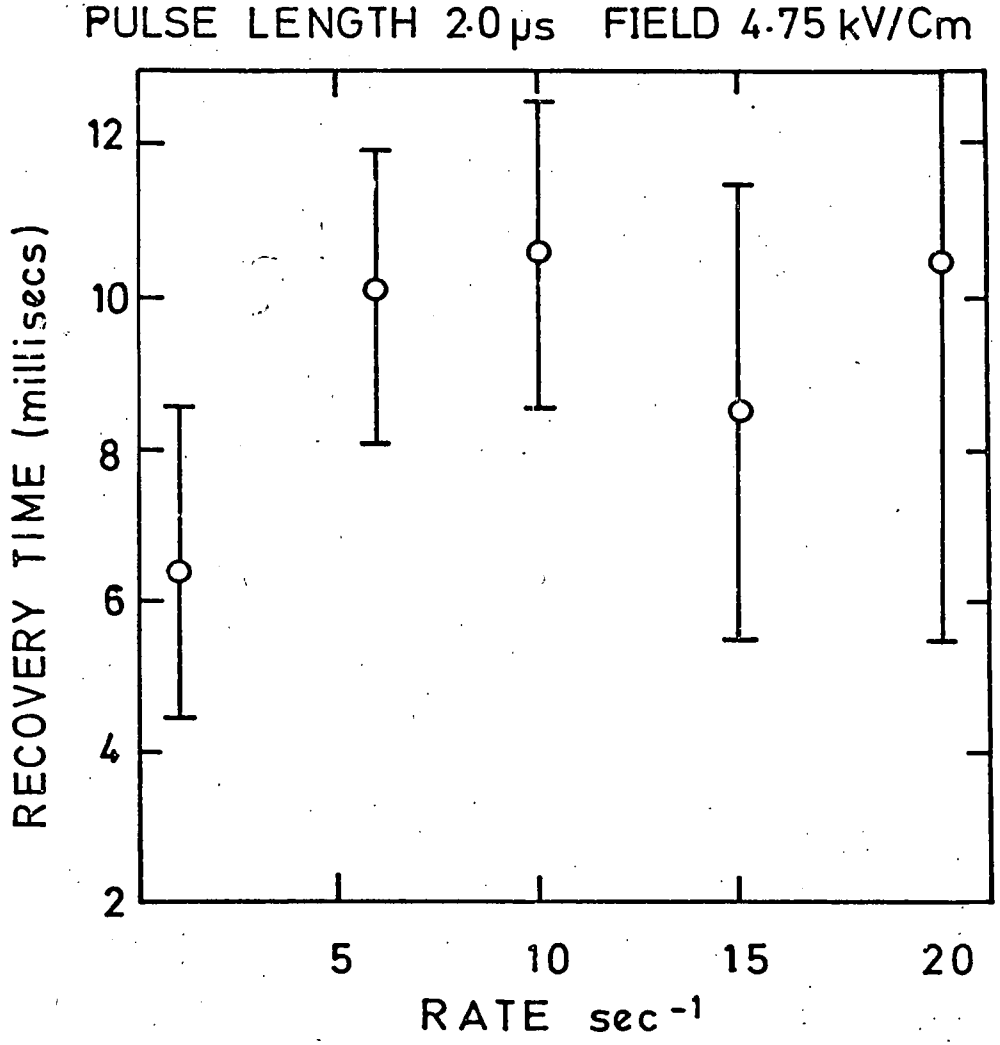

FIGURE 5·32 RECOVERY TIME AS A FUNCTION OF RATE

It is suggested that the rise in the recovery time with event rates is due to the same secondary charge production process which influenced the sensitive time.

5.8.4 Effect of Rate on Energy and Spatial Resolution.

The methods employed in the measurement of energy and position require that the detector responds uniformly to the changing parameters of the electromagnetic shower. It is to be expected that should this response also depend upon the event rate of the detector, it would completely invalidate any attempt to measure the primary energy and position.

Figure 5.33 shows the mean number of tubes igniting as a function of event rate for 1.0 GeV primary energy and 0.6 radiation lengths of target. It can be seen that the mean number of tubes igniting increases dramatically above an event rate of 10 sec^{-1}. This is due to a mechanism, as yet not fully understood but associated with the induced field, which is responsible for the presence of free charge in the gas, resulting in spurious flashing. The fall of the curve beyond a rate of 40 sec^{-1} is due to the almost complete backing off of the applied field by the induced field. Such a dependence on event rate would make it impossible to measure energy by the present method.

The dependence of spatial and angular resolution upon event rate is shown for 1 GeV and 0.6 radiation lengths of lead target in Figure 5.34. It appears that the resolution varies very little with rate, however this is due to the fact that the spurious flashing tubes are located along the axis of the shower, which varies little with successive events, and results in an enhancement of the distribution of flashing tubes in each sampling plane. Should the primary positron be incident over a larger area and a wider range of incident angle, it is expected that the spatial and angular resolution would deteriorate appreciably.

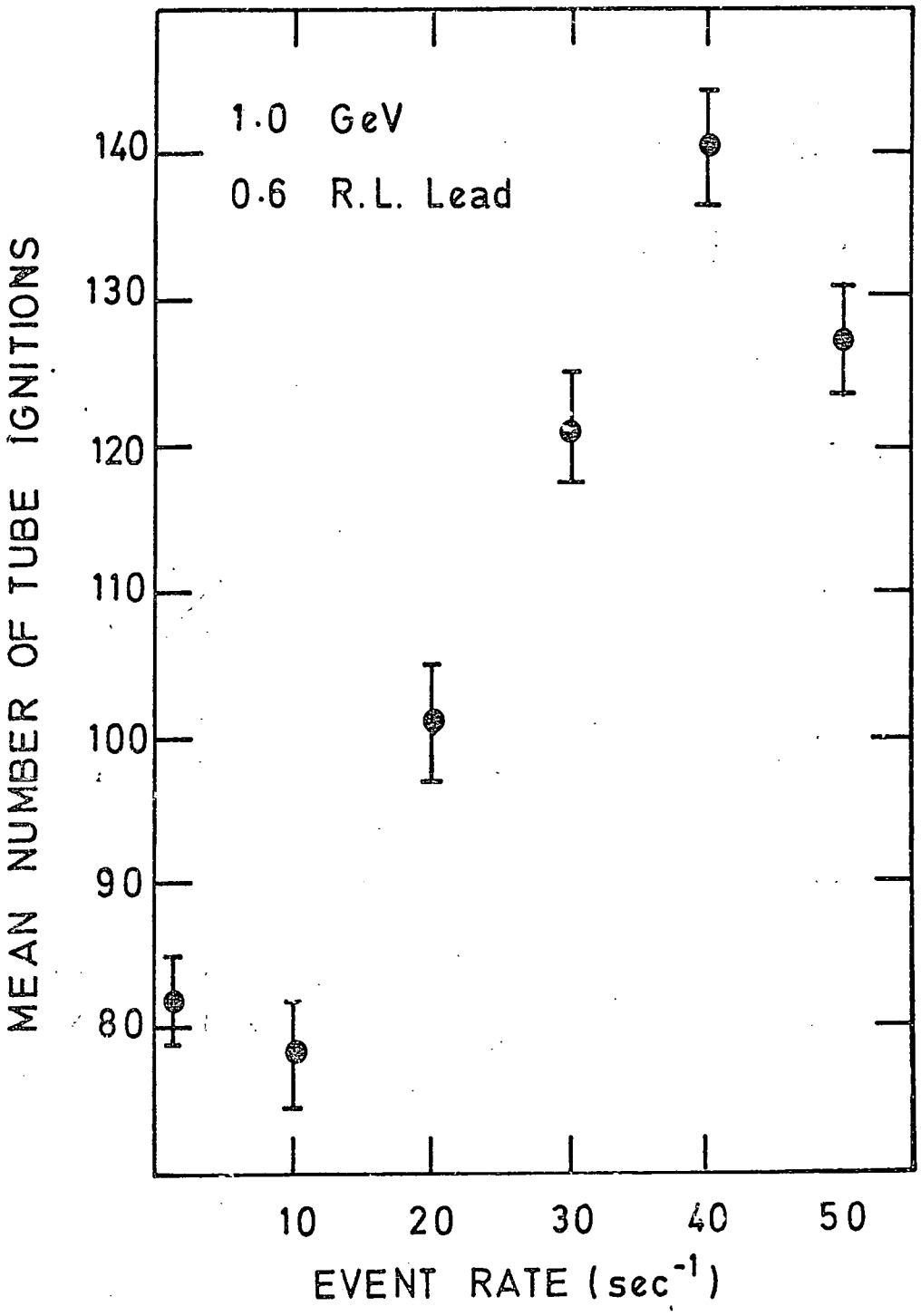

FIGURE 5.33 NUMBER OF TUBE IGNITIONS AS A FUNCTION OF RATE

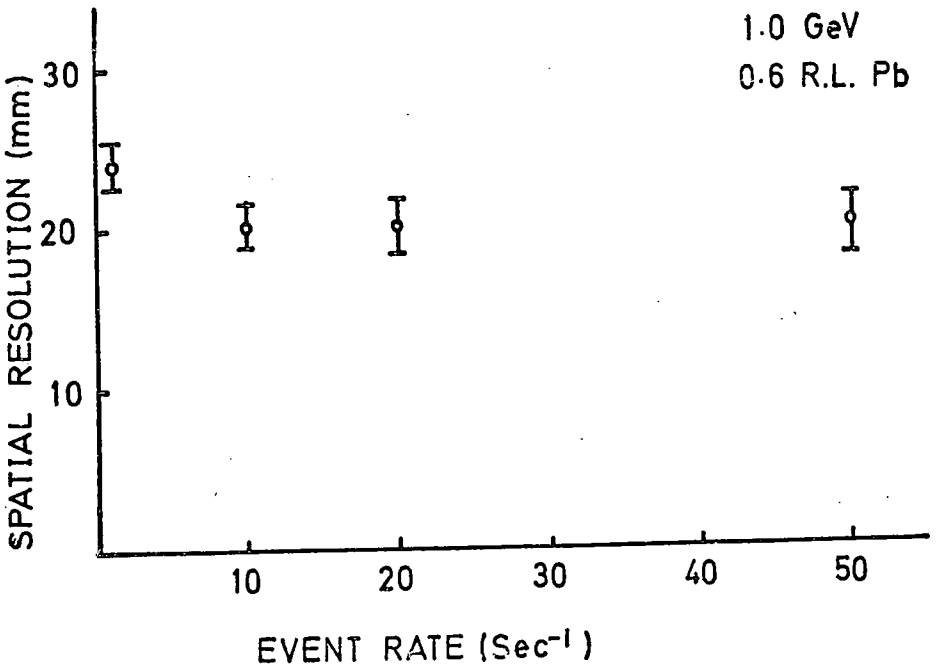

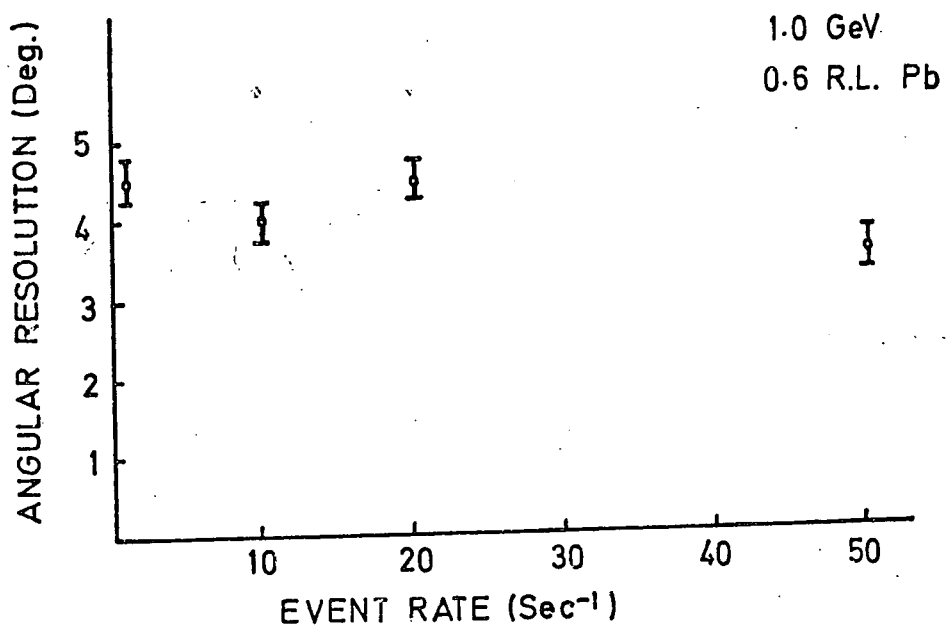

FIGURE 5.34 SPATIAL AND ANGULAR RESOLUTION AS A FUNCTION OF EVENT RATE

5.9 DISCUSSION

The principal aim in designing the low pressure flash tube chamber was to demonstrate that such a detector could offer an energy and spatial resolution comparable to that obtained using high pressure flash tubes, and further, that such a detector could operate at event rates required by typical HEP accelerator based experiments.

The first of these objectives has been achieved. The detector has been shown to work successfully in a high background environment such as experienced on accelerators. An energy resolution of 33% obtained at 1.5 GeV using 0.6 radiation lengths of target compares well with the resolution of 43% obtained with the high pressure flash tube chamber. The energy resolution is seen to follow a $1/\sqrt{E}$ dependence as expected and had it been possible to contain the shower completely at high energies, using 0.6 radiation lengths of target, the figure of 33% is expected to be improved upon. Spatial and angular resolutions of 11 mm and 2^{o} (FWHM) respectively were achieved, compared with 5 mm and 4^{o} obtained with the high pressure flash tube chamber. Both the energy and spatial resolutions are seen to be influenced at high energies, by the inability of the flash tube to resolve individual particles in dense showers, due to the width of the tube. It has been shown that good energy resolution requires almost total containment of the shower, whereas little improvement in spatial and angular resolution is achieved beyond 60% containment. These would be important considerations in the design of a future detector.

The second objective, to operate the chamber at high event rates, produced unexpected results in the light of the experience of previous workers[1]. The low pressure tubes, chosen because of their relative insensitivity to the effect of induced clearing fields at high rate, were seen to become spurious or inefficient at rates in excess of a few per

second, in a similar manner as the high pressure tubes.

The principal difference between the present tubes and those operated by earlier workers at rates of 50 sec^{-1}, is that the former tubes were painted and the latter sleeved in thin PVC tubing. It has been subsequently shown[2] that painting the tube increases the resistivity of the outer surface which has been shown to considerably enhance the effect of the induced field. It is quite probable that the sleeved tubes, at the time of their use, exhibited a much lower external surface resistance, which would explain their successful operation at a rate of 50 sec^{-1}.

The original sleeved tubes were operated in the present detector using identical H.T. pulse characteristics as used for their earlier operation; these tubes were seen to behave in the same manner as the painted tubes. This, however, is not a fair test, since the tubes had been stored in a warm dry atmosphere for 3 years, which would result in an increase in the outer surface resistance.

Although the mechanism by which the internal fields are produced, and the manner by which they reduce the efficiency are well understood[10,11,12], a satisfactory explanation of the mechanism by which free charge is made available to the gas volume has yet to be given. Many processes may produce free charge in an electric field of the magnitude of the induced field. The following phenomena, first observed by Francis[13] is suggested as the most likely cause. It has been found that charges residing on the surface of glass insulators may be easily removed from the surface by the application of DC electric fields of less than 1 kV/Cm. The phenomena was observed whilst studying discharges in neon, contained in a soda glass tube, a similar configuration to that of the flash tube. The charges residing on the surface were conclusively shown

to be responsible for the free charge in the gas, which resulted in spurious discharges.

Fields of the order of 1 kV/Cm have been seen to exist inside the flash tube for long periods after the tube has ignited. Therefore, under the influence of their own electric field the charges are removed from the wall, resulting in the tube flashing spuriously upon application of the next H.T. pulse.

If flash tubes are to be operated successfully at an event rate which satisfies the requirements of the typical accelerator based experiment, the factors influencing the formation and decay of the induced field must be fully understood. Investigations to this effect are described in the following chapter.

REFERENCES : CHAPTER FIVE

(1) Chaney, J.E., Breare, J.M., Nucl. Inst. Meth., 124 (1975), 61.

(2) Breare, J.M., Doe, P.J., Nandi, B.C., Submitted to Nucl.Inst. Meth. (1977).

(3) Hedge, A.R., Internal Report, NI-77-12, (1977) Durham University.

(4) Ayre, C.A., et al., Proc.Int. Conf.on Inst., for High Energy Physics, Frascati, (1973), 215.

(5) Goulding, F., Internal Report, Daresbury Laboratory, April 1974.

(6) Chaney, J.E., Ph.D. Thesis, University of Durham, 1974.

(7) Messel, H., Crawford, D., Electron-Photon Shower Distribution Function, Pergamon Press, (1970).

(8) Backenstoss, G., et al., Nucl.Inst.Meth., 21, (1963), 155.

(9) Siegbahn, K.M.G., Beta and Gamma-Ray Spectroscopy, North Holland Publishing Co., Amsterdam, (1955).

(10) Breare, J.M., Doe, P.J., Nandi, B.C., Submitted to Nucl.Inst.Meth, (1977).

(11) Breare, J.M., Doe, P.J., Nandi, B.C., Nucl. Inst.Meth., 133, (1976), 247.

(12) Holroyd, F.W., Ph.D. Thesis, Durham University (1971).

(13) Francis, G., Proc.Phys. Soc. Lond., B68 (1955), 137.

CHAPTER SIX

A STUDY OF THE FLASH TUBE DISCHARGE MECHANISMS AND FACTORS INFLUENCING THE INDUCED FIELD

6.1 INTRODUCTION

In the light of the unexpected results obtained whilst operating the low pressure flash tubes at high event rates, it is clear that further investigation into the discharge mechanism of the tube is necessary if a solution to the problems of the induced field is to be found.

A novel approach has been made in attempting to understand the discharge mechanisms, by studying the behaviour of the digitisation pulse under various operating conditions. Because of the manner in which the digitisation pulse is formed, this method is particularly sensitive to the plasma density in the tube, which has a bearing upon the resultant internal field, and may be used to estimate the properties of this field.

The significance of the outer surface resistance, which is the most probable explanation of the failure of the present low pressure tubes to operate at the high rates obtained by previous workers[1], has also been investigated. This was achieved by observing the behaviour of the sensitive time, which is field dependent[2], as the outer surface resistance of the tube was changed.

The behaviour of the sensitive time was also used to investigate the dependence of the magnitude of the induced field upon the applied HT pulse parameters, such as pulse length and frequency of an oscillating HT pulse.

The results of these investigations are presented below.

6.2 THE FLASH TUBE DISCHARGE MECHANISM FROM A STUDY OF THE DIGITISATION PULSE

A study of the digitisation pulse may appear to be a rather indirect method of investigating the discharge mechanisms occurring inside the flash tube. However, since the digitisation pulse is formed by a capacitive coupling of the digitisation probe to the HT electrode by way of the gas plasma, the technique is expected to be particularly sensitive to the changing plasma conditions and hence the discharge mechanisms occurring in the tube.

6.2.1 The Discharge Mechanisms

(a) THE TOWNSEND MECHANISM : An energetic charged particle, traversing a gas will lose energy by excitation and ionisation of the gas molecules, resulting in a trail of ionisation along its path. The total amount of ionisation distributed along the track may be found from the following relation,

$$j_{total} = \frac{dE/dX}{V_o}$$

where: j_{total} = total number of ion pairs created per unit length of path.

dE/dX = energy loss by primary particle per unit length of path (eV/Cm).

V_o = average energy to create one ion pair (eV).

For example, a particle in neon at atmospheric pressure is expected to liberate on average some 37 ion pairs/Cm of path. Upon application of an electric field these primary ions will accelerate towards their respective electrodes. If sufficient energy is gained then collisions between the gas atoms and the electrons will liberate further electrons, which in turn accelerate and result in further ionisation. In this manner multiplication

occurs and an avalanche is rapidly built up. The electrons will travel rapidly ($\sim 10^7$ Cm.Sec^{-1}) [3] towards the anode, whilst the more massive positive ions move more slowly ($\sim 10^5$ Cm.sec^{-1}) [4] towards the cathode.

The number of electrons produced by an electron in moving a distance dx is given by

$$dn = \alpha dx$$

where α is the first Townsend ionisation coefficient. Hence the number of electrons produced in length x, by one electron is given by

$$n = \exp(\alpha x)$$

In this manner the number of electrons increases exponentially as the avalanche crosses the tube, and in the case of the flash tube, terminates on the anode wall. The arrival of the positive ions at the cathode wall results in the release of further electrons, which in turn will avalanche across the gas volume.

The discharge in the flash tube is not limited to the immediate volume traversed by the ionising particle. Photo electrons produced in the initial avalanche will result in further charge production, principally by collision with the glass walls remote from the initial avalanche. These photo electrons produced at the cathode wall will result in further avalanches, and in this manner the discharge will propagate down the length of the tube at approximately 0.24 Cm/n.sec [2].

The increasing number of electrons and positive ions deposited on the anode and cathode walls will result in an induced electric field opposing the applied HT field. In this manner the effective HT field across

the gas will decrease until a stage is reached where the field will no longer maintain sufficient multiplication and the discharge is self quenched.

(b) THE STREAMER MECHANISM : When higher electric fields are applied across the gas a second phenomena, the streamer effect, will occur. Some doubt exists as to the exact mechanisms by which the streamer is formed and only a simple model will be presented here.

When the number of ion pairs produced in the Townsend discharge reaches approximately 10^6, the space charge effect caused by the separating clouds of electrons and positive ions becomes significant, and the electron avalanche begins to slow down due to the attraction of the positive ions.

Raether[5] suggested that the criterion for the transition of an avalanche to a streamer is given by

$$\alpha \, x_c = 20$$

where : x_c = the critical length of the avalanche.

This condition is represented by some 10^8 ion pairs, by which the applied field is effectively neutralised by the space charge dipole, and charge recombination starts to occur. This results in the isotropic production of UV photons, which ionise molecules outside the region of the primary avalanche. Those ions produced in this manner, at the head and tail of the avalanche, will experience an enhanced field due to the presence of the electron and positive ion clouds, and will rapidly form new avalanches, and the process continues. Those ions produced at the sides of the avalanche will encounter a reduced field and contribute little to further multiplication.

The new avalanches produced at the head and tail of the original avalanche will merge with it forming the streamer which advances towards the cathode and anode at about 10^8 Cm.sec^{-1}. The streamer will be seen as a

bright filament of highly ionised gas surrounded by a dark region where little multiplication occurs.

The interaction of photons with the cathode wall will produce further avalanches along the length of the tube, which may also develop into streamers. Eventually, as with the Townsend mechanism, the discharge is self-quenched.

Figure 6.1 shows both Townsend and streamer avalanches occurring in a flash tube filled with Ne:He (98:2) at 600 torr. For high fields of 6.4 $kV.Cm^{-1}$ (Figure 6.1 (a)) the bright filaments of the streamers, interspaced with dark low field areas where little multiplication takes place, can be clearly seen. At the lower field of 3.6 $kV.Cm^{-1}$, the tube is filled with a diffuse glow, which is due to the Townsend mechanism alone.

6.2.2 Experimental Technique

The digitisation of flash tubes by the use of an external probe was first introduced by Ayre[6]. The magnitude of the digitisation pulse depends upon the plasma density and the magnitude of the HT pulse at the time of formation of the plasma. It is expected, therefore, that the size and shape of the digitisation pulse will depend upon the discharge mechanism of the flash tube.

The experimental arrangement is shown in Figure 6.2. The flash tube to be studied was placed with its plane end in contact with the head of the digitisation probe, which was held to ground by a 5.7 k Ω resistor chain, across which the digitisation pulse appeared. Single ionising β particles were selected from a 1 m Ci RU 106 source by means of a twofold coincidence of the scintillators S_1 and S_2. Upon obtaining a coincidence the logic was paralysed against further coincidences for a period of time which depended upon the event rate at which it was wished to operate. The

FIGURE 6.1 THE FLASH TUBE DISCHARGE UNDER TWO DIFFERENT APPLIED FIELD STRENGTHS

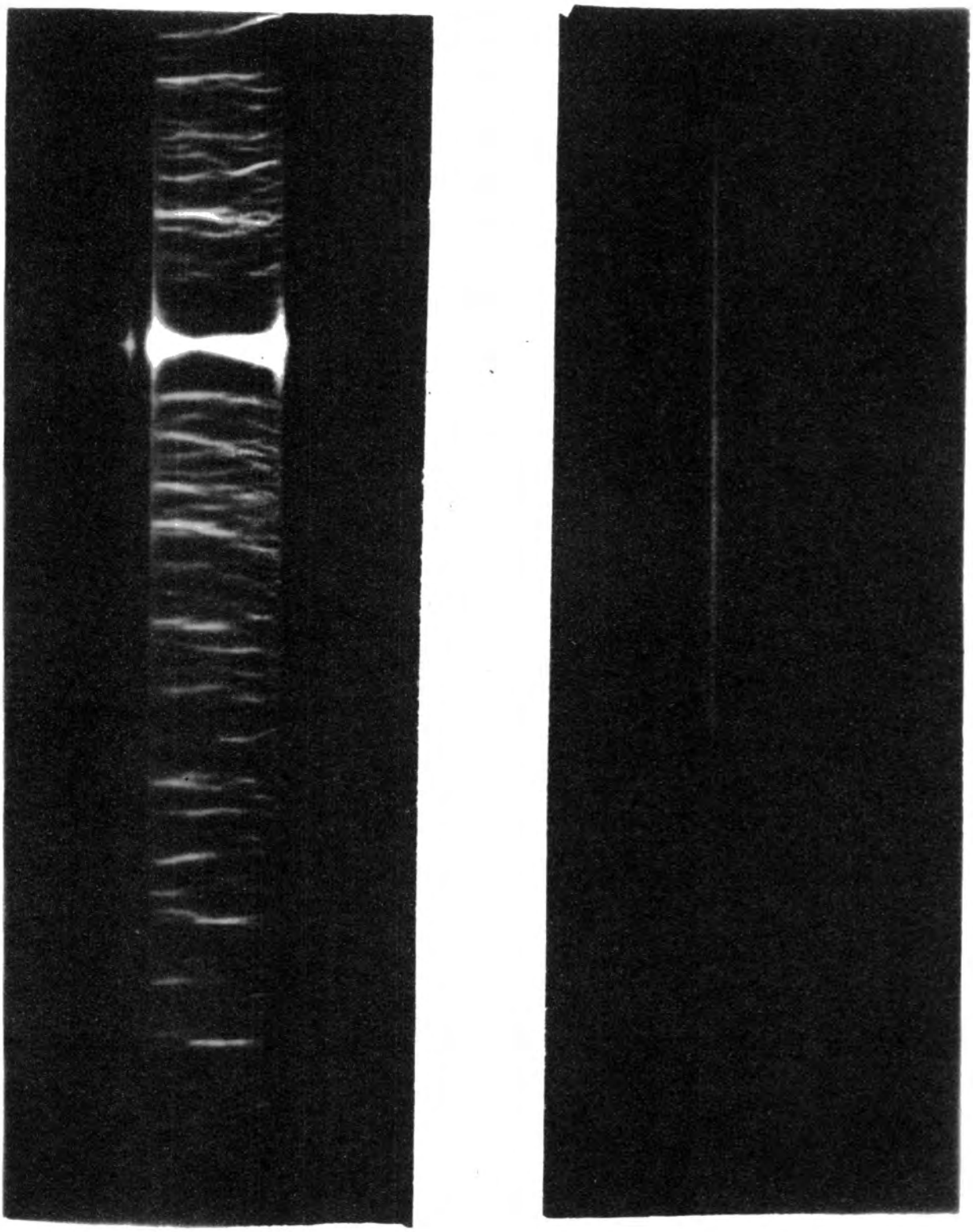

(a)
FIELD 6.4 kV/Cm.

(b)
FIELD 3.6 kV/Cm

GAS COMPOSITION NEON: HELIUM, 98:2, PRESSURE 600 Torr

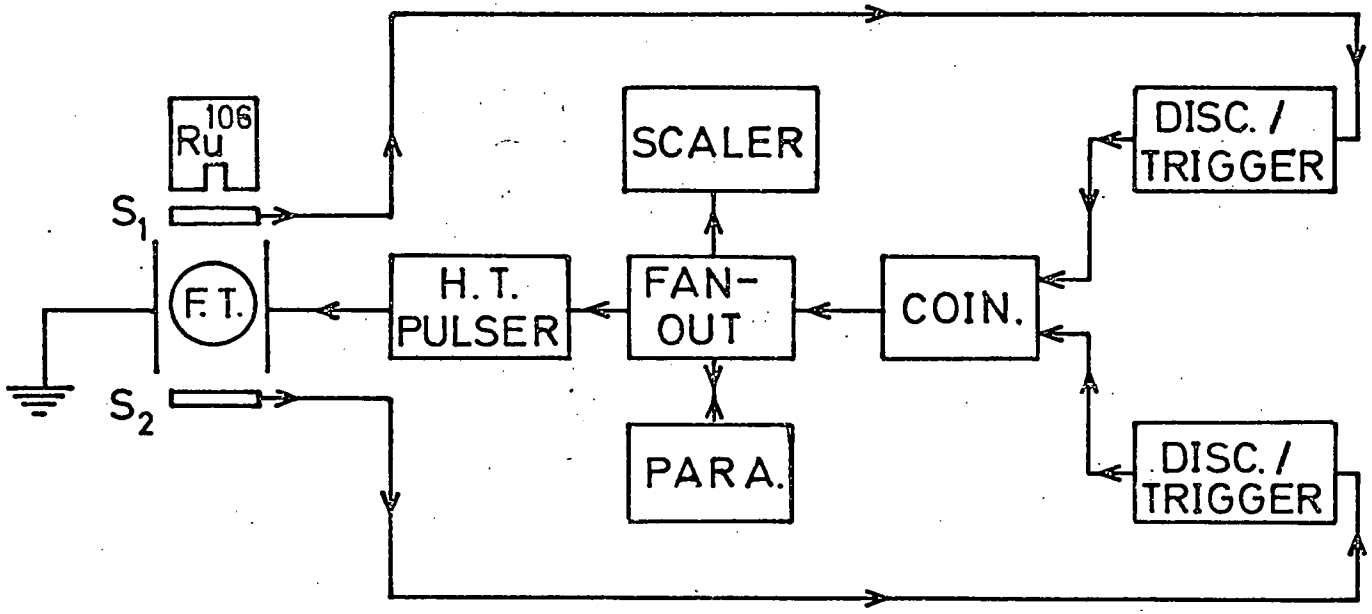

FIGURE 6-2 SCHEMATIC DIAGRAM OF EXPERIMENTAL ARRANGMENT

high voltage thyratron pulser was then triggered, discharging a 3000 pf capacitor through a 3.3 k Ω resistor, resulting in a pulse of rise time 60 ns, and RC decay time of about 10 μs, appearing on the HT electrode.

The tubes under investigation were coated in a thin layer of white enamel paint to reduce the effects of water vapour contaminating the outer surface of the tube, which is known to influence the induced fields occurring in the tube (see section 6.3.3). Three gas mixtures, typically used in flash tubes, were investigated. These were Ne: He (70:30), Ne:He (98:2) and Ne:He (70:30) + 1% CH_4; these will be referred to as gas types I, II and III respectively. The characteristics of the tubes are given in Table 6.1.

TABLE 6.1 : Characteristics of the Tubes

Glass Type	Diameter (mm) Internal	Diameter (mm) External	Pressure (Torr).	Gas Composition (%) Type I	Type II	Type III
S95 Soda Glass	16	18	600	Ne:He 70:30	Ne:He 98:2	Ne:He 70:30 +1% CH_4

6.2.3 The Digitisation Pulse Output

Figure 6.3 shows the digitisation pulse output for a tube filled with type II gas for 3 values of applied field. The pulse shapes were obtained as traces from an oscilloscope photograph. It can be seen that for fields of 3.1 $kV.Cm^{-1}$ the digitisation pulse is small, as may be expected since the discharge is almost solely by the Townsend mechanism and hence the plasma density is low. A small second peak occasionally appears after the Townsend pulse ; this will be seen to be associated with the appearance of

FIGURE 6.3 DIGITISATION OUTPUT PULSES FROM THE FLASH TUBE FOR VARIOUS APPLIED FIELDS

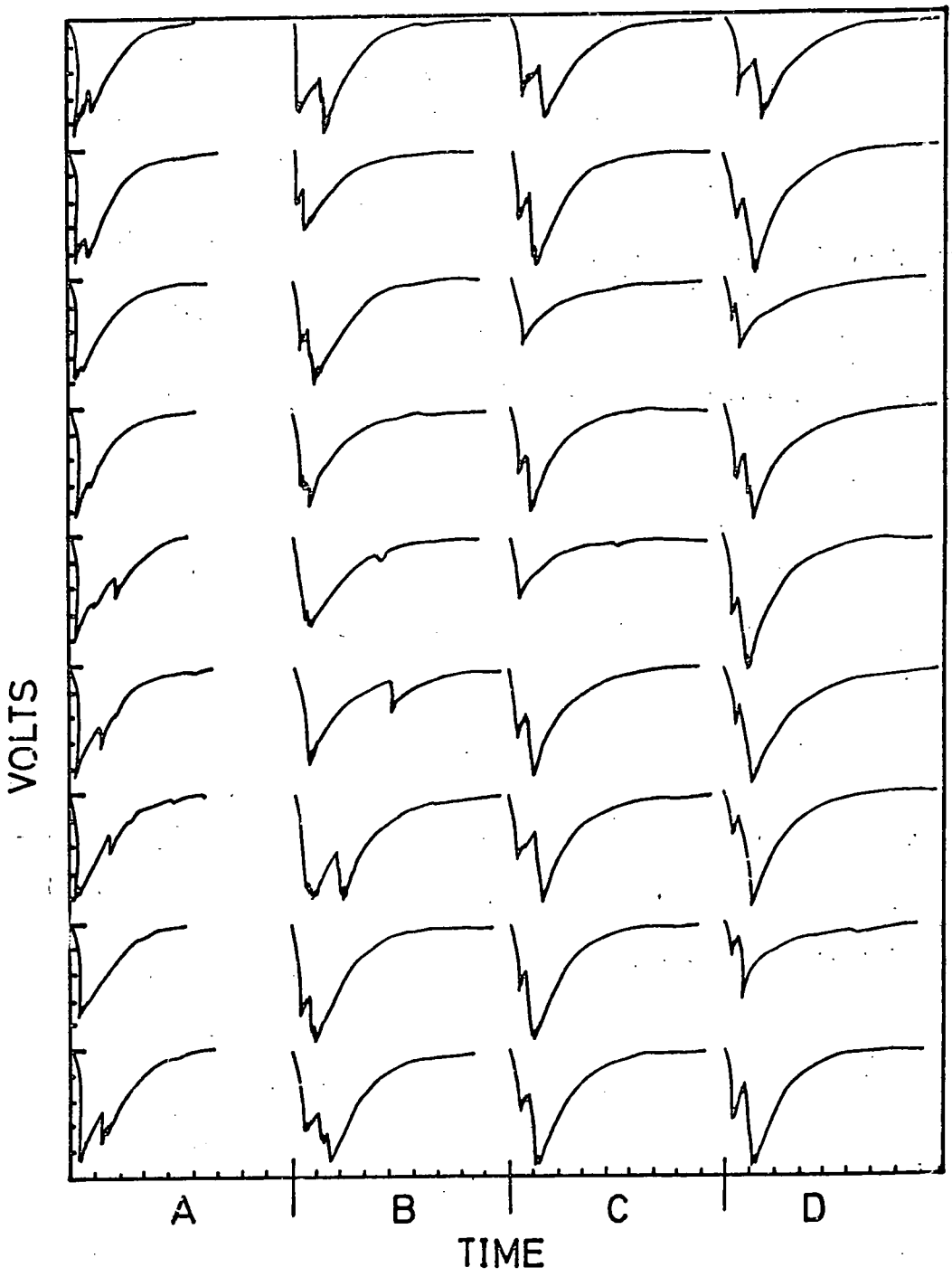

A : FIELD 3·1 kV/cm, SCALE 0·5V/DIV., 500 NS/DIV.
B : " 3·7 " " " 1·0 " 500 "
C : " 4·3 " " " 2·0 " 500 "
D : " 4·9 " " 2·0 " 500 "

very weak streamers. As the field strength is increased, the second pulse increases rapidly in size, as the production of dense streamers rapidly increases the capacitive coupling to the HT electrode. It should be noted that at no time does the streamer pulse occur without the prior appearance of the Townsend pulse, as may be expected. The time between the two pulses is not constant for a fixed field value, however, for higher field values the streamer pulse occurs increasingly earlier.

The distribution of pulse heights obtained for a tube filled with gas type II, using a field of 4.9 $kV.Cm^{-1}$, at a rate of 14 events min^{-1}, is shown in Figure 6.4. It can be seen that there are two distinct groups into which the pulses fall, associated with the two types of discharge mechanism. At low field values some small streamer pulses do occur, as can be seen in 6.3. These will be stored in the PHA as Townsend pulses, since only one peak was recorded for each pulse.

6.2.4 Percentage of Discharges Involving Streamer Formation As A Function of Applied Field

The number of discharges which take place by the Townsend mechanism, and the number involving streamers may be found from the distribution of pulse heights as seen in Figure 6.4. To obtain the transition from discharges solely by Townsend mechanism, to that dominated by the occurrence of streamers, pulse height distributions over a range of field strengths were obtained. Figure 6.5 shows the percentage of discharges involving streamers as a function of applied field of both positive and negative polarity, for a tube filled with gas type I, at an event rate of 10.8 min^{-1}. It can be seen that for a field strength of 5.1 $kV.Cm^{-1}$, 50% of the pulses are due to streamer breakdown, whilst at the higher field of 7.0 $kV.Cm^{-1}$, the streamer mechanism is seen to completely dominate. Similar relationships were

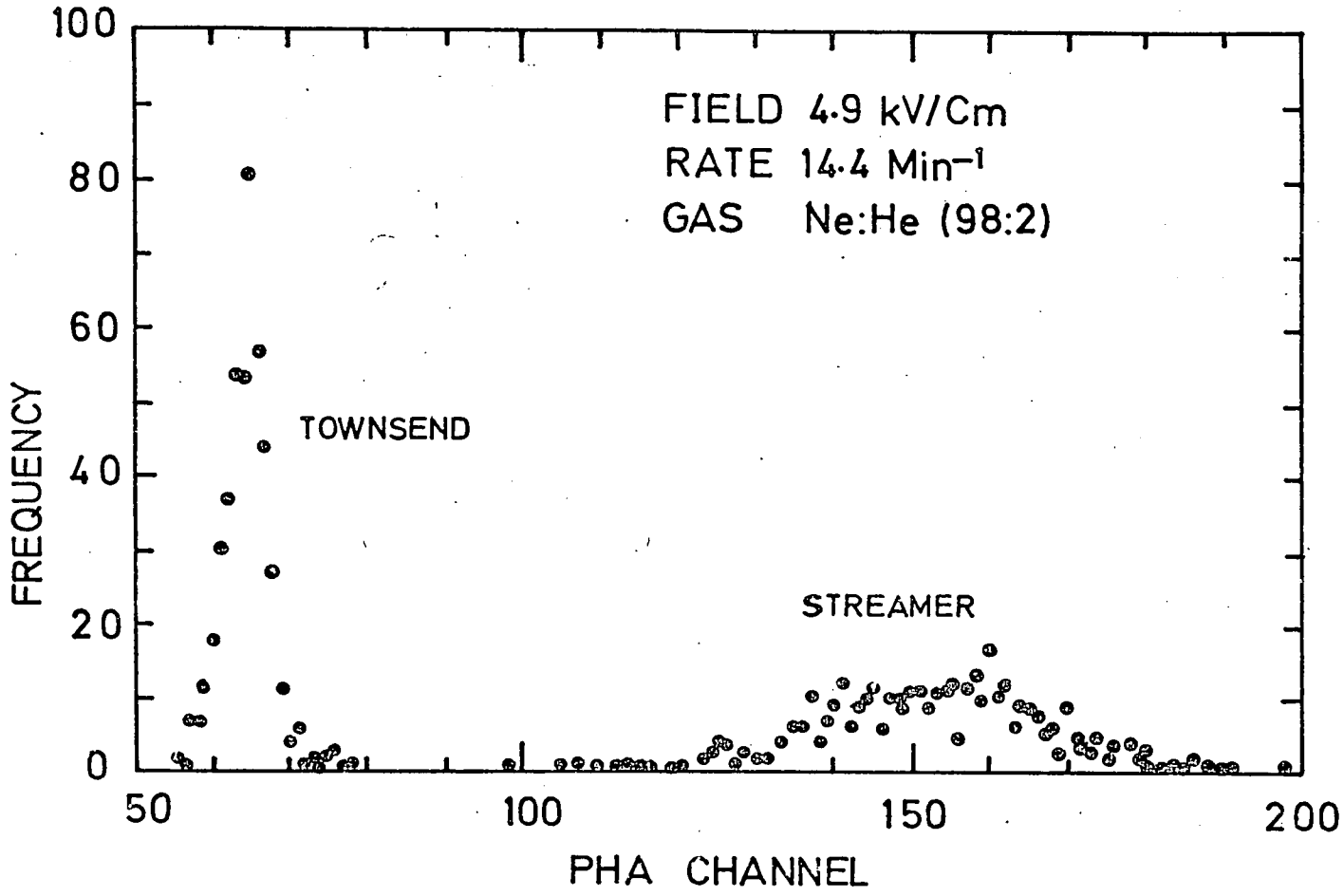

FIGURE 6.4 DISTRIBUTION OF DIGITISATION PULSE HEIGHTS INTO TWO DISTINCT GROUPS ASSOCIATED WITH TOWNSEND AND STREAMER DISCHARGE MECHANISMS

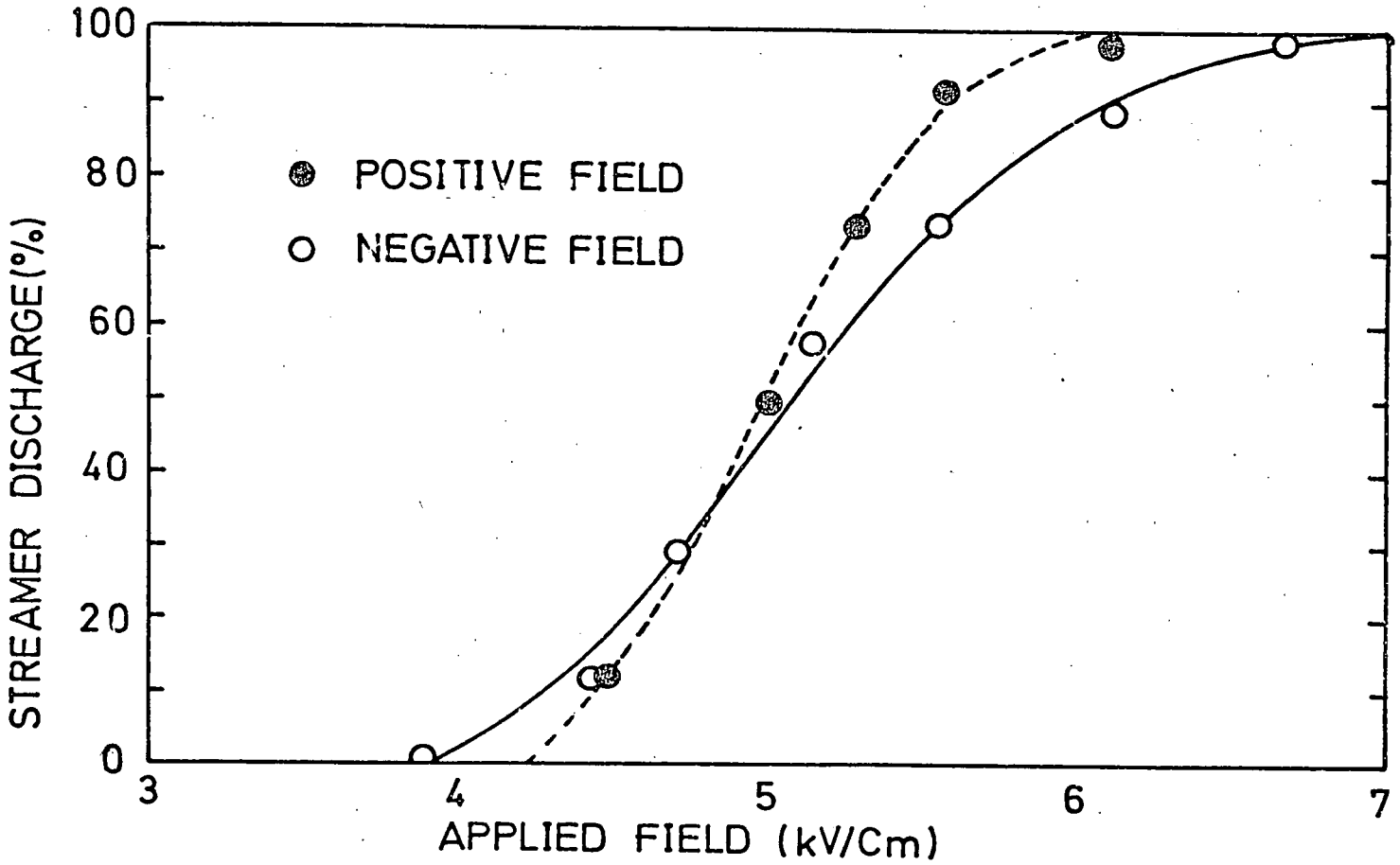

FIGURE 6.5 PROBABABILITY OF STREAMER BREAKDOWN AS A FUNCTION OF APPLIED FIELD (RATE 10.8/MIN.)

obtained for gas types II and III, and the positive and negative field strengths necessary for 50% and 100% probability of streamer formation are given in Table 6.2.

TABLE 6.2 : Field For Streamer Transition

Gas Composition	Negative Applied Field ($kV.Cm^{-1}$)		Positive Applied Field ($kV.Cm^{-1}$)	
	50% Probability	100% Probability	50% Probability	100% Probability
Ne:He (70:30)	5.1	7.0	5.0	6.0
Ne:He (98: 2)	5.9	6.9	5.1	6.4
Ne:He (70:30) +1% CH_4	4.5	6.0	4.5	5.8

It can be seen that there is no significant difference in the applied fields required to give streamer breakdown in the 3 gas types. The probability of a streamer occurring, for a particular applied field value, is greater with a positive HT field, than with a negative one. This is in agreement with the results of Breare[7] who found that with the high pressure flash tubes the induced field was significantly less with a positive HT field, and consequently streamer formation occurs at a lower applied field.

An approximate value of the field strength necessary for the formation of streamers may be simply obtained by the theory developed by Meek[8], who proposed that the transition from avalanche to streamer takes place when the field intensity due to the positive ion cloud becomes comparable to the applied field. This may be expressed in the following manner.

$$N_+ = \frac{\alpha \exp \alpha X_o}{\pi r_o^2} \qquad (1)$$

where : N_+ = positive ion density

α = first Townsend coefficient

X_o = distance of advance of the avalanche

r_o = radius of electron avalanche head.

The radius of the avalanche head may be expressed using the one dimensional diffusion equation

$$r_o = \sqrt{2Dt}$$

$$= \sqrt{2DX_o/V} \qquad (2)$$

where : D = electron diffusion coefficient

V = electron drift velocity

Assuming the positive ions are uniformly distributed within a sphere of radius r_o, then the electric field intensity (E_r) at the surface of the sphere may be calculated using Gauss's law.

$$E_r = \frac{4}{3} \pi r_o^3 N_+ e \Big/ 4\pi\varepsilon_o r_o^2 \qquad (3)$$

substituting for N_+ and r_o into equation (3) gives

$$E_r = \frac{e \alpha \exp (\alpha X_o)}{3 \pi \varepsilon_o} \sqrt{\frac{V}{2DX_o}} \qquad (4)$$

where e is the charge of the electron.

Using Meeks criteria for the transition to streamer breakdown, $E = E_r$, where E is the external applied field, and using the relationship $\alpha = \eta E$, one obtains

$$\eta E X_o = \ln \left\{ \frac{3\pi \varepsilon \sqrt{2DX_o/V}}{e\eta} \right\} \qquad (5)$$

In deriving this relationship a number of assumptions have been made. Owing to space charge effects there exists some uncertainty as to the field experienced by the electrons, and therefore their drift velocity, V. However, it can be seen from equation (5) that $\eta E X_o$ is not strongly dependent on the value of V. Further, it is assumed that $E = E_r$, as suggested by Meek, however it was noted by Hopwood[9] that the electrons at the rear of the advancing electron cloud, ahead of the positive space charge, experiences a reduced field due to space charge effects, and therefore $E_r = KE$ where $K < 1$. However, $\eta E X_o$ is seen to vary little for values of K between 0.1 and 1.

Substituting the values $\varepsilon_o = 8.854 \times 10^{-12}$ F.M^{-1}, $e = 1.6 \times 10^{-19}$ C, $D = 2 \times 10^{-1}$ M^2.sec^{-1}, $V = 10^5$ M.sec^{-1} into equation (5) one obtains,

$$\eta E X_o \simeq \ln \left\{ \frac{10^5 \sqrt{X_o}}{\eta} \right\} \qquad (6)$$

From this relationship the field intensity required for streamer formation may be obtained by means of a graphic method. By plotting equation (6), for given values of pressure (P) and X_o, on a graph of η as a function of E/P[10], by knowing the value of E/P at the crossing point of the two curves, one can obtain the field intensity for streamer formation.

This is shown in Figure 6.6 for P = 600 torr and X_o = 0.5 cm, 1.0 cm and 1.5 cm. The values of E required for streamer formation are given in Table 6.3.

TABLE 6.3 : Calculated Field For Streamer Transition

X_o (Cm)	0.5	1.0	1.5
E (kV/Cm)	6.0	4.92	4.26

Considering the crudeness of the calculation, and that it was carried out for pure neon, the calculated field values are in reasonable agreement with those obtained experimentally using 1.6 cm internal diameter tubes, as given in Table 6.2.

6.2.5 The Effect of Rate on the Probability of Streamer Production - The Induced Field

The discharge that occurs in a flash tube, as discussed in section 6.2.1, is self-quenching, due to the backing-off of the applied field, due to charge deposited on the inner wall of the tube. These charges are expected to be removed by movement around the walls, enabling opposite charges to neutralise. The field due to these charges has been observed to decay according to

$$E = E_o \exp(-t/\tau) \qquad (7)$$

where: E_o = field at time t = 0

E = field at time t

τ = decay constant.

FIGURE 6.6 GRAPHIC METHOD OF ESTIMATING THE BREAK-DOWN FIELD INTENSITY IN NEON

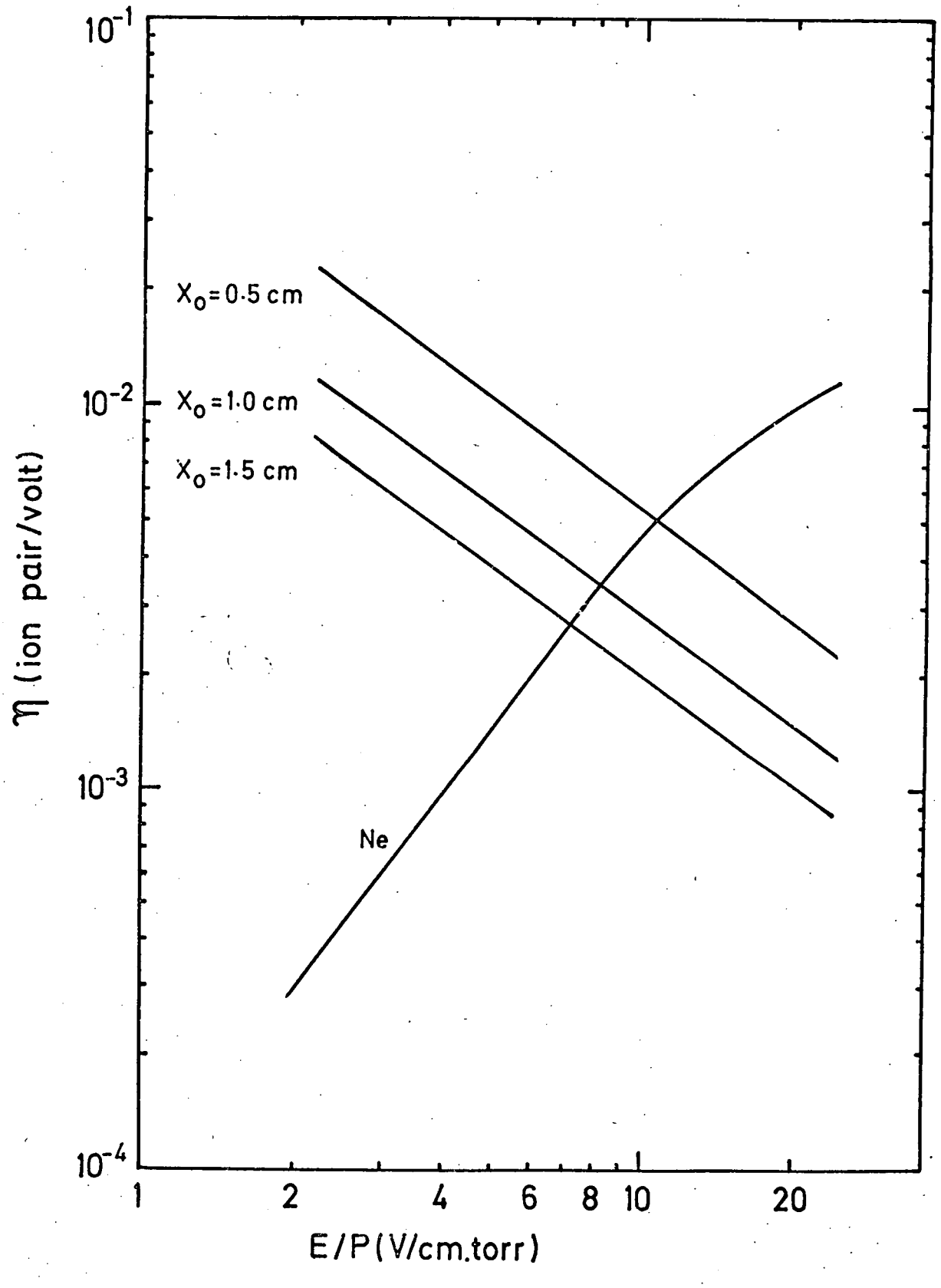

The decay constant, τ, may be expressed as $\tau = RC$, where R is the resistance of the glass surface and C is the intrinsic capacitance of the tube.

The magnitude of the induced field will increase with increasing flashing rate, and this will exhibit itself by a decrease in the percentage of discharges involving streamers, at a particular applied field. The percentage of streamers occurring as a function of event rate, for an applied field of 5.6 $kV.Cm^{-1}$, is shown in Figure 6. 7, for a tube filled with gas Type I. The percentage of discharges involving streamers is seen to fall with increasing event rate, indicating an increase in the induced field. Similar variations were observed for tubes filled with gas Types II and III.

Since the fall in the percentage of streamers is directly due to the presence of the induced field, an attempt was made to obtain a value for the induced field and its decay, by relating the data contained in Figures 6.5 and 6.7. This was achieved by taking the difference (for a particular percentage of streamer discharges) in the applied field at a high event rate (Figure 6.7), and the applied field at a low event rate (Figure 6.5), where the effect of the induced field is negligible. This difference is accounted for by the size of the induced field.

The decay of the induced field with time, obtained in this manner, is given in Figure 6.8, for a tube filled with gas Type I. Although there exists a slight difference in the decay rate of the induced field, for negative and positive applied fields, it is insignificant compared with the differences obtained by Breare[11] using the high pressure tubes, this may be due to the large fields ($\simeq$ 11 $kV.Cm^{-1}$) required to operate these tubes.

The general shape of the decay curve is in agreement with that obtained by more direct methods[12]. The field is seen to initially decay rapidly, and then, after a few seconds, the rate of decay slows. It is

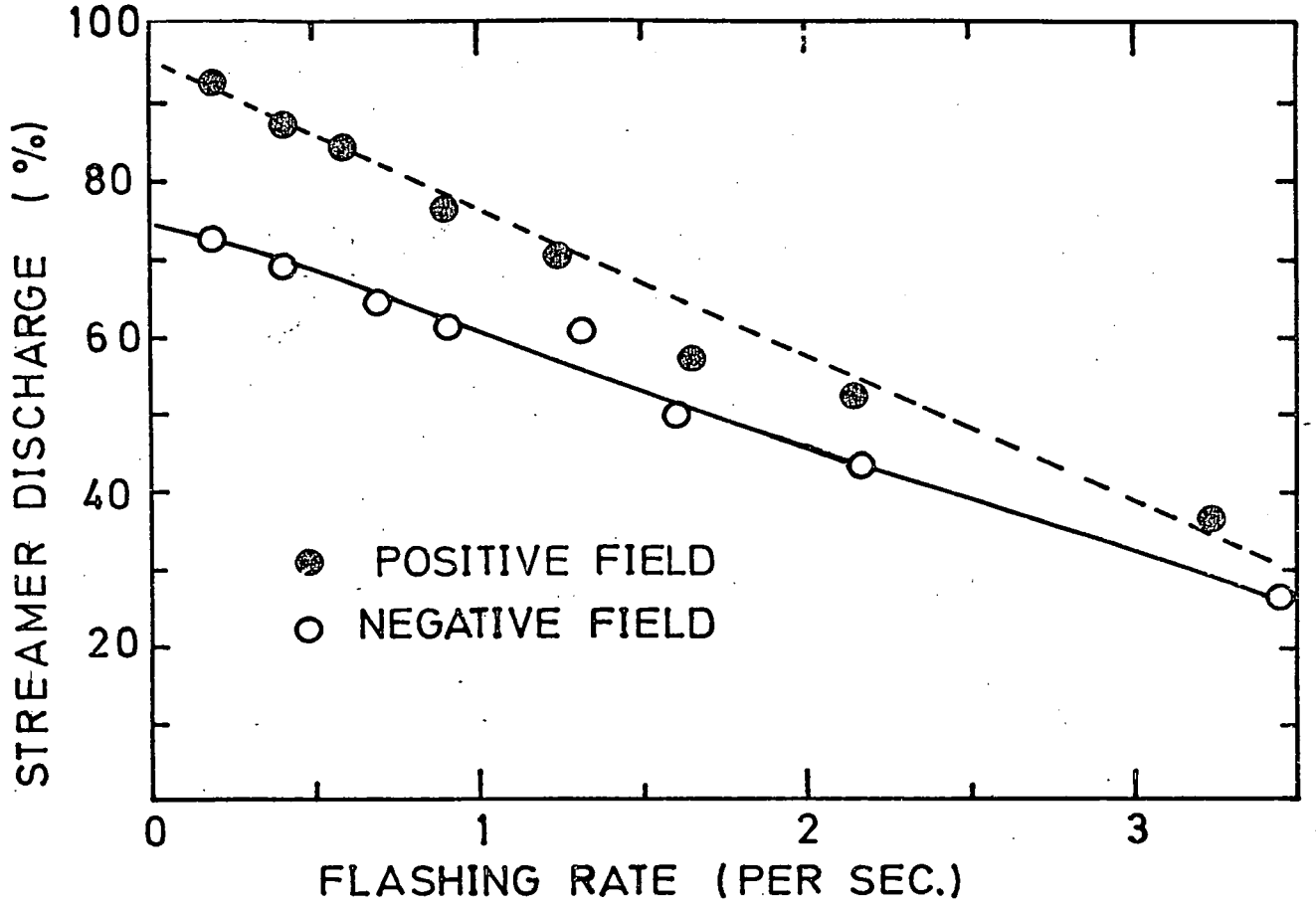

FIGURE 6.7 PROBABILITY OF STREAMER DISCHARGE AS A FUNCTION OF EVENT RATE FOR AN APPLIED FIELD OF 5.56 kV/cm

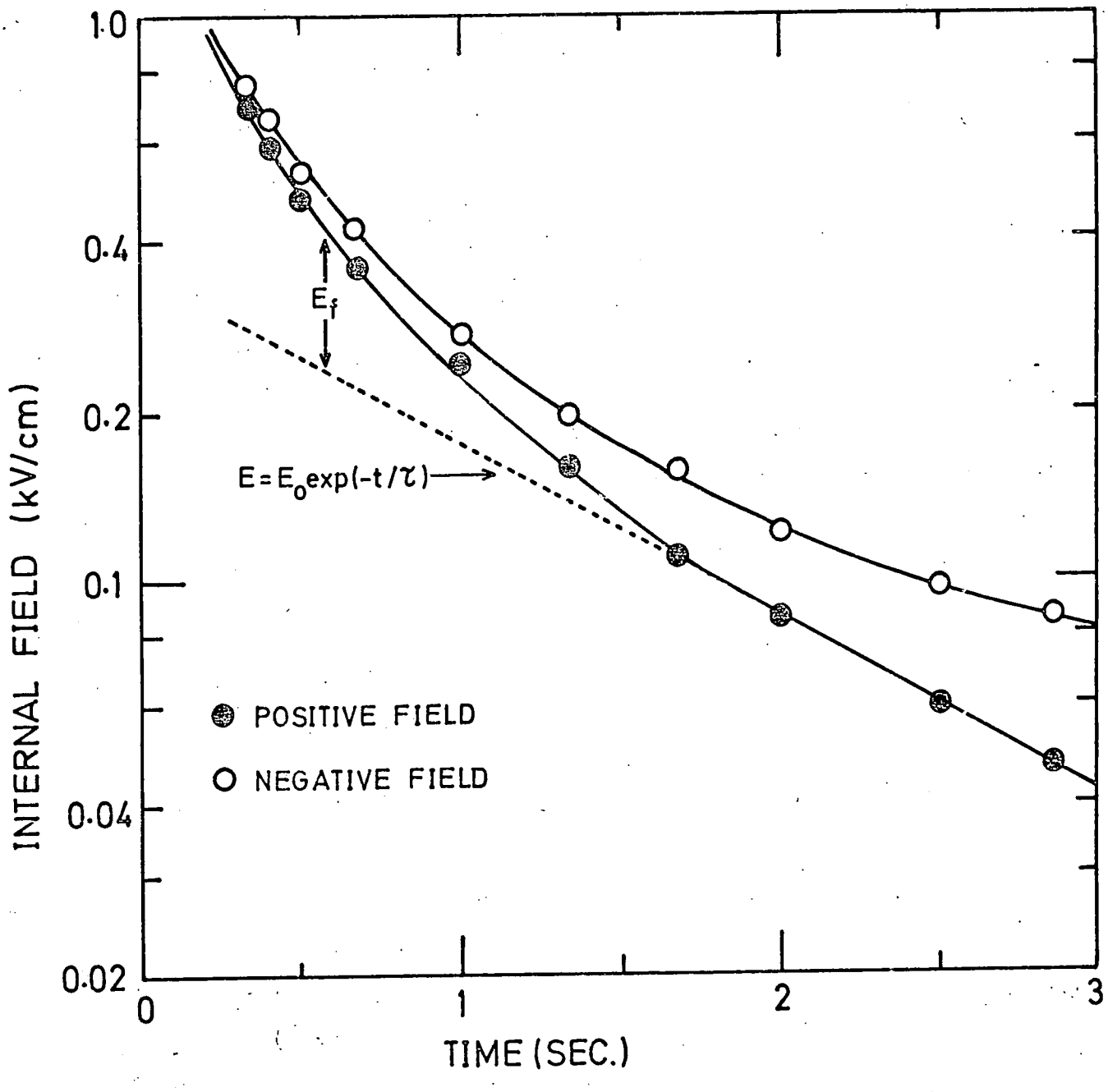

FIGURE 6·8 DECAY OF THE INTERNAL FIELD WITH TIME FOR APPLIED FIELDS OF 5·56 kV/cm

suggested that there are two mechanisms responsible for the decay of the induced field. At low field values ($E < 0.2$ kV.Cm^{-1}), the dominant mechanism is by conduction of charge around the inner walls, as described by equation (7). At higher field values where the induced field decays more rapidly a second mechanism, first observed by Francis[13], whereby the charges are freed from the walls under the influence of their own field and cross the gas volume, becomes of significance. An estimation of the contribution of this second mechanism to the decay of the induced field and to the spurious behaviour of the tube was made in the following manner.

A least squares fit of equation (7) to the decay curve, for values of induced field less than 0.1 kV.Cm^{-1} was made. In this region the decay is exponential and due to movement of the charge around the tube wall. The effect observed by Francis is considered insignificant at these field values, since the tube did not exhibit spuriousness at rates of less than 1 sec^{-1}, which indicates the absence of free charge in the gas. The decay of the induced field associated with the positive applied field obeyed the following relation,

$$E = 3.8 \exp(-t/1.35) \qquad (8)$$

which, assuming a value of 5 pf[2] for the capacitance of the tube, gives a value of 0.3×10^{12} Ω for the resistance of the inner wall of the flash tube.

Above field values of 0.1 kV.Cm^{-1}, the field decays more rapidly due to the freeing of charge from the wall into the gas volume. Assuming an electron drift velocity of 5×10^{6} Cm.Sec^{-1}[3], charge will cross the tube in 0.3 μs, for these field and pressure values. The difference

between the decay rate given by equation (8), and the decay rate observed at high field values (E_f in Figure 6.8) gives a measure of the contribution of the removal of charge from the walls to the decay of the induced field.

These differences are plotted in Figure 6.9. It can be seen that the decay of the induced field due to this effect follows an exponential relationship given by

$$E_f = A \exp(-\lambda t) \qquad (9)$$

since E_f is due to the charges residing on the tube walls, equation (9) can be rewritten as,

$$E_f = \frac{ne}{4\pi\varepsilon_o d^2} = A \exp(-\lambda t)$$

where: n = number of charges residing on the wall.

d = diameter of the tube.

Therefore the rate of loss of charge from the wall is given by,

$$\frac{dn}{dt} = -\frac{4\pi\varepsilon_o d^2}{e} A\lambda \exp(-\lambda t) \qquad (10)$$

This relation is particularly significant since it allows an estimate to be made of the rate of injection of free charge into the gas volume, and hence the onset of spurious flashing.

Values of λ and A were obtained by means of a least squares fit of equation (9), to the points in Figure 6.9, and assuming a value of 0.3 for the probability of a single electron to initiate a discharge[2], then the probability of 50% spurious flashing occurs at time values of 3.5 sec. This is equivalent to a rate of approximately 0.3 events.sec^{-1}, which is

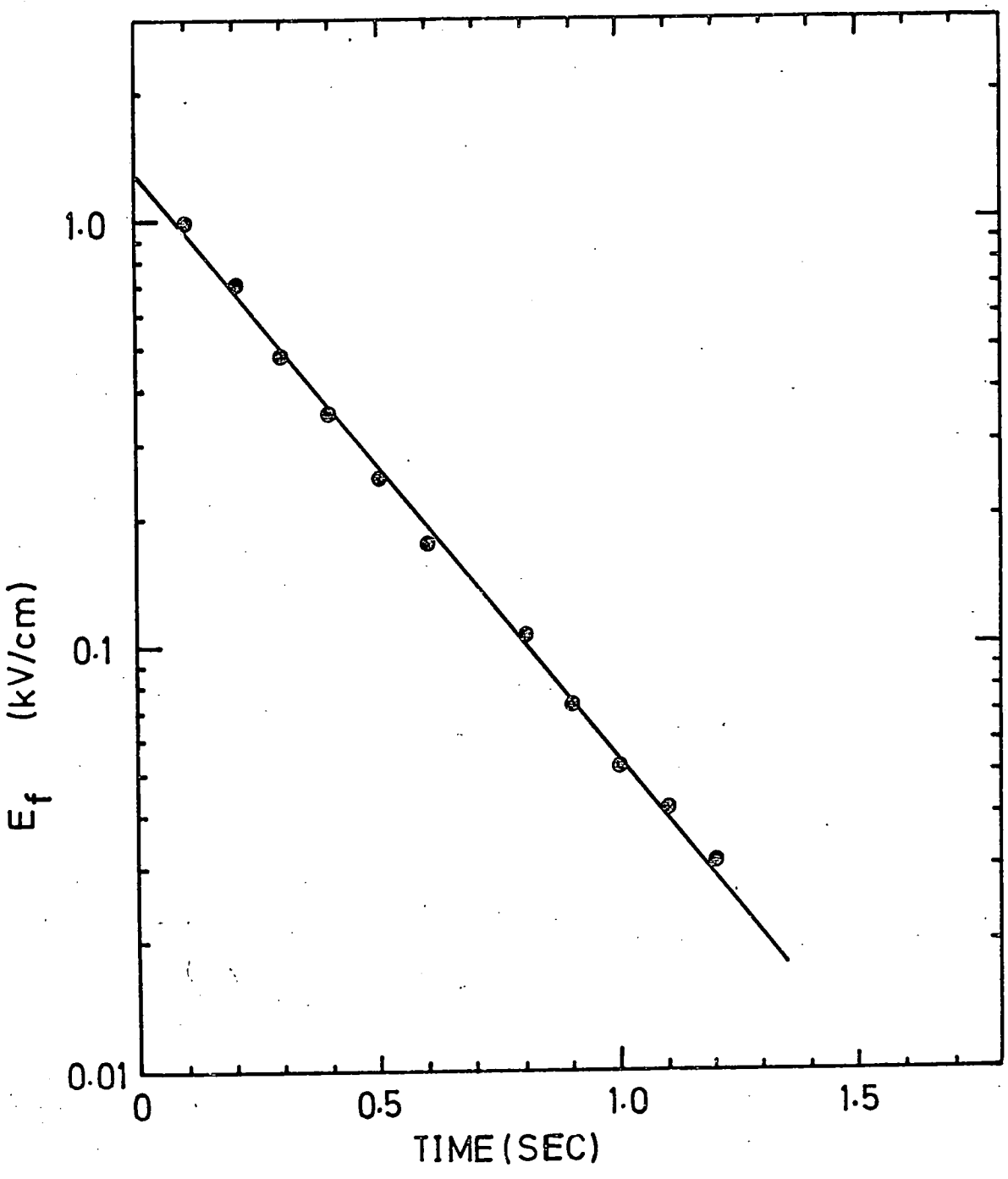

FIGURE 6.9 DECAY OF THE INTERNAL FIELD DUE TO REMOVAL OF CHARGE FROM THE TUBE WALL

somewhat lower than the value of > 1.0 events.sec^{-1} at which the tubes were observed to become spurious. However, considering the approximate manner in which the rate of emission of charge was arrived at, and the neglect of such effects as charge recombination in the gas, the agreement is quite good.

It has been suggested that back sparking may also be the cause of the rapid initial decay of the induced field[2], however, although this has been seen to occur, such a violent exchange of charge across the tube would probably result in a discontinuity in the decay curve.

6.2.6 Townsend and Streamer Pulse Height as a Function of Applied Field and Event Rate

Due to the capacitive coupling of the digitisation probe to the HT electrode the digitisation pulse height is expected to be sensitive to changes in the effective applied field across the tube. The mean Townsend and streamer pulse heights were obtained for slow event rates from the distribution of pulse heights, as seen in Figure 6.4. The variation of Townsend and streamer pulse height with applied field is given in Figure 6.10, for a tube filled with gas type I. Very little difference in behaviour of the pulse height, with the 3 gas types was observed. The difference in pulse height obtained using positive and negative applied fields was also insignificant, unlike the results obtained by Breare[7], who found that the pulse heights were considerably higher using a positive applied field. The variation of the Townsend pulse height with applied field is much less than that observed with the streamer. This is to be expected since there is an upper limit to the charge density (defined by the Reather criteria[5]), beyond which the Townsend avalanche transforms into a streamer.

The mean Townsend and streamer pulse heights, as a function of flashing rate, is given in Figure 6.11, for a tube filled with gas type I. After an initial decrease in pulse height, up to an event rate of

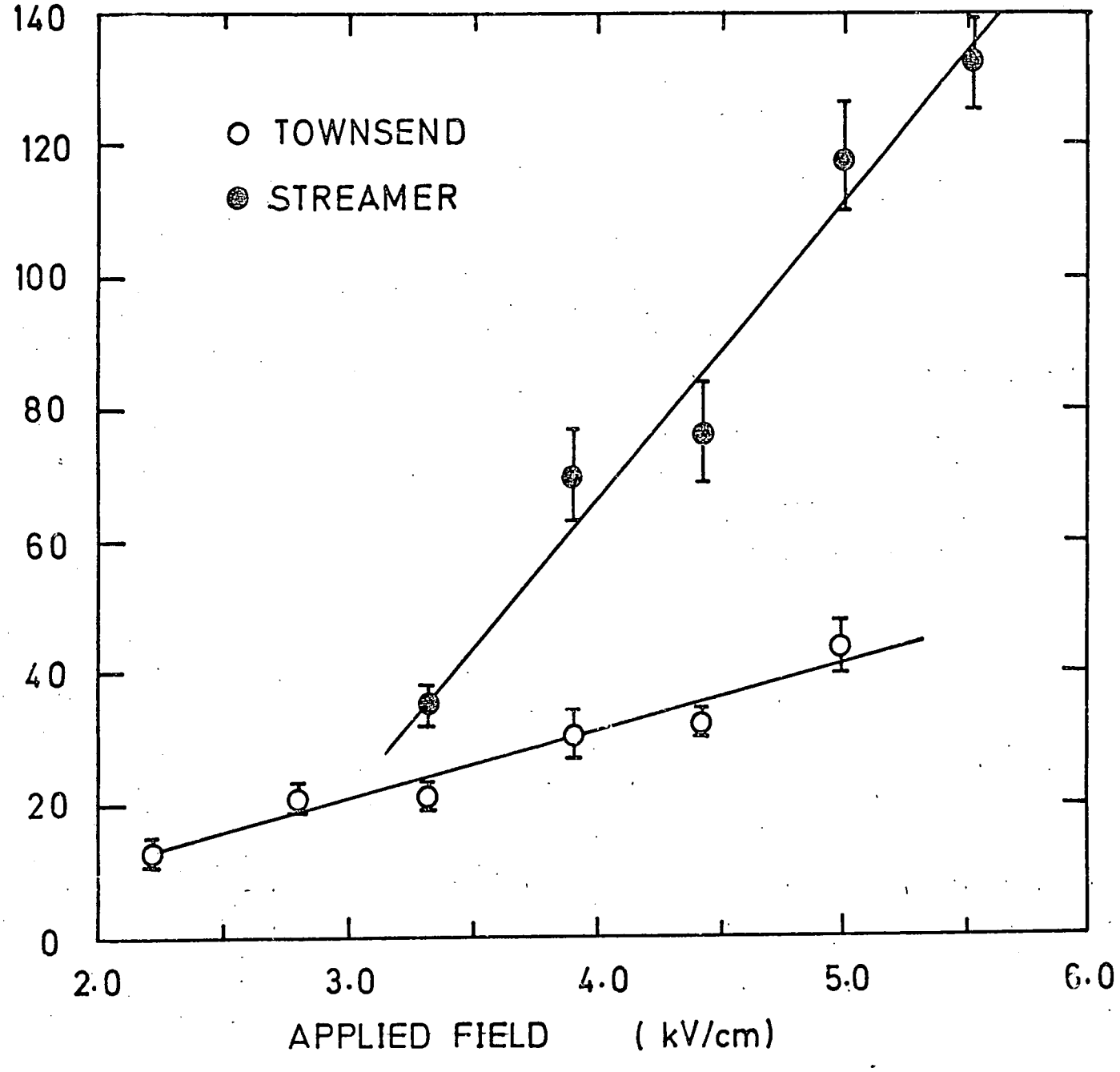

FIGURE 6.10 DEPENDENCE OF MEAN PULSE HEIGHT ON THE APPLIED FIELD

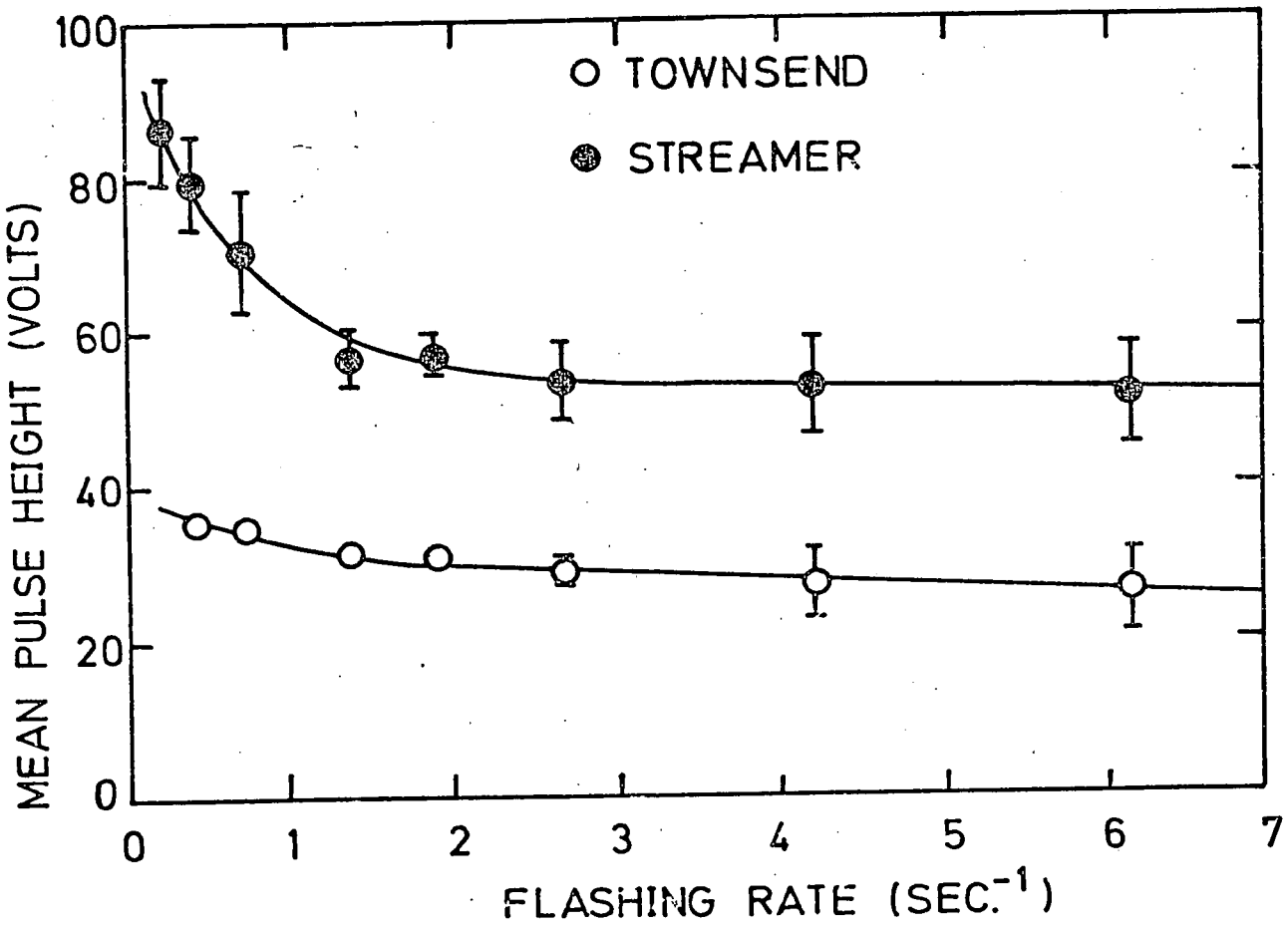

FIGURE 6.11 MEAN PULSE HEIGHT AS A FUNCTION OF FLASHING RATE

approximately 2 sec^{-1}, the mean pulse height of both the Townsend and the streamer discharge is seen to remain almost constant. A similar behaviour was observed with the other gas fillings and the difference resulting from using positive and negative applied fields was found to be insignificant.

6.3 EFFECT OF INDUCED FIELDS UPON THE PERFORMANCE OF THE FLASH TUBE

Two types of induced field are expected to occur in the flash tube, one due to charge deposited on the inner wall of the flash tube, and the other due to charge induced upon the outer wall of the tube. These fields were studied with respect to the resistance of the outer surface and the shape of the applied HT pulse, by observing the sensitive time of the tube in the manner described below.

6.3.1 Influence of the Induced Field upon the Sensitive Time

A convenient method of studying the effect of induced fields upon the performance of a flash tube is to observe its sensitive time under various operating conditions. The sensitive time is defined as that period of time between the passage of an ionising particle through the tube, and the application of the HT pulse, necessary for the internal efficiency of the tube to fall to 50%. An analytical solution to the sensitive time of the flash tube was first performed by Lloyd[14], who considered diffusion to the tube walls and recombination as the sole means of loss of the primary ionisation, and obtained a value of approximately 100 μs for the sensitive time.

For low event rates this figure is in agreement with experiment, however, as the event rate is increased, loss of the primary ionisation to the tube walls, by drifting under the influence of the internal fields occurs, and the sensitive time rapidly decreases.

Holroyd[15] has performed Monte Carlo simulations to estimate the effect of different drift velocities (and therefore internal fields) upon the sensitive time of a flash tube. The results obtained in neon at 760 torr, for various drift velocities opposing the applied field, are given in Figure 6.12. Velocities above 10^{-3} Cm.sec^{-1} (corresponding to fields of less than 10^{-3} V.cm^{-1} [2]), have a considerable effect upon the sensitive time of the tube, and use can be made of this to provide an indication of the magnitude of the internal fields.

6.3.2 Experimental Arrangement

The tests were conducted using tubes of S95 soda glass, 16 mm internal diameter, with 1 mm thick walls, approximately 500 mm long, filled with commercial grade neon at 600 torr pressure. Individual tubes were initially sleeved in thin black polythene, to prevent cross ignitions by photons. The tubes were arranged in four layers, each layer containing six tubes. Cosmic rays were used as a source of ionising particles, triggering being provided by means of a scintillator telescope, giving an event rate of approximately 9 min^{-1}. The tubes were fired by means of a high voltage pulse, of 60 ns rise time, formed by discharging a condenser through a 3mH inductance and a series resistor. Two types of HT pulse were used for the investigations, and are shown in Figure 6.13. Figure 6.13 (a) shows a non-oscillatory pulse obtained by use of a large series damping resistor ; the oscillating pulse shown in Figure 6.13 (b) was obtained by removing the resistor. A field strength of approximately 5.0 kV.Cm^{-1} was necessary to ensure efficient operation of the tubes.

The layer efficiency of the assembly of tubes was obtained by recording the number of tubes igniting along the cosmic ray track. Since the tubes in each layer were in physical contact, the layer efficiency was related to the internal efficiency by the ratio of the internal and external tube diameters.

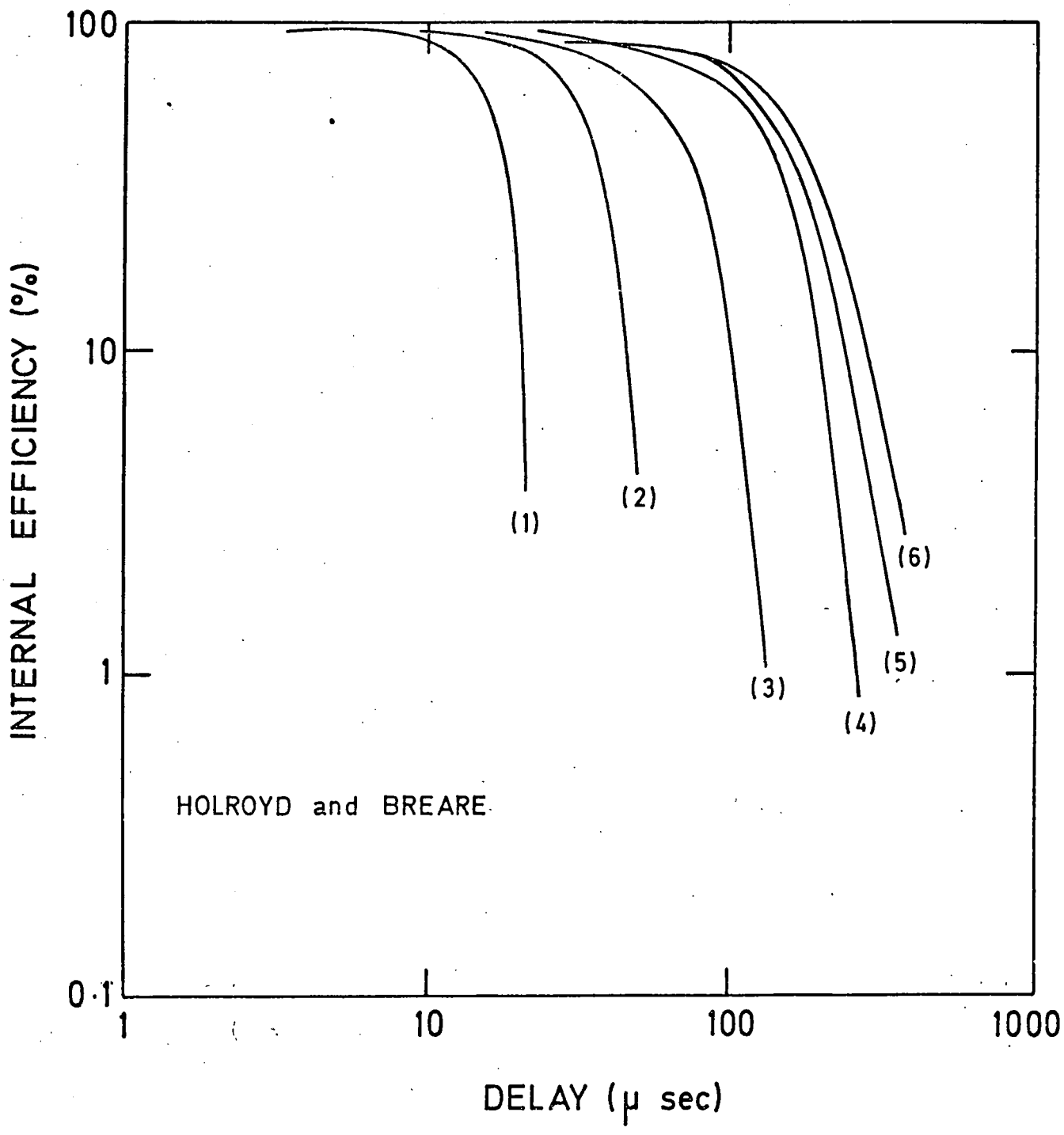

(1) $V = 10^5$ cm/sec
(2) $V = 5 \times 10^4$ cm/sec
(3) $V = 2{\cdot}5 \times 10^4$ cm/sec
(4) $V = 10^4$ cm/sec
(5) $V = 4 \times 10^3$ cm/sec
(6) $V = 0$

FIGURE 6.12 EFFICIENCY AS A FUNCTION OF DELAY FOR DRIFT VELOCITIES OPPOSING THE APPLIED FIELD

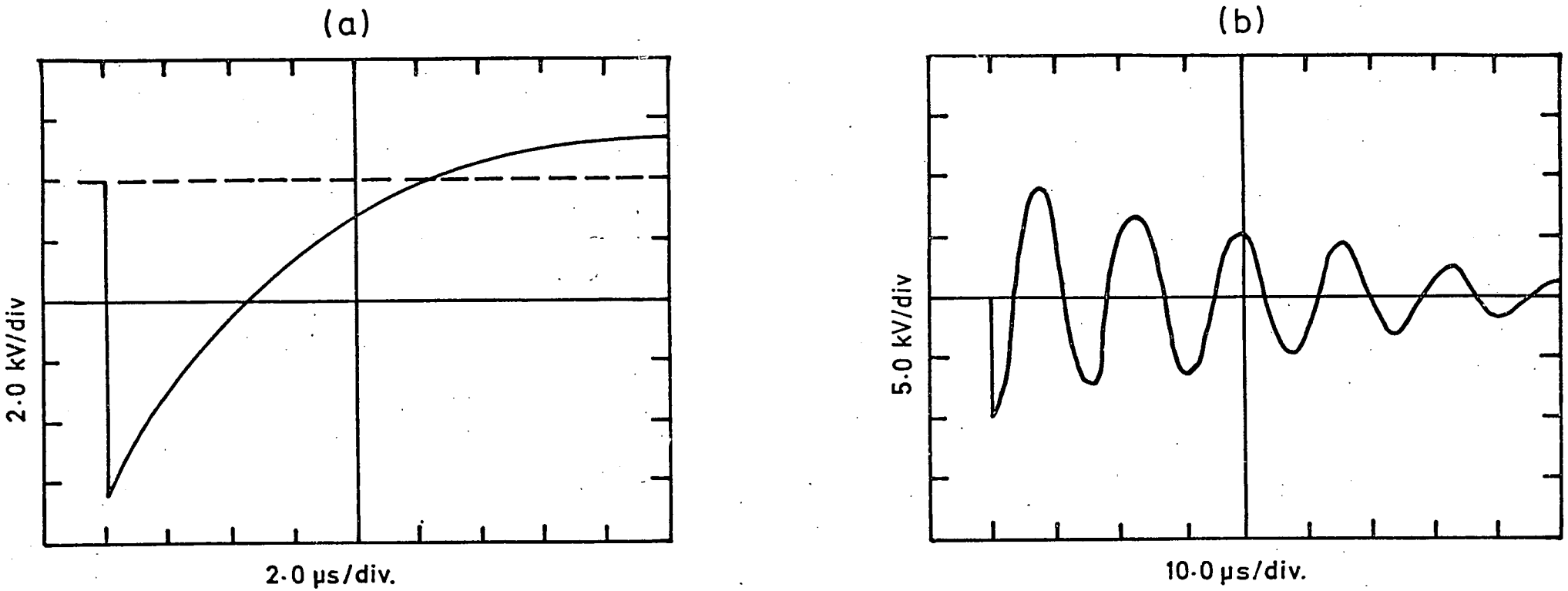

FIGURE 6·13 OSCILLOSCOPE TRACES OF: (a) NON-OSCILLATORY, (b) BI-POLAR RINGING APPLIED HT PULSE

6.3.3 Effect of the Outer Surface Resistance Upon the Induced Field

The efficiency of the flash tube array was measured for two different values of outer surface resistance which occurred :-

(1) Immediately after manufacture, when the effect of surface contamination is expected to result in a low surface resistance.

(2) After the tubes had been cleaned and heated (to drive off water vapour) and painted with white cellulose paint, and therefore exhibited a high surface resistance.

The resultant variation of layer efficiency with time delay for the two surface conditions, using the non-oscillatory HT pulse is given in Figure 6.14 for an event rate of 9 events min^{-1}. The resultant sensitive times of 11.0 μs and 2.5 μs obtained before and after cleaning and painting the tubes respectively, indicate that the conditions of the outer surface of the flash tube has a considerable influence upon the effect of the induced field appearing across the gas of the tube.

It is assumed that the conductivity of the outer surface of the flash tube influences the availability of free charge on the outer surface of the tube. This charge induced on the outer surface of the tube results in a field in opposition to that due to the charge adhering to the inner surface of the tube, resulting in a reduction of the clearing field appearing across the gas volume. The resistance of the outer surface was determined by attaching aluminium foil to each end of the flash tube, which was then connected in series with a capacitor and a 2 kV power supply. By observing the rate of charging of the capacitor a value of the time constant was obtained and hence the resistance. Values of 10^{13} and 10^{14} Ω were obtained before and after painting.

An estimate of the magnitude of the field resulting from the charge residing on the outer surface was obtained in the following manner. The

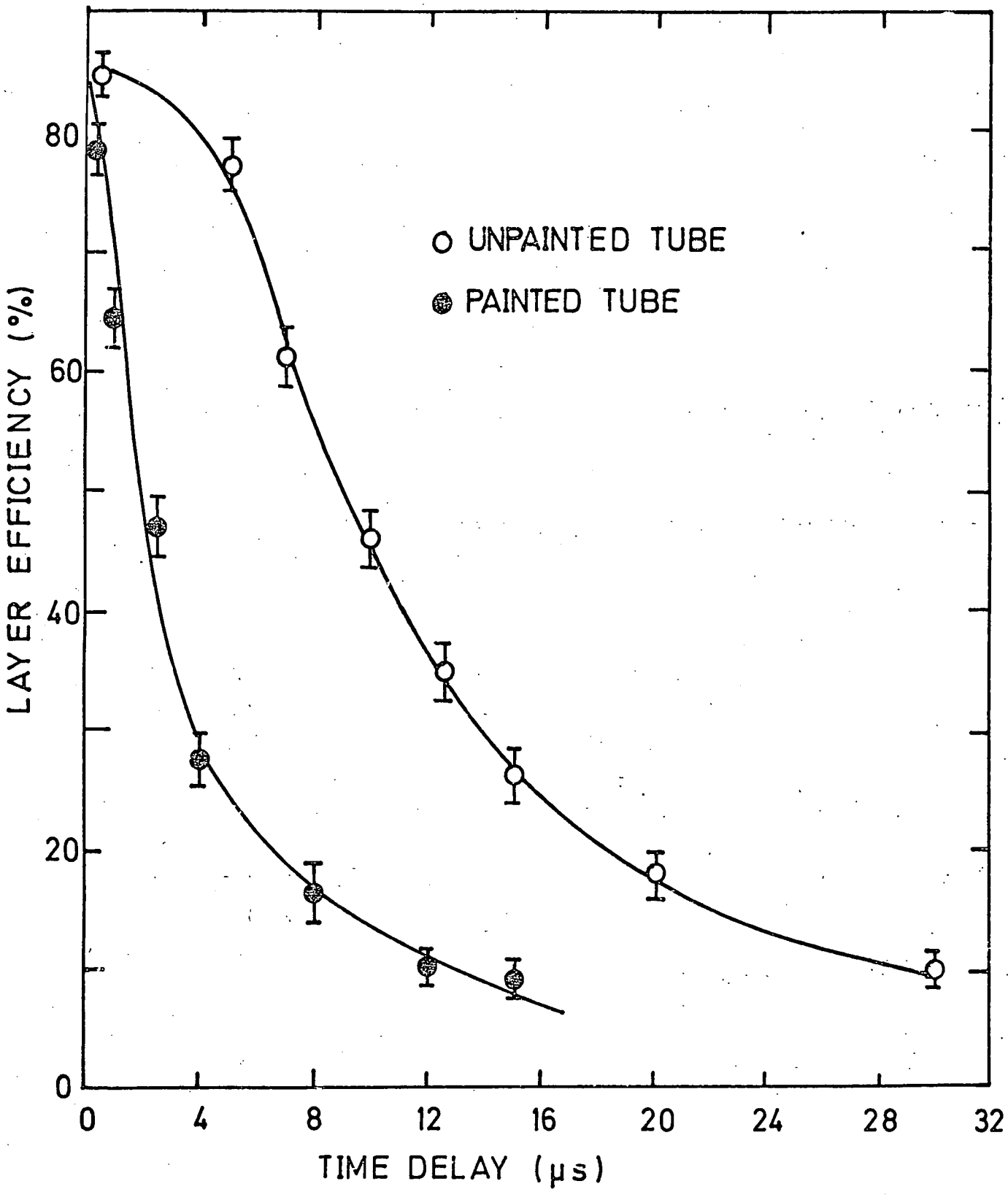

IGURE 6·14 LAYER EFFICIENCY AS A FUNCTION OF TIME DELAY FOR PAINTED AND UNPAINTED TUBES

field (E), appearing across the gas volume may be expressed as,

$$E = E_i - E_x$$

where: E_i = field due to internal charge

E_x = field due to external charge

From Holroyds Monte Carlo data, given in Figure 6.11, a graph of sensitive time as a function of drift velocity may be obtained. From this graph, drift velocities of 1.3×10^5 cm.sec^{-1} and 2.9×10^5 cm.sec^{-1} are associated with sensitive times of 11.0 μs and 2.5 μs respectively. Using the data of Pack and Phelps[3] for electron drift velocities in neon, this is equivalent to fields (E) of 2 V.cm and 30 V.cm. Since the field (E), is small compared with the applied field and the two sensitive times were obtained at the same flashing rates, it is expected that the field due to the internal charge (E_i), should be the same in both cases, and hence one can write

$$2 + E_{x_1} = 30 + E_{x_2}$$

where E_{x_1} and E_{x_2} are the fields due to external charge on the high and low resistance outer surfaces respectively. Thus a change in outer surface resistance from 10^{13} Ω to 10^{14} Ω, produces a 28 V.cm^{-1} change in the external field and a resultant change in sensitive time of 11.0 μs to 2.5 μs.

The variation of sensitive time with flashing rate is given in Figure 6.15, for unpainted and painted tubes with surface resistances of 10^{12} Ω and 2×10^{13} Ω respectively. The sensitive time of both sets of tubes falls with increasing rate, although the fall is less rapid for the

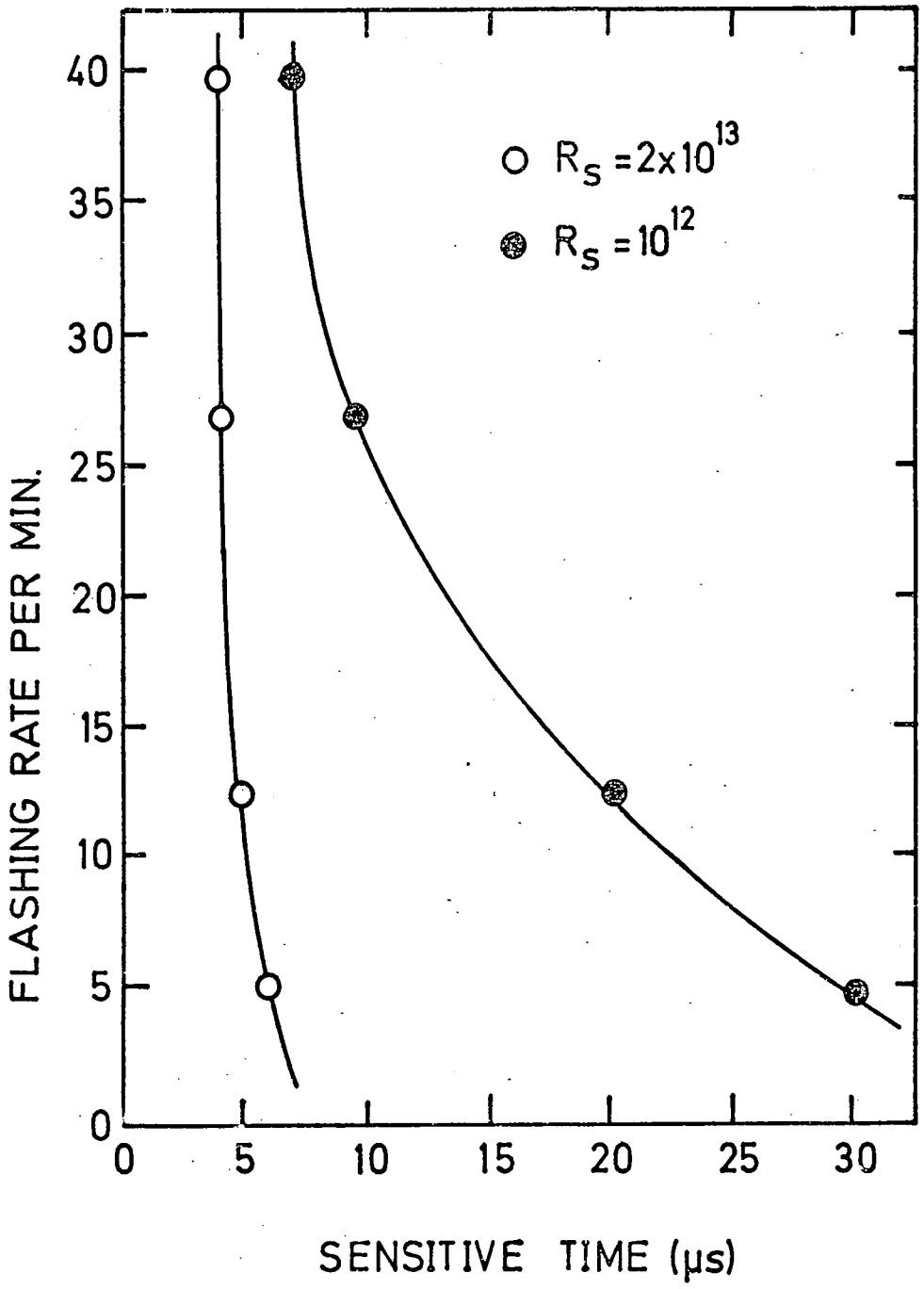

FIGURE 6.15 SENSITIVE TIME AS A FUNCTION OF FLASHING RATE, FOR TWO VALUES OF OUTER SURFACE RESISTANCE (R_s)

tubes with the lower surface resistance, indicating a greater availability of free charge on its outer surface.

6.3.4 Dependence of the Induced Field Upon the HT Pulse Length

It is to be expected that the amount of charge deposited on the walls of the flash tube will depend upon the length of the HT pulse. With electron drift velocities of approximately 5×10^6 cm.sec^{-1} (3), for the typical field and gas pressure of the neon tubes, the electrons are expected to be swept to the walls in approximately 300 ns, which is in agreement with the observed duration of the discharge of about 150 ns (2). However, the positive ions, with a drift velocity of 5×10^4 cm.sec^{-1} (4), remain almost stationary in this time, and HT pulse lengths of approximately 30 μs are required to remove these ions from the gas volume. For pulse lengths shorter than this the fraction of the ions not adhering to the wall will drift back, recombine and neutralise an equivalent number of electrons on the opposing wall, resulting in a reduction of the induced field.

The rate of increase in the number of positive charges residing on the tube wall (dn/dt) may be expressed in the following way

$$\frac{dn}{dt} = D - \frac{n}{\lambda}$$

where: D = rate of deposition of charge on the wall

λ = decay constant of charges moving around the wall.

If the tube is considered to contain a uniform distribution of positive ions within its volume (the electrons having been swept from the gas), then since the positive ion drift velocity is proportional to the electric field it experiences,

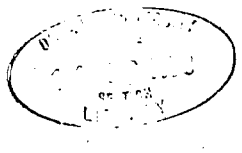

$$D = KV$$

where: V = field

K = a constant

and therefore,

$$\frac{dn}{dt} = KV - \frac{n}{\lambda}$$

If, for this simple treatment, one ignores the effect of space charge, then the field across the gas (V) is equal to the applied field minus the field due to charges on the wall, i.e:

$$V = V_o \exp(-t/\tau) - c\,n$$

where: V_o = initial value of applied field at t = 0

τ = decay constant of the applied field

n = number of charges residing on the tube wall

c = a constant.

and therefore,

$$\frac{dn}{dt} = K(V_o \exp(-t/\tau) - cn) - \frac{n}{\lambda}$$

or,

$$\frac{dn}{dt} + n\,(cK + {}^{1}/_{\lambda}) = KV_o \exp(-t/\tau)$$

Therefore, the number of charges (n), residing on the tube wall after a time t, is given by,

$$n = \frac{KV_o}{A} \exp(-t/\tau)\,(1 - \exp(-At))$$

where $A = cK + {}^{1}/_{\lambda} - {}^{1}/_{\tau}$

It can be seen that the amount of charge deposited on the tube walls is exponentially dependent upon the pulse length. A more rigorous treatment would include the time dependence of the components of A, since K, C and λ will all depend upon the field strength, which varies with time.

To investigate the dependence of the induced field upon pulse length the non-oscillatory pulse was used, and the variation of the efficiency with time delay of the HT pulse, for various pulse lengths (base width) was recorded, and is shown in Figure 6.16. It is clear from the behaviour of the sensitive time that the internal field increases with HT pulse length. The dependence of the sensitive time upon pulse length is given in Figure 6.17, and is seen to increase exponentially with increasing pulse length, as predicted by the above relationship. Beyond a pulse length of 10 μs, no further decrease in sensitive time was observed, indicating that all the positive ions had been swept from the gas volume ; this is in reasonable agreement with the crude estimate of 30 μs, obtained from the drift velocity.

Although the use of a short HT pulse reduced the effect of the induced field, it was also noted that the light intensity of the discharge decreased with decreasing pulse length, indicating a corresponding decrease in the plasma density, which may have a significant effect on the digitisation pulse height.

6.3.5 Effect of an Oscillating HT Pulse on the Induced Field

The use of an oscillating pulse is expected to decrease the internal field, since the charge will oscillate about a mean position, instead of being swept in one direction, thus reducing the probability of collision with the tube wall. As the frequency increases so the amplitude of the oscillation will decrease, reducing further the amount of charge available to the wall. Furthermore, charges of both signs will be deposited on the

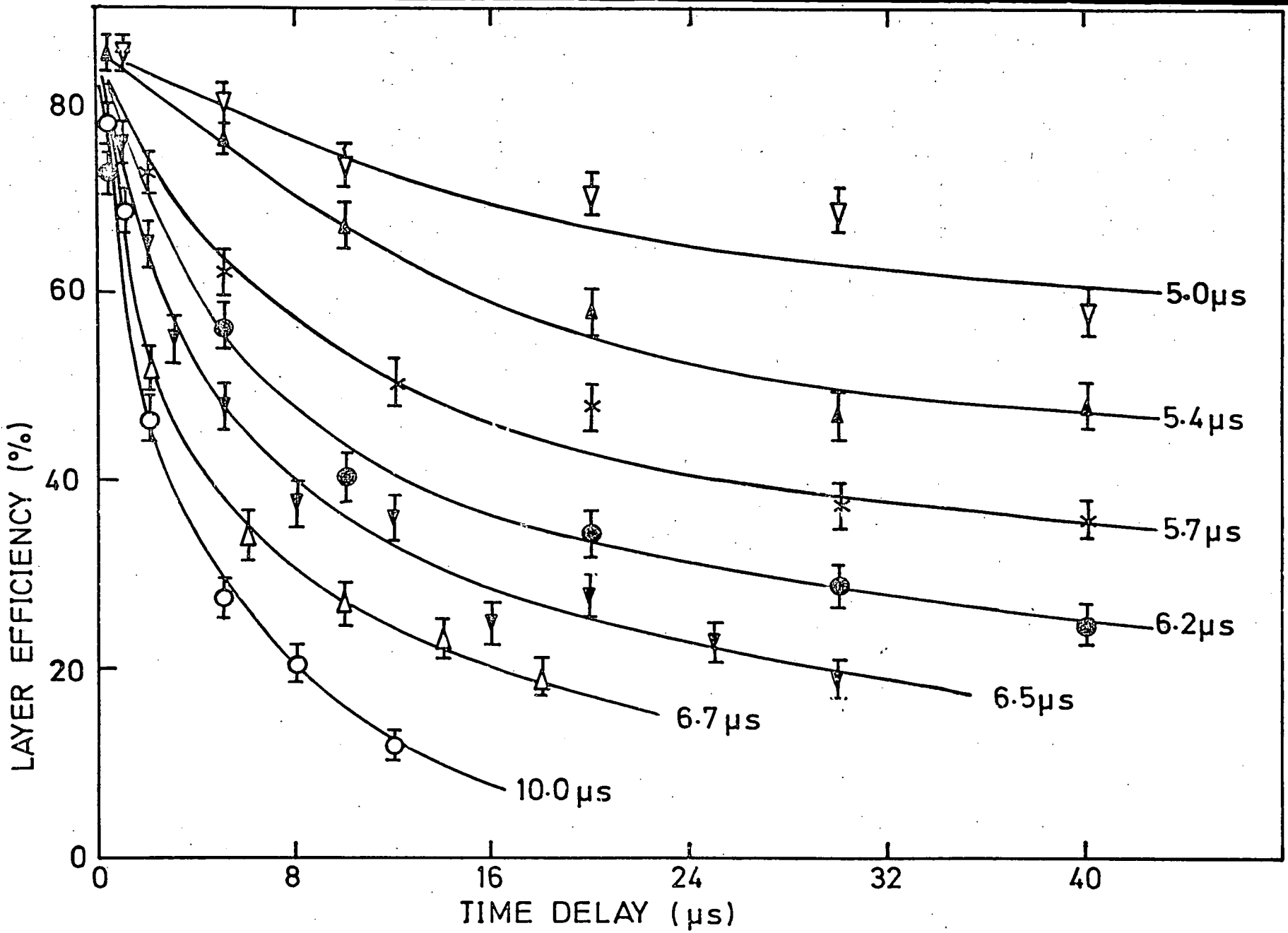

FIGURE 6.16 EFFICIENCY AS A FUNCTION OF DELAY FOR VARIOUS PULSE LENGTHS

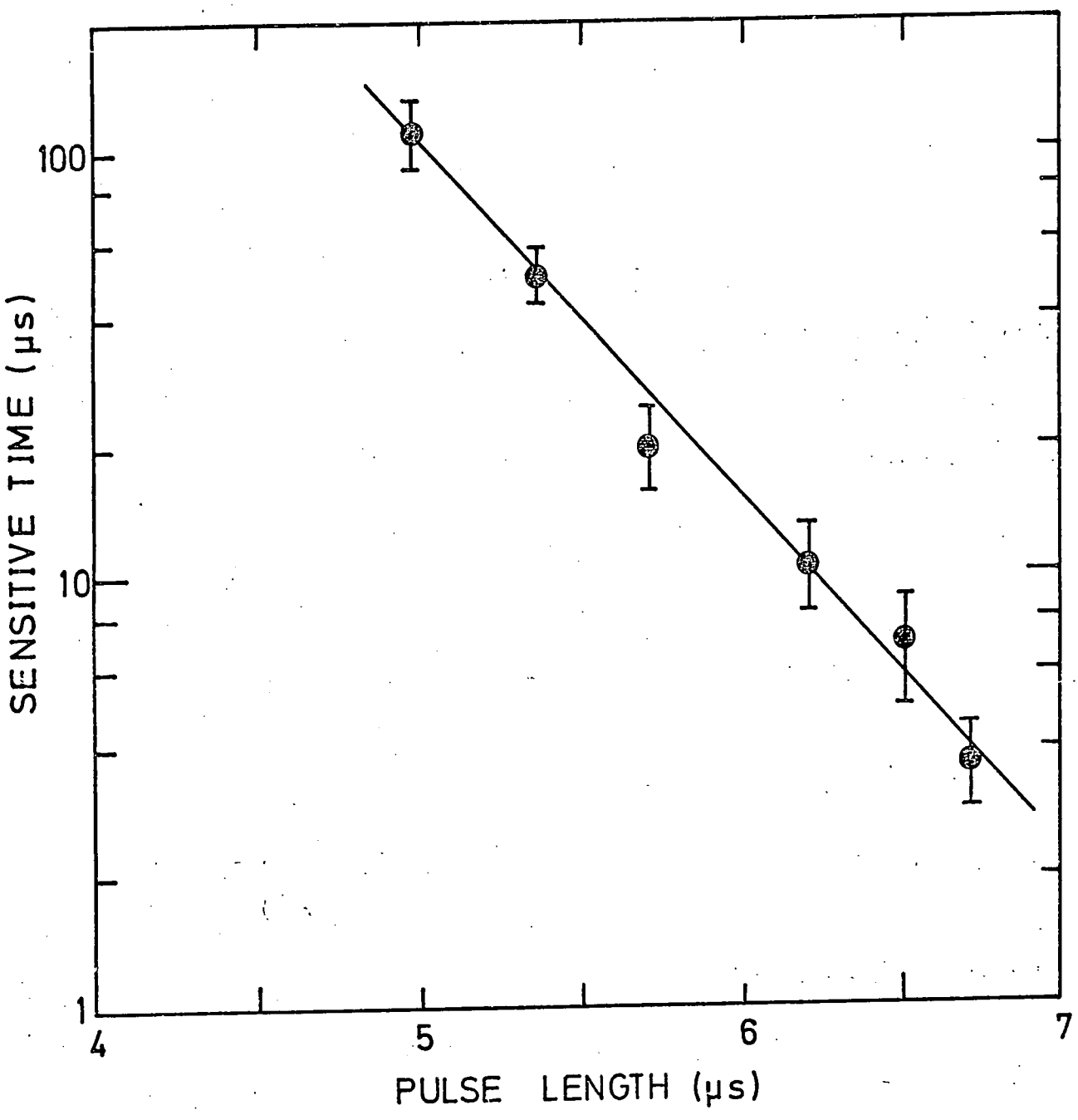

FIGURE 6·17 VARIATION OF SENSITIVE TIME WITH APPLIED H T PULSE LENGTH

same wall, resulting in a further reduction of the internal field.

To investigate the effect of an oscillating HT pulse upon the sensitive time the resistive load was removed from the LCR pulse forming circuit, resulting in an oscillating pulse, as shown in Figure 13 (b). The behaviour of the layer efficiency as a function of delay, for a number of different frequency pulses, is shown in Figure 6.18; the sensitive time is seen to increase with increasing frequency indicating that less charge is swept to the tube walls. The dependence of sensitive time upon pulse frequency is shown in Figure 6.19, it can be seen that the rate of increase of sensitive time falls above a pulse frequency of 80 k Hz. It may be necessary to apply pulses of frequency greater than 1 M Hz to ensure minimal charge deposition. Holroyd[2] found that using pulses of 2 M Hz, the efficiency time delay curves were in good agreement with the theoretical predictions of Lloyd[15], which indicates a very small internal field.

6.4 DISCUSSION

It has been seen that the discharge mechanisms occurring in a flash tube may be studied by observing the digitisation output pulse. The coupling of the digitisation probe to the HT electrode is sensitive to the plasma conditions inside the discharging tube, and two plasma states are evident, since the distribution of digitisation pulse heights fall into two distinct categories. The behaviour of these two groups, under changing applied field conditions, indicates that they are associated with the Townsend and streamer discharge mechanisms. This view is further supported by the observation that the field strength required for transition from predominantly Townsend discharge to predominantly streamer, measured using this technique, is in agreement with simple theoretical calculations.

This technique for studying the flash tube discharge mechanism may be improved upon, principally by more sophisticated processing of the raw output pulse, since the present method cannot distinguish between

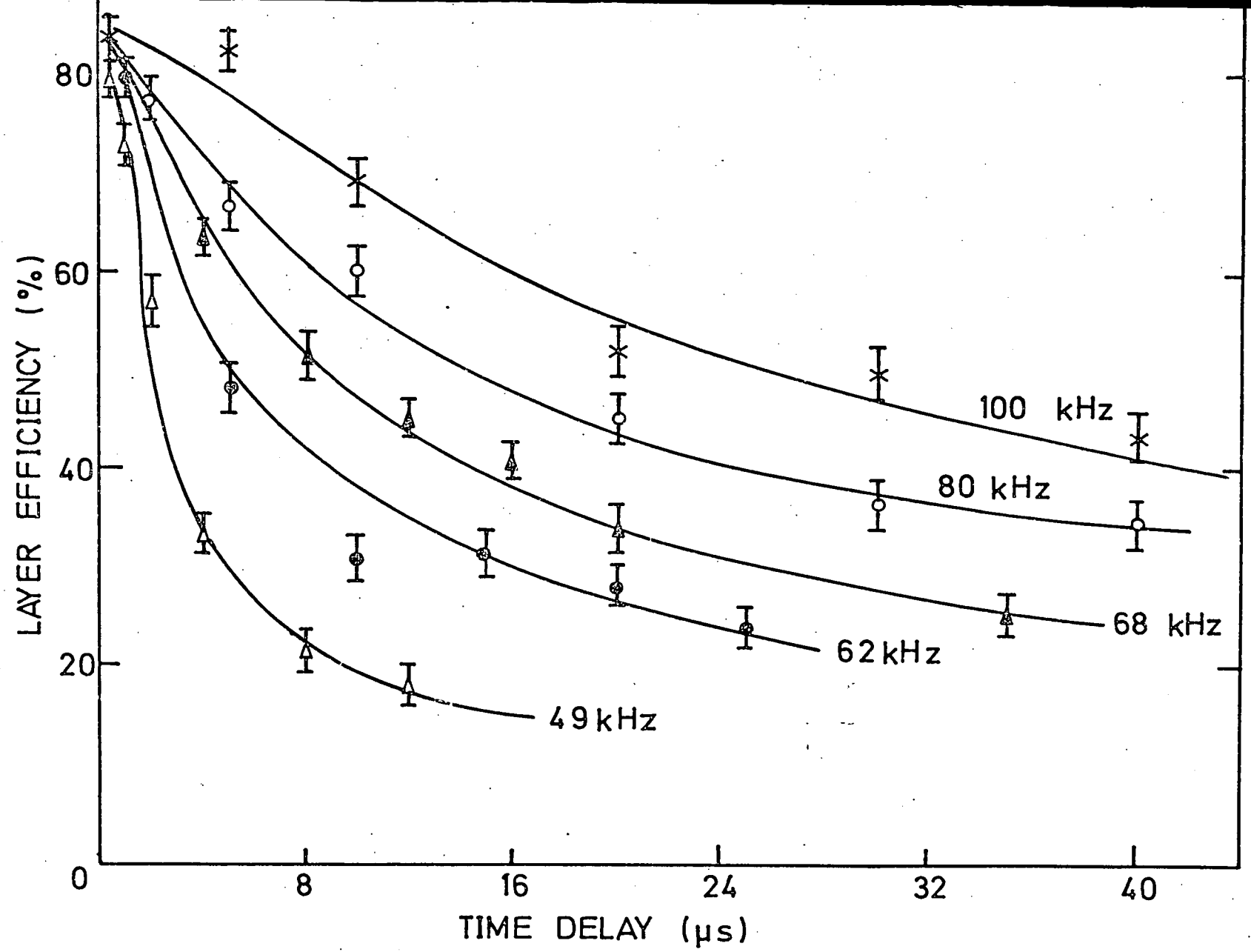

FIGURE 6.18 LAYER EFFICIENCY AS A FUNCTION OF TIME DELAY FOR VARIOUS FREQUENCIES OF APPLIED HT PULSE

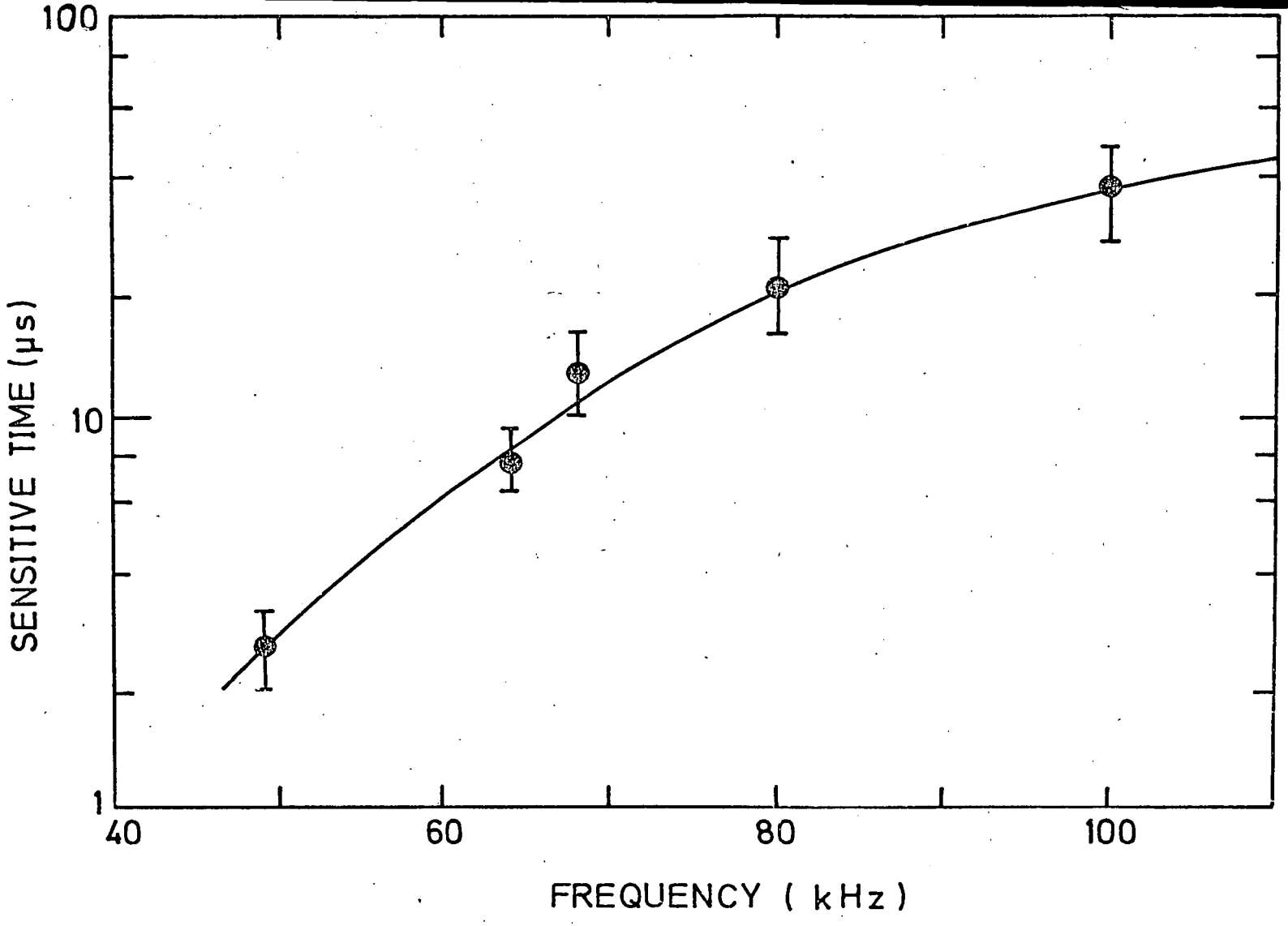

FIGURE 6·19 DEPENDENCE OF THE SENSITIVE TIME ON THE FREQUENCY OF THE APPLIED H T PULSE

Townsend and streamer pulses of approximately the same magnitude, which occur at low applied field values. With refinement the technique may represent a useful tool in the study of gas discharges themselves.

A study of the percentage of discharges occurring by Townsend or streamer mechanism, for varying field strengths, using the above technique, has allowed the decay of the internal field to be measured. Two decay constants are apparent ; at long time values the field decays by movement of charge around the inner wall, the value of the decay constant depending on the inner surface resistance and the intrinsic capacitance of the tube. For shorter time values and hence larger fields, a second mechanism becomes dominant, whereby charges are removed from the walls of the tube into the gas. The field values at which this effect becomes of significance is seen to be > 0.2 $kV.cm^{-1}$, which is in agreement with the observations of earlier workers[13]. The rate of injection of free charge into the gas, as a function of field, has been obtained and is in reasonable agreement with the time period associated with the onset of spurious flashing, which supports the idea that the emission of charge from the walls is the main source of spurious flashing as the event rate is increased.

The resistance of the outer surface of the flash tube is seen to have considerable influence upon the magnitude of the induced field occurring across the gas volume. The induced field is reduced for low values of outer surface resistance, which suggests that it is the availability of charge to the outer surface which results in a field in opposition to that due to the charges adhering to the inner walls, resulting in a lower induced field across the gas. This may result in raising the threshold at which spurious flashing occurs, and is the most likely explanation of the differences observed in the performance of the present tubes and those of earlier workers.

The quantity of charge deposited on the inner wall of the tube may be considerably reduced by the use of a shorter HT pulse or an oscillating pulse. The former may present problems due to the weakness of the discharge effecting the digitisation pulse height. The use of a well defined square pulse from a Blumlein line will remove the long tail associated with the RC formed pulse, which is responsible for a large proportion of the charge swept to the wall, and possibly at the same time maintain an intense discharge. An oscillating pulse of frequency greater than 1 MHz will ensure almost complete removal of the internal field effects, however difficulty may be encountered in applying such a high frequency pulse to large capacitive systems, also the electrical noise may present problems.

It is clear that the problems of operating flash tubes at high rates stem directly from the presence of charges deposited on the inner wall of the tube. Attention to the above details, plus the use of low resistance materials (such as JENA 16 B glass) in the construction of the tubes, will enable them to be operated at higher event rates than at present, without the problems of inefficiency or spuriousness.

REFERENCES : CHAPTER SIX

(1) Chaney, J.E., Breare, J.M, Nucl.Inst.Meth., 124, (1975), 61.

(2) Holroyd, F.W., Ph.D. Thesis, University of Durham, (1971).

(3) Pack, J.C., Phelps, A.V., Phys. Rev., 121, (1961), 798.

(4) Honrbeck, J.A., Phys. Rev., 84, (1951), 615.

(5) Raether, H., Electron Avalanches and Breakdown in Gases, Butterworths Press, London, (1964).

(6) Ayre, C.A. et al., Proc.Int.Conf. on Inst.for High Energy Physics, Frascati, (1973), 215.

(7) Breare, J.M., Nandi, B.C., Tait, I.D., Nucl.Inst.Meth., 133, (1976), 415.

(8) Meek, J.M., Phys. Rev. 57, (1940), 722.

(9) Hopwood, W., Proc. Phys. Soc., 62 B, (1949), 657.

(10) Druyvesteyn, M.J., Penning, F.M., Rev.Mod. Phys., 12, (1940), 87.

(11) Breare, J.M., Nandi, B.C., Tait, I.D., Nucl. Inst.Meth., 138, (1976), 457.

(12) Breare, J.M., Doe, P.J., Nucl. Inst.Meth., 133, (1976), 247.

(13) Francis, G., Proc. Phys. Soc. Lond., B68, (1955), 137.

(14) Lloyd, J.L., Proc. Phys. Soc., 75, (1960), 387.

(15) Holroyd, F.W., Breare, J.M., Nucl.Inst.Meth., 100, (1972), 277.

CHAPTER SEVEN

CONCLUSIONS AND SUGGESTED FUTURE WORK

7.1 CONCLUSIONS

It has been shown that a calorimeter of the sampled shower type, using planes of flash tubes as the sampling elements can be successfully operated in an accelerator type environment. The simple elemental nature of the detector allows large sensitive volumes to be obtained, inexpensively, in keeping with the anticipated requirements of the current trend of accelerator based HEP experiments. Furthermore, the simple method of outputting information, by means of digitisation probes, has been shown to be highly compatible with CAMAC data acquisition/control systems.

The detectors performance was evaluated using a mono-energetic positron beam over the energy range 0.5 to 4.0 GeV. The number of tubes igniting in a shower may be used as a measure of the primary energy, also the trajectory of the primary may be determined by means of a weighted fit to the centroids of the groups of tubes igniting in each layer. In order to resolve the maximum number of individual particles in the dense showers, the detector employed small diameter (8 mm internal diameter), high pressure (2.2 atmospheres) flash tubes. With this detector an energy resolution of approximately 40 % and spatial and angular resolutions of $\pm$ 5 mm and 4^{o} (FWHM) respectively, were achieved, which compares favourably with more complex and expensive devices.

The performance of the detector was influenced at high energies by the inability of the tubes to resolve individual particles in the dense showers, and by shower leakage from the rear and sides of the detector. These problems may be reduced, or eliminated, by improvements in the

detector design. The sensitive time, (approximately 2 μs), of the tubes, ensured successful operation in the backgrounds experienced in the experimental area, no spurious flashing being observed. A more serious problem arose when attempts were made to operate the detector at high event rates. The recovery time of the tubes, (approximately 0.6 ms), should in theory allow event rates of up to 1 KHz, however at rates in excess of 1 per second, the tubes were observed to become inefficient or to flash spuriously. This behaviour is a direct result of internal fields, associated with the charges from the discharge adhering to the inner wall of the tube. Attempts to reduce the amount of charge deposited on the walls, by the use of alternate polarity and oscillating HT pulses were unsuccessful, due principally to the narrow HT plateau over which the tubes can be operated.

In order to demonstrate that useful resolutions may be obtained at the high event rates demanded by typical accelerator based experiments, a further detector was built using large diameter (16 mm internal diameter) low pressure (600 torr) flash tubes, which had been shown to operate at rates of at least 50 Hz, with no detectable deterioration in efficiency. In order to improve the poor multiparticle efficiency of the detecting planes, (due to the relatively large tube diameter), two staggered layers of tubes were employed in each sampling plane. A system of drift chambers was also incorporated to obtain an improved estimate of the spatial resolution of the detector. An energy resolution of 33% and spatial and angular resolutions of 10.5 mm and 2^{o} (FWHM), were obtained, which compares well with those of the earlier detector. Unexpectedly, the tubes behaved in a similar manner to the high pressure tubes, at event rates in excess of a few per second.

Investigations were therefore made into the discharge mechanisms and the formation of the internal field. These investigations were

carried out by observation of the digitisation pulse, a method which may prove of use to other investigators of gas discharge phenomena. The results showed that the quantity of charge deposited on the inner wall can be considerably reduced by use of a shorter HT pulse, and possibly removed completely by means of a high frequency (> 1 MHz) oscillatory pulse. Furthermore, the resistance of the outer surface of the flash tube has been shown to have considerable influence on the strength of the internal field, due to the ability of charge to accumulate on the outer surface, resulting in a field in opposition to that resulting from charge deposited on the inner surface. This is the most probable explanation of the failure of the present low pressure tubes to operate at a high event rate, since their painted surface offered a high resistance to charge movement.

The source of free charge to the gas filling, which results in spurious flashing, has been shown to be due to a mechanism, whereby charges are liberated from the wall into the gas volume under the influence of their own field. The internal field threshold for this effect is approximately 0.2 $kV.cm^{-1}$, beyond which spurious flashing will occur upon the application of the HT pulse.

Although the present event rates are sufficient to satisfy a number of machine based experiments (see below), it is essential that if the useful properties of the flash tube shower detector are to become available to a wide range of experiments, methods of reducing the deposited charge, and speeding its decay,must be found, allowing the detector to operate at high event rates.

7.2 SUGGESTIONS FOR FUTURE WORK

In spite of the present rate restrictions, large volume detectors, employing flash tubes are being proposed and constructed for experiments

(principally hadron shower detectors for neutrino investigations) in a number of laboratories[2,3,4,5,6]. These detectors primarily employ plastic flash chambers consisting of honeycomb extrusions, mainly of polypropylene. These chambers are considerably simpler to construct than the traditional glass flash tubes, and allow a wide range of geometries to be simply obtained. They do, however, have one drawback, in as much as the outgassing of the plastic material requires a constant gas flow through the detector to prevent poisoning by electronegative impurities. For large volume detectors this may prove expensive (in the case of venting) or complicated and unreliable (in the case of recycling). Although the lower resistance of the plastic removes the problems associated with clearing fields, at the event rates so far obtained (< 10 per sec), the eventual rate limit is determined by the recovery time of these tubes, which at present stands at approximately 70 ms[5].

Consideration is also being given to installing flash tubes around the inner walls of hydrogen bubble chambers[7,8]. The flash tube is ideal for this application since because of its simple construction and operation, it requires a minimal amount of attention, and hence avoids expensive shut down of the bubble chamber. Furthermore, since the spill time through the bubble chamber is accurately known, the flash tubes may be made permanently sensitive, by application of a HT pulse of the same duration as the spill, allowing event reconstruction in time, as well as space. If such a system is to be expected to operate at the rate of the present rapid cycling bubble chambers, considerable research must be made into the decay of the internal fields,which will be very slow at liquid hydrogen temperature.

In the light of these developments and future trends, it is suggested that further work should focus around the following three main areas.

A) A more complete understanding of the factors affecting the formation and decay of the internal fields, also information concerning the surface phenomena which sets the lower threshold for removal of charge from the surface of the tube, since this determines the onset of spurious flashing. A search for an "ideal" material from which to construct flash tubes. This material should have a low resistance (approximately 10^7 Ω), and be easily workable (i.e. extrudable plastic), and machinable, yet show little tendency to outgas, allowing the use of a sealed system. It is unlikely that a material satisfying all these criteria and remaining inexpensive, will be found.

B) A Monte Carlo simulation of electromagnetic/lepton and hadron induced showers in the inhomogeneous absorber of the detector would allow the design parameters to be optimised for particular applications. Such factors as sampling frequency diameter of tubes or degree of shower containment for maximum energy or spatial resolution will vary according to the demands of the experiment. The present experimental results, and those of other workers, are insufficient to predict the dependence of the performance upon these parameters. The problem lends itself ideally to the Monte Carlo technique, and in the light of the anticipated wide application of flash tubes, such a study will be very valuable.

C) A wide range of readout is available to the flash tube, apart from the digitisation probes used in the present experiment, normal photographic techniques, or iconoscopic systems, based on the vidicon tube may be used. Further the optical problems of viewing a large array may be overcome by the use of optical fibres, up to several metres long, to locate the light signals to a small area where they can be more conveniently recorded. The use of digitisation probes in conjunction with a magnetostrictive wand (of the type commonly used in spark chambers), may enable a whole plane of tubes to be read out quite simply.

As the size of detectors increase, so the cost of the readout will become a dominant factor in the overall cost of the detector, and consideration should be given to the type of readout most suitable for a particular application. For example, for a detector whose sole requirement is measurement of energy, it may simply be sufficient to sum the total light output, using a photomultiplier tube and optical fibres to obtain a sufficiently accurate estimate of the energy, especially if the detector forms part of a trigger, requiring a rapid determination of an upper or lower energy threshold. Alternatively, if the centroids of shower samples are required, a digital method, possibly employing magnetostrictive wands may offer the best solution. Further, this digital information is ideal for handling by hard-wired processors[9], whereby trigger decisions (i.e. to fire a bubble chamber) can be rapidly made, or data compressed for maximum tape utilisation. The use of such processors with digitised flash tubes has already successfully demonstrated the potential of such a technique. Should the flash tubes be operated in the continually sensitive mode, then timing information will be required to record the exact moment of passage of the particle through the tube. A jitter in the formation time of the discharge is to be expected, and this will be further accentuated by the response of the particular readout system. An investigation into the timing jitter associated with the optical and electrical probe methods should be made to determine the system best suited to timing requirements.

In conclusion, it can be said that the flash tube, which was the forerunner of many of the gaseous discharge chambers in present use, after many years of neglect, is likely to become an invaluable addition to the tools of the future accelerator based physicist. However, many problems remain to be solved before its general use throughout the high energy physics community.

REFERENCES : CHAPTER SEVEN

(1) Chaney, J.E., Breare, J.M., Nucl.Inst. Meth., 124 (1975), 61.

(2) Walker, J.K., Fermi Laboratory, private communication,(1977).

(3) Chen, H.H., U.C. I./LAMPF, private communication, (1977).

(4) Hand, L.N., Fermi Laboratory, proposal No. 553, (1977).

(5) Ceradini, F., Conversi, M., submitted to Nucl.Inst. Meth., (1977).

(6) Conversi, M., Nature (Phys. Sciences), 241 , (1973), 160.

(7) Miller, D., Rutherford Laboratory, private communication to J.M.Breare, Durham University, (1977).

(8) Mannelli, I., Rosso, E., CERN Report, EF/ER/mk, (17/2/77).

(9) Verkerk, C., CERN Report, DD/arh, (June 1977).

APPENDIX I

RELATIONSHIP BETWEEN THE NUMBER OF PARTICLES INCIDENT UPON A LAYER OF FLASH TUBES AND THE NUMBER OF TUBES OBSERVED TO FLASH

One of the major problems associated with the use of flash tubes as elements of a shower detector is the inability to distinguish between one, or more than one, ionising particle passing through the sensitive volume of the tube. Therefore when the density of particles (assumed uniform) increases beyond a certain value, the number of flashed tubes no longer equals the number of ionising particles crossing the layer. A relationship between the number of incident particles and the observed number of tube ignitions can be obtained in the following manner.

Suppose a uniform flux of K particles is incident normally upon a layer of M_o flash tubes, as shown in Figure AI.a, if all tubes are in contact the likelihood of a particular tube being hit, for one particle incident on a layer of M_o tubes, is given by

$$\text{Prob. hit} = {}^{1}/_{M_o}$$

the probability of this tube flashing is given by

$$\text{Prob. flashing} = \eta . {}^{1}/_{M_o}$$

where η is the layer efficiency of the tubes.

The probability of the tube not flashing is given by

$$\text{Prob. not flashing} = 1 - {}^{\eta}/_{M_o}$$

(a)

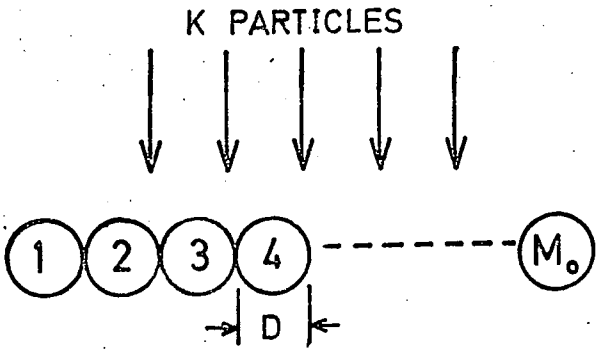

LAYER EFFIENCY = η

MEAN NUMBER OF TUBE IGNITIONS = $\bar{M}$

$$\bar{M} = M_o\left[1-(1-\eta/M_o)^K\right]$$

(b)

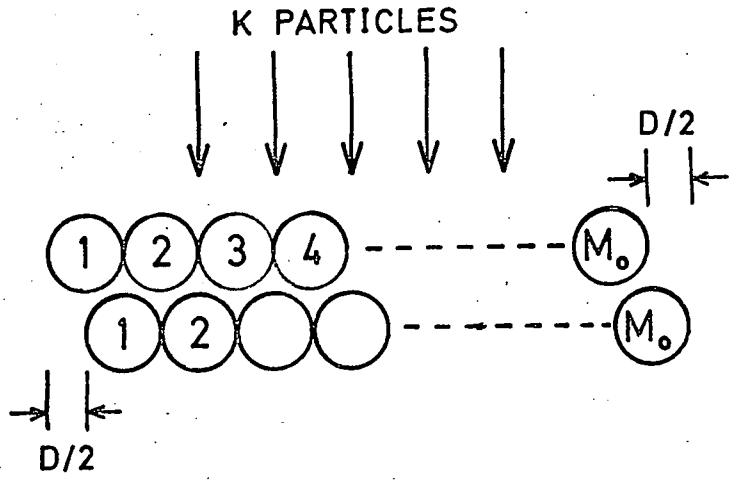

$$\bar{M} = 2M_o\left[1-(1-\eta/M_o+\tfrac{1}{2})^K\right]$$

FIGURE AI·1 MEAN NUMBER OF TUBE IGNITIONS ($\bar{M}$) FOR K PARTICLES INCIDENT ON M_o TUBES

Therefore for K particles incident upon the layer, the probability of a particular tube not flashing will be given by

$$\text{Prob. not flashing (K particles)} = \left(1 - {}^{\eta}/_{M_o}\right)^K$$

The probability of the tube flashing is therefore given by

$$\text{Prob. flashing (K particles)} = 1 - \left(1 - {}^{\eta}/_{M_o}\right)^K$$

and the mean number of tubes flashing in a layer containing M_o tubes is given by

$$\bar{M} = M_o \left\{ 1 - \left\{ 1 - {}^{\eta}/_{M_o} \right\}^K \right\}$$

A similar approach may be used to predict the mean number of tubes flashing in a system of two staggered layers. If the two layers are displaced by half a tube width, as shown in Figure AI.b, then the likelihood of a particular tube being struck for a single particle incident upon the layer is given by

$$\text{Prob. hit} = {}^{1}/_{(M_o + \frac{1}{2})}$$

Following the previous reasoning, the mean number of tubes flashing in a layer of M_o tubes, $M_o + \frac{1}{2}$ wide, with a uniform flux of K particles incident normally upon the layer is given by

$$\bar{M} = M_o \left\{ 1 - \left\{ 1 - {}^{\eta}/_{(M_o + \frac{1}{2})} \right\}^K \right\}$$

and the mean number igniting in two independent layers is given by

$$\bar{M}_{tot} = 2 M_o \left\{ 1 - \left\{ 1 - {}^{\eta}/_{(M_o + \frac{1}{2})} \right\}^K \right\}$$

The relationship between K and $\bar{M}$ for 1 layer and 2 staggered layers of tubes, for $M_o = 16$ and $\eta = 0.8$ is shown in Figure AI.2. It can be seen that the use of two layers results in an over-estimate of $\bar{M}$ up to K = 20, after which the value of $\bar{M}$ falls below that of K. The significance of the width of the flash tubes may be seen from Figure AI.3, which shows $\bar{M}$ as a function of K for 5 values of M_o. As M_o increases, which is equivalent to decreasing the width of the flash tube, the curve approaches the linear relationship between $\bar{M}$ and K, for $\eta = 0.8$, assuming an infinitely narrow sensitive volume for the flash tube.

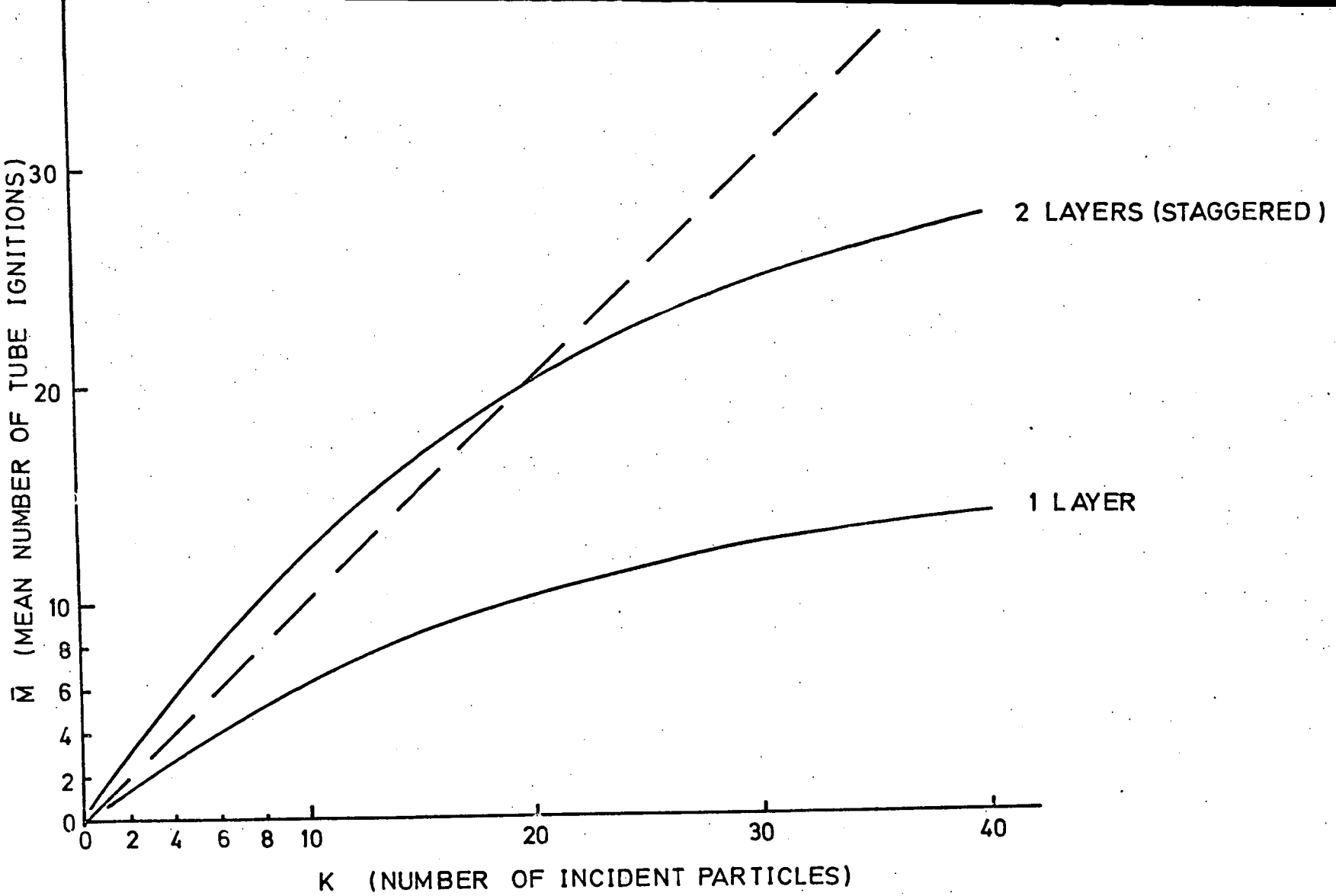

FIGURE AI·2 RELATION BETWEEN NUMBER OF INCIDENT PARTICLES AND NUMBER OF TUBE IGNITIONS

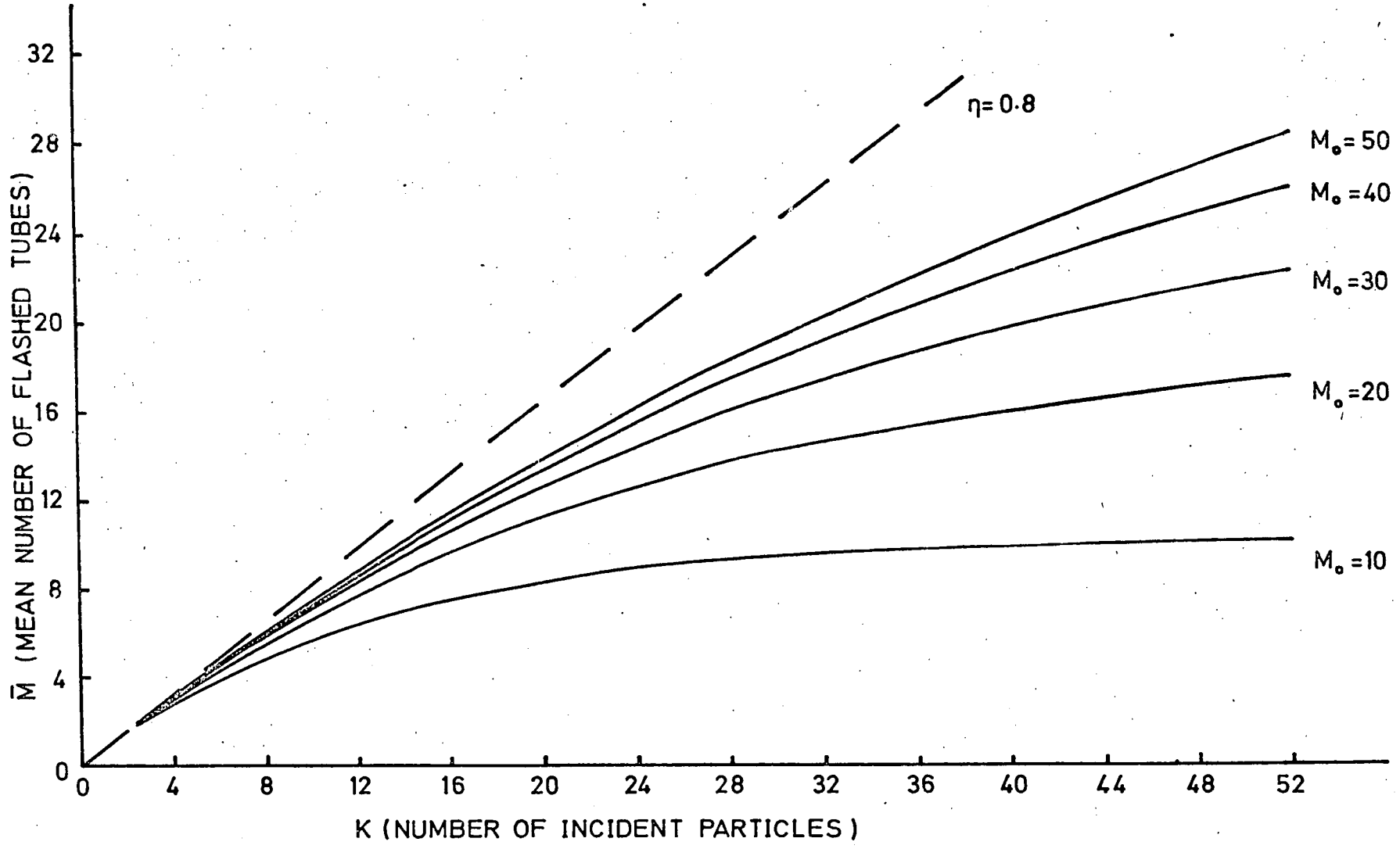

FIGURE AI·3 MEAN NUMBER OF FLASHED TUBES AS A FUNCTION OF THE NUMBER OF INCIDENT PARTICLES FOR DIFFERENT VALUES OF M_o

ACKNOWLEDGEMENTS

The author would like to thank Professor A.W.Wolfendale for his support of this work and use of the laboratory facilities.

He is indebted to his supervisor, Dr.J. M. Breare, for his guidance, assistance and patience shown throughout this work, also to past and present members of the Nuclear Instrumentation Group, Dr. B.C. Nandi, Mr. A.R. Hedge, Mr. A. Campbell, Mr. A. Humrich, Mr. M. Comyn, Dr. I.D. Tait and Mr. W. el Disouki, who have been of invaluable assistance throughout all stages of this work. Mr.J.Webster, Mr. R. McDermot and Mr. J. Scott are thanked for the excellent technical support provided in building the apparatus.

The Daresbury Laboratory is thanked for the use of their experimental and computing facilities. In particular, Dr. P. Ridley, Mr. A. Rush and Dr. P. Richmond are thanked for their help and interest, also the many members of the Machine Physics Group, for their constant effort to satisfy the beam requirements of a very minor user.

He would also like to thank Mrs. S. Mellanby for undertaking the unenviable task of typing this thesis.

Finally, the Science Research Council is thanked for providing a Research Studentship.